KEK Internal 83- 4
September 1983
I/E/B

KENS REPORT-Ⅳ

Edited by

Y. ISHIKAWA
N. NIIMURA
S. IKEDA

NATIONAL LABORATORY FOR
HIGH ENERGY PHYSICS

National Laboratory for High Energy Physics, 1983

KEK Reports are available from:

Technical Information Office
National Laboratory for High Energy Physics
Oho-machi, Tsukuba-gun
Ibaraki-ken, 305
JAPAN

Phone: 0298-64-1171
Telex: 3652-534 (Domestic)
(0)3652-534 (International)
Cable: KEKOHO

PREFACE

The present report follows a previous issue, KENS REPORT III published in June 1982. This volume collects the summaries of the works performed at KENS during the 1982 fiscal year. This is the second issue of the report on the academic works at KENS.

Our neutron source was operated satisfactorily throughout the 1982 FY. The first W target was replaced by a new one at the bigining of this FY, because of a serious erosion of covering metals due to condensation of NO_x gas generated in air by irradiation. The second target which was installed in an improved environment has been operative since then without any serious radiation damage. The total machine time allocated to KENS in the 1982 FY was 1,439 hrs.

One of the highlight of this FY was that flat cold moderator was replaced by the grooved one at the end of the FY, which increased the intensity of cold neutrons by 1.4. The results of studies performed in connection with the new moderator are reported in three papers.

The most of academic works have been carried out employing eight spectometers, HIT, MAX, CAT, FOX, LAM, LAM-D, SAN and TOP which are reported in 52 papers. A significant effort has also been paid for development of new spectrometers. They are summarized in another 11 papers. RAT has made a good progress in improving the energy resolution. PRE-PEN was removed and the installation of PEN, the final version of the polarized epithermal neutron spectrometer, was completed at the end of the FY. The test experiment for the μeV spectroscopy carried out using the cold neutrons from the guide tube C_2 was found quite successful,which made us decide to install a new high energy resolution spectrometer, LAM-80 in the 1983 FY. The instrument for producing and measuring ultra cold neutrons, UCN has also been accomplished.

We should also mention that there was a rush of the international conferences concerning neutron scattering researches in the summer of 1982,

as ICANS meeting (Argonne), Yamada Conference(Hakone), ICM'82(Kyoto), Conference Celebrating 50 Years Anniversary of Neutron Discovery (Cambridge), Symposium on Utilization of Pulsed Neutrons (Oxford) and Polarized Neutron Conference (Grenoble). We were happy to have been able to make a good contribution to each of these conferences by presenting our current yields from KENS, which we heard, impressed many of the wide neutron scattering communities and convinced them of the potentials of the pulsed neutron sources for the study of condensed matters.

The details of each paper will be published in original journals. Any one who has an interest in the details is asked to make a direct contact with the authers.

August 15, 1983

Editors : Y. Ishikawa
N. Niimura
S. Ikeda

CONTENTS

SAN

Present Status of BSF Operation

Toshikazu ADACHI, Yoshiro IRIE, Naokatsu KANEKO
Masayuki MIKI, Yoshiharu YANO and Hiroshi SASAKI

National Laboratory for High Energy Physics
Oho-machi, Tsukuba-gun, Ibaraki 305, Japan

The summary of the BSF operation in the Fy 1982 is shown in Table 1. The beam time used for physics experiments, medical use and beam line tuning amounts to 3,242 hours, which corresponds to 89 % of the total operations time of the accelerator, 3,652 hours. In comparison with the operations in Fy 1981, the available beam time increased by 12 % and the "REJECT" time of the experimental facilities decreased, however the downtime of the beam line equipments increased by a factor of 3. These failures were mainly due to troubles of the pulsed magnet power supplies. The power supply, which switches the beam from the main ring injection line to the BSF beam line, was transferred to the room beside the beam dump room. Thus we can expect the repairs would be carried out without disturbing the main ring synchrotron operations when the power supply breaks down.

An alarm is furnished to warn the console operator when the beam pulses hit somewhere else other than pass through the beam line. The alarm signals

Table 1 Summary of BSF operations since April 1982 through March 1983. (All units are "hours", unless otherwise specified.)

	NEUTRON EXPERIMENT	MESON EXPERIMENT	MEDICAL USE	TOTAL
BEAM UTILITY	1509.29	1529.62	180.27	3219.18
BEAM ON	1439.06	1431.17	166.49	3036.72
REJECT	3.72	7.32	4.83	15.87
BEAM LINE TROUBLE	15.58	37.74	3.01	56.33
ACCELERATOR TROUBLE	50.93	53.39	8.94	113.26
BEAM LINE TUNING	14.92	7.03	0.75	22.7
AVERAGE INTENSITY (10^{11} protons/pulse)	4.79 ± 0.66	4.68 ± 0.57	5.17 ± 0.47	
BEAM TRANSMISSION FROM SYNCHROTRON TO TARGET (%)	91.4 ± 8.2	89.3 ± 7.9	93.7 ± 5.4	

are produced by an anti-coincidence circuit which is connected with the beam bunch signal and the booster synchrotron extraction kicker pulse for BSF use. The reasons for such alarms are drifts of the power supply outputs, beam fluctuations in the upper stream, and so on. The alarm helps to reduce the radioactivity along the beam line.

Downstream from the pulsed switching magnet (PHB2), a beam shutter of stainless steel was installed in the beam line (Fig. 1). The shutter has a cylindrical shape of 180 mm in diameter and 250 mm in length which is enough to stop the 500 MeV proton beam. The moving time of the shutter from one end (on-line limit or off-line limit) to the other end is about 5 seconds by means of an air cylinder. ON/OFF operations of the shutter are made at the BSF control desk by request of the particle radiation medical science center. The vacuum vessel including the shutter and the upper stream chamber are separated by two thin stainless steel foils such as 50 μm and 100 μm in thickness respectively. The shutter vessel is evacuated by a 260 ℓ/min rotary pump. When the shutter is set on the on-line limit the access to the medical treatment room with neutrons is always possible without stopping the beam supply to the meson experimental facility and the medical treatment room with protons.

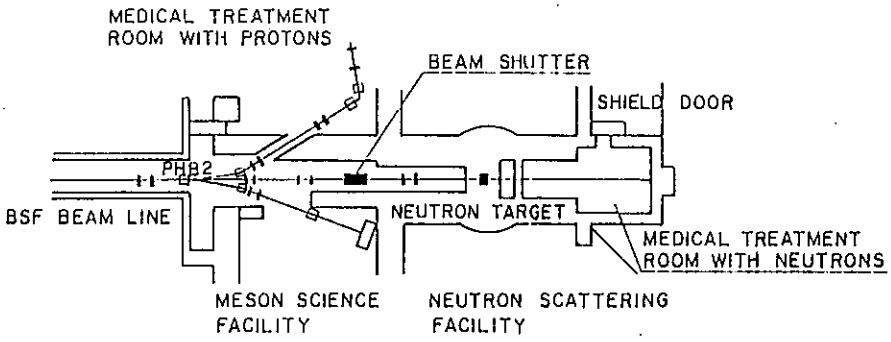

Fig. 1 Installation of the 500 MeV proton beam shutter.

The procedures for the beam intensity calibration were laborious so far. Recently a fast storagescope with a scan converter tube (Iwasaki's TS-8123) has become available. It has memories of 512 bytes and can be connected to a computer through GP-IB. The new calibration system with TS-8123 is shown in Fig. 2. As is shown a bunch signal is divided into two signals, one of which is fed to the sample and hold (S/H) module and the other fed to TS-8123. When the bunch signal is detected, TS-8123 writes the signal shape into the memories and triggers the digital volt meter (DVM) to

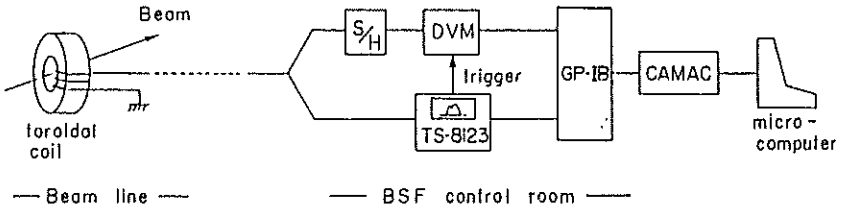

Fig. 2 Block diagram of an intensity calibration system.

hold the current output value of the S/H module. Then both the signal shape and the digitized S/H output are transmitted to a microcomputer through CAMAC controlled GP-IB. The microcomputer integrates the beam charge and calculates the calibration constant which is the ratio of the intergrated beam charge to the digitized S/H output. Consequently a relative error of the calibration constant is less than 5 %.

The linkage between BSF MELCOM-70 and KEK satellite computer S-2 is completed. The beam intensity along the BSF beam line in units of protons per pulse are transmitted to the S-2. For more information a video system is also provided. This system uses a Fujitsu Micro-7 personal computer which has the video output interface. Digital and analogue input interfaces were designed and made by means of which beam profile signals, booster extraction kicker pulses and other data are interfaced. The video information transmitted to KEK CATV center covers the beam pulse number available for BSF operations, the beam intensity at the entrance of the BSF beam line, the distributed pulse number for each experimental facility, beam profiles averaged over one main ring synchrotron cycle where the background spectra are subtracted, and the beam request status of the experimental facilities. Fig. 3 is an example displayed on the channel 3 of KEK CATV.

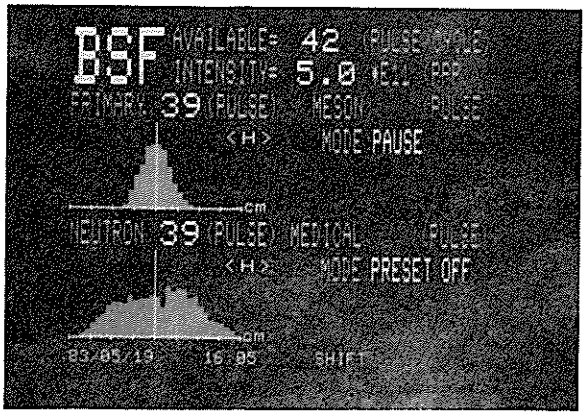

Fig. 3 Video information on BSF displayed on the channel 3 of KEK CATV.

Numerical Study of Grooved Moderator for Pulsed Neutron Source

Keichiro Tsuchihashi

Japan Atomic Energy Research Institute

Tokai-mura Ibaraki-ken 319-11

A numerical study has been done to find the mechanism of the increase of neutron beam currents from the grooved surface by a computer simulation, and also through the geometrical parameter survey about polyethylene moderators to find optimum parameters so as to yields the maximum beam currents of thermal neutrons.

Numerical Analysis

The reference grooved moderator for the numerical simulation is of polyethylene ρ=0.923 g/cc, overall 14.4* 10.* 10. cm dimension with 1.6 cm wide * 5. cm deep grooves are placed 1.6 cm apart. Another moderator of polyethylene, overall dimension 14.4 * 7.5 * 10. cm is taken as the reference flat moderator which preserves the volume of polyethylene used in the grooved one.

A two dimensional SN transport code TWOTRAN-II[1] was used due to the lack of any available 3D SN code. Then the geometry under consideration is reduced to the infinitely long column as the section is shown in Fig.1.

The distributed sources for the SN calculations were calculated beforehand as the spatial distribution of the first flight collision from the line source. The nine group neutron cross sections were calculated by the SRAC code[2] .

As a demonstration, shown in Fig.2 are the spatial distributions along y-direction of the beam currents of the eighth energy group (.04 ev -.01 ev) from the grooved and the flat moderators. Both curves are normalized by the unit line source. We can see the sharp shoots of beam currents appearing from the bottom of grooves.

In Table 1, the neutron balance is compared between two reference moderators. Due to the wider solid angle spanned from the line source, the first flight collision in the grooved moderator occurs about 15 % more than in the flat one. Hereafter we use the term G/F for the ratio of some physical quantity of the grooved moderator to that of the flat one. The net fast neutron leakage in the grooved moderator occurs in a little higher rate as the G/F 1.17 than the G/F of the first collision rate 1.15, especially the right leakage occurs remarkably as the G/F 1.26. The increased fast neutron leakage results in the decrease of the slowing down source to the thermal energy range to the G/F 1.11. In spite of this decrease of the G/F the net thermal neutron leakage in the grooved moderator is elevated up to the G/F 1.18. As to the thermal leakage from the right boundary this trend is stressed up to 1.45. On the contrary the neutron absorption in the grooved moderator is depressed apparently 3 %.

On the lower lines of the table the integrated beam components multiplied by an undefinite scale factor are compared. The G/F for the beam components of fast neutron 1.13 is rather low compared with the G/F of the right leakage 1.26. The G/F of the thermal beam currents, however, amounts to 1.73. This situation is shown in detail in Fig.3 where the spectra of beam currents integrated along y-direction and the G/F's by energy group are shown. We should note that the G/F at the highest energy group is less than unity and that the G/F's for other fast groups are same as those of the right leakage. In the thermal energy range we can find not only the increased beam intensity but also the softer spectrum from the grooved surface.

Shown in Fig.4 are the spectra of scalar fluxes at the central position of both moderators. We can find the thermal neutron flux in the bulk of the grooved moderator has, inversely, lower intensity and harder spectrum than those in the flat one.

Now we shall summarize the mechanism of the increase of beam currents from the grooved moderator comparing with the currents from the flat one. At first we have to note that the increase of distributed source of about 15 % due to the wider solid angle from the line source. At the highest energy group the neutron distribution is strongly affected by the source distribution and the right leakage occurs mainly from fin part with less beam components than the isotropic. In other fast groups the increased G/F's for the beam components are obtained as well as those for the right leakages. There occurs no effective absorption and the mean free path is only one tenth of the dimension of the moderator so that the flux is fairly flat in beam direction. The increase of G/F in the epithermal energy range comes from the biased distribution of the increased source neutrons to the right side so as to make the right leakage more. In the thermal neutron range where the absorption occurs in the same rate of the leakage , the flux in the edge of fins is much lower than in the central part of the moderator. Because of the geometry of the grooved surface the neutron beam comes out directly from the bottom of grooves. The total beam currents of the thermal neutrons amount to 1.73 times of those from the flat moderator in spite of the lower neutron density.
On the contrary the beam currents from the flat moderator is hardened due to the absorption which takes place more strongly for the slower neutrons during the diffusion from the inside to the surface in spite of the softer neutron spectrum in the bulk moderator.

Parameter Survey

The overall dimension and the parameters of the grooved surface such as the width and the depth of grooves, and the width of fins, have to be optimized in view point of yielding the most high beam currents.

As the result of the parameter survey, it has been found that the extension to the backward from the beam direction, the longer fin length, and the shorter groove-fin pitch increase the thermal beam currents and that the ratio of groove width to fin's as 1:1, and the x-position of target on the plane across the bottoms of grooves maximize the beam currents.

A grooved moderator is proposed to demonstrate the possible gain by the modification of geometrical parameters of the reference grooved one The modification consists of 1 cm extension of the moderator to the

left direction, 2 cm extension of fin length, and the reduction of groove pitch from 3.2 to 2.4 cm upon keeping the width ratio of groove's to fin's 1:1 and the number of grooves 4. Due to the reduction of pitch, the width of the remotest fin from the target is changed from 1.6 to 4.8 cm which might work as backward reflector. The gain of 1.38 was obtained by the modification.

Comments to the cold neutron source under planning

For the design of the moderator for the cold neutron source of KENS-II under planning we can suggest as follows,

1. The gain by the grooved structure will be increased for the cold moderator due to the stronger absorption in the lower energy range.
2. The width ratio of groove's to fin's should be 1:1.
3. The fin length is preferable to be as long as possible. If the sharp pulse shape is desired, the top surfaces of fins could be covered by the absorber with the sacrifice of loss of less than 15 % of beam currents.
4. The groove pitch is preferable as short as possible.
5. We propose the insertion of any low absorbing metal like zirconium into grooves which might decrease undesirable leakage of fast and thermal neutrons and behave as transparent material to neutrons below Bragg cut off energy.

References

1) Lathrop K.D. and Brinkley F.W. 'An Interfaced, Exportable Version of the TWOTRAN Code for Two-Dimensional Transport', Los Alamos Scientific Laboratory report LA-4432-MS, July 1973
2) Tsuchihashi K. et al 'SRAC : JAERI Thermal Reactor Standard Code System for Reactor Design and Analysis', JAERI-1285, January 1983

Table 1 Neutron Balance Table for Reference Moderators

Reaction (range)	Grooved Moderator	Flat Moderator	Ratio G / F
Source	.2656	.2309	1.15
Absorption	.0260	.0269	0.97
Net Leakage	.2396	.2040	1.17
(fast)	(.1816)	(.1550)	(1.16)
(thermal)	(.0580)	(.0490)	(1.18)
Right Leakage	.0667	.0510	1.30
(fast)	(.0451)	(.0358)	(1.26)
(thermal)	(.0217)	(.0151)	(1.45)
Slowing Down to Thermal	.0835	.0754	1.11
Right Beam *	3.044	2.315	1.31
(fast)	(1.785)	(1.586)	(1.13)
(thermal)	(1.259)	(0.729)	(1.73)

* An undefinite scale factor is multiplied to the right beam components.

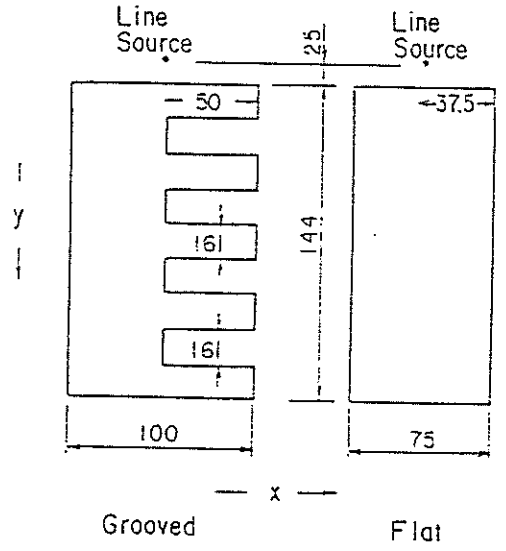

Fig.1 Two-Dimensional Model for Reference Moderators

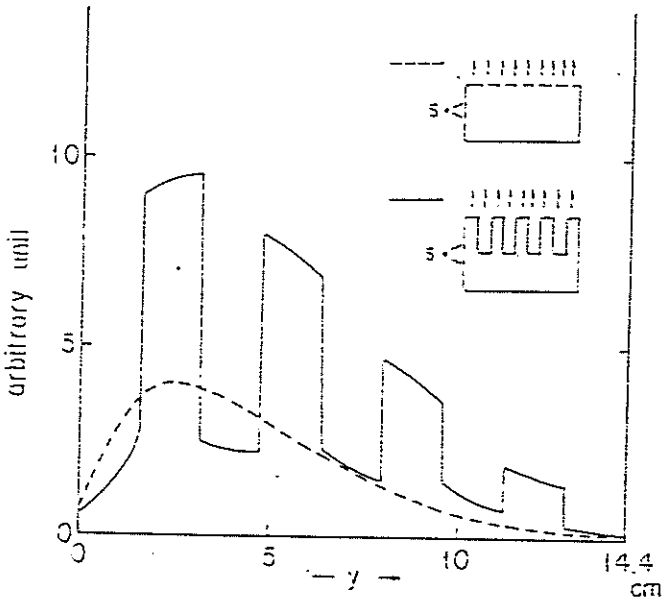

Fig.2 Y-Dependence of Beam Currents (8th group) from the Reference Moderators

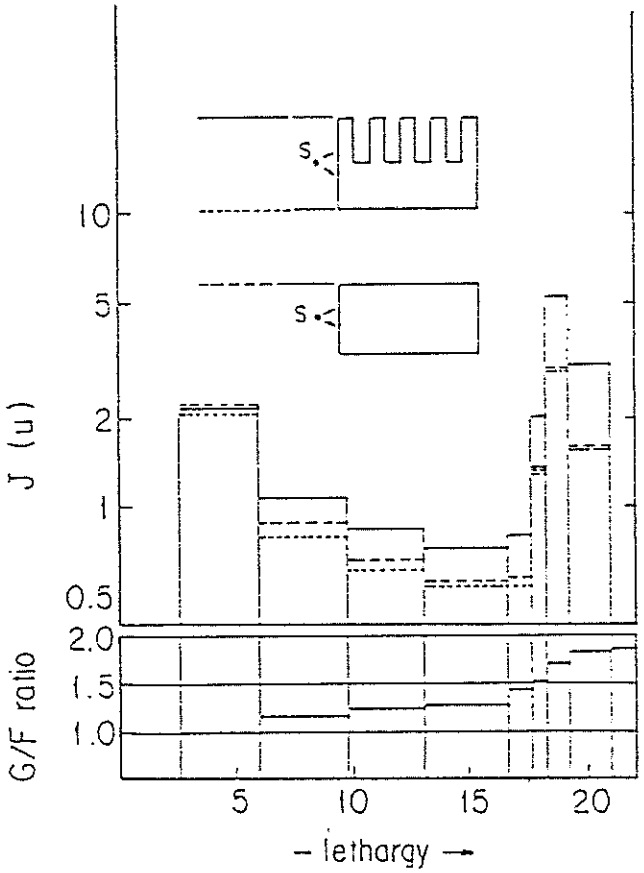

Fig.3 Spectra of Beam Currents from the Reference Moderators Integrated over Each Right Surface and Their G/F's by Energy Group

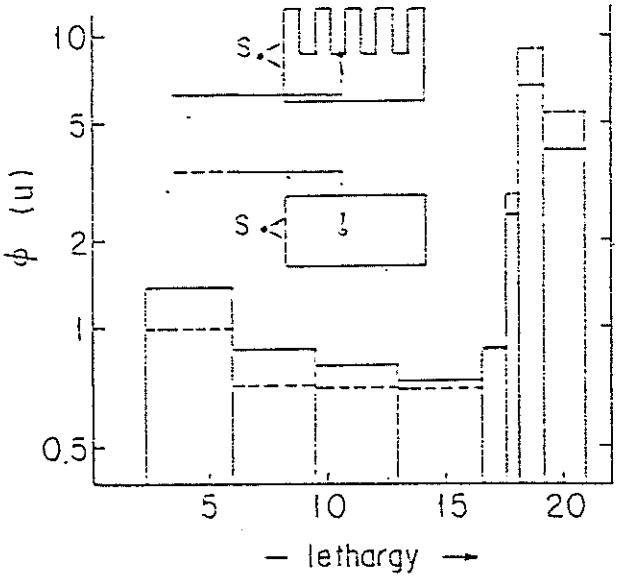

Fig.4 Spectra of Scalar Fluxes in the Reference Moderators at x=5.0 cm, y=5.8 cm

Thermal Grooved Moderator Experiments

Yoshiaki KIYANAGI*, Kazuhiko INOUE*, Yoshikazu ISHIKAWA**,
Noboru WATANABE*** and Hirokatsu IWASA*

* Department of Nuclear Engineering, Hokkaido University, Sapporo, 060 Hokkaido, Japan
** Physics Department, Tohoku University, Sendai, 980,Japan
*** National Laboratory for High Energy Physics, Oho-machi, Tsukuba-gun, 305 Ibaraki-ken, Japan

We surveyed design parameters of KENS grooved cold moderator by using polyethylene thermal moderators at Hokkaido University. A reflector imitating the shape of the upper half of KENS one was used but the material was graphite. Time-of-flight spectra from $15 \times 15 \times 5$ cm^3 flat moderator and $15 \times 15 \times 10$ cm^3 grooved modertor with 5 cm depth grooves are indicated in Fig. 1. The grooved surface consisted of six fins and five grooves. The intensity gain is about 1.5 times around the spectrum peaks. Comparing with the same volume flat moderator, $15 \times 15 \times 8$ cm^3, the gain factor is about 1.4. The moderator thickness

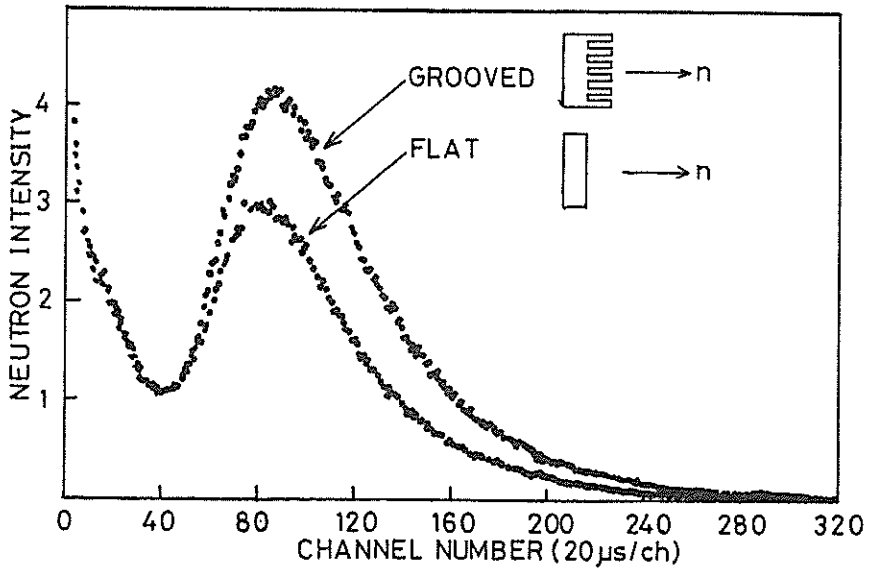

Fig. 1 Time-of-flight spectra from grooved and flat moderators.

was limited to 10 cm because of spatial allowance in KENS Be reflector while the neutron intensity can be increased by elongating the length of fins. We examine next the effect of depth of grooves under the condition of the constant moderator volume. Figure 2 shows the results for four grooved moderators of 2, 3, 4 and 5 cm depths of grooves, respectively. The 5 cm depth is best in this condition. Figure 3 shows the neutron intensities from the grooved moderators with various heights of the lowest fins. Neutron intensity is not so sensitive to the height in a range of 1 ∿ 2 cm.

We decided the grooved cold moderator dimension taking into account above results as well as the refregeration efficiency. The increase in intensity is expected to be 30∿50 %.

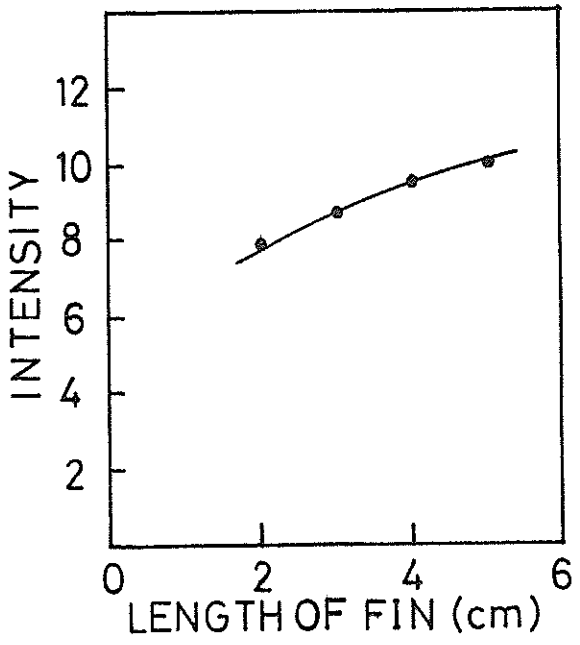

Fig. 2 Effect of length of fins.

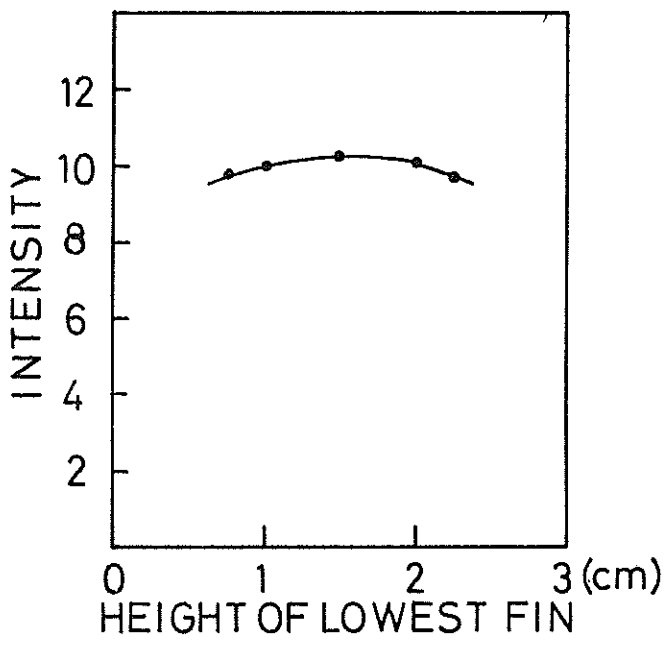

Fig. 3 Effect of hight of the lowest fin.

Grooved Cold Moderator at KENS

Yoshikazu ISHIKAWA, Susumu IKEDA*, Noboru WATANABE*, Kazuhiko INOUE**, Yoshiaki KIYANAGI** and Hirokatsu IWASA**

Physics Department, Tohoku University
Sendai 980, Japan

*National Laboratory for High Energy Physics
Oho-machi, Tsukuba-gun, Ibaraki 305, Japan

**Department of Nuclear Engineering, Hokkaido University
Sapporo 060, Japan

The KENS first cold moderator made by solid methane of 50 x 120 x 150 mm^3 in size[1] (flat moderator) had been operative without any trouble for more than two years and a half and had proved a satisfactory performance for its high coupling efficiency and effective cooling ability. However, recent mock-up tests using Hokkaido University LINAC[2),3)] and a simulation calculation by Tsuchihashi[4)] have suggested that a cold moderator with a grooved surface would increase the intensity of cold neutrons further, if it is installed in the KENS target station. After a carful survey and design, we finally made a grooved cold moderator and replaced it with the old one in March 1983. The paper describes the design and performance of the new moderator.

Figure 1(a) is the side view of the grooved moderator we finally constructed with its photograph in Fig. 1(b). The dimension of the new moderator, the ratio of groove width to fin's (1.28), number of fins and depth of grooves given in Fig. 1(a) are determined based on the results of mock-up test and calculation as reported in preceding three papers[2-4)]. The methane container is made by pure Aℓ, and the wall of fins is only 2 mm thick, while other parts of the container have the thickness of either 4 or 5 mm. The container is cooled by the same method as the previous moderator[1)] with some improvement. The total volume of methane is 1,544 cc, which is the 70 % increase of volume compared with the old one.

The result of cooling performance with and without proton beams are displayed in Fig. 2. Without the proton beams, the methane could be cooled

down to 16.8 K, the lowest temperature that our refrigerator (PGH 105) can attain. The temperature of methane was found to rise up to 20 K by full proton currents (1.5 μA). The amount of heat q deposited in the moderator by nuclear radiation could be estimated from the temperature rising curve in Fig. 2 as was done in the previous paper[1]. The temperature rise $\Delta T(t)$ is given by

$$\Delta T(t) = g(1 - e^{-ht}),$$

with $g = q/\bar{K}$ and $h = \bar{K}/C$, $\bar{K}$ and C being thermal conductance and heat capacity of the moderator respectively. By employing the parameters g and h determined from Fig. 2, q was estimated to be $q = ghC = 4.9$ watt. Note that the result in Fig. 2 was obtained with the proton currents slightly reduced from the maximum value to get an accurate temperature rise.

The heat deposit thus estimated is almost four times larger than that in the old moderator as is compared in Table 1. If the total deposit is normalized by proton current, the total volume of moderator and ratio of the first flight collision rate $\eta = G/F = 1.15$ estimated by a transport calculation[4], the normalized heat deposit becomes 1.9 times larger than the flat one. It is not clear whether such a discrepancy is due to the real change of situations or is simply due to the accuracy of the approximate calculation for q. Note that the normalized heat deposit estimated for the flat moderator at the end of its use (Feb. 1983) is 1.3 times higher than that measured at the beginning (Jul. 1980).

The energy spectra at the exit of the neutron guide tube from the new grooved and old flat moderators were measured by the neutron scattering from a standard vanadium sample. Their intensities were normalized by measuring epithermal neutron current from an ambient temperature moderator located at the opposite side of the target. An appreciable change was found in the energy spectra as seen in Fig. 3. The ratio of the intensity of cold neutrons from the grooved moderator I_g to that from flat one I_f was found to be wave length dependent. The ratio is 1.4 ∿ 1.5 in the wave length range 5 ∿ 8 A which is important for the spectrometers with neutron guide tubes (SAN, TOP and LAM-80), while the value is only 1.2 at the Maxwellian peak of the cold spectrum (λ = 4 A). (Note that the energy spectra shown in Fig. 3 are modified by the transmittance of the neutron guide tube and are different from the real one.) The values are less than those anticipated from the mock-up tests, presumably due to the better reflector system for KENS.

The time spectra of cold neutrons were measured by back scattering from a mica single crystal and are displayed in Fig. 4. The spectra have a

time-structure in the rising part, which becomes substantial for longer wave lengths. However, it is confirmed that the structure gives no serious problem to the profile analysis for the quasi-elastic spectrometer LAM-40 which utilizes 4 A neutrons. This was turned out to be also the case for the high resolution quasi-elastic spectrometer LAM-80 even if it employs the neutrons of 6.6 A. The total cost for realization of the increase is about ¥16.5 x 10^6 including the expenses for the mock-up tests and for the modification of the Be reflector.

It should be noted that the replacement gave us an opportunity for examining the inside of the old cold moderator container to find the deposits created by irradiation during the 2.5 years operation. This would give us an important information on the decomposition process of solid methane by spallation neutrons. This examination will be carried out as soon as the radiation level of the cold moderator container reduces to the accessible one.

References

1) S. Ikeda, Y. Ishikawa and K. Inoue, Proc. ICANS-IV (KEK) (1981) 200.
2) K. Inoue, Y. Kiyanagi, H. Iwasa, N. Watanabe, S. Ikeda, J. M. Carpenter and Y. Ishikawa, Proc. ICANS-IV (ANL) (1983) 392.
3) Y. Kiyanagi, K. Inoue, Y. Ishikawa, N. Watanabe and H. Iwasa, KENS Report-IV (1983) preceding paper.
4) K. Tsuchihashi, ibid.

Table 1 Heat Deposit in Cold Moderators by Nuclear Radiation

	Flat Moderator (Jul. 1980)	Flat Moderator (Feb. 1983)	Grooved Moderator (Jul. 1983)
Proton Intensity (current I, μA)	7.3 x 10^{12} protons/sec (1.2)	8.0 x 10^{12} protons/sec (1.3)	6.5 x 10^{12} protons/sec (1.0)
Volume V (cm^3)	900	900	1,544
Bottom Area S (cm^2)	60	60	131
Temperature Rise (K)	1.0	1.4	2.0
Thermal Conductance K(J/K·sec)	1.08	1.09	2.46
Total Heat Deposit q(W)	1.2	1.7	4.9
Normalized Heat Deposit (= q/VηI) ($mW/cm^3 \cdot \mu A$)	1.11	1.44	2.75

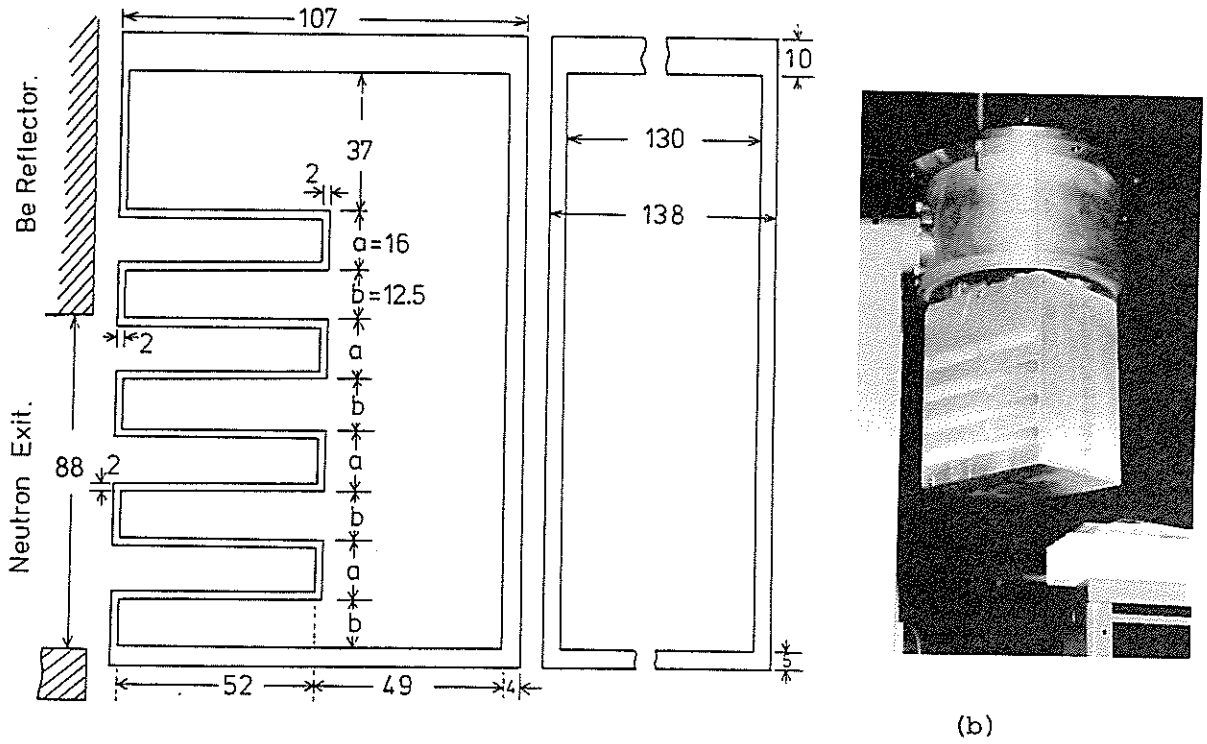

Fig.1(a) The side view of grooved moderator and (b) its photograph.

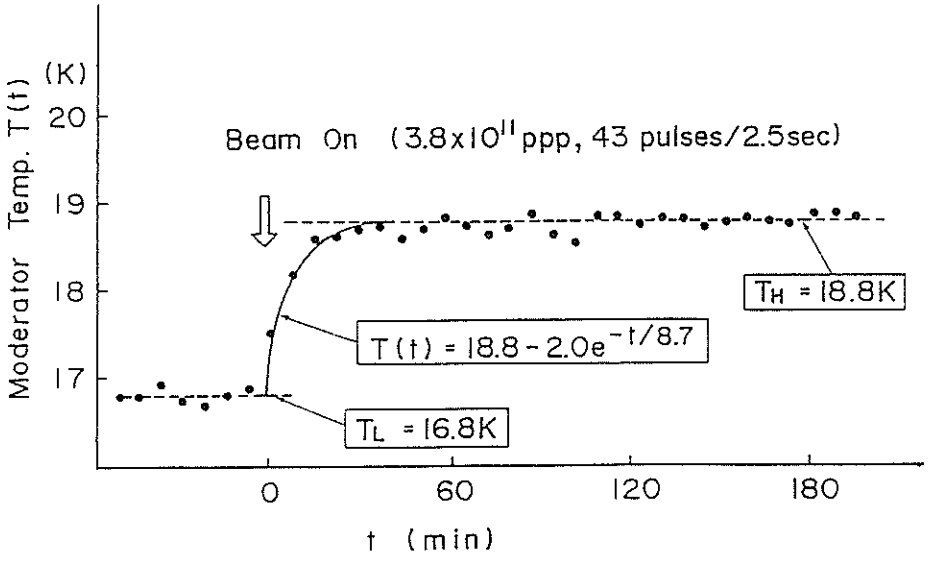

Fig.2 Temperature rise of grooved moderator by nuclear radiation.

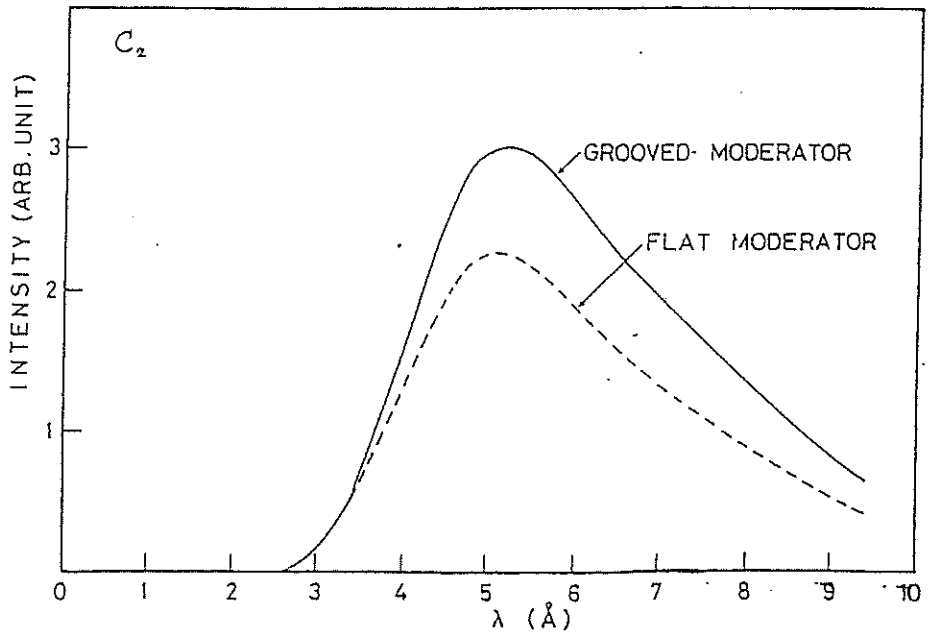

Fig.3 Energy spectra of grooved and flat moderators.

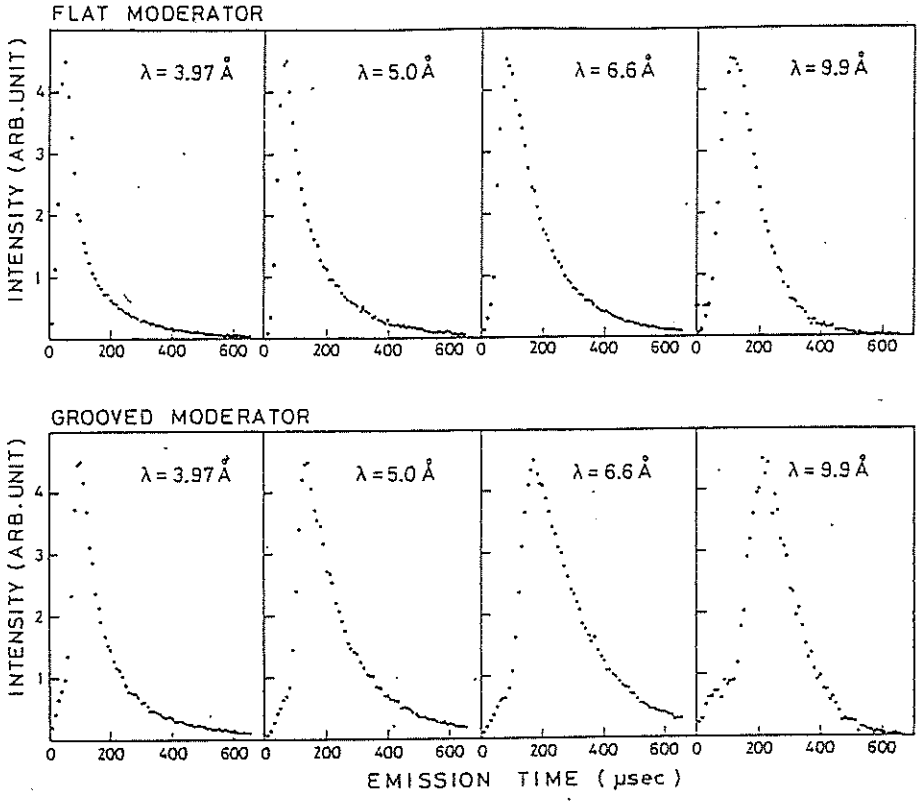

Fig.4. Time spectra of grooved and flat moderators.

Radiation Decomposition of the Solid Methane used as a Neutron Moderator in the KENS Target Assembly

K. Kondo and S. Ikeda

National Laboratory for High Energy Physics
Oho-machi, Tsukuba-gun, Ibaraki, 305, Japan

The solid methane used as a cold neutron moderator, which is placed just upon the W target, is exposed to high radiations of secondary particles and photons during machine operation. After each cycle of machine operation, the methane used is evaporated and transfered to a reservior tank of 0.5 m^3, from which the gas is released into air through a stack. The preliminary chemical analysis of radiation decomposition products in the exhausted gas was conducted in July 1980. Hydrogen, ethylene and ethane were detected, and most abundant hydrogen was 0.15 % for the irradiation of an average beam current 1.2 μA for 52.7 hrs.[1)]

In this experiment, the methane exposed to different radiation doses was assayed in order to examine more precisely the correlation between concentration of decomposition products and radiation dose, and the analytical results are presented, being compared with the previous one.

The sample gases A and B to be assayed were taken from the reservoir tank, and the total number of 500 MeV protons on the W target were 2.74×10^{18} for the sample A and 1.35×10^{18} for the sample B respectively. The chemical analysis was

performed by gaschromatography under the following conditions; column: 3 mm diameter, 1.5 m long, column packing: molecular sieve 5A, 80 ~ 100 mesh, column temperature: temperature programmed at the rate of 10°C/min. from 30°C to 220°c, carrier gas: N_2, TCD filament current and temparature: 70 mA, 150°C. The retention times of H_2, C_2H_4 and C_2H_6 and their sensitivities to TCD were determined in advance using standard gases prepared at various mixing ratios of these gases. Fig. 1 shows one of the gas-chromatograms obtained for the sample A. H_2, C_2H_4 and C_2H_6 were identified as decomposition products the same as those in the previous result.[1] The concentrations of individual products were calculated from the peak area in the gas-chromatograms and sensitivity of each gas to TCD. The results were listed in Table 1, together with total number of protons for each sample. As far as the present results are concerned, the concentrations of decomposition products in the sample A are about twice as great as those for the sample B, in proportion to the total number of protons on the W target, and it is expected that H_2 concentration does not exceed ~ 1 % for the case of total number of protons less than about 3.3×10^{18}. However the above results were largely different from the previous one.[1] At present there is no explanation pertinent to this discrepancy, but it seems supposedly to arise from the procedures of gas sampling and/or chemical assay. The confirmative results have to await further analysis.

Reference

1. K. Kondo and K. Hozumi: KENS Report II (1981) 381

Table 1 Product Yields Due to the Radiation Decomposition of Solid CH_4 Moderator

	H_2 (%)	CH_4 (%)	C_2H_6 (%)	C_2H_4 (%)	Other (%)	H_2 Production Rate (%/10^{18} protons)
Sample A (Feb. '83)	0.81	98.8	0.15	0.2	0.1	0.30
Sample B (Mar. '83)	0.35	99.5	0.1	<0.1	<0.1	0.26
Sample C (Jul. '80)	0.15	∿100	0.03	0.06	0.03	0.11

Irradiation condition

	Proton Current (μA)	Irradiation Time (hours)	Total Protons (x 10^{18})
Sample A	1.40	87.0	2.74
Sample B	1.47	40.9	1.35
Sample C	1.2	52.7	1.42

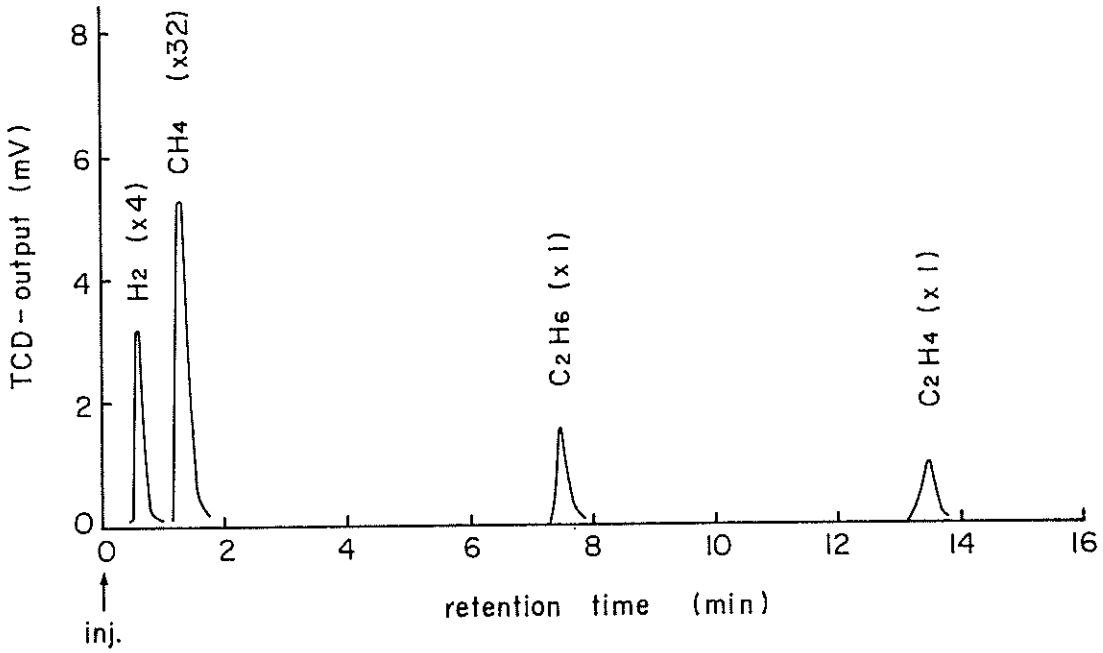

Fig.1 Gas-chromatogram of the irradiated methane moderator (sample A)

Structural Study of the Glass Transition of P_2Se_3 Glass

Masakatsu MISAWA and Noboru WATANABE*

The Research Institute for Iron, Steel and Other Metals, Tohoku University, Sendai 980, Japan

*National Laboratory for High Energy Physics, Oho-machi, Tsukuba-gun, Ibaraki 305, Japan

Numerous papers on the glass transition have been published. However almost all were concerned with the thermodynamical and kinematical properties. Recently Busse and Nagel[1] have measured the temperature dependence of X-ray structure factor of As_2Se_3 glass up to the glass transition temperature T_g. Even in the limited temperature range, they found an anomalous temperature dependence of a first peak in the S(Q). In order to understand the structural origin of the glass transition, structural study over a wide temperature range from glassy state to supercooled liquid state must be made.

The aim of this study is to examine the structural nature of the glass transition of P_2Se_3 glass by means of pulsed neutron total scattering using HIT spectrometer.

The P_2Se_3 glass was sealed in vacua in a silica tube. The measurements of the structure factor S(Q) were carried out at various temperatures; 25, 55, 90, 120, 170, 230 and 340°C. The glass transition temperature of P_2Se_3 glass determined by DTA and DSC measurements was around 100°C.[2,3] Although the liquidus temperature at the composition of P_2Se_3 in a phase diagram varies from 250 to 320°C depending on the investigators[4,5], the temperature range studied in this work covered glassy state, supercooled liquid state and equilibrium liquid state. It has been reported that the glass of P-Se system is quite stable even in a supercooled liquid state[2]. In fact, we did not find any indication of crystalization during S(Q) measurements, although the sample was kept at each temperature for about 4 hours.

The S(Q)'s measured at various temperatures were shown in Fig. 1. The S(Q)'s at temperature below 120°C were measured both on heating and on cooling in order to check whether the change in S(Q) is reversible or not. The S(Q)'s measured at both conditions agree with each other within an

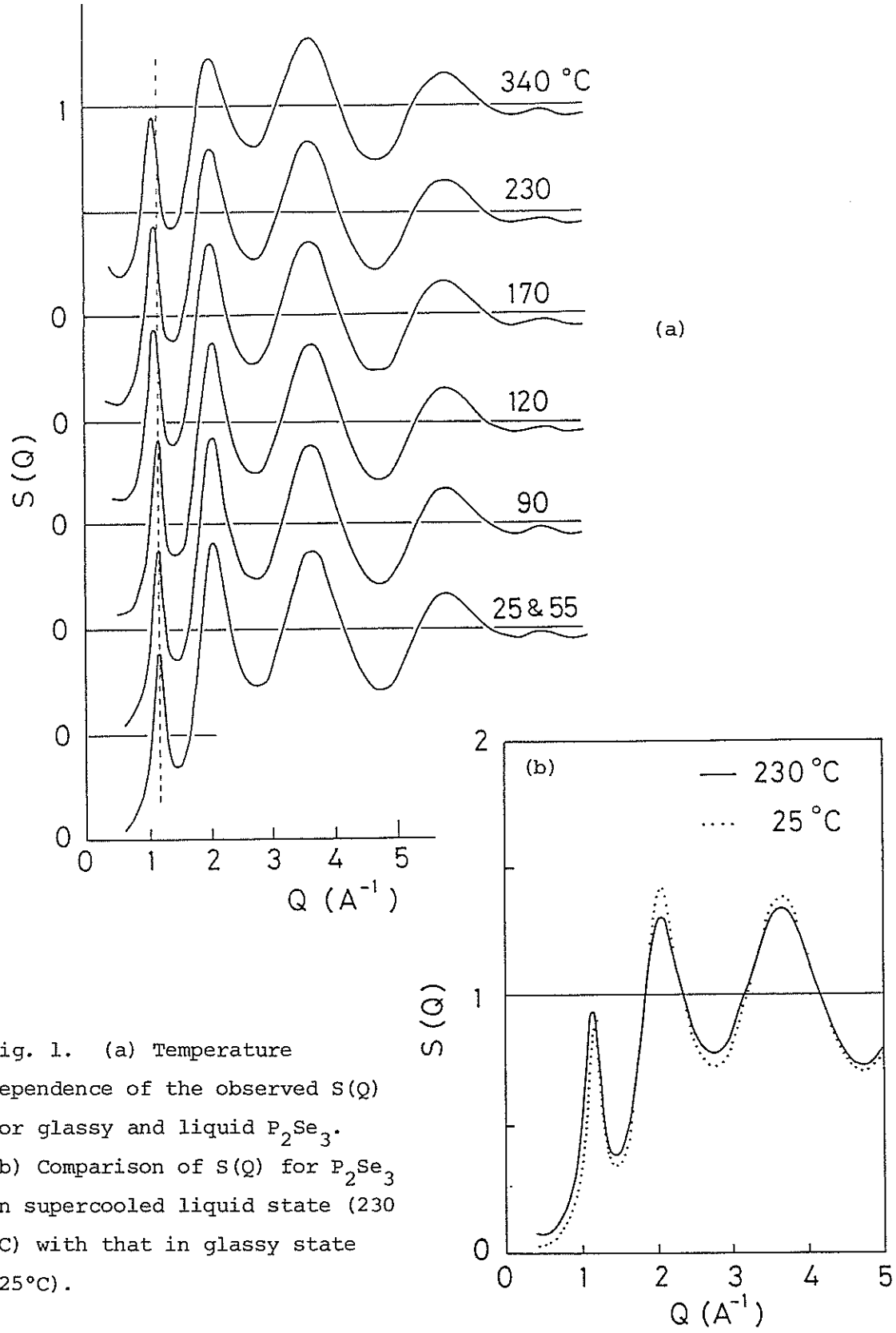

Fig. 1. (a) Temperature dependence of the observed S(Q) for glassy and liquid P_2Se_3. (b) Comparison of S(Q) for P_2Se_3 in supercooled liquid state (230 °C) with that in glassy state (25°C).

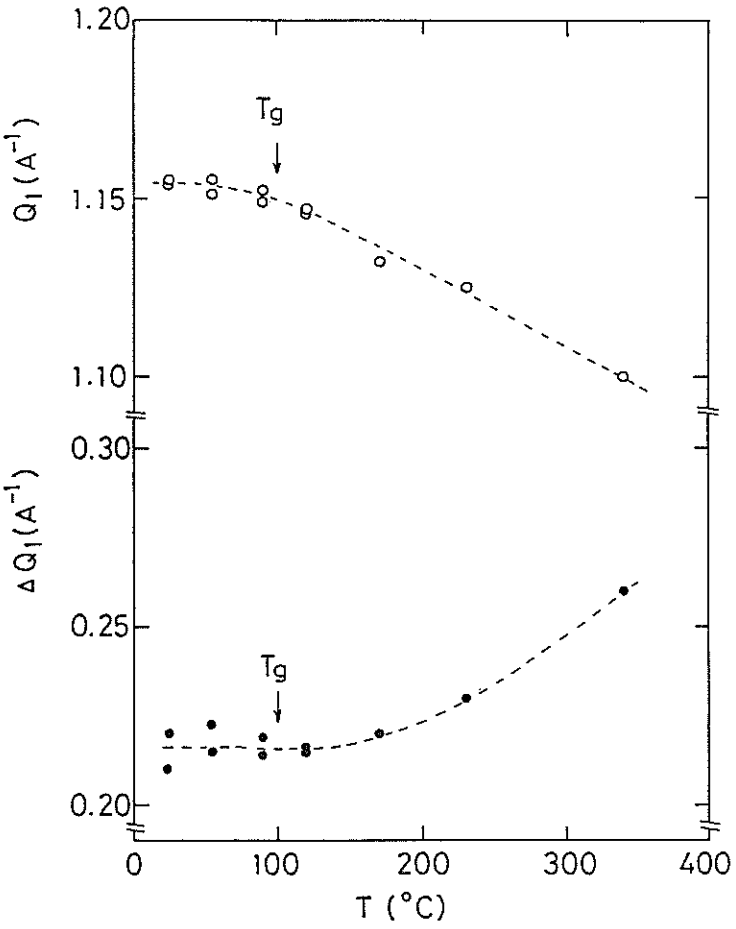

Fig. 2. Temperature dependences of the position Q_1 and the width ΔQ_1 of the first sharp peak in S(Q) for glassy and liquid P_2Se_3.

experimental error, indicating that the temperature dependence of the S(Q) shown in Fig. 1 is reversible. From Fig. 1, the two remarkable features on S(Q) were found: (1) The first sharp peak located around Q=1.1-1.2 A^{-1} shifts toward lower Q value with increasing temperature, while the others do not shift. This characteristic feature is clearly shown in Fig. 2 where the position of the first sharp peak Q_1 was plotted against temperature. (2) The height of the first sharp peak increases with increasing temperature, while the other peaks decrease with increasing temperature. This characteristic behavior is shown in Fig. 3 where the values of $S(Q_1)$ at first sharp peak and $S(Q_2)$ at second peak were plotted as a function of temperature. In Fig.2 are also shown the width of the first sharp peak ΔQ_1 (FWHM) as a function of temperature. The ΔQ_1's shown in Fig. 2 are approximate values, because subtraction of the overall background due to the tail of the second peak from the first sharp peak is ambiguous.

As shown in Fig. 2, drastic change in Q_1 and ΔQ_1 occurs at around 100°C where glass transition was observed. The temperature dependence of the first sharp peak $S(Q_1)$ shown in Fig. 3 is anormal because it increases with increasing temperature while the other peaks attenuate with increasing temperature as usually observed in many liquids. These experi-

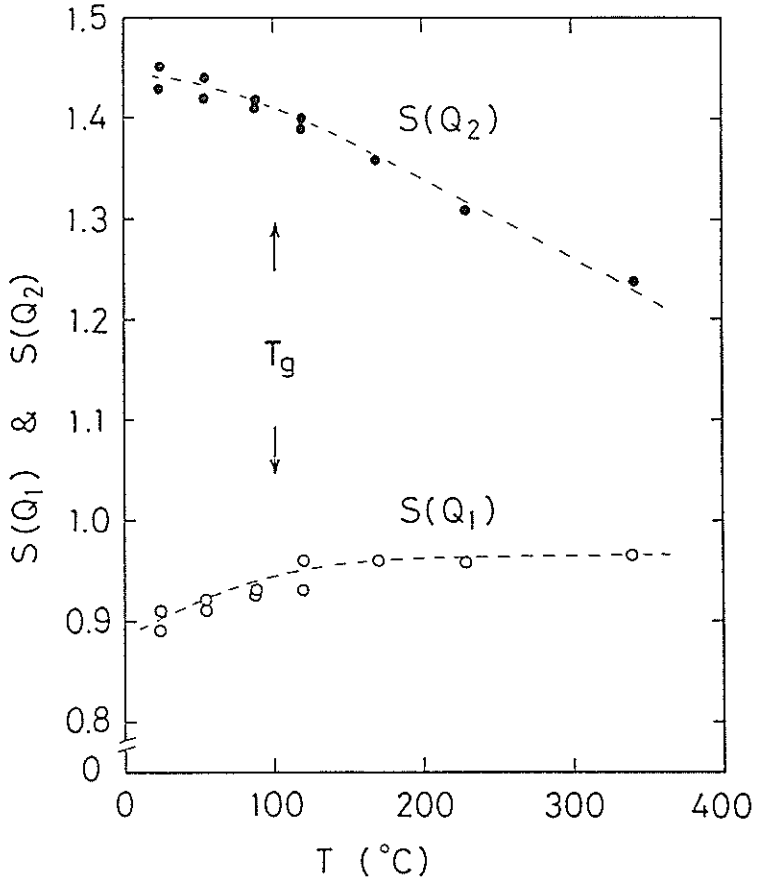

Fig. 3. Temperature dependences of the value of S(Q) for the first sharp peak at Q_1=1.1-1.2 A^{-1} and for the second peak at Q_2= 2.04 A^{-1} for glassy and liquid P_2Se_3.

mental findings suggest that the origin of the first sharp peak is different from the other peaks. If one adopts the layered structure model for the appearance of the first sharp peak, the value of $2\pi/Q_1$ gives the mean separation of the layers which was estimated to decrease from 5.7 A in liquid state at 340°C to 5.4 A in glassy state below 90°C. The correlation length of these layers estimated by $2\pi/\Delta Q_1$ increases from 24 A(∿4 layer spacing) to 29 A(∿5 layer spacing) in the same temperature change.

These experimental results suggest the following : As the P_2Se_3 is cooled from the liquid state, the spacing between the two adjacent layers possibly existing in the liquid decreases with decreasing temperature but at a patricular temperature it reaches a minimum value below which further decrease is impossible, then the glass transition occurs.

References

1) L. E. Busse and S. R. Nagel, Phys. Rev. Lett. 47, 1848(1981).
2) Y. Monteil and H. Vincent, Z. anorg. allg. Chem. 428, 259(1977).
3) R. Blachnik and A. Hoppe, J. Non-cryst. Solids 34, 191(1979).
4) E. I. Kim, A. P. Chernov, S. A. Dembovskii and Z. U. Borisova, Russ. Inorg. Mat'ls 12, 856(1976).
5) Y. Monteil and H. Vincent, J. Inorg. nucl. Chem. 37, 2053(1975).

Structure of Sputter-deposited SiO_2 Amorphous Film

Yoshifumi KOBAYASHI, Toshiharu FUKUNAGA, Masakatsu MISAWA, Noboru WATANABE* and Kenji SUZUKI

The Research Institute for Iron, Steel and Other Metals, Tohoku University, Sendai 980, Japan

* National Laboratory for High Energy Physics, Oho-machi, Tsukuba-gun, Ibaraki 305, Japan

Silicon dioxide is one of the materials most extensively used in various engineering applications. In electronic and optical devices, much attentions have been paid to characterize and control the structure defects included inherently in SiO_2 films prepared by deposition from gaseous phases.[1)]

The aim of this study is to examine what difference exists in the structure between sputter-deposited SiO_2 amorphous films and ordinary melt quenched SiO_2 glass by means of pulsed neutron total scattering.

SiO_2 amorphous film was prepared in argon gas atmosphere using RF sputter-deposition technique. The chemical analysis of the resulting SiO_2 amorphous film(hereafter referred to as a-SiO_2 film) indicated a small oxygen deficiency with a composition of $SiO_{1.97}$. The density of the a-SiO_2 film was 2.16 ± 0.09 g/cm^3, while the density of the ordinary melt quenched SiO_2 glass (hereafter referred to as SiO_2glass) used in this study as a standard was 2.20 ± 0.09 g/cm^3. The sputter-deposited SiO_2 film is colorless and transparent, but hygroscopic.

Pulsed neutron total scattering experiments on the a-SiO_2 film and the SiO_2 glass were carried out using the high intensity total scattering spectromrter(HIT). The observed structure factor S(Q) of a-SiO_2 film is compared with that of SiO_2 glass in Fig. 1. There are two remarkable differences in S(Q) between a-SiO_2 film and SiO_2 glass: (1) The intense small angle scattering is observed in S(Q) of a-SiO_2 film, indicating the existence of inhomogeneity in this film. (2) The first peak in S(Q) of a-SiO_2 film is drastically attenuated in comparison with that of SiO_2 glass.

The analysis of the small angle scattering intensity suggests the existence of voids of the order of about 10 A in effective diameter with a volume fraction of about 4%.

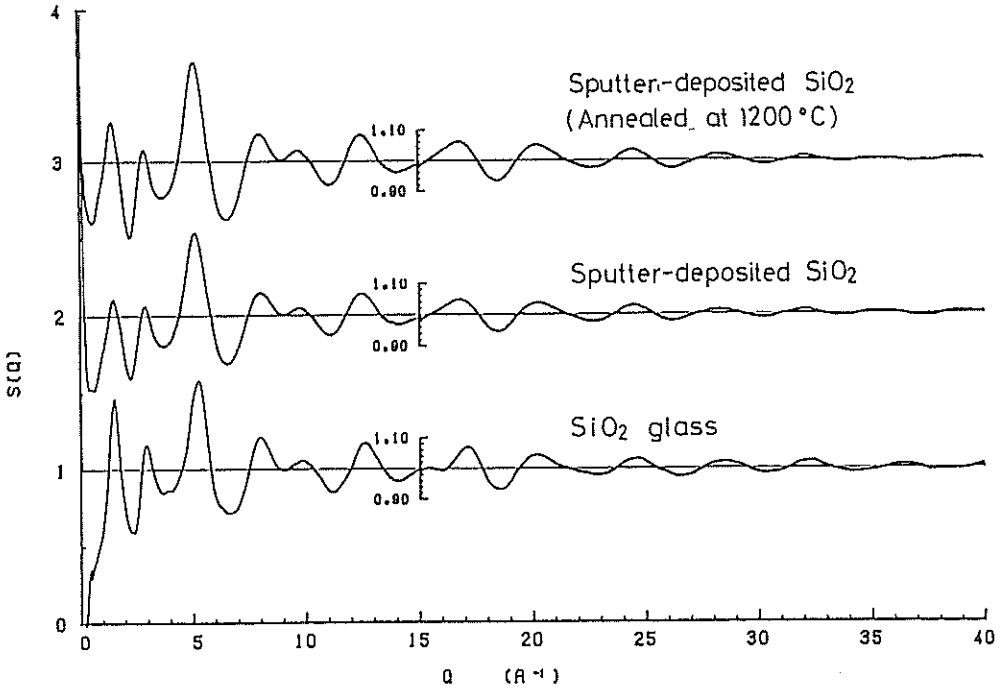

Fig. 1. Structure factors S(Q) of sputter-deposited a-SiO_2 film before and after annealing, and SiO_2 glass.

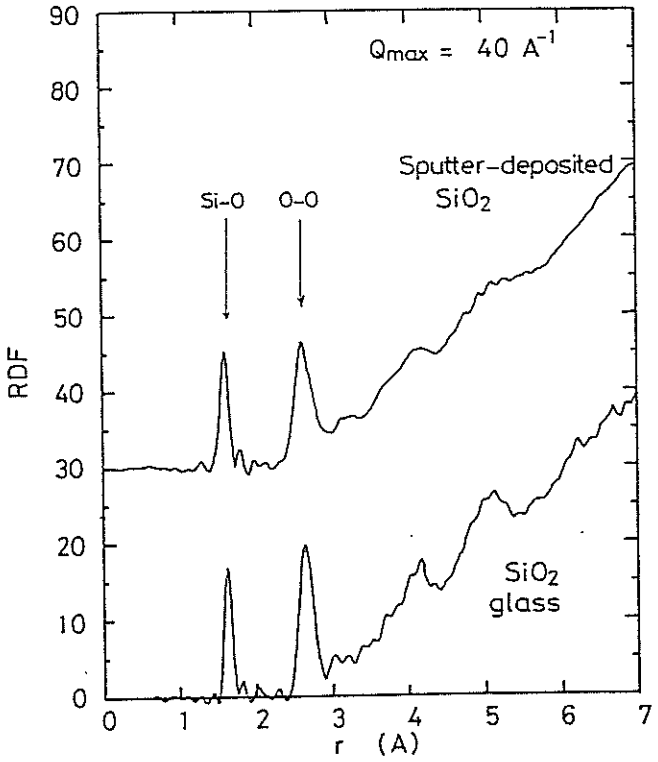

Fig. 2. Radial distribution functions (RDF) of sputter-deposited a-SiO_2 film and SiO_2 glass.

Table 1. Experimental values for atomic distance(l), its fluctuation(Δl) and coordination number(n_{A-B}) for A-B pairs in a-SiO_2 film and SiO_2 glass. ∠A-B-A is the bond angle of A-B-A bond.

	Si-O			O-O				Si-Si	
	l(A)	Δl(A)	n_{Si-O}	l(A)	Δl(A)	n_{O-O}	∠O-Si-O	l(A)	∠Si-O-Si
a-SiO_2 film	1.62	0.05	4.0	2.64	0.11	5.6	109.9	3.12	146.3
SiO_2 glass	1.60	0.04	4.0	2.62	0.09	5.5	109.1	3.14	151.5

Fig. 2 shows the radial distribution functions (RDF) of a-SiO_2 film and SiO_2 glass obtained as Fourier transforms of the S(Q) shown in Fig. 1. The analysis of the RDF shown in Fig. 2 in combination with the RDF obtained by X-ray diffraction experiment gives the following structural data listed in Table 1. From the results listed in table 1 and RDF shown in Fig. 2, the following conclusions can be made: (1) The silicon-oxygen average distance is slightly longer in a-SiO_2 film than in SiO_2 glass. (2) The structure unit in a-SiO_2 film is a [SiO_4] tetrahedron as well as in SiO_2 glass. However the fluctuations of Si-O bond length and O-O atomic distance are larger in a-SiO_2 film than in SiO_2 glass. (3) The angle of Si-O-Si bond is slightly smaller in a-SiO_2 film than in SiO_2 glass. (4) The atomic distribution of a-SiO_2 film is smeared out rapidly beyound 4 A.

The strong attenuation of the first peak in S(Q) for a-SiO_2 film shown in Fig. 1 and the broadening of the atomic distribution at large r in a-SiO_2 film shown in Fig. 2 imply that the atomic arrangement is more disordered in a-SiO_2 film than in SiO_2 glass. The similar attenuation of the first peak of S(Q) has been observed in neutron irradiated vitreous SiO_2[2,3,4].

In order to evaluate the degree of disorder in a-SiO_2 film, one may introduce a broadening function α(r) with which the pair distribution function g(r) of a-SiO_2 film is given by the next equation

$$g(r) - 1 = \alpha(r)[g_0(r) - 1], \qquad (1)$$

where $g_0(r)$ is the pair distribution function of SiO_2 glass. One of the simplest forms of the α(r) is approximated as follows

$$\alpha(r) = 1 - \frac{3}{2}\left(\frac{r}{2R_s}\right) + \frac{1}{2}\left(\frac{r}{2R_s}\right)^3, \qquad (2)$$

where $2R_s$ denotes the characteristic length beyond which atomic correlation disappears. Inverse Fourier transformation of (g(r)-1) gives the S(Q). The calculated S(Q)'s are shown in Fig. 3. The S(Q) with the value of R_s around

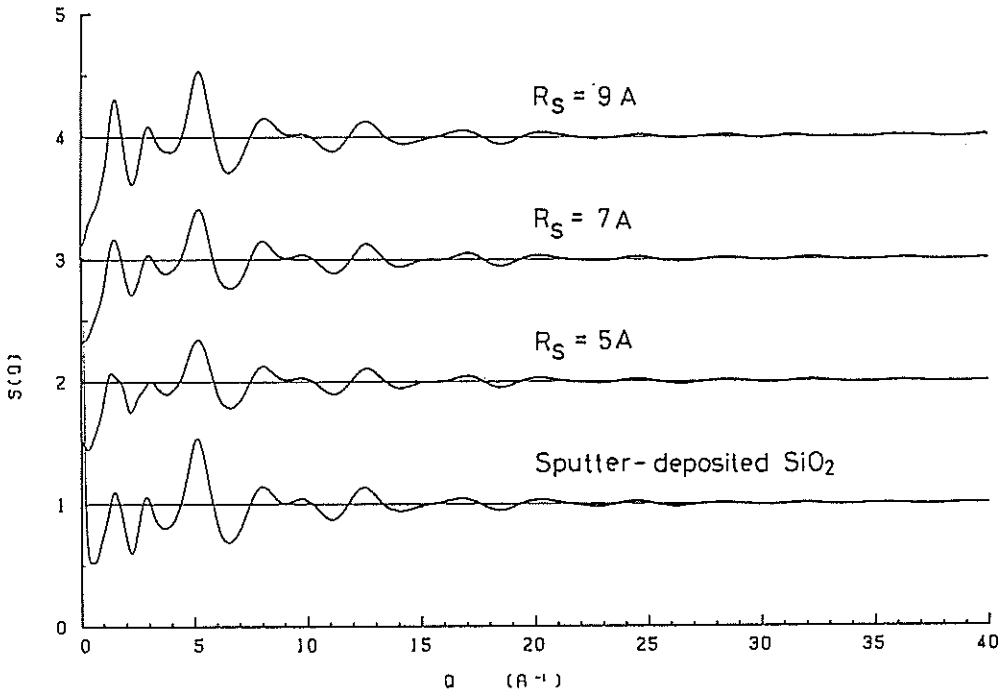

Fig. 3. Comparison of the S(Q)'s calculated with R_s=5, 7 and 9 A in eq. (2) with the observed S(Q) of a-SiO_2 film.

7 A can reproduce the experimental S(Q) quite well. Therefore, it is concluded that the atomic correlation in a-SiO_2 film disappears beyond 14 A, while the atomic correlation in SiO_2 glass persists up to 30 A or more.

The geometrical distortion and connection of SiO_4-tetrahedra in RF sputter-deposited SiO_2 film approaches the state found in ordinary melt quenched SiO_2 glass by annealing at 1200°C, but the void still remains as shown in Fig. 1.

References

1) J. J. Hauser, G. A. Pasteur, A. Staudinger and R. S. Hutton, J. Non-cryst. Solids 46, 59(1981).
2) J. S. Lukesh, Phys. Rev. 97, 345(1955).
3) I. Simon, J. Amer. Ceram. Soc. 40, 150(1957).
4) K. Doi, J. Non-cryst. Solids 51, 367(1982).

Structure Factors of Ge-Se and Te-Se Chalcogenide Glasses determined by a Pulse Neutron Scattering

Shinichiro HATTA, Shigeru YODA, Tadashi MIZOGUCHI and Noboru WATANABE*

Faculty of Science, Gakushuin University, Mejiro, Tokyo 171, JAPAN
* National Laboratory for High Energy Physics, Oho-machi, Tsukuba-gun, Ibaraki 305, JAPAN

This paper reports results of neutron diffractions for Ge_xSe_{1-x} (x=0.150, 0.250,0.333) and Te_ySe_{1-y} (y=0.150,0.200) chalcogenide glasses, which were measured by a high intensity total scattering spectrometer (HIT) at KENS. The chalcogenide glasses were made from mixtures of fine powder with purity of 99.99%. The mixture was heated in a sealed quartz tube, with keeping molten state for 5h. After the treatment, the molten glass was quenched into water to prepare the specimen. In order to check whether any crystallization takes place or not, X ray diffraction patterns were observed for every specimen before the neutron diffraction experiments. A total correlation function

$$G(r)=4\pi r(\rho(r)-\rho_o)$$

was calculated by using S(Q) up to 36Å^{-1}.

At a stoichiometric composition of $GeSe_2$, we have a crystal including a tetrahedral arrangement, whose bond length between Ge and Se was measured to be 2.36Å. The second nearest Ge-Ge and Se-Se distances were also measured to be 3.48Å and 3.83Å, respectively.[1] For the crystalline $GeSe_2$, there is a layer structure constructed with the Ge-Se tetrahedral units. As shown in Fig.1, the pre-peaks can be seen at about $Q=1\text{Å}^{-1}$ in glassy state. These pre-peaks are thought to be produced by a layer-layer correlation, which is still left even in a glassy state. However, in G(r), we can not find any clear peak due to the layer- layer correlation. In the $GeSe_2$ glass , the bonds in a random network are almost Ge-Se, while the number of Ge-Ge or Se-Se bonds is very small. Therefore a first peak of G(r) shows

the Ge-Se correlation with the bond length of 2.37 Å , as shown in Fig.2. The second peak is divided to two peaks. One of the peaks at 4.03Å becomes high with increasing Ge content. In Fig.2, the values of distances for Ge-Se, Se-Se and Ge-Ge for the crystalline $GeSe_2$ are also shown as arrow marks. This indicates that the bond length of Ge-Se in the glassy state is very equal to the value for the corresponding crystal. However, correlations of second nearest neighbors (Ge-Ge and Se-Se) in the glasses are quite different from those of the crystal,as shown in Fig.2. For the crystalline $GeSe_2$, the bond angles of Ge-Se-Ge and Se-Ge-Se are definite as 93.6° and 109.3°, respectively.[1] Therefore it is found that the chalcogenide glasses indicate the characteristics of the covalent random network, which has the rigid bond length and the random bond angles.

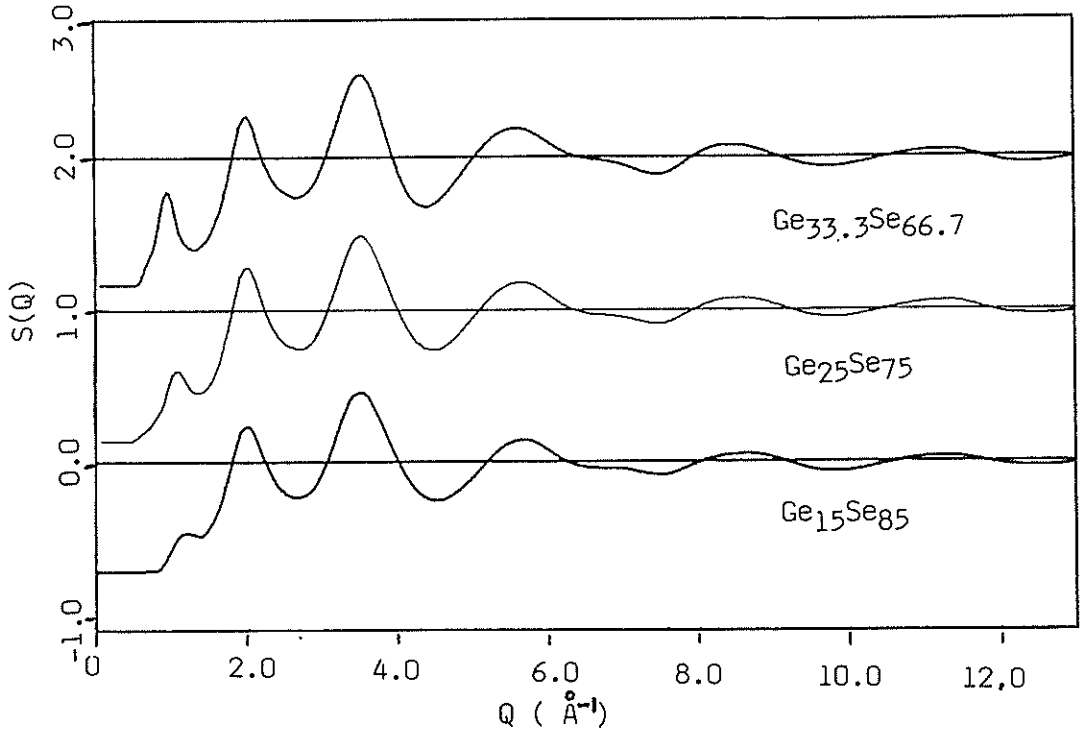

Fig.1 S(Q) for Ge_xSe_{1-x} glasses

In S(Q) for Te_ySe_{1-y} glasses, there is not any clear pre-peak due to the layer-layer correlation in Ge-Se glasses as seen in Fig.1. As shown in Fig.3, G(r) for Te_ySe_{1-y} are very similar to those for Ge_xSe_{1-x}. If G(r) for $Te_{15}Se_{85}$ is carefully compared with that for $Ge_{15}Se_{85}$, we can see that the peak positions coincide with each other not only at the first peak but also at a few following peaks. The result suggests that the short range structure does not suffer a significant change , even if Ge is replaced by Te in the chalcogenide glasses.

reference

1) V.G.Dittmar and H.Schaefer, Acta Cryst. B32 (1976) 2726

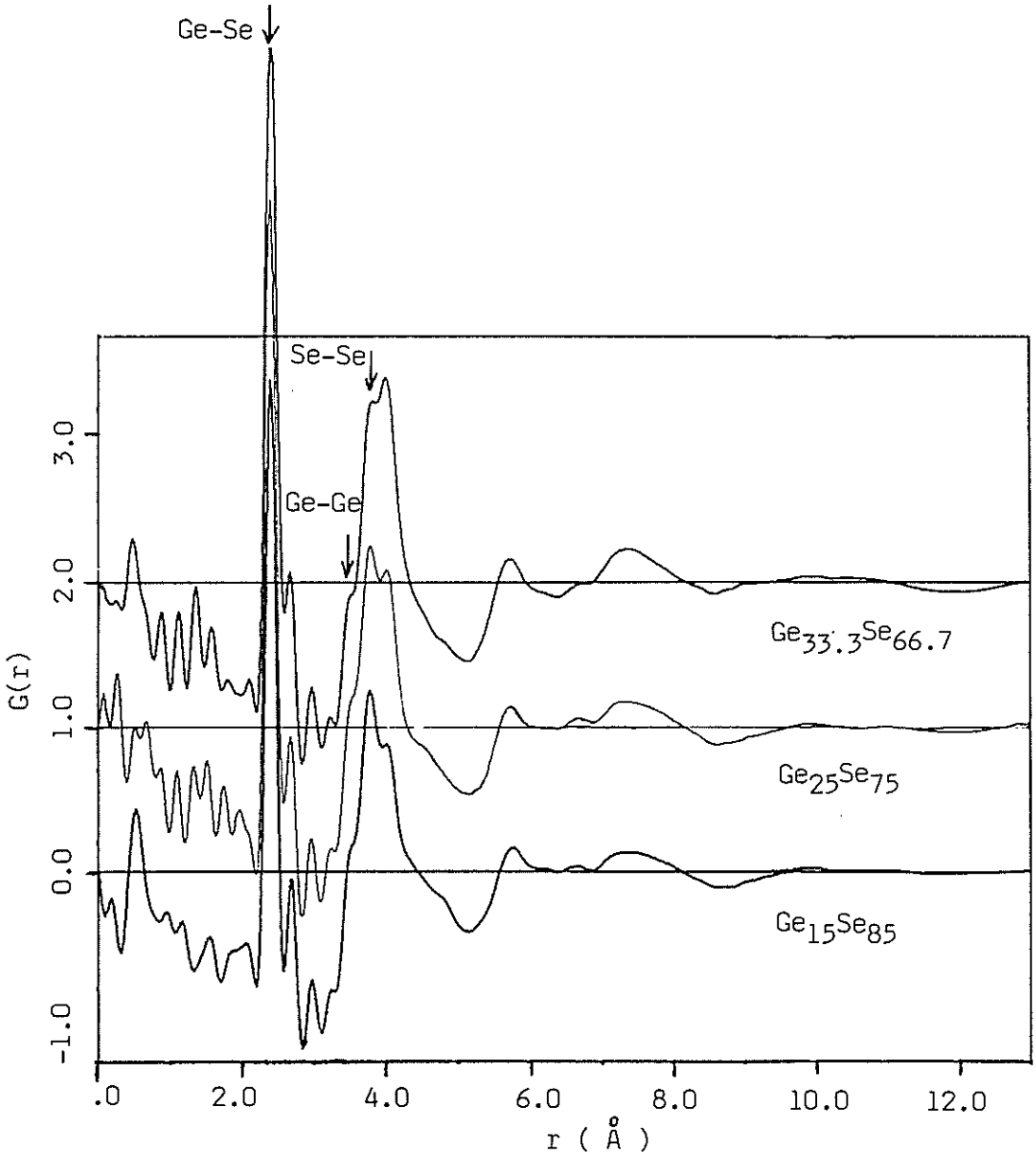

Fig.2 G(r) for Ge_xSe_{1-x} glasses. Arrow marks show bond length for $GeSe_2$ crystal.

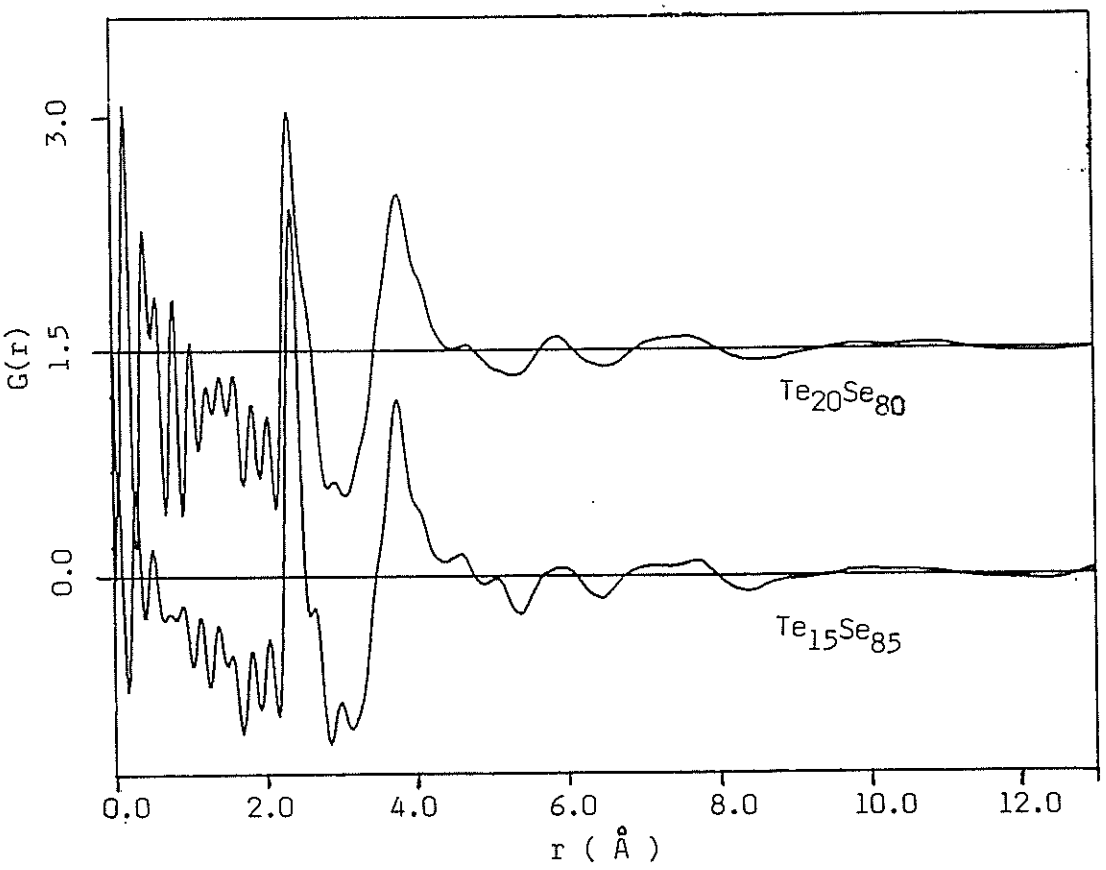

Fig.3 G(r) for Te_ySe_{1-y} glasses

Layer Correlation in a-$As_2(Se_xS_{1-x})_3$ Systems

Tatsuo MORI, Hiroshi YASUOKA, Hiroaki SAEGUSA, Katsumi OKAWA,
Michio KATO, Toshihiro ARAI, Toshiharu FUKUNAGA†
and Noboru WATANABE†

Institute of Applied Physics, University of Tsukuba
Sakura, Ibaraki 305, Japan

†National Laboratory for High Energy Physics
Oho-machi, Ibaraki 305, Japan

It is well known that amorphous As_2S_3 and As_2Se_3 have layer-like structure from X-ray and neutron diffraction[1)-3)]. The vibrational and electronic properties of these glasses are affected by the interlayer correlation[4)]. In this paper we report the neutron diffraction measurements for the $As_2(Se_xS_{1-x})_3$ glasses, the change in the structure factor S(Q) with the composition x and the analysis of the interlayer correlation in these systems.

The samples of $As_2(Se_xS_{1-x})_3$, (x = 0.0, 0.1, 0.2, 0.35, 0.5, 0.65, 0.9, 1.0) were prepared by direct systhesis from properly weighted high purity As, Se and S. The raw materials sealed in evacuated quartz ampoules ($1x10^{-5}$ Torr, 8 mm in diameter) were rocked at 600°C for 24 hours. They were then quenched in the air at room temperature and annealed for 24 hours at 120°C. Since each sample shows only one glass transition temperature in the thermal analysis, the phase separation has not occurred in these samples. The neutron diffraction measurements using the time-of-flight method were carried out using High Intensity Total Scattering Spectrometer (HIT) at the pulsed spallation neutron source KENS.

The structure factors of each sample which are related to the layer correlation are shown in Fig. 1. In order to investigate the change of the pre-peak at $Q \sim 1.2$ A^{-1} with composition x, the peaks were fitted by Gaussian functions. In table I, the parameters obtained by fitting are listed. Q_0 is a peak position, ΔQ_0 is a full width at half maximum (FWHM), and S is a peak height. From these results, the peak position hardly

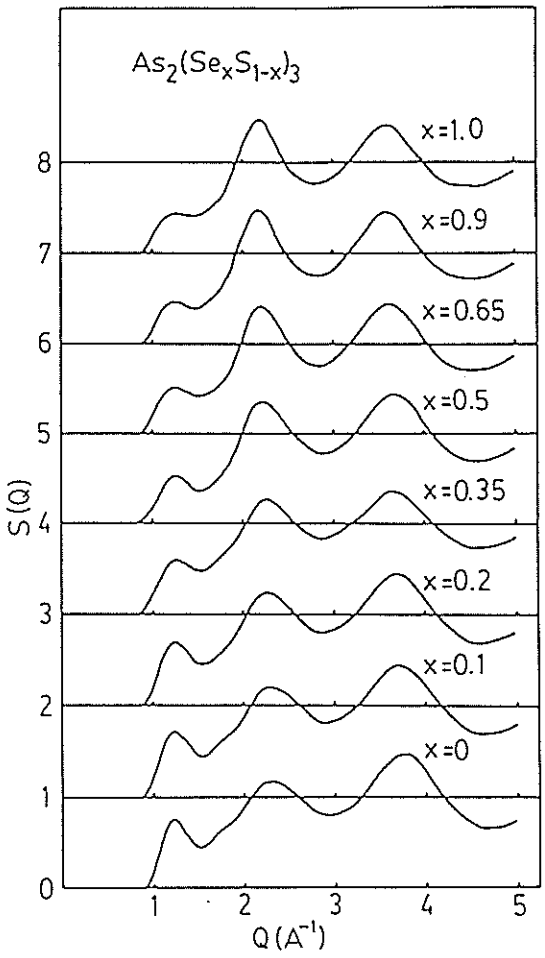

Fig. 1 Structure factors of $As_2(Se_xS_{1-x})_3$ glasses.

shifts. These systems, therefore, have same interlayer distance $r_0=2\pi/Q_0$, about 5A. This value is reasonable because the crystalline As_2S_3 and As_2Se_3 are the same crystal structure and the mean interlayer distances are about 4.8 and 4.9 A, respectively. From FWHM, the interlayer correlation length R can be estimated[1] as

$$R = r_0Q_0/\Delta Q_0 \qquad (1)$$

The values calculated by eq.(1) are also shown in table I. These results indicate that the interlayer correlation ranges extend to three layers in a-As_2Se_3 and to four layers in a-As_2S_3, as the mean interlayer distance is about 5 A, and that there are three- or four-layer correlations in the medium composition. The origin of the change in the correlation lengths in these systems may be due to the difference in the strength of the interlayer interaction,

Table I. Positions Q_0, FWHM's ΔQ_0 and heights S of the pre-peaks and interlayer correlation lengths R in $As_2(Se_xS_{1-x})_3$ glasses.

x	$Q_0(A^{-1})$	$\Delta Q_0(A^{-1})$	S	R(A)
0.0	1.22	0.31	0.76	20
0.1	1.24	0.36	0.72	17
0.2	1.24	0.36	0.69	17
0.35	1.25	0.40	0.60	16
0.5	1.24	0.38	0.53	17
0.65	1.23	0.38	0.51	17
0.9	1.25	0.45	0.48	14
1.0	1.24	0.43	0.45	15

which is van der Waals force. The heights of the pre-peak decrease remarkably with increasing Se concentration. Since the peak height depends strongly on the neutron scattering amplitude of each atom, it is difficult to relate the decrease of the height of the pre-peak to the change in the correlation length. From the comparison between the structure factors obtained from RDF's, which were broadened by Gaussian functions, of the crystalline As_2Se_3 and As_2S_3, it becomes clear that the peak height at about 1.25 A^{-1} for As_2Se_3 is lower than that for As_2S_3 and the peaks at about 2.2 A^{-1} in two systems behave conversely. The decrease of the pre-peak height, therefore, does not always correspond to the decrease of the interlayer correlation length. From these results, it may be concluded that all these systems have the similar layer structure.

In summary, all the $As_2(Se_xS_{1-x})_3$ glassy systems have the layer structure and the nearly constant interlayer distances of about 5 A. The interlayer correlation length of a-As_2S_3 is slightly longer than that for a-As_2Se_3 and the interlayer correlation ranges in these systems extend to three or four layers.

References

1) A. J. Readbetter and A. J. Apling : J. Non-Cryst. Solids 15 (1974) 250
2) O. Uemura, Y. Sagara, D. Muno and T. Satow : J. Non-cryst. Solids 30 (1978) 155
3) L. E. Busse and S. R. Nagel : Phys. Rev. Lett. 47 (1981) 1848
4) J. C. Phillips : J. Non-cryst. Solids 43 (1981) 37

Neutron Diffraction Study of Li_2O-B_2O_3 Glasses

Toshiharu FUKUNAGA, Noriyuki HAYASHI, Masakatsu MISAWA,
Noboru WATANABE*and Kenji SUZUKI

The Research Institute for Iron, Steel and Other Metals, Tohoku University, Sendai 980, Japan.

*National Laboratory for High Energy Physics, Oho-machi, Tsukuba-gun, Ibaraki 305, Japan.

Borate glasses including alkali oxides exhibit often anomalous Physical properties which are well known as "boron oxide anomaly". For example, the thermal expansion coefficient of an alkali borate glass shows the minimum at about 16 mol% alkali oxide and increases abruptly above about 30 mol% alkali oxide. This anomaly has been reported to be due to the change of oxygen atom configurations around a boron atom from BO_3-triangle to BO_4-tetrahedron with increasing alkali oxide content up to about 30 mol%, beyond which non-bridging oxygen atoms appear and BO_4-tetrahedra are again transformed to BO_3-triangle.

In this work, the high resolution observation of the short-range structure was carried out to find the atomic scale mechanism of $BO_3 \leftrightarrow BO_4$ transition in Li_2O-B_2O_3 glasses.

Six $(Li_2O)_X(B_2O_3)_{1-X}$ glasses(X=0.1, 0.2, 0.3, 0.4, 0.5 and 0.6) were prepared by mixing reagent grade lithium carbonate(Li_2CO_3) and orthoboric acid(H_3BO_3) enriched to contain 95.14at% ^{11}B-isotope. The measurments of the coherent neutron scattering intensity from the oxide glasses were carried out at room temperature in vacua by using the High Intensity Total scattering spectrometer(HIT). The advantage of the pulsed neutron scattering experiment for Li_2O-B_2O_3 glasses is not only the high Q observation but also the fact in that the neutron scattering length for ^{11}B-isotope is slightly greater than that for oxygen and Li atom has a negative neutron scattering length in contrast to X-ray diffraction where oxygen atom is a predominant scatterer. This means that the B-B and O-B correlations in the glass predominantly to the experimental total correlation function and the Li-O and Li-B correlations are characterized as negative contributions to total correlation function.

Figure 1 shows the neutron total structure factors S(Q) of Li_2O-B_2O_3 glasses. The oscillation in the S(Q) can be definitely observed to persist up to Q~60 A^{-1}, which allows us to obtain the high resolution short-range structure. The position of the small peak located between the first and second large peaks moves drastically to the high Q side around 30mol% Li_2O content.

Further careful data analysis is in progress to elucidate the local atomic arrangement which controls the $BO_3 \leftrightarrow BO_4$ transition in Li_2O-B_2O_3 glasses.

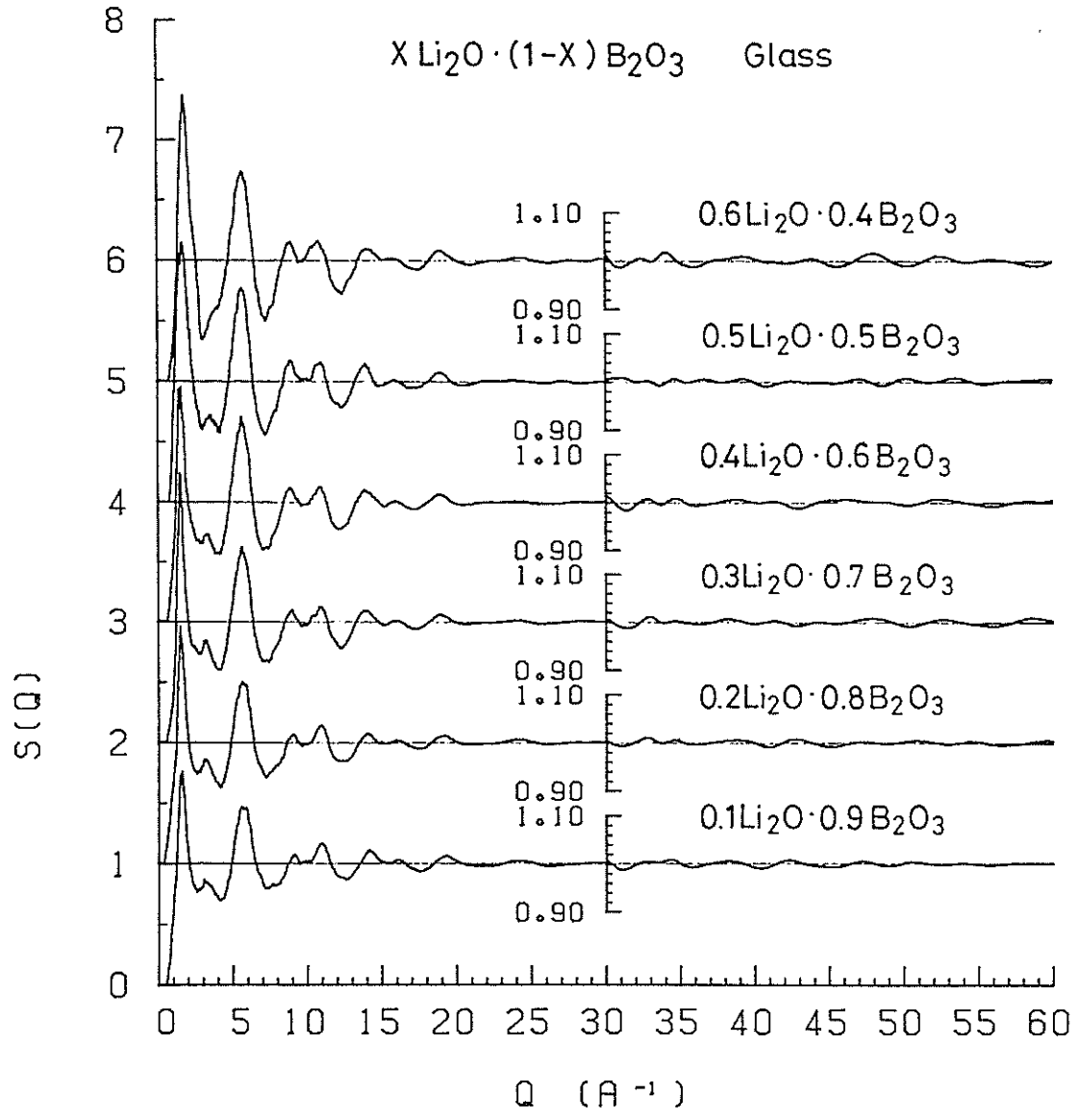

Fig. 1. Total structure factors of $(Li_2O)_X$-$(B_2O_3)_{1-X}$ glasses (X=0.1, 0.2, 0.3, 0.4, 0.5 and 0.6).

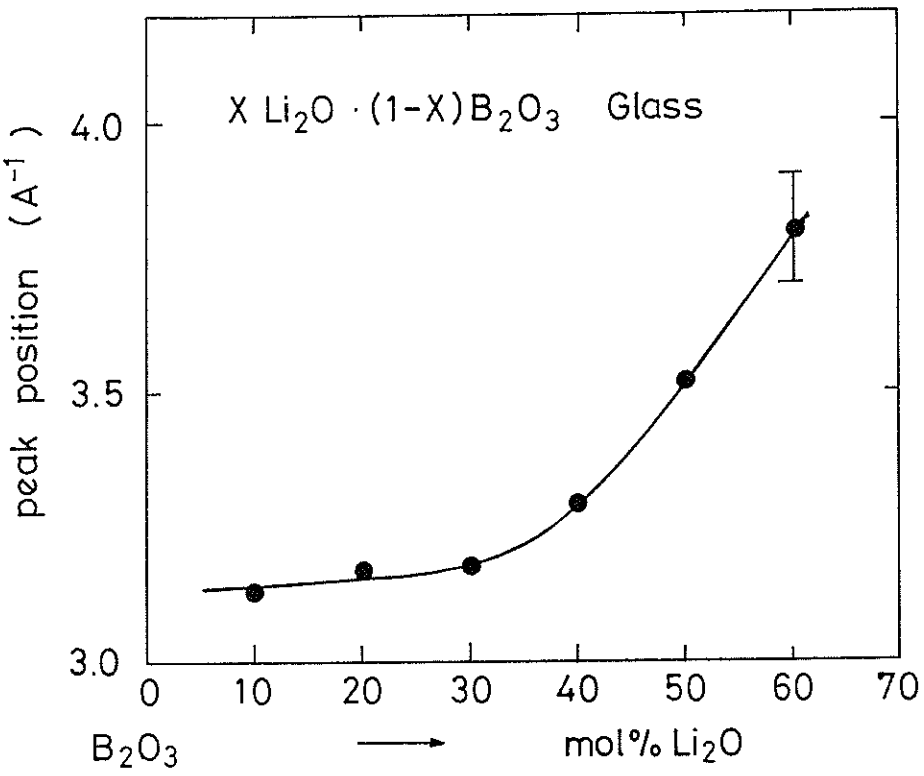

Fig. 2. Variation of the position of the small peak located between the first and second peaks in S(Q).

References

1) L. Shatsis, W. Capps and S. Spinner, J. Am. Cer. Soc., 36 (1953) 35.

2) J. Krogh-Moe, Phys. Chem. Glasses, 3 (1962) 1.

Neutron Diffraction of Ni-Ti Neutron Zero-Scattering Alloy Glasses

Toshiharu FUKUNAGA, Noriyuki HAYASHI, Kenzo KAI, Noboru WATANABE* and Kenji SUZUKI

The Research Institute for Iron, Steel and Other Metals, Tohoku University, Sendai 980, Japan

*National Laboratory for High Energy Physics Oho-machi, Tsukuba-gun, Ibaraki 305, Japan

High resolution observation of the short-range structure is crucially needed to characterize the stability and various properties of metallic glasses. The authers have reported that the chemical short-range structure of metal-metal alloy glasses is quite close to that of the corresponding crystal structure as well as metal-metalloid alloy glasses in previous papers[1),2)]. However, nobody has studied yet the effect of alloy composition on the chemical short-range order of metal-metal alloy glasses.

The aim of this study is to find how the chemical short-range order does depend on the change in alloy composition in metal-metal alloy glasses through the high resolution observation of the radial concentration correlation function using the pulsed neutron total scattering technique. The Ni-Ti alloy glasses containing 74, 67 and 60 at%Ti were prepared by rapid quenching from the molten state and the average coherent scattering length of these alloy glasses were artificially adjusted to zero by ^{60}Ni-isotope substitution. Therefore, experimental Bhatia-Thornton neutron total structure factors S(Q)[3)] of the alloy glasses provide exclusively the concentration-concentration structure factor $S_{CC}(Q)$.

The experimental S(Q)'s of Ni-Ti neutron zero-scattering alloy glasses with three different alloy compositions are shown in Fig. 1 together with that of Ni-67at%Ti neutron off-zero scattering alloy glass. Figure 2 shows the $G_{CC}(r)$'s for the Ni-Ti neutron zero-scattering alloy glasses and G(r) for Ni-67at%Ti neutron off-zero scattering alloy glass obtained as the Fourier transform of S(Q)'s shown in Fig. 1. The $G_{CC}(r)$'s of Ni-Ti neutron zero-scattering alloy glasses exhibit a negative peak located at $r \sim 2.54$ A, of which position shifts quite slightly to large distance with increasing Ti

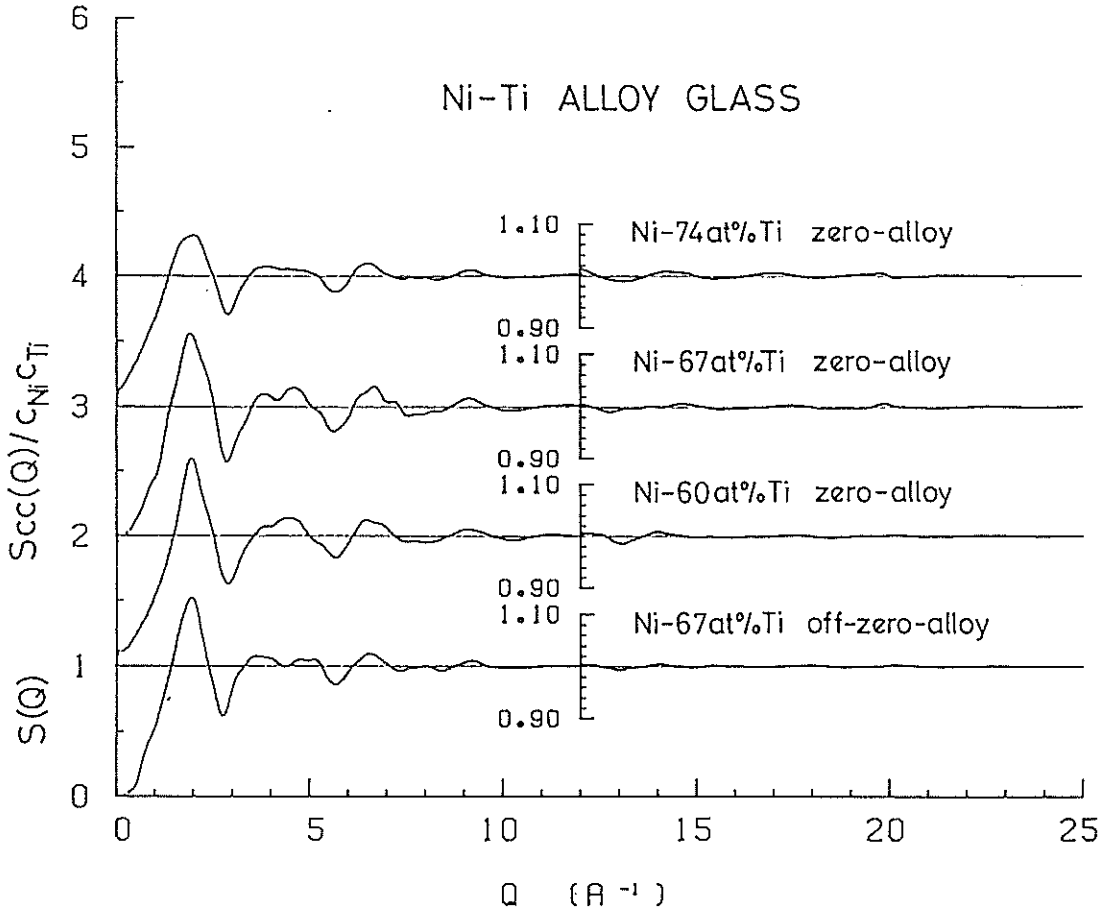

Fig. 1. Concentration-concentration structure factors $S_{CC}(Q)/C_{Ni}C_{Ti}$ of Ni-74at%Ti, Ni-67at%Ti and Ni-60at%Ti neutron zero-scattering alloy glasses, and Bhatia-Thornton total structure factor S(Q) of Ni-67at%Ti neutron off-zero scattering alloy glass.

content. These negative peaks indicate the preference for Ni-Ti unlike atom pairs in Ni-Ti alloy glasses. By comparison between the crystal structure of $NiTi_2$ compound(Fe_3W_3C-type)[4] and the $G_{CC}(r)$ of Ni-Ti neutron zero-scattering alloy glasses the negative peak at r=2.54 A in $G_{CC}(r)$ is found to correspond to the Ni-Ti unlike atom pairs in $NiTi_2$ crystalline compound.

To examine further this point, we evaluated the Warren chemical short-range order parameter[5] (α) of Ni-Ti neutron zero-scattering alloy glasses as a function of alloy composition by the following equation

$$\alpha = \frac{1}{Z}\int_{\Delta r} rG_{CC}(r)\,dr = 1 - \frac{Z_{AB}}{C_B Z} \quad , \qquad (1)$$

where Z is the coordination number of the first neighbor obtained from the X-ray radial distribution function, Z_{AB} is the coordination number of B atoms surrounding an A atom and C_B is the concentration of B atom. The calculated values of α are negative, i.e. α=-0.102, -0.141 and -0.116 for

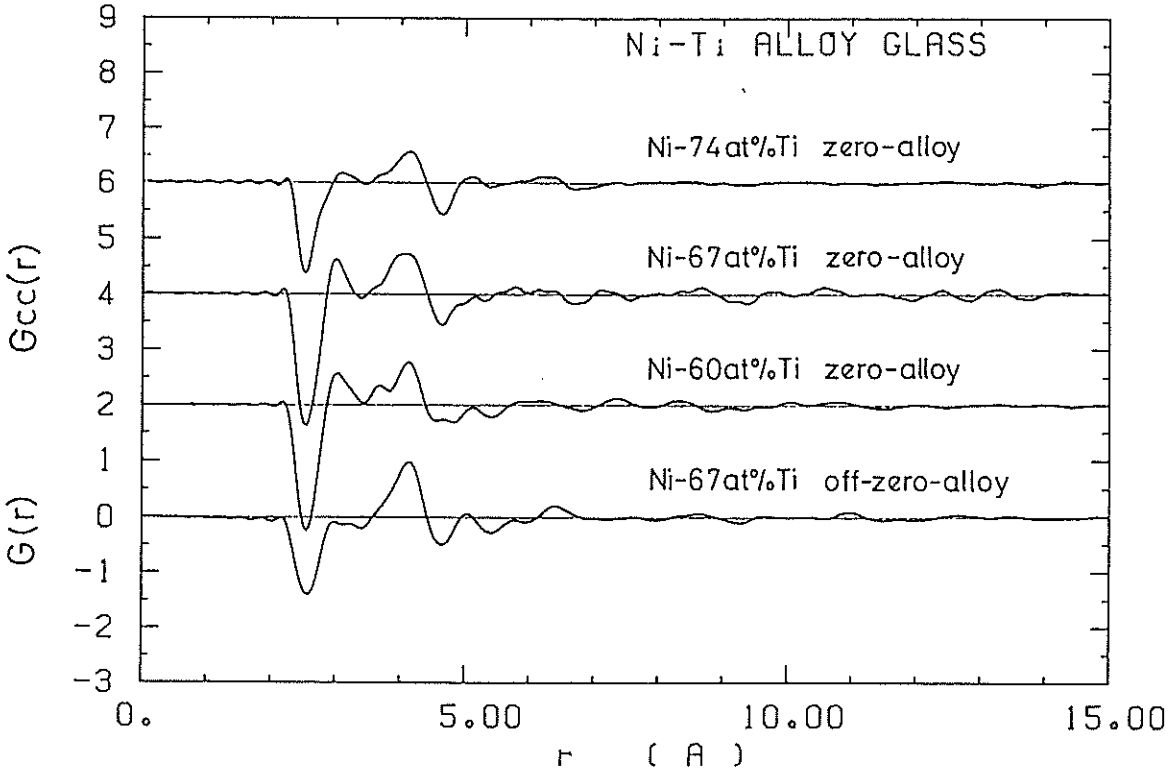

Fig. 2. Reduced concentration correlation functions $G_{CC}(r)$ of Ni-74at%Ti, Ni-67at%Ti and Ni-60at%Ti neutron zero-scattering alloy glasses, and Bhatia-Thornton total reduced atomic distribution function G(r) of Ni-67at%Ti neutron off-zero scattering alloy glass.

Ni-74at%Ti, Ni-67at%Ti and Ni-60at%Ti neutron zero-scattering alloy glasses, respectively. This certainly means the preferential existence of Ni-Ti unlike atom pairs in the first nearest neighbor coordination over the whole Ni-Ti glass formation range. The coordination numbers(Z_{NiTi}) of Ti atoms around a Ni atom in Ni-Ti neutron zero-scattering alloy glasses calculated using the values of α obtained above are plotted as a function of Ti content in Fig. 3 together with the coordination numbers(Z^{R}_{NiTi}) calculated for statistically random distribution alloys. It is noteworthy that the values of Z_{NiTi} in Ni-Ti alloy glasses are well located in the straight line connecting the Z_{NiTi} values found in crystalline $NiTi_2$ and NiTi compound.

We conclude that the chemical short-range structure even in metal-metal glasses is quite analogous to that in corresponding crystalline compounds over whole glass forming composition range.

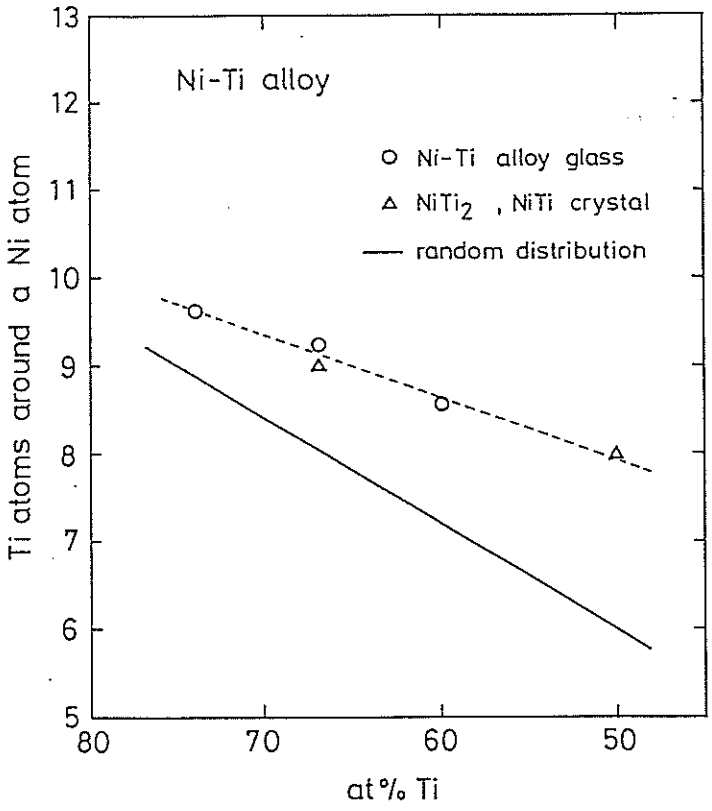

Fig. 3. Coordination numbers of Ti atoms around a Ni atom in Ni-Ti alloy glasses, and crystalline $NiTi_2$ and NiTi compound. A solid line means the coordination number of Ti atoms around a Ni atom in case of statistically random distribution under the total coordination number of 12 atoms.

References

1) T. Fukunaga and K. Suzuki, Sci. Rep. Res. Inst. Tohoku Univ., A-29 (1981) 153.

2) T. Fukunaga, K. Kai, M. Naka, N. Watanabe and K. Suzuki, Proc. 4th Inter. Conf. Rapidly Quenched Metals(edited by T. Masumoto and K. Suzuki, The Japan Institute of Metals, Sendai, 1982) p.347.

3) A. B. Bhatia and D. E. Thornton, Phys. Rev., B2 (1970) 3004.

4) W. Rostoker, Trans. AIME, 194 (1952) 209.

5) B. E. Warren, B. L. Averbach and B. W. Roberts, J. Appl. Phys., 22 (1951) 1493.

Partial Structures of $Ni_{40}Ti_{60}$ Alloy Glass

Toshiharu FUKUNAGA, Noboru WATANABE* and Kenji SUZUKI

The Research Institute for Iron, Steel and Other Metals, Tohoku University, Sendai 980, Japan

*National Laboratory for High Energy Physics, Oho-machi, Tsukuba-gun, Ibaraki 305, Japan

Up to date the high resolution observation of the short-range structure and the determination of the partial structures have been carried out to explore the topological and chemical short-range structure of metal-metalloid and metal-metal alloy glasses. It has been reported that metal-metalloid alloy glasses are chemically ordered in the short-range atomic arrangement[1]. Recently the chemical short-range orders have been analysed not only in metal-metalloid alloy glasses but also in metal-metal alloy glasses[2] using the Bhatia-Thornton correlation functions.

The aim of this study is to investigate more precisely the local atomic arrangement and chemical short-range order in terms of both the Bhatia-Thornton and the Faber-Ziman three partial distribution functions.

Thin ribbons of Ni-60at%Ti neutron zero and off-zero scattering alloy glasses were prepared by rapid quenching from the molten state using single roll technique under Ar-gas atomosphere. The measurements of the neutron scattering intensity from the alloy glasses were carried out at room temperature in vacua by using the High Intensity Total scattering spectrometer(HIT). X-ray diffraction pattern was measured by θ-2θ scanning reflection mode using Mo-Kα radiation.

Figure 1 shows the Bhatia-Thornton total structure factor[3] $S^{BT}(Q)$'s observed for Ni-60at%Ti alloy glasses by X-ray and neutron diffraction. In the case of the neutron zero-scattering alloy glass the $S^{BT}(Q)$ observed provides exclusively the concentration-concentration partial structure factor $S_{CC}(Q)$. Therefore, the number density-number density partial structure factor $S_{NN}(Q)$ and the partial structure factor $S_{NC}(Q)$ presenting the cross correlation between density and concentration fluctuation can be easily caluculated from X-ray and neutron $S^{BT}(Q)$'s for Ni-60at%Ti neutron off-zero scattering alloy glass using the $S_{CC}(Q)$ obtained above, as shown

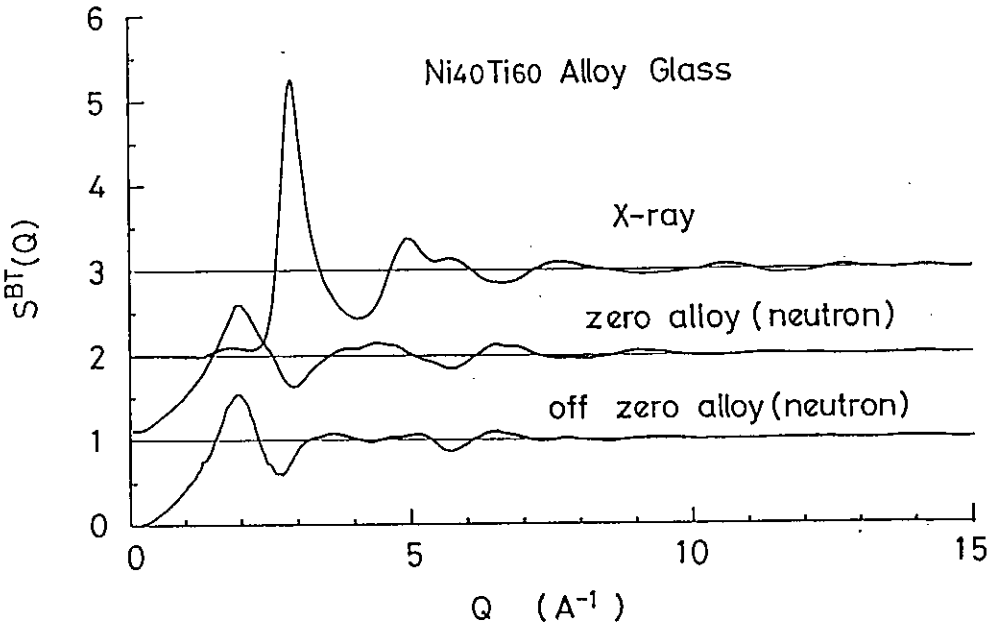

Fig. 1. Bhatia-Thornton total structure factors $S^{BT}(Q)$ of Ni-60at%Ti alloy glasses by X-ray and neutron diffraction.

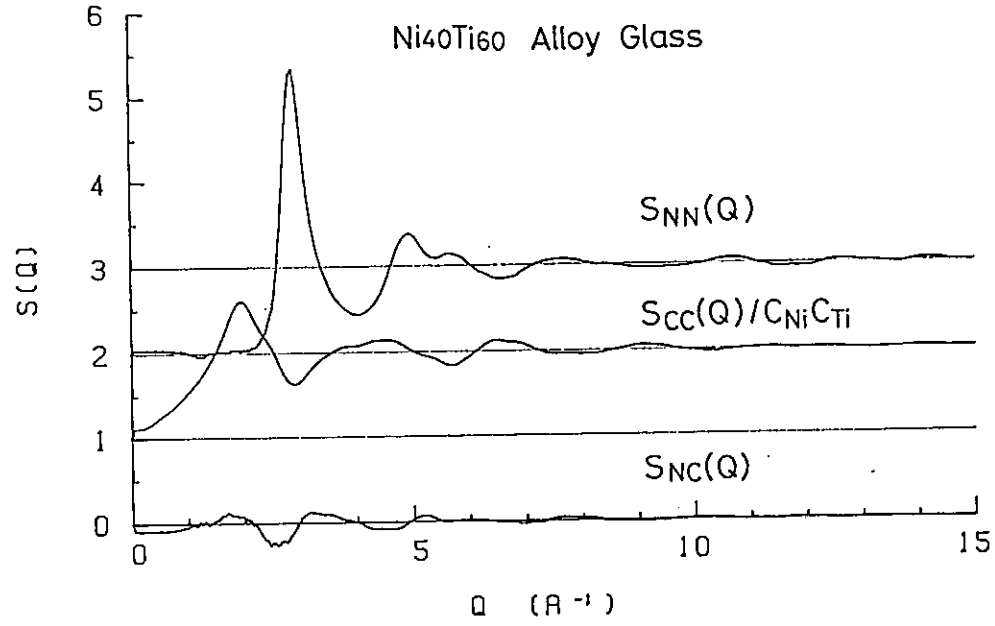

Fig. 2. Bhatia-Thornton partial structure factors $S_{NN}(Q)$, $S_{NC}(Q)$ and $S_{CC}(Q)$ of Ni-60at%Ti alloy glass.

in Fig. 2.

Figure 3 shows the Faber-Ziman partial structure factors[4] $S_{NiNi}(Q)$, $S_{NiTi}(Q)$ and $S_{TiTi}(Q)$ calculated from the Bhatia-Thornton partial structure factors $S_{NN}(Q)$, $S_{NC}(Q)$ and $S_{CC}(Q)$. It is noteworthy that the evidence for the large peak situated at $Q \sim 1.9$ A^{-1} in $S_{NiNi}(Q)$, which has not been

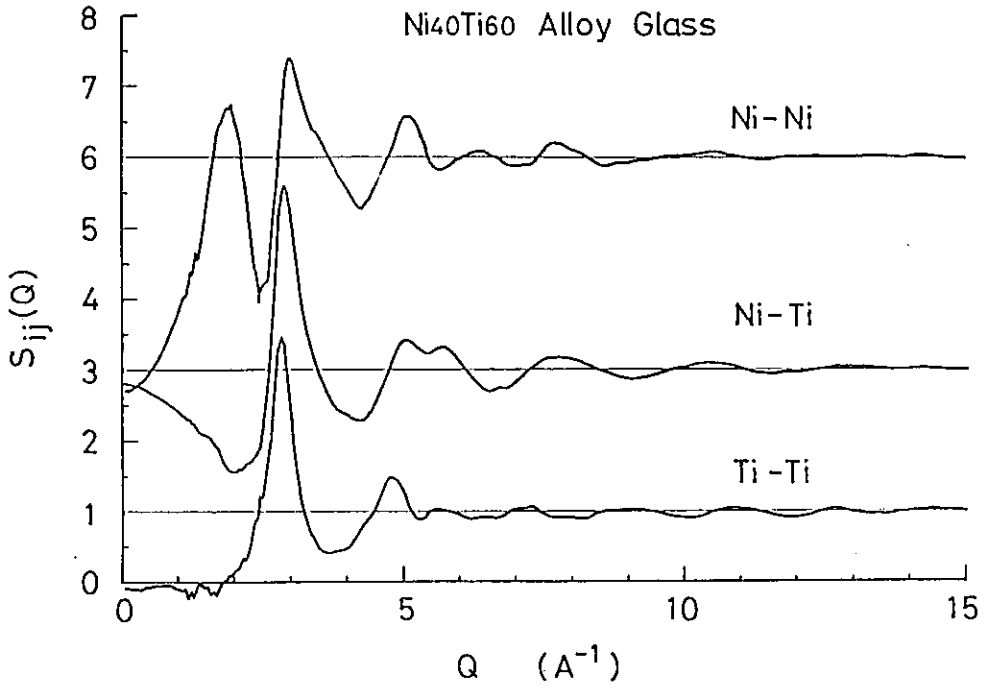

Fig. 3. Faber-Ziman partial structure factors $S_{NiNi}(Q)$, $S_{NiTi}(Q)$ and $S_{TiTi}(Q)$ of Ni-60at%Ti alloy glass.

resolved in metal-metal alloy glasses so far, is definitely found near $Q \simeq 1.9$ A^{-1} in the X-ray $S^{BT}(Q)$ because the atomic number of Ni is larger than that of Ti. Appearance of this peak indicates that the Ni-Ni correlation in Ni-60at%Ti alloy glass is much deviated from the random mixture of Ni and Ti atoms, and rather preserves some orders over the intermediate range around the second nearest neighbor position.

Figure 4 shows the Faber-Ziman partial radial distribution functions $(RDF)_{NiNi}$, $(RDF)_{NiTi}$ and $(RDF)_{TiTi}$ obtained as the Fourier transforms of $S_{NiNi}(Q)$, $S_{NiTi}(Q)$ and $S_{TiTi}(Q)$. The nearest neighbor distances of Ni-Ni, Ni-Ti and Ti-Ti correlations are r_1=2.626 A, 2.60 A and 3.01 A repectively. It is noticeable that the Ni-Ni and Ti-Ti interatomic distances are larger than the Ni and Ti atomic diameters[5] (σ_{Ni}=2.48 A and σ_{Ti}=2.94 A), but the Ni-Ti interatomic distance is much smaller than the mean value of the Ni and Ti atomic diameters. This means that Ni atoms never exist in contact each other but the first nearest neighbor position is predominantly occupied by Ni-Ti unlike atom pair. The preference for unlike atom neighbors indicates that the amorphous structure is essentially stabilized by the chemical bonding between Ni and Ti atoms. The coordination numbers between the nearest neighbor atoms calculated from the first peak areas in the partial RDF's of Ni-60at%Ti alloy glass are almostly similar to

those of $NiTi_2$ crystalline compound[6].

It is clearly concluded that there is the chemical short-range order in the atomic arrangement of Ni-60at%Ti alloy glass, which is almost analogous to that of $NiTi_2$ crystalline compound.

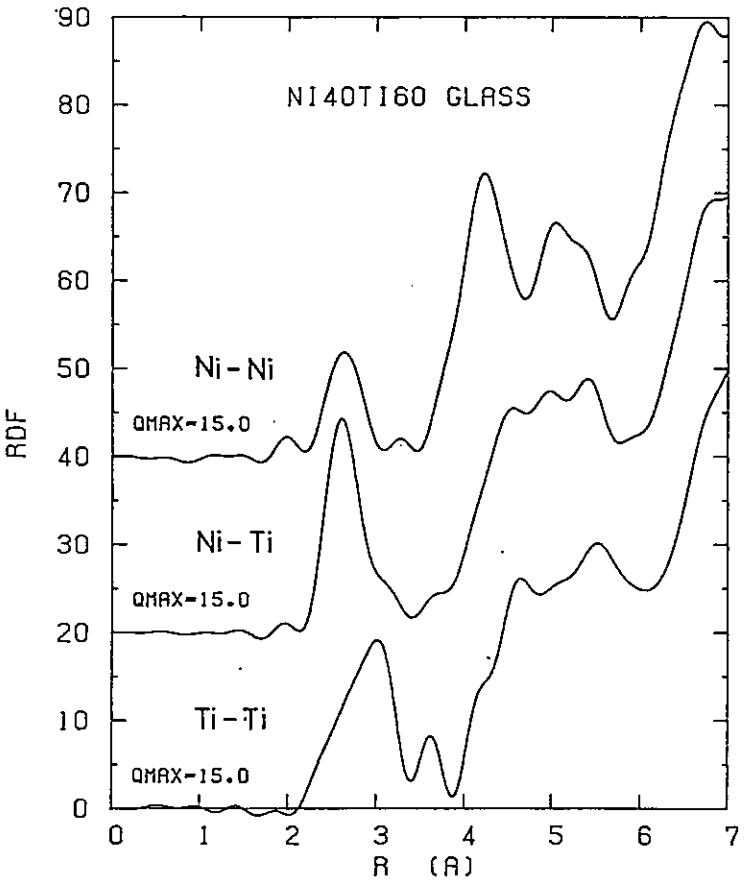

Fig. 4. Partial radial distribution functions of Ni-Ni, Ni-Ti and Ti-Ti correlations in Ni-60at%Ti alloy glass.

References

1) G. S. Cargill III and F. Spaepen, J. Non-Cryst Solids, 43(1981)91.
2) C. N. J. Wagner, J. Non-Cryst. Solids, 42(1980)3
3) A. B. Bhatia and D. E. Thornton, Phys. Rev., B2(1970)3004.
4) T. E. Faber and J. M. Ziman, Phil. Mag., 11(1965)153.
5) R. D. Shannon and C. T. Prewitt, Acta. Cryst., B25(1969)925.
6) W. Rostoker, Trans. AIME, 194(1952)209.

Partial Structures of an Amorphous $Ni_{.36}Zr_{.64}$ Alloy

T. MIZOGUCHI, S. YODA, N. AKUTSU, S. YAMADA
J. NISHIOKA, T. SUEMASA and N. WATANABE*

Faculty of Science, Gakushuin University
Mejiro, Toshima-ku, Tokyo 171 Japan

*National Laboratory for High Energy Physics
Oho-machi, Tsukuba-gun, Ibaraki 305 Japan

The partial structures of amorphous $Ni_{.36}Zr_{.64}$ alloys were studied by neutron diffraction, using isotopic substitution method. Three samples which contained natural Ni, 99.08% enriched ^{60}Ni and mixed Ni (68.3% natural Ni and 31.7% ^{60}Ni) were prepared by the melt quenching technique. TOF neutron diffraction experiments were done at room temperature, using HIT spectrometer at KENS facility of KEK Laboratory. The total interference functions, S(Q), of these three samples were obtained after necessary corrections for absorption, multiple scattering and incoherent scattering. They are expressed as the weighted sum of the three partial interference functions, $S_{NiNi}(Q)$, $S_{NiZr}(Q)$ and $S_{ZrZr}(Q)$. Since we have got the three total S(Q)s with the different weighting factors, the three partial interference functions can be obtained by solving the linear equations. The results are shown in Fig. 1. By Fourier transforming the partial $S_{IJ}(Q)$ we get the partial pair correlation functions $g_{NiNi}(r)$, $g_{NiZr}(r)$ and $g_{ZrZr}(r)$. They are shown in Fig. 2. The first peak position, r_p, and the first minimun position, r_m, in $g_{IJ}(r)$ are listed in Table 1. The partial coordination number Z_{IJ} was calculated by integrating the partial pair correlation functions up to r_m as follows,

$$Z_{IJ} = \int_0^{r_m} 4\pi r \rho_0 c_J g_{IJ}(r) dr$$

where ρ_o is the total number density and c_J is the concentration of an element J. The results are listed in Table 2.

It is interesting to compare these results to those for a crystalline $NiZr_2$. In the amorphous alloy the Ni-Ni pair peak position is smaller by about 6% than that in the crystalline $NiZr_2$. The Ni-Zr pair distance is close to the average of the Ni-Ni and Zr-Zr pair distances in the amorphous phase. This suggests that the topological atomic configurartion is more or less close to the random close packing of spheres of different sizes thanks to a lack of constraint of long range ordering. In the crystal a Ni atom is surrounded by 2 Ni and 8 Zr atoms and a Zr atom is surrounded by 4 Ni and 9 Zr atoms[1]. In the amorphous alloy the ratio of partial coordination number is closer to that of the total concentration. In the crystal there is poor Ni-Ni nearerst neighbor pair correlation while in the amorphous phase there seems to be a moderate chemical short range order with somewhat prevailing Ni-Zr nearest neighbor pair correlation.

atomic pair	1st peak	1st min
Ni-Ni	2.45 A	3.55 A
Ni-Zr	2.85 A	4.00 A
Zr-Zr	3.15 A	4.30 A

Table 1. The first peak and the first minimum position of the partial pair correlation function $g_{IJ}(r)$ of an amorphous $Ni_{.36}Zr_{.64}$ alloy.

center	nearest neighbor		
atom	Ni	Zr	total
Ni	3.8 (33%)	8.6 (66%)	11.4
Zr	6.8 (38%)	11.0 (62%)	17.8

Table 2. The partial coordination number of an amorphous $Ni_{.36}Zr_{.64}$ alloy.

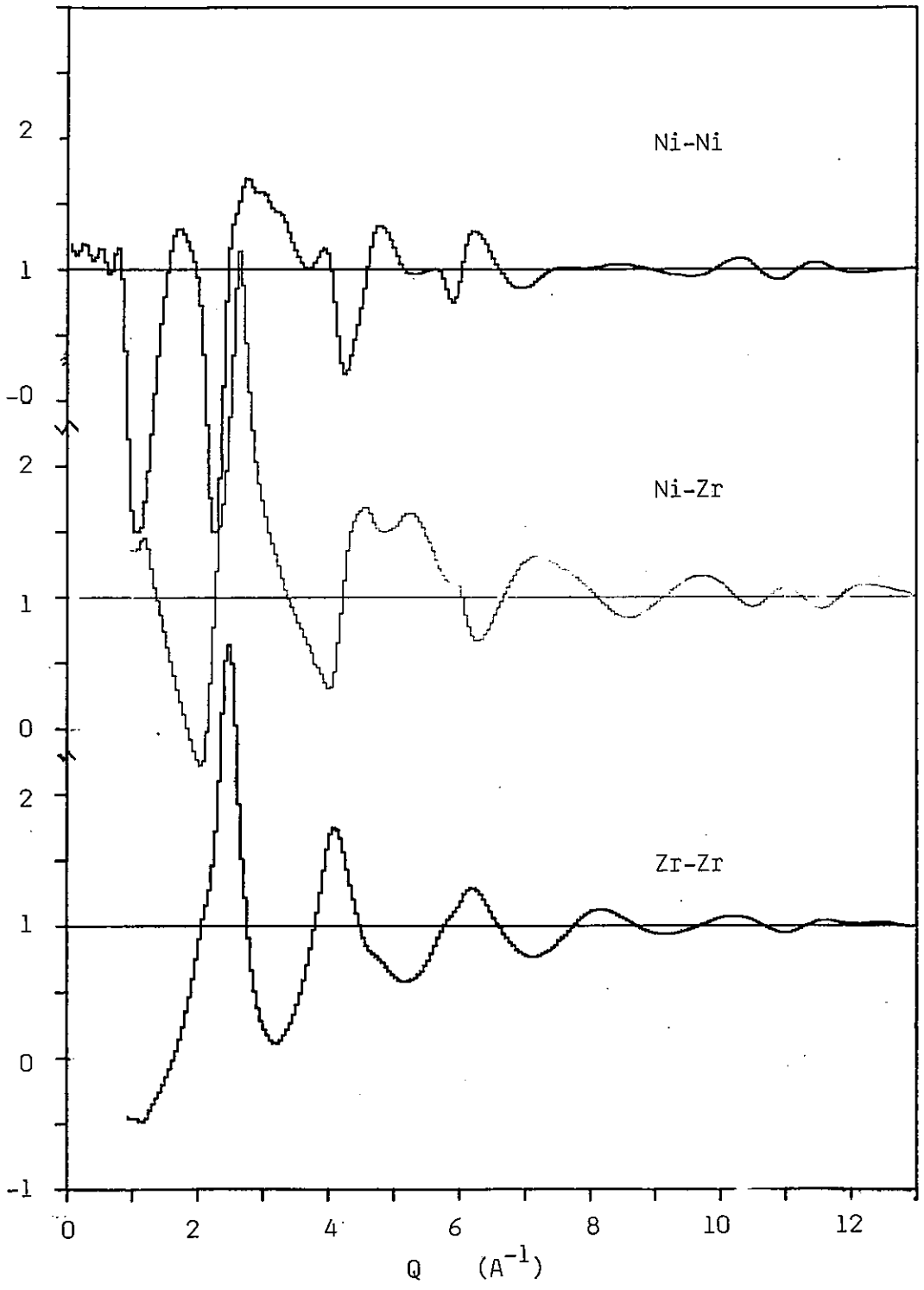

Fig. 1. The partial interference functions, $S_{NiNi}(Q)$(upper), $S_{NiZr}(Q)$ (middle) and $S_{ZrZr}(Q)$(bottom) of an amorphous $Ni_{.36}Zr_{.64}$ alloy.

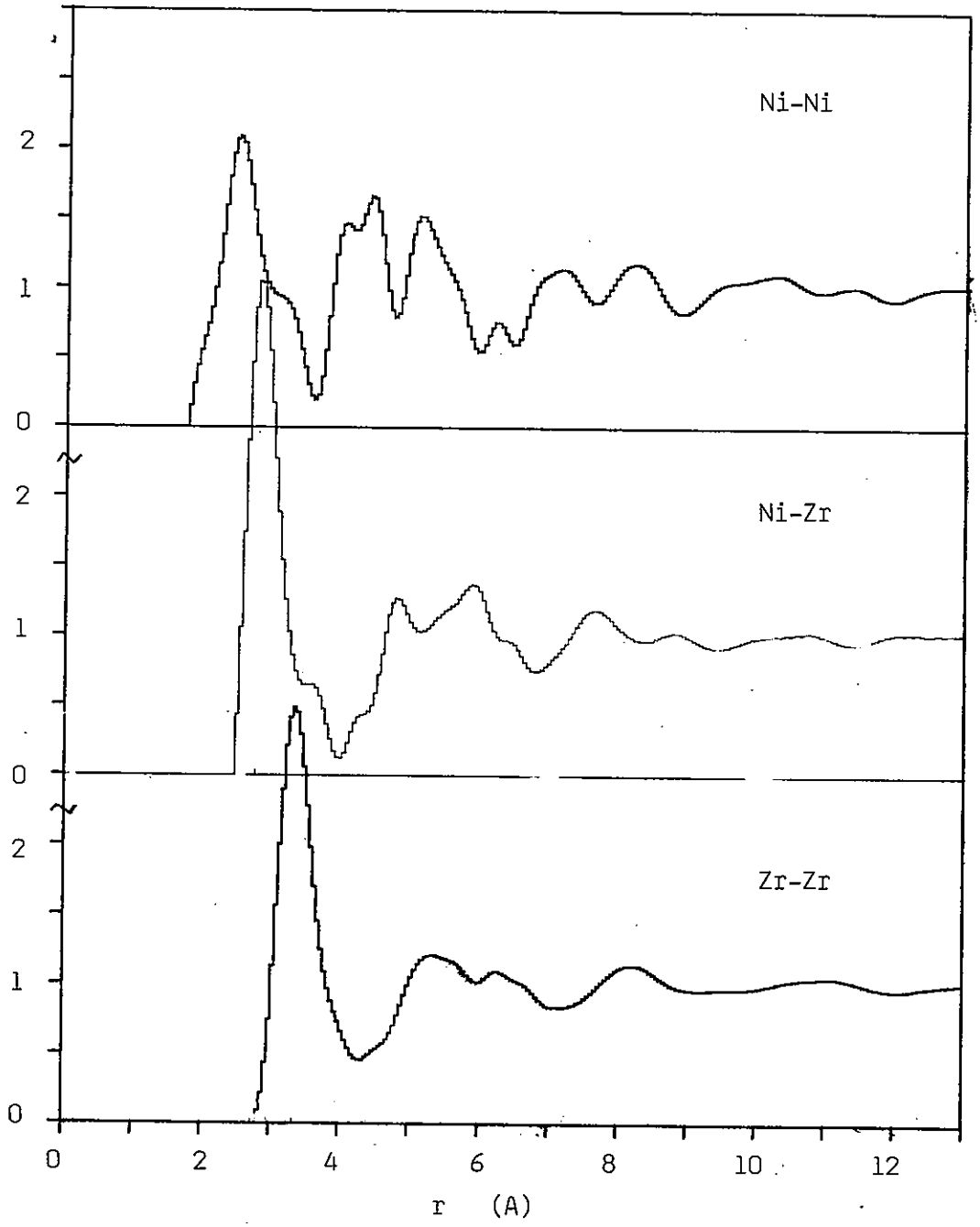

Fig. 2 The partial pair correlation functions, $g_{NiNi}(r)$(upper), $g_{NiZr}(r)$(middle) and $g_{ZrZr}(r)$(bottom) of an amorphous $Ni_{.36}Zr_{.64}$ alloy.

Reference

(1). M. E. Kirkpatrick, D. M. Bailey and J. F. Smith, Act. Cryst. 15 (1962) 252.

Chemical Short Range Order in $Ni_{60}Nb_{40}$ glass

M. SAKATA, S. HASHIBA, S. YODA*, N. AKUTSU* and T. MIZOGUCHI*

Applied Physics Department, Nagoya University, Nagoya 464, Japan

*Faculty of Science, Gakushuin University, Tokyo, Japan

It is now the well established fact that the Chemical Short Range Order (CSRO) exists in some alloy glasses like CuTi and NiTi[1]. From the study of the variation with composition of the CSRO parameter and the crystallization temperature for CuTi glasses[2], it was found that the CSRO appear to have a substantial effect on enhancing the thermal stability of the alloy glasses. If an alloy glass has the CSRO which means the preference of unlike atoms as the first nearest neighbours (FNN), there appears longer pseudo-periodicity which causes so called prepeak in S(Q) pattern around Q=1.9 A^{-1}. For many amorphous alloy systems, however, such a prepeak can not be observable because of the poor contrast in X-ray and neutron diffraction methods[3], even if there exists maximum CSRO. It is, therefore, not possible to examine the existence of CSRO for all the amorphous alloys experimentally and it is an unsolved problem whether CSRO is the ordinary feature of amorphous alloys which implies that the existence of CSRO is the necessity to stablize amorphous alloys.

For amorphous $Ni_{60}Nb_{40}$ alloy, there is a controversy whether a small prepeak of neutron S(Q) pattern is due to the CSRO[3] or the correlation between density and concentration fluctuation[4]. To finalize the controversy would be regarded as the forward step toward answering the above problem. The aim of this work is to try to do this.

Three different isotope composition $Ni_{60}Nb_{40}$ amorphous alloys, i.e. $^{Nat}Ni_{60}Nb_{40}$, $(^{Nat}Ni_{58}{}^{60}Ni_{42})_{60}Nb_{40}$ (abbreviated as $^{Nat+60}Ni_{60}Nb_{40}$) and $^{60}Ni_{60}Nb_{40}$, have been prepared by melt-spinning method. For the $^{Nat+60}Ni_{60}Nb_{40}$ specimen, only the structure factor of density fluctuation should be observed, while for the other two specimens there will be prepeak if CSRO exists in this amorphous alloy.

The neutron total scattering were measured up to Q=24 A^{-1} with HIT installed at KENS, National Laboratory for High Energy Physics, Tsukuba.

The total structure factor S(Q) of the samples are shown in Fig. 1. The RDF (radial distribution function) for them are shown in Fig. 2.
The small prepeak is clearly seen in $^{Nat}Ni_{60}Nb_{40}$ S(Q) pattern as expected. It is certain that the prepeak is not seen in the S(Q) pattern of $^{Nat+60}Ni_{60}Nb_{40}$, although the small Q range data suffer from the poor statistics. Unfortunately, nothing definite can be said on the prepeak for $^{60}Ni_{60}Nb_{40}$.

These results are obviously compatible with the explation of the prepeak as the CSRO but it is not sufficient to conclude it decisively and the further study is required to finalize the controversy on the prepeak observed in $Ni_{60}Nb_{40}$ neutron S(Q) pattern.

References:

1) For examples, M. Sakata, N. Cowlam and H. A. Davies; J. Physique 4 (1980) C8-190 and H. Ruppersberg, D. Lee and C. N. J. Wagner; J. Phys. F10, (1980) 1645
2) M. Sakata, N. Cowlam and H.A. Davies; Proc. RQ4, p327 (1982)
3) M. Sakata, N. cowlam and H.A. Davies; J. Non-Cryst. Solids 46 (1981) 329
4) H. Ruppersberg and C. N. J. Wagner; To be published in J. Non-Crst. Solids

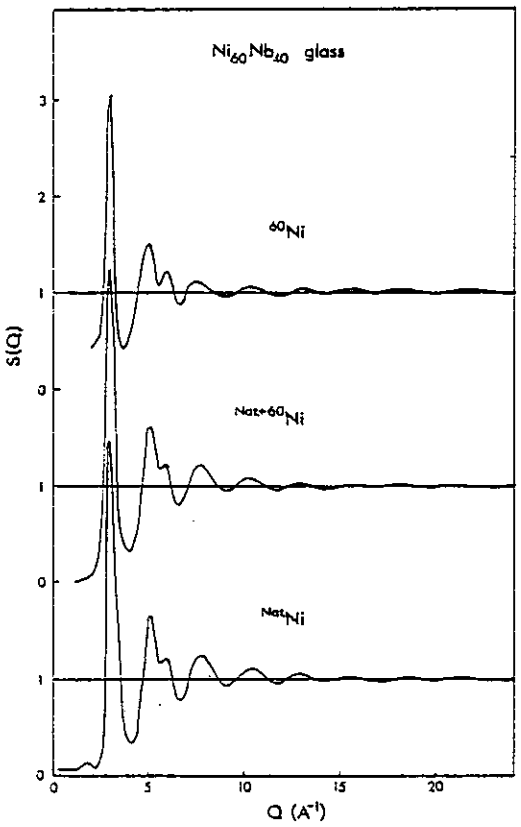

Fig. 1 The total S(Q) of Ni-Nb.

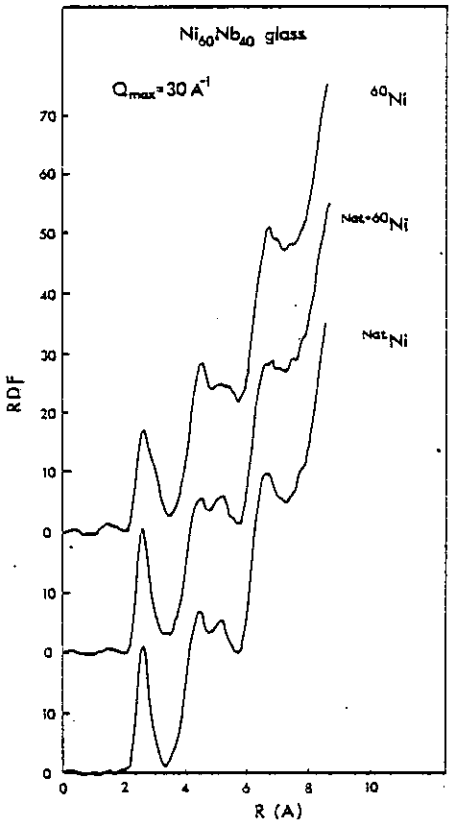

Fig. 2. RDF of Ni-Nb glass.

Neutron Diffraction of Hydrogenated Alloy Glasses Zr-Ni-D

Noriyuki HAYASHI, Yuuji TOMITSUKA, Toshiharu FUKUNAGA,
Kenzo KAI, Noboru WATANABE* and Kenji SUZUKI

The research Institute for Iron, Steel and Other Metals,
Tohoku University, Sendai 980, Japan.

*National Laboratory for High Energy Physics, Oho-machi,
Tsukuba-gun, Ibaraki 305 Japan.

The aim of this study is to examine what kind of atomic sites in Zr_YNi_{1-Y}(Y=0.67, 0.5 and 0.35) alloy glasses are occupied by hydrogen atoms. The measurement of S(Q) for $Zr_{0.67}Ni_{0.33}D_X$(X=0.0, 0.18, 0.25, 0.61, 0.79 and 1.32), $Zr_{0.50}Ni_{0.50}D_X$(X=0.0, 0.15, 0.29, 0.48 and 0.86) and $Zr_{0.35}Ni_{0.65}D_X$(X=0.0, 0.16, 0.39 and 0.50) alloy glasses was curried out by a High Intensity Total scattering spectrometer(HIT) installed at a spallation neutron source of KEK.

Alloy glasses were prepared into a form of thin ribbons with about 2 mm in width and 30 μm in thickness by rapid quenching from their melts using single roll method under Ar-gas atomosphere. Deuterium atoms were absorved into the glass ribbons by a gas-charge method under 20 Kg/cm^2 pressure at 160 °C.

The structure factors S(Q) of $Zr_{0.50}Ni_{0.50}D_X$ alloy glasses obtained in this study are shown in Fig. 1. The height of the first peak in S(Q) decreases with increasing D concentration, while the width increases. A small peak in S(Q) at lower Q side of the first peak becomes inconspicuous due to the broadening of the first peak. The profile of the second peak obviously varies with D concentration. Some modifications of the oscillation in S(Q) over high Q region ($Q \gtrsim 15$ A^{-1}) are observed with different D concentrations. Such a characteristic behavior in S(Q) appears depending on both the D and Zr concentration in Zr-Ni-D alloy glasses.

Figure 2 shows the pair distribution functions g(r) of $Zr_{0.50}Ni_{0.50}D_X$ alloy glasses obtained as Fourier transforms of S(Q) truncated at $Q_{max} \simeq 25$ A^{-1}. Two new peaks appear inside the first peak, when D atoms are absorbed. One($r \sim 1.7$ A) is likely to correspond to D-Ni pair correlation

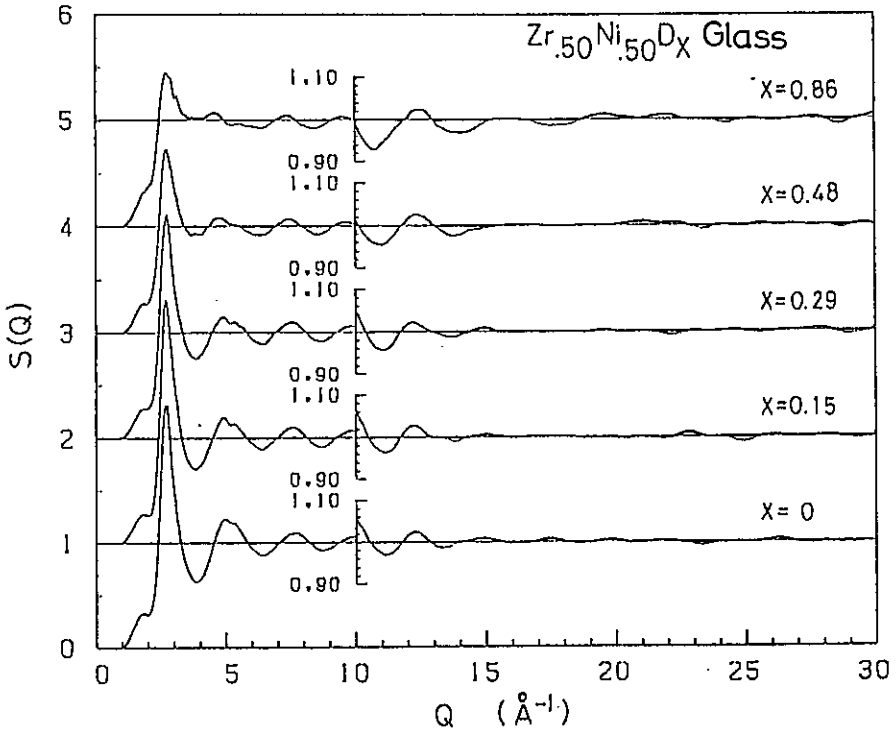

Fig. 1. Structure factors of $Zr_{0.50}Ni_{0.50}D_X$ alloy glasses.

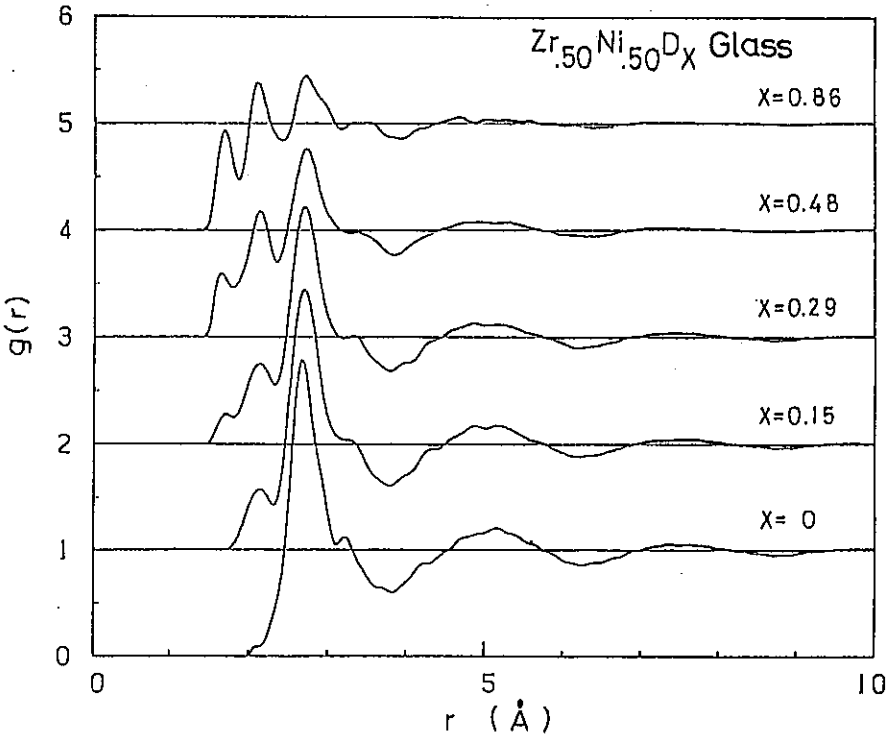

Fig. 2. Pair distribution functions of $Zr_{0.50}Ni_{0.50}D_X$ alloy glasses obtained by Fourier transforming the S(Q).

and the other(r~2.1 A) is regarded as D-Zr pair correlation. The height of both peaks increases with increasing D concentration. In the case of other two hydrogenated alloy glasses, $Zr_{0.67}Ni_{0.33}D_X$ and $Zr_{0.35}Ni_{0.65}D_X$, the behavior of g(r) is essentially similar to that of $Zr_{0.50}Ni_{0.50}D_X$ alloy glass. The D-Zr pair correlation always appears in Zr-Ni-D alloy glasses, while the appearance of the D-Ni pair correlation critically depends on the Ni/Zr ratio and D content in Zr-Ni-D alloy glasses.

Figure 3 shows the nearest neighbor coordination numbers of Ni and Zr atoms arround a D atom obtained by a two Gaussian curves-fitting from the radial distribution functions of Zr-Ni-D alloy glasses. In $Zr_{0.67}Ni_{0.33}D_X$ alloy glasses, at the low D concentration of $X \lesssim 0.61$, a D atom is surrounded by about 4.2~4.6 Zr atoms, while at the high D concentration of X=0.79 and 1.32, a D atom is surrounded by about 4 metal atoms including Zr and Ni

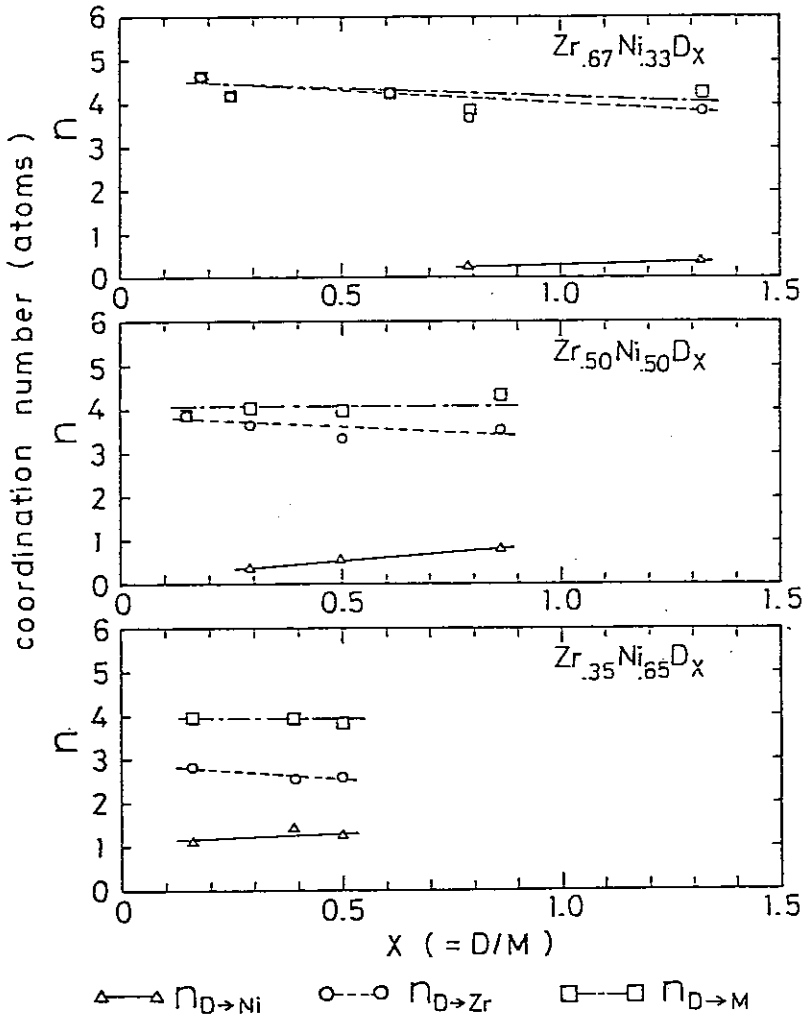

Fig. 3. Nearest neighbor coordination numbers arround a D atom in Zr-Ni-D alloy glasses.

atoms. In $Zr_{0.50}Ni_{0.50}D_X$ and $Zr_{0.35}Ni_{0.65}D_X$ alloy glasses, a D atom is surrounded by about 4 metal atoms over whole D concentration. If Zr-Ni-D alloy glasses have high Zr and low D content, D atoms prefer to occupy the interstitial hole surrounded by 4 Zr atoms. With increasing Ni and D content in Zr-Ni-D alloy glasses, D atoms asymptotically sit in the hole surrounded by 3Zr and 1Ni atoms.

Figure 3 indicate that D atoms may be surrounded by more than 4Zr atoms in the amorphous alloy with high Zr content and sit in the tetrahedral site consisting of 2Zr and 2Ni atoms in the amorphous alloy with high Ni content. These points will be studied by more precise measurements of g(r) and hydrogen atom vibration spectra[1].

Reference

1) K. Kai, N. Hayashi, Y. Tomitsuka, S. Ikeda, N. Watanabe and K. Suzuki, Local Vibration Energy Spectra of H Atoms in Amorphous and Crystalline $ZrNiH_X$, in this volume.

Neutron Diffraction of Hydrogenated Alloy Glass $Ni_{33}Ti_{67}D_X$(X=0∿60)

Kenzo KAI, Toshiharu FUKUNAGA, Noriyuki HAYASHI, Noboru WATANABE*
and Kenji SUZUKI

The Research Institute for Iron, Steel and Other Metals,
Tohoku University, Sendai 980, Japan

*National Laboratory for High Energy Physics Oho-machi, Tsukuba-gun,
Ibaraki 305, Japan

Current technological attentions have been paid to the potential application of metallic glass hydrides as a medium of hydrogen-energy storage and conversion. From the view point of fundamental studies, hydrogen atoms serve as an unique probe to investigate the topological and chemical configurations of polyhedral structure units composing metallic glasses, because the central holes of polyhedra are selectively occupied by hydrogen atoms as a function of hydrogen concentration. Therefore, the aim of this work is to investigate the local environment of hydrogen atoms absorbed into $Ni_{33}Ti_{67}$ alloy glass through the high resolution observation of the radial distribution function.

Thin ribbons of $Ni_{33}Ti_{67}$ metallic glass were prepared by rapid quenching from the molten state in Ar-atomosphere using single roll technique. Deuterium atoms were charged into $Ni_{33}Ti_{67}$ metallic glass at 130 °C under about 30 atoms D_2-gas pressure. Deuterium contents absorbed were controlled by measuring the changes in D_2-gas pressure during absorption and in sample weight and then analyzed by Ar-gas carrier chromatography. The total structure factors were measured by a High Intensity Total scattering spectrometer (HIT).

Since $Ni_{33}Ti_{67}$ alloy glass is near the neutron zero-scattering alloy composition, we derive the Bhatia-Thornton neutron total structure factor $S(Q)$[1] as shown in Fig. 1. The first and second peak profiles in $S(Q)$ are significantly modified for the $Ni_{33}Ti_{67}D_X$ glass hydrides beyond X=26. The oscillation in $S(Q)$ of the glass hydrides is rather enhanced over a high Q region compared with that of the alloy glass before hydrogen charge.

Figure 2 shows the reduced atomic distribution function $G'(r)$ obtained as the Fourier transform of $S(Q)$ truncated at $Q_{max}=25\ A^{-1}$. A negative peak

at r=2.56 A in G(r) of $Ni_{33}Ti_{67}$ alloy glass is mainly contributed from the preference for Ni-Ti unlike atom pairs. This peak vanishes and a negative peak appears at the position around r~1.95 A with increasing D content.

The atomic distances for D-Ni and D-Ti pairs in $NiTi_2D_{1.5}$ crystal[2] are expected to be $r_{DNi} \simeq 1.8$ A and $r_{DTi} \simeq 2.0$ A from its crystal structure, respectively. The both atomic distances are too close each other and so we consider that the negative first peaks appearing at r~1.95 A are a result of the overlapping of D-Ti negative peak and D-Ni positive peak. The hydrogen atom vibration spectrum of $Ni_{50}Ti_{50}H_{150}$ glass hydride[3] indicates that greater part of hydrogen atoms prefer to sit in the tetrahedral site. Therefore, presuming that D atoms occupy only the tetrahedral holes, we have calculated the number of Ni or Ti atom around a D atom from the negative first peak located at r~1.95 A in $Ni_{33}Ti_{67}D_X$ alloy glasses.

It is considered that the D atom occupies the tetrahedral hole consisting of 4Ti atoms in $Ni_{33}Ti_{67}D_X$ glass hydrides up to X~11 and above this D content the D atom occupies the tetrahedral hole consisting of Ti and Ni atoms, for example, 3Ti and a Ni atom, 2Ti and 2Ni atoms and so on.

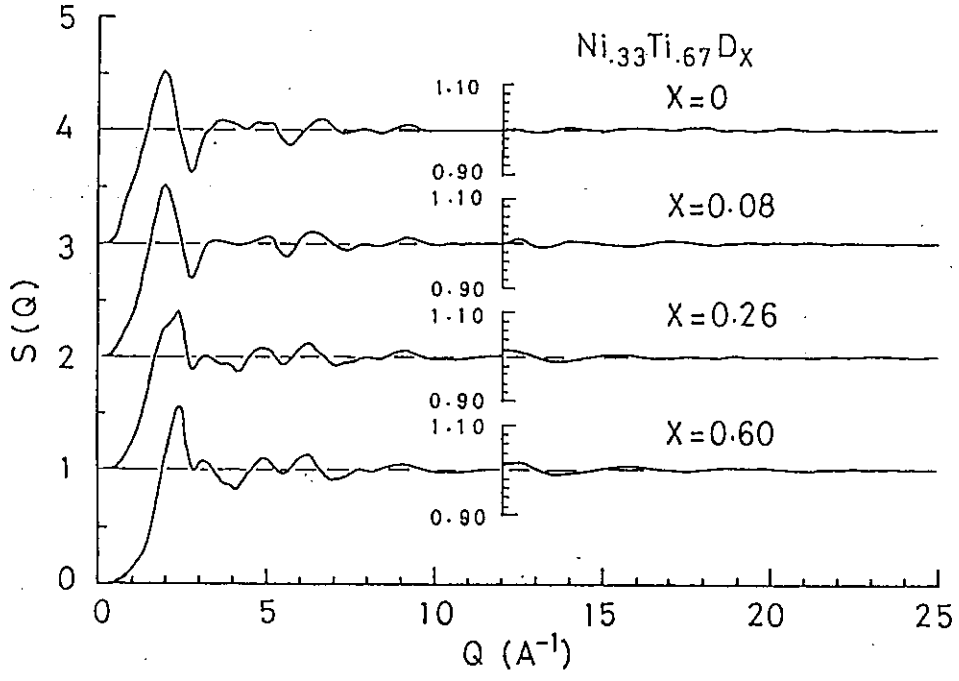

Fig. 1. Bhatia-Thornton type neutron total structure factors of $Ni_{33}Ti_{67}D_X$(X=0, 8, 26 and 60) glass hydrides.

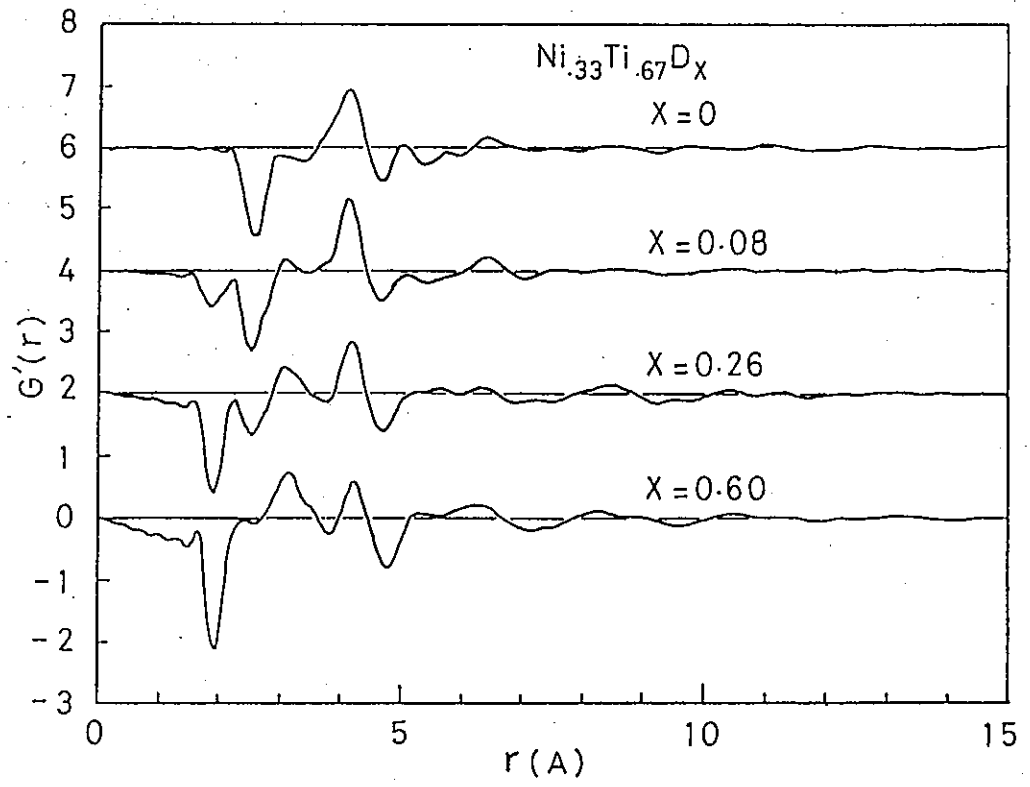

Fig. 2. Reduced atomic correlation functions G'(r) of $Ni_{33}Ti_{67}D_X$ (X=0, 8, 26 and 60) glass hydrides.

References

1) A. B. Bhatia and D. E. Thornton, Phys. Rev. B2(1970)3004.

2) H. Buchner, M. A. Gutijar, K-D. Beccu and H. Saufferer, Z. Metald. 63(1972)497.

3) K. Kai, S. Ikeda, T. Fukunaga, N. Watanabe and K. Suzuki, Physica (1983) in press.

Measurement of Magnetic Scattering from Amorphous Invar Alloys, $Fe_{1-x}B_x$

Ze. Xianyu[§], Y. Ishikawa, T. Fukunaga[+] and N. Watanabe[++]

Physics Department, [+]Institute for Iron Steel and Other Metals, Tohoku Univ., Sendai 980 and [++]National Laboratory for High Energy Physics, Tukuba

The amorphous $Fe_{1-x}B_x$ alloys are the unique system which has the stable amorphous phase in a wide range of composition and their physical properties depend strongly on composition. The magnetization at 0 K becomes maximum around x = 0.17 and the invar effect which is quite large in $Fe_{86}B_{14}$ is significantly reduced when x aproaches to 0.25. In order to find the origin of the invar effect of this alloy system, we have studied the compositional variation of local atomic order as well as of magnetic moment on iron atoms. The paper discusses mainly the magnetic contribution to the scattering.

The amorphous $Fe_{1-x}{}^{11}B_x$ samples with x = 0.14, 0.17 and 0.25 were prepared by rapid quenching method and the neutron scattering experiments were carried out on HIT in a magnetic field H of 5 K Oe applied parallel (I") and perpendicular ($I^{\perp}$) to the scattering vector Q in order to separate the magnetic contribution. The scattering was detected by three He^3 counters with scattering angles of 29.6, 31.5 and 43.9 degrees. The numbers of the nearest neighboring Fe-B and Fe-Fe pairs could be separately determined from the radial distrubution functions RDF for three samples. The results suggest that the numbers of the nearest neighboring Fe and B atoms with respect to a central Fe atom is approximately twelve and seven respectively, independent of composition, suggesting that the local atomic order of iron atoms is nearly the same as that of the f.c.c. structure and it does not suffer an appreciable change with composition.

The magnetic scattering function obtained by a simple substraction of I" from $I^{\perp}$ shows that the magnetic first peak is significantly large for $Fe_{86}B_{14}$, while it almost desappears for $Fe_{75}B_{25}$ as shown in Fig.1. We also found that for $Fe_{86}B_{14}$ the background has a positive slope, while it becomes negative for $Fe_{75}B_{25}$. This is due to the fact that the normalization factor K of

§ Present address ; Northeast Institute of Technology, China

parallel scattering $I^{\parallel}$ with respect to the perpendicular scattering $I^{\perp}$ is slightly misestimated for both $Fe_{86}B_{14}$ and $Fe_{75}B_{25}$. In another word, we can determined the normalization factor so as that the difference of $I^{\parallel}$ and $I^{\perp}$ has no slope above $Q = 5.00\ A^{-1}$. This is the most accurate method for determining K. Such an accurate determination of K seems to be quite important, because the magnetic contribution to the first peak is only 20% of

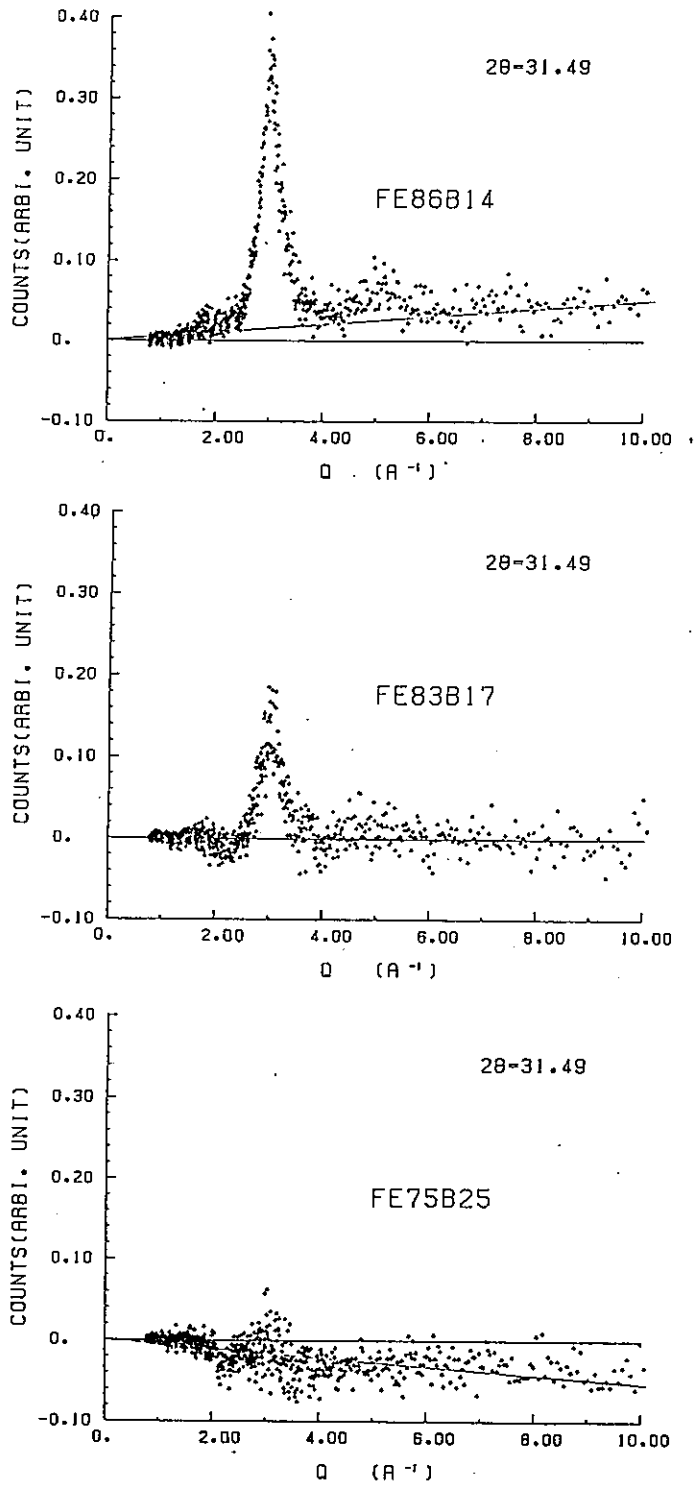

Fig.1. Magnetic scattering function obtained by simple subtraction of scattering with $H \parallel Q$, $I^{\parallel}$ from that with $H \perp Q$, $I^{\perp}$ for three samples.

the nuclear peak and K should be determined in an accuracy of a few percents. Such an accuacy cannot be obtained by the conventional method which takes only an account of the outer shape of the sample, because there seems to be a slight change of orientation of the sample pieces inside the sample holder when the magnetic field is applied in different directions.

The magnetic scattering thus determined is plotted against Q in Figs.2(a),

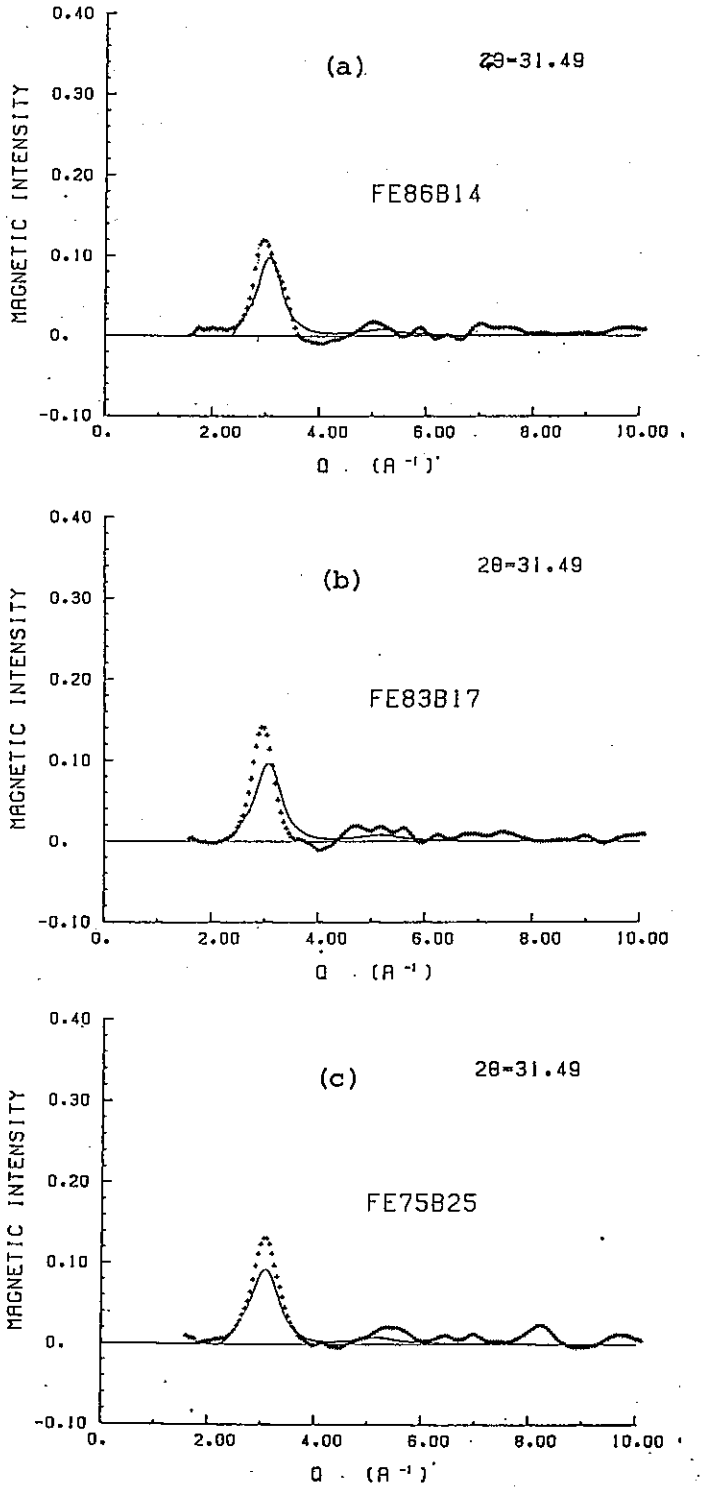

Fig.2. Magnetic scattering obtained by subtracting $KI_{\parallel}$ from $I_{\perp}$ with K determined experimentally. Solid lines were calculated with nuclear scattering function of Fe atoms determined by X-ray, observed magnetization and calculated magnetic form factor of Fe atom.

(b) and (c) after making smoothing correction. The solid line in each figure is calculated by using the scattering function $S_{Fe-Fe}(Q)$ of Fe atoms derived by X ray scattering[1] and the magnetic moment determined by the magnetization measurements. For the magnetic form factor, a following analytic form was assumed.

$$f(Q) = A \exp(-aWQ^2) + B \exp(-bWQ^2) + C, \qquad (1)$$

with W = 1 and A, B, C, and b calculated for Fe atoms[2]. The results show that the calculated magnetic peaks are about 20% lower than the observation for three samples. In Fig.3 is plotted the magnetic moment of iron atoms calculated from the observed magnetic peak by assuming W = 1 in (1). If we assume W = 0.8, the calculated magnetic moment agrees reasonably with that of the average magnetization as also shown in the figure. The value of W = 0.8 is consistent with other observations[3], suggesting that the magnetic electrons are slightly expanded in the amorphous materials.

In conclusion in $Fe_{1-x}B_x$, there is no significant variation of local atomic and magnetic order with composition ranging between x = 0.14 and x = 0.25. Therefore, the distinct change of the invar properties in these alloys should be attributed to the electronic origin.

References

1). T. Fukunaga, M. Misawa, K. Fukamichi, T. Masumoto and K. Suzuki: Proc, 3rd. Int. Conf. R.Q.M. 2(1978)325.

2). E. J. Liher and J. B. Forsyth: Act Cryst A27(1971)545.

3). J. Bletry and J. F. Sadoc. J. Phys. F: Metal Phys. 5(1975)L110.

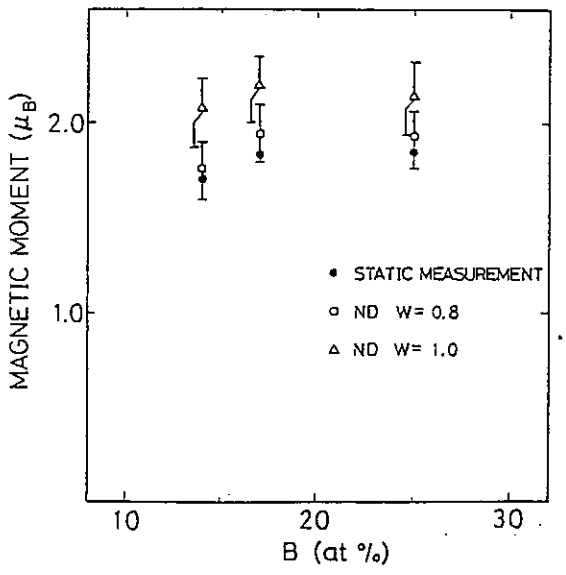

Fig.3. Compositional dependence of magnetic moment determined from the first magnetic peak of magnetic scattering.

Neutron Diffraction Pattern and Structure of the Water + LiCl System

Kazuhiko Ichikawa, Takaaki Matsumoto*,
Yasuo Kameda and Noboru Watanabe**

Chemical Department and *Nuclear Department,
Hokkaido University, Sapporo 060, Japan

**National Laboratory for High Energy Physics.
Tsukuba-gun, Ibaraki 305, Japan

Up to the present, no one simple model can be expected to cover the entire range of electrolyte solutions from dilute solution to fused salt, and an exact statistical-mechanical treatment remains in the future . For the H_2O + LiCl system, Fig. 1 shows the different concentration domains wherein these concentration ranges overlap and have only qualitative meaning. In the LiCl-rich side corresponding to the C and D areas the

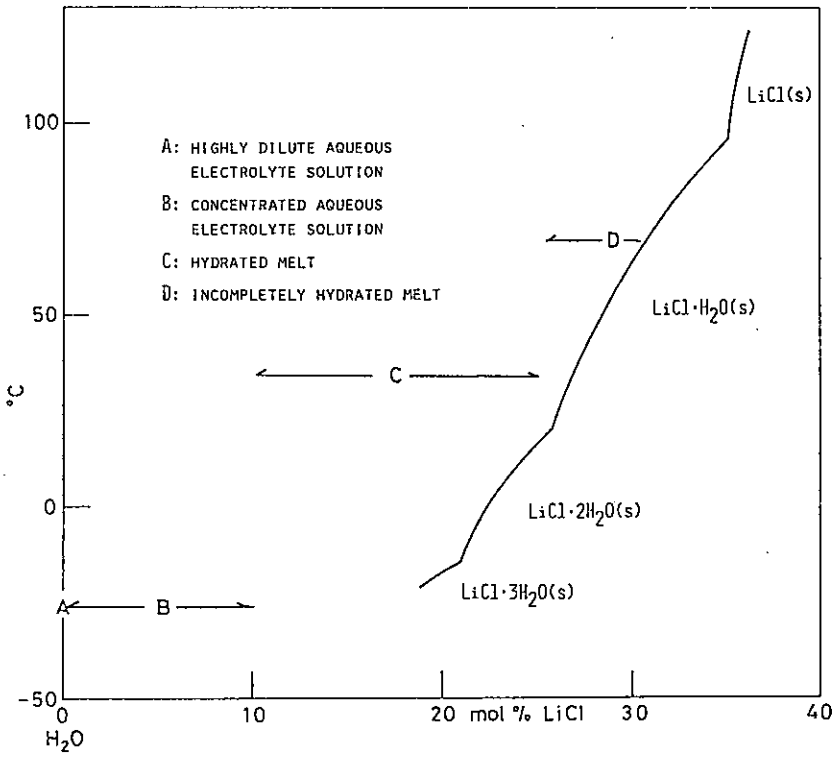

Figure 1. Binary system of aqueous LiCl solution

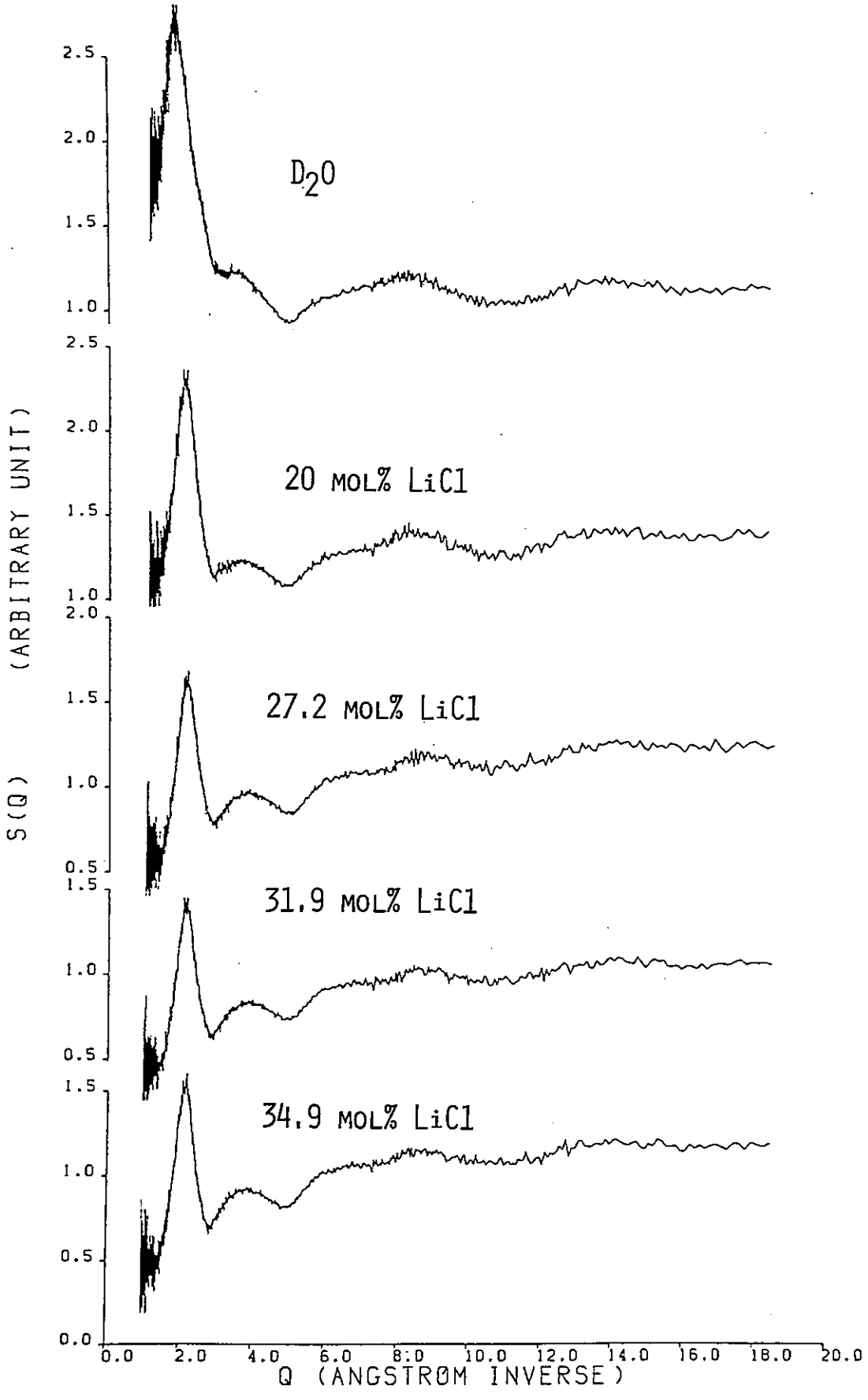

Figure 2. The dependence of S(Q) on the composition at ca. 120°C

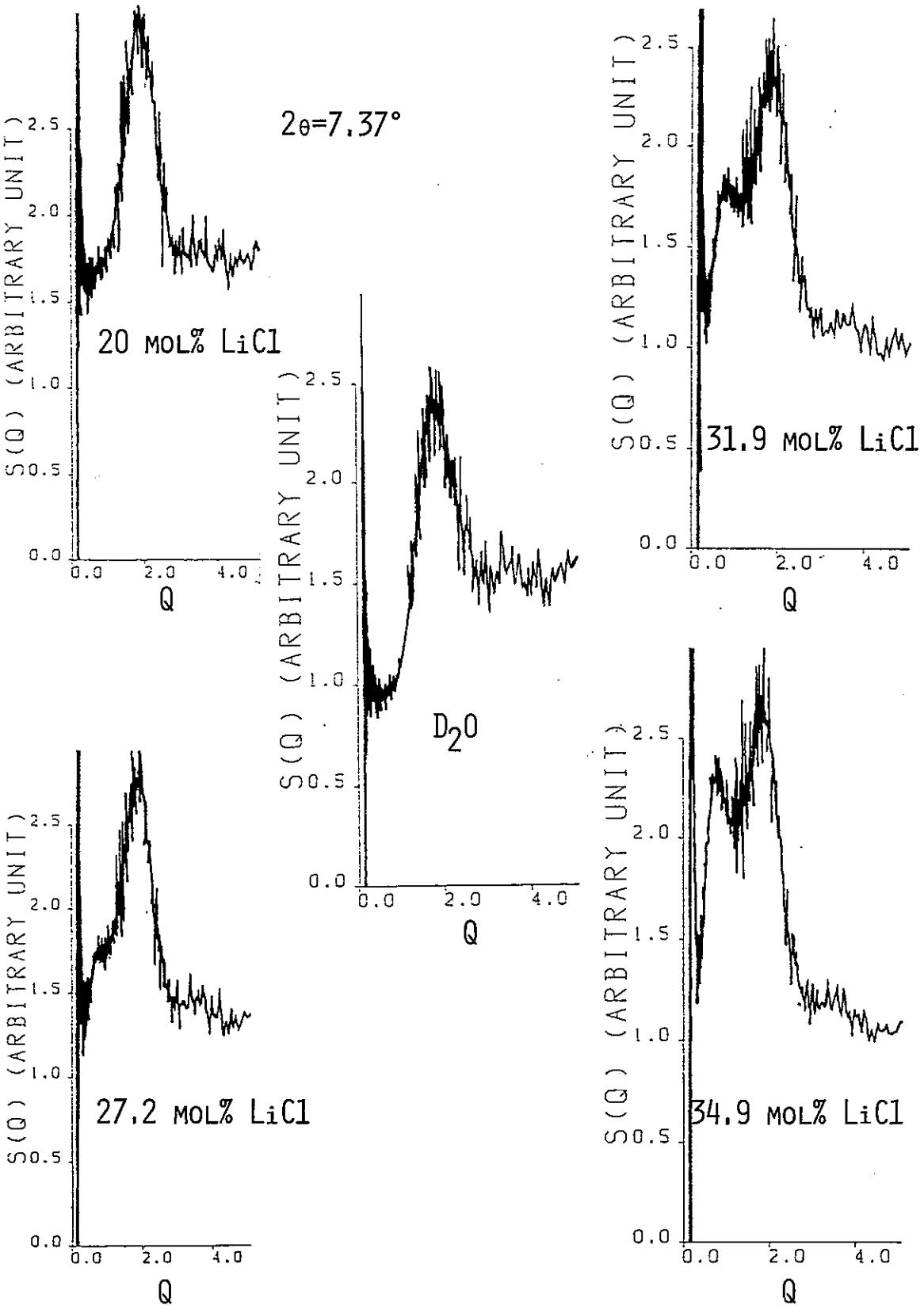

Figure 3. The dependence of S(Q) on the composition in low Q region and at ca. 120°C

ionic atmosphere appeared in the Debye-Hückel equation cannot be defined precisely because the usual correlation between the central ion in the hydration sheath and the counter ions in the hydration sheath is no longer possible on account of a deficiency of the coordinated D_2O molecules around the central ion. The structural change between the C and D ranges may take place and the intramolecular OD and DD distances of the water component may be affected by the large ionic strength.

This paper reports the preliminary results of the TOF neutron-diffraction experiments of the D_2O + LiCl system using the HIT equipment. Figures 2 and 3 show the structure factors S(Q) of the scattering angles (2θ), 49.9° and 7.37°, respectively, for the solutions at 20, 27.2, 31.9 and 34.9 mol% LiCl and for the heavy water at ca. 120°C. The S(Q) values for 2θ=49.9° increase in the higher Q region because the absorption correction, which is important in particular for the nuclei Li and Cl, had not been carried out. In order to check the experimental accuracy in our measurement we have determined the intramolecular OD and DD distances for pure D_2O liquid and compared with the reported value. The measured values in our experiment are ca. 0.95 Å and 1.54 Å respectively which agree well with the existing data by Narten within an experimental accuracy of ±0.01 Å.[1] Figure 3 shows the saddle or peak , for the first time, observed in S(Q) at the low Q side of the first peak for the LiCl-rich solutions at larger than 27 mol% LiCl (i.e., at the D area in Fig. 1).

1) A. H. Narten, J. Chem. Phys. 56, 1972, 5681.

Short range order in a binary critical mixture of perfluoro(methylcyclohexane)—carbon tetrachloride

Yoshinobu IZUMI, Yasuhiro MIYAKE, Toshiharu FUKUNAGA*, Noriyuki HAYASHI*, Noboru WATANABE** and Kenji SUZUKI*

Department of Polymer Science, Faculty of Science, Hokkaido University, Sapporo 060, Japan

*The Research Institute for Iron, Steel and Other Metals, Tohoku University, Sendai 980, Japan

**National Laboratory for High Energy Physics, Oho-machi, Tsukuba-gun, Ibaraki-ken 305, Japan

Binary mixtures as well as fluids, ferromagnetic and ferroelectric systems exhibit many interesting properties in the vicinity of the critical point. The behavior near the critical point is usually described by the use of various critical exponents. A great deal of efforts has been made to characterize the effects in terms of long wavelength fluctuations, which are observed at small wave vectors, while the studies of the short range order near the critical point have scarcely been made except in rubidium[1], liquid lithium—sodium alloys[2] and in fluids[3].

From the results of x-ray small-angle scattering measurements, Brady et al considered a rod-like cluster formation in the critical region[4]. It is therefore very interesting to study the interrelation between the cluster formation and the short range order of the radial distribution function (RDF). In this report, the short range order and its temperature variation of the binary critical mixture of perfluoro(methylcyclohexane)—carbon tetrachloride have been studied by a high intensity total scattering spectrometer (HIT) installed at a spallation neutron source of KEK.

The critical solution of perfluoro(methylcyclohexane)—carbon tetrachloride was prepared[5),6)] and measured only at 29.6°C(ΔT=1.0°) and 42.0°C(ΔT=13.4°). As a reference sample, only perfluoro(methylcyclohexane) was measured at 25°C, because carbon tetrachloride was already measured by Misawa[7]. Preliminary results are shown in Figs. 1 and 2. It is noted

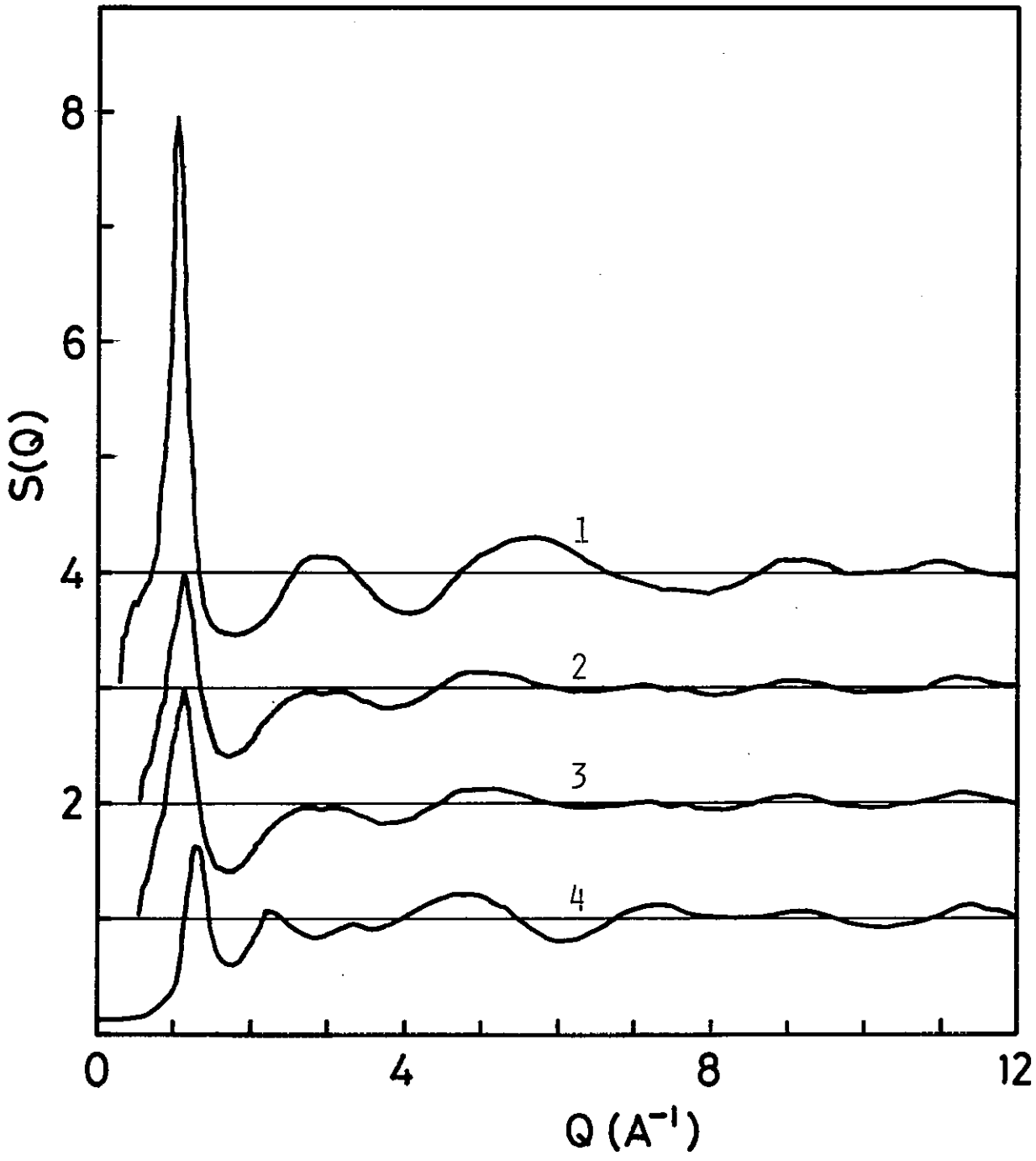

Fig. 1. Structure factors by perfluoro(methylcyclohexane)(1), critical mixture at 42.0°C (2), at 29.6°C (3), and carbon tetrachloride (4).

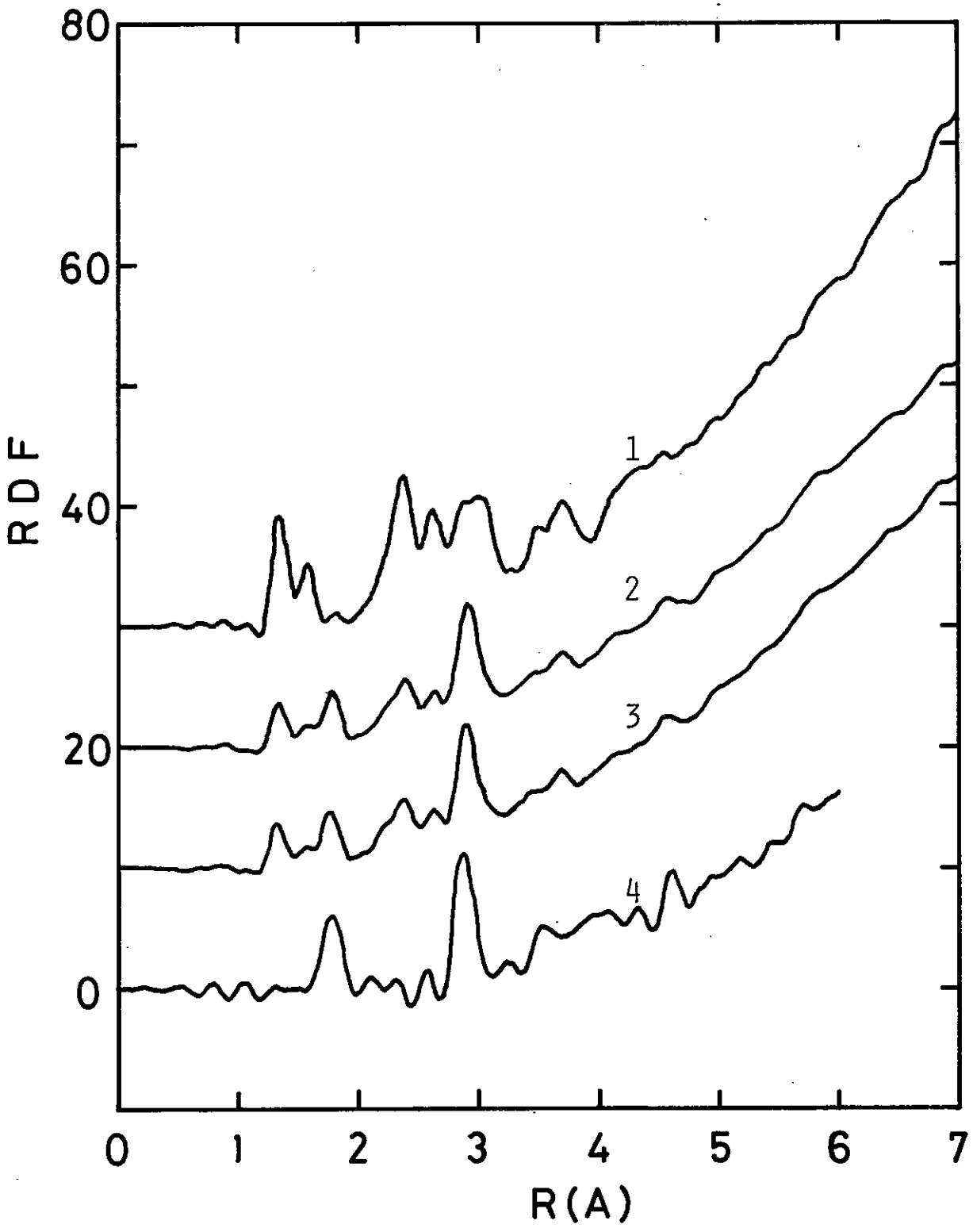

Fig. 2. Radial distribution functions (RDF) of the same systems (1–4) in Fig. 1.

that there is no appreciable change in the profiles of S(Q) and RDF in these measurements, irrespective that the critical point is approached or not. Further experiments in low Q range and near T_c are desirable.

References

1)G.Franz, W.Freyland, W.Glaser, F.Hensel and E.Schneider, J.Phys.(Paris), 41(1980)C8-194.

2)H.Ruppersberg and W.Knoll, Z.Naturforsch. 32a(1977)1374.

3)F.Mandel, J.Chem.Phys. 59(1973)3907.

4)G.W.Brady, J.Chem.Phys.40(1964)2747 and references cited herein.

5)B.Chu, D.Thiel, W.Tscharnuter, D.V.Fenby, J.Phys.(Paris),33(1972),C1-11.

6)D.R.Thompson and O.K.Rice, J.Amer.Chem.Soc. 86(1964)3547.

7)M.Misawa, Thesis, Tohoku University.

Magnetic phase diagram of MnSi near the critical temperature studied by SAN

Y. Ishikawa and M. Arai

Physics Department, Tohoku University, Sendai

MnSi has a helical spin structure below T_c=29K with a period of 180Å(q=0.035) at 4K[1]. It becomes ferromagnetic in a magnetic field of 6kOe.[1] The magnetic phase diagram of MnSi has been studied by neutron small angle scattering[1], ultrasonic attenuation[2], ESR[3] and other techniques[4]. The results near T_c is reproduced in Fig.1. We have studied by neutron small angle scattering the magnetic phase diagram in the vicinity of T_c with the intention (i)to determine the magnetic structure of phase A predicted by many techniques and (ii)to determine accurately the temperature variation of the sublattice magnetization $\langle S_q(T)\rangle$ in zero field near T_c. The latter problem is related with the fact that the magnetic phase boundary $H_c(T)$ drops almost discontinuously to zero at T_c, suggesting that the phase transition at T_c is of the first order. The mean field theories suggest that $H_c(T)$ is proportional to $\langle S_q(T)\rangle$[5)6)7)].

A [100] cylindrical single crystal was mounted in a low temperature cryostat with a cryopump (Cryo-Mini) and the measurement was carried out with SAN in a magnetic field less than 5kOe. The intensity of the satellite peak measured by different wave lengths was found to be free from the extinction effect near T_c and $\langle S_q(T)\rangle$ thus obtained is also plotted by a chain line in Fig.1 after normalized by $H_c(0)/\langle S_q(0)\rangle$. The result shows clearly that $H_c(T)$ deviates substantially from $\langle S_q(T)\rangle$. In Fig.2 are displayed the two dimensional scattering patterns in the (110) reciprocal plane when the magnetic field is applied at 28K in the horizontal direction ([1$\bar{1}$0]). The solid lines are the contour maps of the equal intensities written in logarithmic scale. When the magnetic field of 1kOe is applied(Fig.2(b)), the direction of the q vector of the helical structure coincides with the field direction and in a field of 2kOe(Fig.2(c)) which corresponds to the phase A in Fig.1, the satellites disappear with only an isotropic ring around the center, suggesting that the magnetic structure in the phase A is almost the same as that realized just above T_c in zero field; the state is paramagnetic. When the field is

increased to 4kOe(Fig.2(d)),however,the satellites recover again in the field direction with the short range order developing around them. In Fig. 3 are plotted the intensity of Bragg peaks as well as that of the ring ridge between the satellite against the applied field. The results suggest strongly that the phase A is "paramagnetic".

The magnetic phase diagram of MnSi has been discussed by Kataoka-Nakanishi[6] and Plumer-Walter.[7] Although the latter authors have argued that the phase A is paramagnetic[7], it is because of the deviation of q vector from the field direction, which is actually not the case. Although the origin of the phase A is still unclear, it should be pointed out that the existence of this phase is related with the fact that $H_c(T)$ varies with temperature much slower than $\langle S_q(T) \rangle$ near T_c; there should exist a mechanism which stabilizes the helical structure by increasing the static component $\langle S_z \rangle$ of the magnetization. A simple calculation based on this model, however, failed to explain the phase diagram.

References

1) Y. Ishikawa, K. Tajima, D. Bloch and M. Roth ; Solid State Commun. 19(1976) 525.
2) S. Kusaka, K. Yamamoto, T. Komatsubara and Y. Ishikawa ; Solid State Commun. 20(1976)927.
3) M. Date, K. Okuda and K. Kadowaki, J.Phys.Soc.Jpn 42(1977)1555.
4) K. Kadowaki, K. Okuda and M. Date ; J. Phys.Soc.Jpn 51(1982)2433.
5) T. Moriya; Solid State Commun. 20(1976)291.
6) M. Kataoka and O. Nakanishi ; J.Phys.Soc.Jpn 50(1981)3888.
7) M.L.Plumer and M.B. Watler ; J.Phys.C14('81)4689.

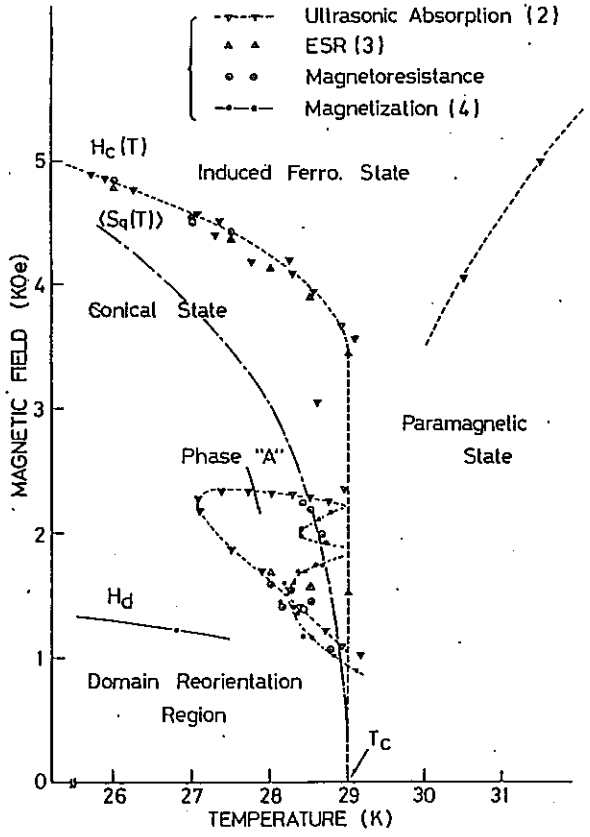

Fig.1 Magnetic phase diagram of MnSi near the critical temperature.

Fig.2 Two dimentional display of small angle scattering from MnSi at 28K in various magnetic fields.

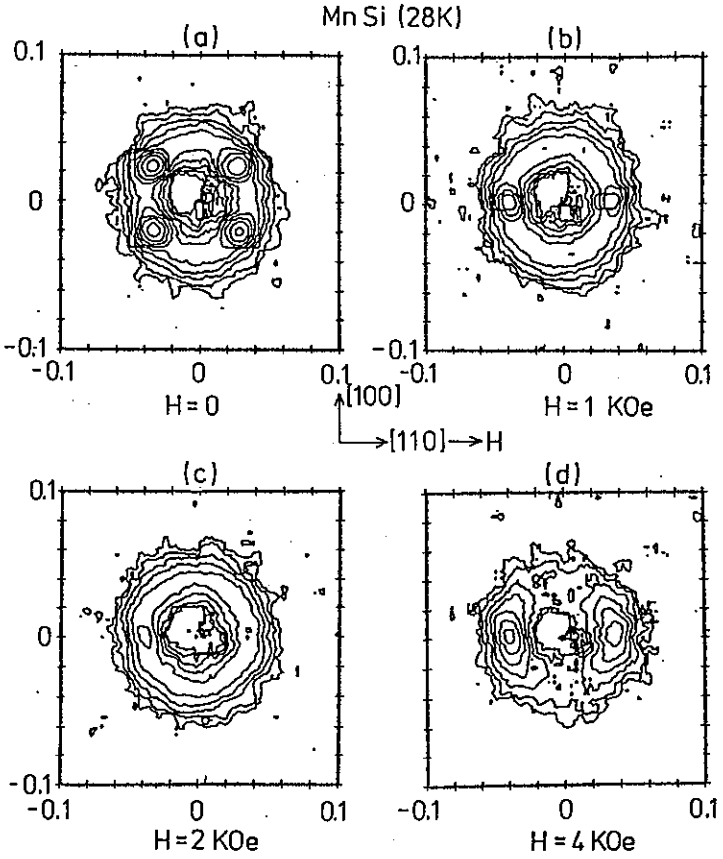

Fig.2

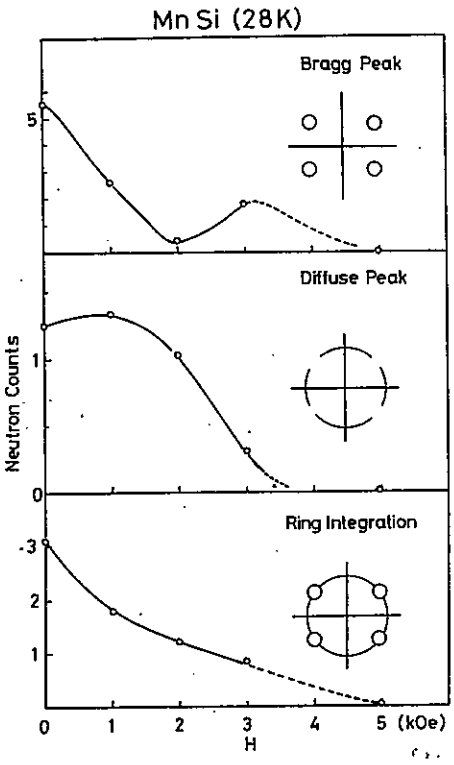

Fig.3 Field dependence of scattering intensity at 28K.

Small Angle Scattering of $Cr_{1/3}NbS_2$

Masatoshi Arai, Yoshikazu Ishikawa and Tomonao Miyadai[†]

Department of Physics, Faculty of Science, Tohoku University, Sendai, 980, Japan,
[†]Department of Physics, Faculty of Science, Hokkaido University, Sapporo, 060, Japan.

We have performed small angle scattering measurements on a powder sample of $Cr_{1/3}NbS_2$ by means of the Small Angle Neutron Scattering Instrument (SAN), and observed a long period helical spin structure.

$Cr_{1/3}NbS_2$ is an intercalate of 2H-type NbS_2 with layer structure and is reported as a metallic ferromagnet[1]. Cr is considered to be in the trivalent state and to have a localized moment. Cr atoms form an h.c.p. lattice. According to our magnetic measurements[2] on single crystals, this compound is approximately an easy-plane type ferromagnet. The magnetization curve along the hard axis (c axis) shows a usual form which is observed for a uniaxial ferromagnet. However, the magnetization curve in the c plane shows a metamagnetic behavior, although the critical field of which is as low as about 1.5 kOe. We supposed a helical structure with the spins in c plane and with its wave vector q along c axis. We made neutron diffraction measurements on a powder sample. We could not detect any satellite but were able to fit the observed powder pattern by the ferromagnetic order with the spins in c plane. However, there remained a a possibility of a long period helical structure, considering that the observed nuclear relfections include the magnetic part in its width. Moriya et al[3] argued the possibility of the helical spin structure due to the antisymmetric exchange interaction and estimated a long period of 480 Å ($Q = 0.013$ Å^{-1}) for this compound from the observed magnetic data including the critical field of the metamagnetic behavior.

The purpose of this paper is to detect the existence of the long period helical spin structure. We have made small angle scattering measurements on the powder sample of about 5g, which was used for the earlier neutron diffraction measurements. The sample was mounted in a

cylindrical aluminium-vessel. Measurements were made at 13K, 100K using a refrigerator and at RT. A strong small-angle scattering was observed at RT, presumably because of fine particle size of the sample. However, as shown in Fig.1, a clear magnetic Bragg peak was detected at Q = 0.013 ± 0.0005 $\mathring{A}^{-1}$, by subtracting the RT data from those at low temperatures. Further, the intensty of the peak at 100 K relative to that at 13 K is in good agreement with the temperature dependence obtained from the magnetic measurements. In Fig.2, the values of the magnetization determined by the present data are indicated by crosses. The value of Q remains unchanged at both temperatures.

Thus we confirmed the existence of the helical spin structure with a long period, and the measured period is in excellent agreement with the one estimated by Moriya et al[3]. The present results are included in reference 4).

The authors would like to thank Prof. H. Kondo of Saitama University for providing them with the sample. One of the authors (T.M.) also thanks Prof. T. Moriya for the theoretical side of the present work.

1) F. Hulliger and E. Pobitschka: J. Solid State Chem. 1 (1970) 117.
R. H. Friend, A. R. Beal and A. D. Yoffe: Philos. Mag. 35 (1977) 1269;
S. S. P. Parkin and R. H. Friend: ibid. 41 (1980) 65, 95.
2) T. Miyadai, K. Kikuchi, H. Kondo and S. Sakka: Ferrites; Proc. Int. Conf. on Ferrites (Kyoto, 1980) p.922.
3) T. Moriya and T. Miyadai: Solid State Commun. 42 (1982) 209.
4) T. Miyadai, K. Kikuchi, H. Kondo, S. Sakka, M. Arai, and Y. Ishikawa: J. Phys. Soc. Jpn. 52 (1983) 1394.

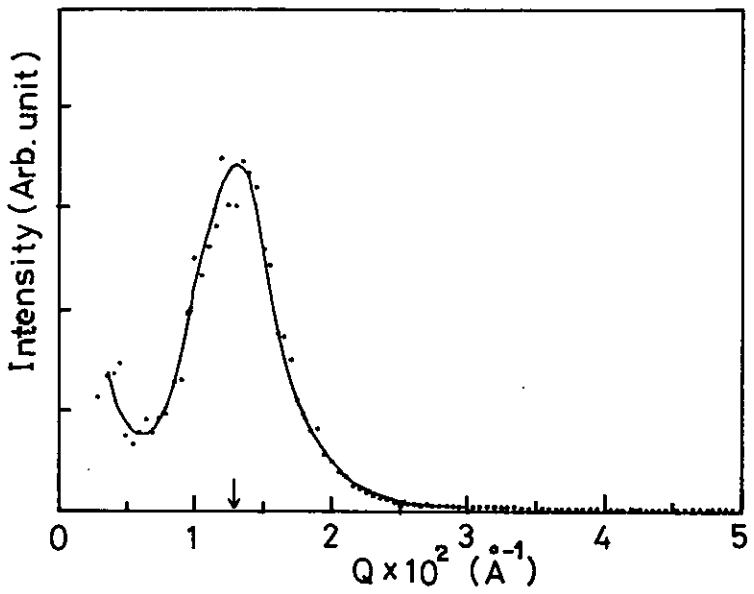

Fig. 1. One dimensional display of small angle scattering at 13 K obtained by summing all data with the same |Q| around (0,0,0). The data at room temperature was subtracted as the background.

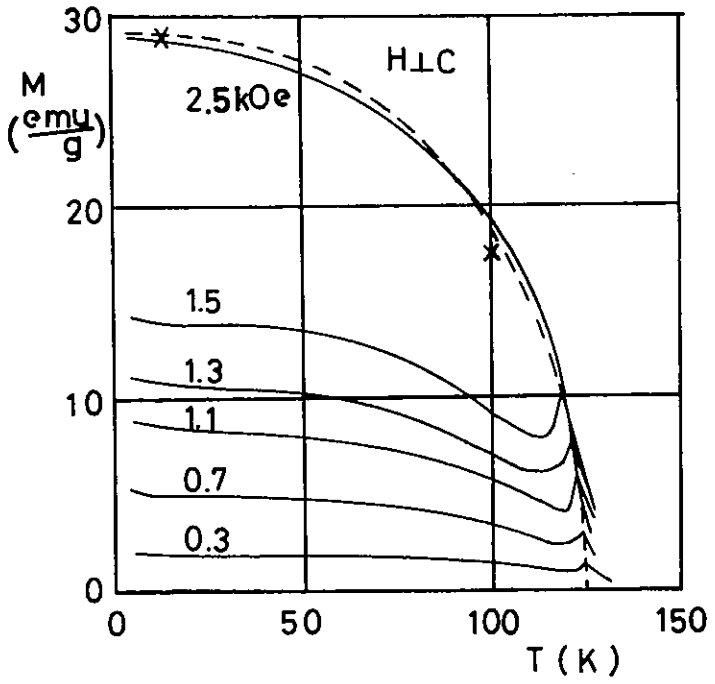

Fig. 2. Temperature variations of the magnetization in c-plane (H⊥C) at various fields (the solid curves), Crosses denote the magnetization estimated from the present data (normalized at 13 K).

Magnetic correlations in a competing interaction system, $79FeTiO_3$-$21Fe_2O_3$ with re-entrant spin glass properties

M. Arai, Y. Ishikawa, N. Saito and H. Takei*

Physics department, Institute for Iron Steel and Other Metals, Tohoku University, Sendai 980

The paper discusses the re-entrant behaviors newly found in a randomly mixed oxide system with competing interactions, $79FeTiO_3$-$21Fe_2O_3$. This is an extention of a previous study of $88FeTiO_3$-$12Fe_2O_3$ with the cluster type spin-glass behaviors[1]. As the concentration of Fe_2O_3 exceeds over the percolation limit to have the ilmenite-hematite type ferrimagnetic order[2], the sample becomes ferrimagnetic below 220K and the re-entrant spinglass behaviors appear below T_g^R=80K as shown in the inset to Fig.2; the magnetization along the c plane measured in a weak magnetic field of 10 Oe exhibits a substantial decrease below T_g^R.

The temperature evolution of the magnetic correlation around (0,0,0) has been studied by small angle neutron scattering (KENS-SAN). Typical examples of the two dimensional displays of the scattering measured at four different temperatures are shown in Fig.1., where the scattering intensity at room temperature had been subtracted as background. In the figure the c* axis nearly concides with the horizontal direction. The figure shows clearly that the magnetic correlation is quite anisotropic. Moreover the direction of the anisotropy does not vary with temperature; the spins are mainly confined in the c plane.

The magnetic correlation between the parallel and perpendicular components was found not to be able to be separated from the small angle scattering data, in contrast with the previous case of $88FeTiO_3$-$12Fe_2O_3$. This is because $\langle S^{\alpha}_{-q} S^{\alpha}_{q} \rangle$ was found to be strongly anisotropic with respect to the q direction. Therefore only the spin correlation between the perpendicular components $\langle S^{\perp}_{-qc} S^{\perp}_{qc} \rangle$ was estimated from the scattering profile along the c* axis and was analyzed by the combination of two functions of Lorentzian and squared Lorentzian;

$$\langle S^{\perp}_{-q} S^{\perp}_{q} \rangle = \frac{A}{\kappa^2 + q^2} + \frac{B}{(\kappa^2 + q^2)^2} \qquad (1)$$

The temperature evolution of A and B is plotted against temperature in Fig.2. In the vicinity of the Curie-temperature, the scattering profile has predominantly the Lorentzian shape as is anticipated for the critical scattering. However below 100°K the squared Lorentzian term becomes significant, suggesting that the ferromagnetic region is decomposed into a domain state by the random field from the surrounding spin glass clusters. Note that B takes a maximum around T_g^R, but it increases again below 60K.

The temperature evolution of $\kappa_\perp$ determined by eq(1) is displayed in Fig.3. The inverse correlation length $\kappa_\perp$ takes a weak minimum at T_c=220K and decreases again further with decreasing temperature below T_g^R. The behavior is quite similar to what have been observed for a number of re-entrant spin glass system as Fe_xCr_{1-x}[3], $(Fe_xMn_{1-x})_{75}P_{16}B_6Al_3$ (amorphous system)[4], but different behaviors have been observed for $Eu_xSr_{1-x}S$[5] and Fe_xAl_{1-x}[6]. Note that we have found that by the measurement of Bragg peak with TUNS(JAERI), the c axis component starts to develope below 80K. It can therefore be anticipated that the development of the correlation below T_g^R would be related with the development of the long range order along the c axis. Gabay and Toulouse has suggested[7] that the spin correlation in the perpendicular directions can possibly behave in the quite different ways in the re-entrant spin glass system. Our mixed oxide system with the large anisotropy may provide an experimental support to this theory.

References

(1) Y. Ishikawa, M. Arai, N. Saito, M. Kohgi and H. Takei
J. Mag. Mag. Mats. 31(1983)1381

(2) G. Shirane, S. J. Pickart, R. Nathans and Y. Ishikawa
Phys. Chem. Solids 10(1959)35.

(3) S. K. Burke and B. D. Rainford
J. Phys. F 13(1983)471

(4) B. D. Rainford, S. K. Burke, J. R. Davis and W. Howarth
1982 Am. Inst. Phys. Conf. Proc. to be published.
G. Aeppli, S. M. Shapiro, R. J. Birgenean and H. S. Chen
Phys. Rev. B25(1982)4882

(5) H. Maletta, G. Aeppli and S. M. Shapiro
Phys. Rev. Lett. 48(1982)1490

(6) S. M. Shapiro et.al. to be published.

(7) M. Gabay and G. Toulouse
Phys. Rev. Lett. 47(1981)201

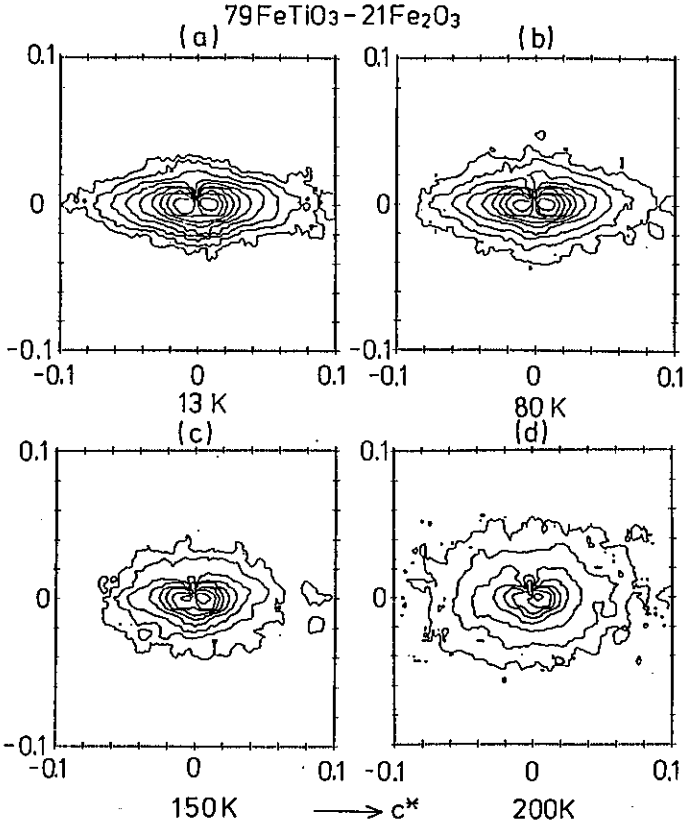

Fig.1 Two dimensional display of small angle neutron scattering from $79FeTiO_3$-$21Fe_2O_3$ at different temperatures.

Fig.3 Temperature evolution of inverse correlation length of in plane spin correlation.

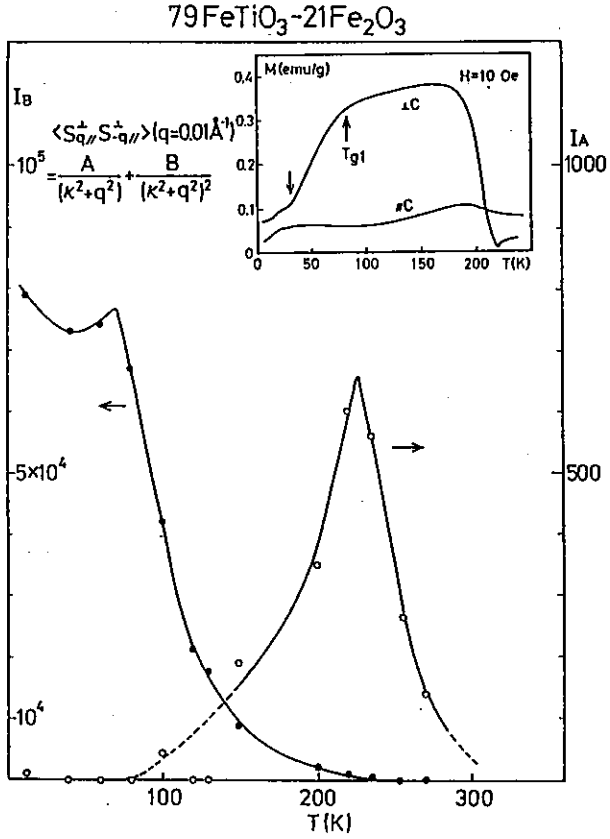

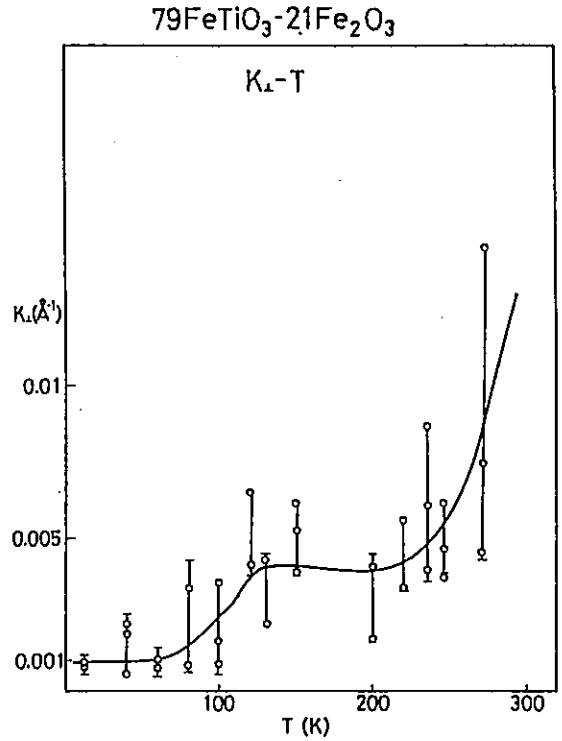

Fig.2 Temperature evolution of magnetic correlation of inplane spin components analyzed by Lorentzian (I_A) and squared Lorentzian (I_B) terms.

Magnetic correlations in a competing interaction system $88FeTiO_3$-$12Fe_2O_3$ with spin glass behaviors II

M. Arai, Y. Ishikawa and H. Takei*

Physics department, *Institute for Iron, Steel and Other Metals, Tohoku University, Sendai 980

$88FeTiO_3$-$12Fe_2O_3$ exhibits the typical cluster type spin glass properties below 38K. The evolution of magnetic correlation has been studied by neutron small angle scattering (KENS-SAN) using a single crystal. A preliminary result was reported in a previous paper[1]. This paper discusses the results of the detailed analysis.

We have found that the profiles of the two dimensional display of small angle neutron scattering can be reproduced by the magnetic correlations between the parallel components $\langle S^{//}_{-q} S^{//}_{q} \rangle$ and perpendicular ones $\langle S^{\perp}_{-q} S^{\perp}_{q} \rangle$, where "parallel" is referred to the c axis. This indicates that $\langle S^{\alpha}_{-q} S^{\alpha}_{q} \rangle$ is isotropic with respect to the q direction as was anticipated in the previous paper[1]. The magnetic correlations have been fitted by two functions, Lorentzian and squared Lorentzian.

$$\langle S^{\alpha}_{-q} S^{\alpha}_{q} \rangle = \frac{A}{\kappa_\alpha^2 + q^2} + \frac{B}{(\kappa_\alpha^2 + q^2)^2}, \qquad (1)$$

where $\alpha = //$ or $\perp$, and the inverse correlation lengths for both component correlations are plotted against temperature in Fig.1. The inverse correlation length of the perpendicular components $\kappa_\perp$ decreases linearly with decreasing temperature down to 50K($=T_N$) where the parallel components start to appear. Moreover the parallel inverse correlation length $\kappa_{//}$ has the minimum around 30K, in contrast with the behaviors in the percolation limit materials[2]; the transverse component correlation $\kappa_\perp$ for a one-dimensional anisotropic chain shows a weak minimum, whilst the longitudinal component tends to divergent ($\kappa_{//} \to 0$) at low temperatures. This tendency in κ can be explained by the evolution of antiferromagnetic correlation in the cluster below T_g, which suppresses the development of the ferromagnetic correlations. In Fig.2 are shown the temperature evolution of the antiferromagnetic and ferromagnetic correlations at $q = 0.048\text{Å}^{-1}$, the former information was obtained

from the diffuse scattering around (1,0,-0.5).

The magnetic radial distrubution function RDF was calculated by the Fourier-transform of the scattering functions for both components. The RDF obtained at different temperatures is displayed in Fig.3, which shows clearly (i)that the ferromagnetic (ferrimagnetic)correlation extends to 125A, accompanied by another ferromagnetic regions with the spins antiparallel to the central cluster, (ii)that the antiferromagnetically coupled configuration persists even above T_g(=38°K) where the sample behaves superparamagnetic and (iii) that there is a rotation of the spin axis in the cluster from the c plane (above 50K) to the c axis (below T_g) without a substantial change of the cluster size. In Fig.4 are plotted the average angle of the spin from the c plane estimated from the ratio of $\langle S''_{-q} S''_{q}\rangle / \langle S^{\perp}_{-q} S^{\perp}_{q}\rangle$ at different q values. The value of 60 degrees at the lowest temperature is consistent with the result obtained by Mössbauer effect[3].

References

1). Y. Ishikawa, M. Arai, N. Saito, M. Kohgi and H. Takei, J. Mag. Mag. Mats 31-34 (1983) 1381

2). P. B. Stinchcombe, J. Phys. C13 ('80) L133

3). A. Itoh, Private communication

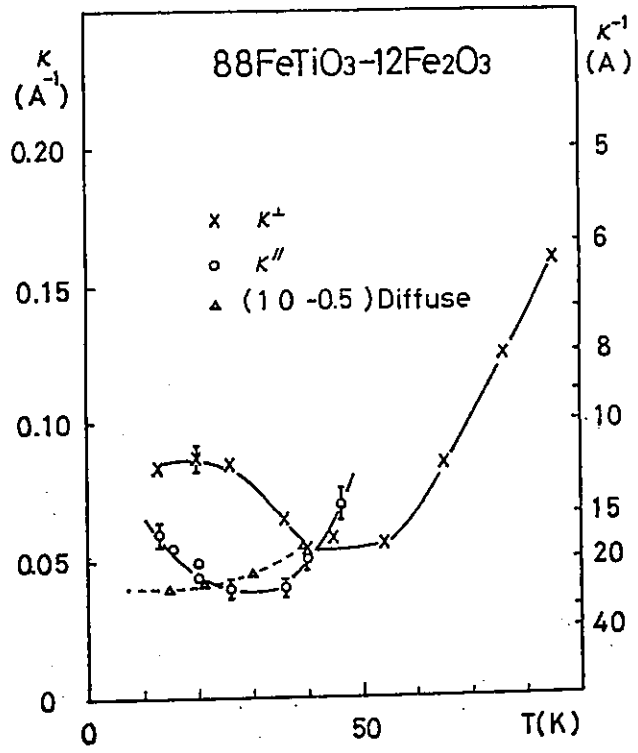

Fig.1 Temperature dependence of inverse correlation lengths of perpendicular spin correlation $\kappa_{\perp}$ and of parallel correlation $\kappa_{//}$. Δ : that of antiferromagnetic correlation.

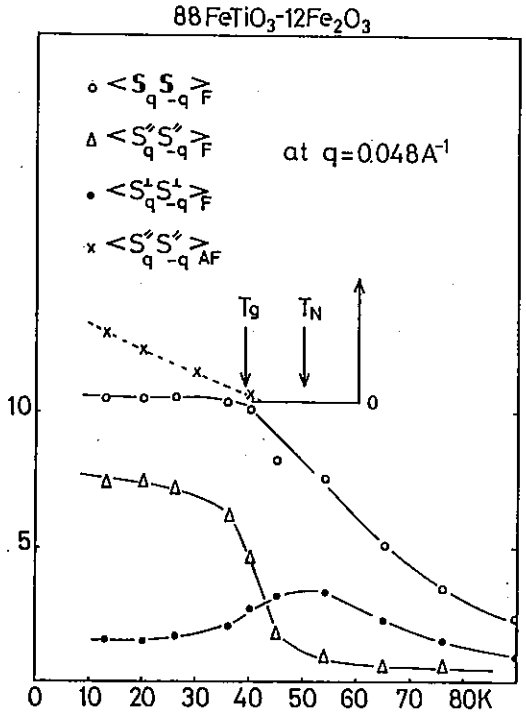

Fig.2 Temperature dependence of spin correlation at $q = 0.048A^{-1}$.

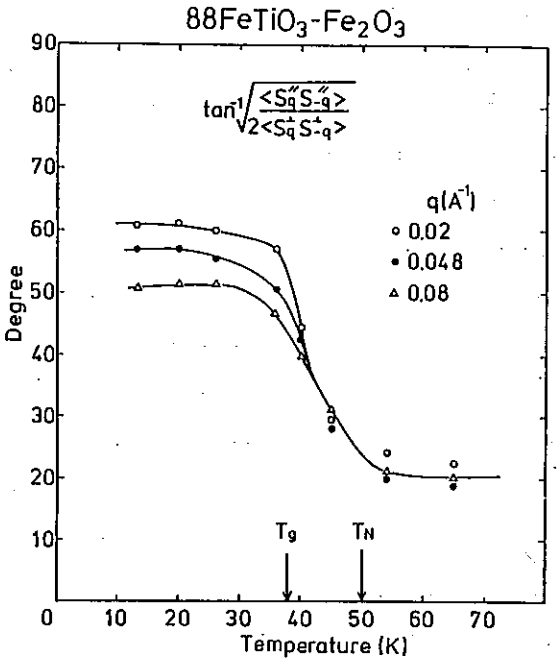

Fig.4 Temperature dependence of average rotation angles of spins from the c plane.

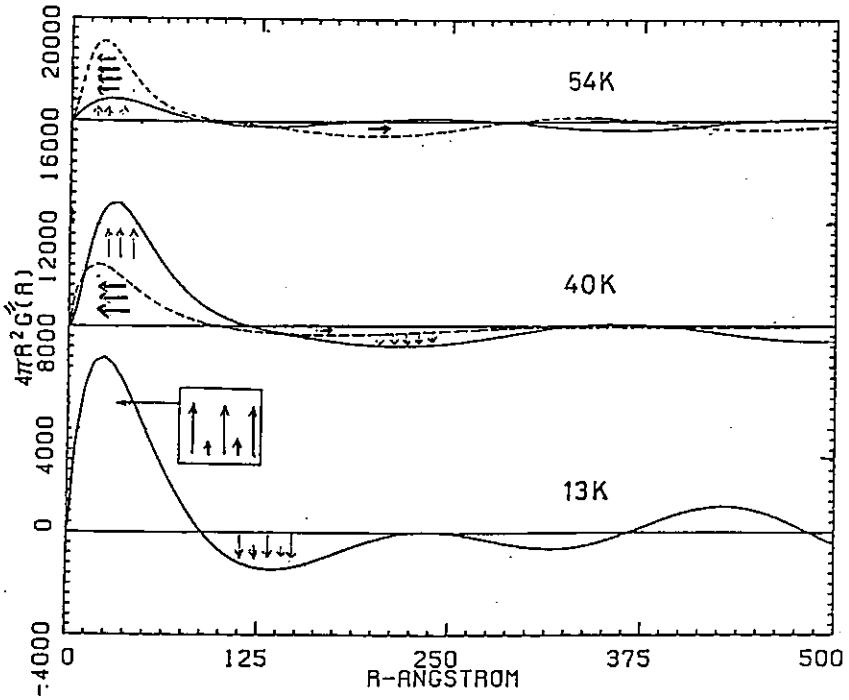

Fig. 3 Temperature variation of randial distribution function of parallel spin component R"(r) (——) and that of perpendicular component (.....).

Real time neutron spectroscopy by means of small angle neutron scattering (KENS-SAN)

Y. Ishikawa, M. Arai, M. Furusaka and M. Mera

Physics Department of Tohoku University, Sendai 980

The paper reports a preliminary result of the real time spectroscopy measurements using small angle neutron scattering instrument SAN. By the real time spectroscopy we mean a technique to study in real time the slow relaxation phenomena with the relaxation time slower than μsec. The method consists of varying abruptly an external condition as magnetic or electric field, pressure or temperature and measuring in real time the temporal variation of the state which is induced by the external force.The SAN is the most promissing for this kind of measurements, because it is the semi-macro structure which has a long relaxation time. The block diagram of the data acquisition system to practise the measurement is shown in Fig.1(a) and (b). Two kinds of signals are supplied from the booster proton synchrotron to the microprocesser (LSI11/23) through CAMAC data way. One is the 20 Hz B-TOP pulse produced in synchronizing with the synchrotron and another is the gate pulse which is switched on only when the protons come to the neutron target (Fig.1 (b)). By using these two signals, the processer controls the time of changing the external condition as well as the mode of data acquisition. When the relaxation time is much slower than 50msec; the time of one neutron burst measurement, the external condition is kept constant over the several neutron pulses, and the 88K words neutron scattering data obtained for each neutron burst through the multi-dimensional time analyzer is transfered as one set to one data accumulation area (f,ex,AREA 1 in Fig.1(a)) in the external bulk memory. (BLM,2M bytes). The next set of 88 K words can be stored in the next area, and in this way eight different states successively induced by a change of the external condition can be measured. The change of the external condition is repeated synchronizing with the neutron spulses until the statistics of the data accumulated in each area become satisfactory. All data are then sent to the central mini-computor OKITAC50/60 for further analysis and are displayed through one of the peripheries. If the relaxation time is faster than 50msec, the data in each channel can give an information on a state at the different time. The relax-

ation time of order of1 msec or less can,in principle,be measured with SAN.

We have applied this technique to study the relaxation phenomena in the magnetization process in the cluster type spin glass $88FeTiO_3$-$12Fe_2O_3$ at low temperatures. It has been reported that the relaxation time becomes significantly long below T_g and it cannot be measured by a conventional method of inelastic scattering. A small electromagnet which can apply the square magnetic field of 5kOe with a rising time of 8msec was specially made by using thin plates of Fe-Si steel for the commercial transformer. The decending time was found to be about 20msec. Typical examples of measurements in cases of applying and switching off the magnetic field of 5kOe along the c*axis are shown in Fig.2 and 3 respectively, where the temporal variation of the scattering intensity at 13K are plotted against the measured time t. In the upper part of Fig.2 are also shown two dimensional displays of small angle scattering for three different states. Note that the relaxation time is shorter for larger valuse of q and the relaxation time is of the order of 100msec for q=0.03. The results show clearly that this type of measurement can successfully be carried out with SAN. The quantitative analysis of the data as well as the measurements at different temperatures are now in progress.

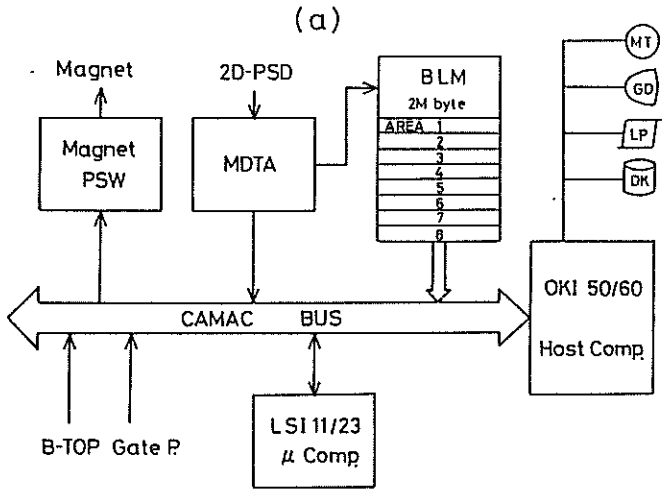

Fig.1(a) Block diagram of the data acquisition system of SAN for real time spectroscopy.

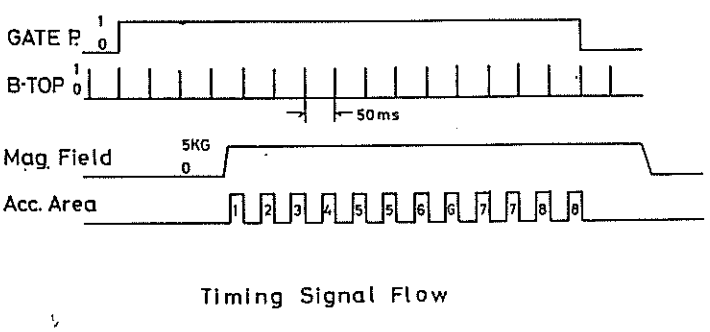

Fig.1(b) Signals controling the time sequence of measurements.

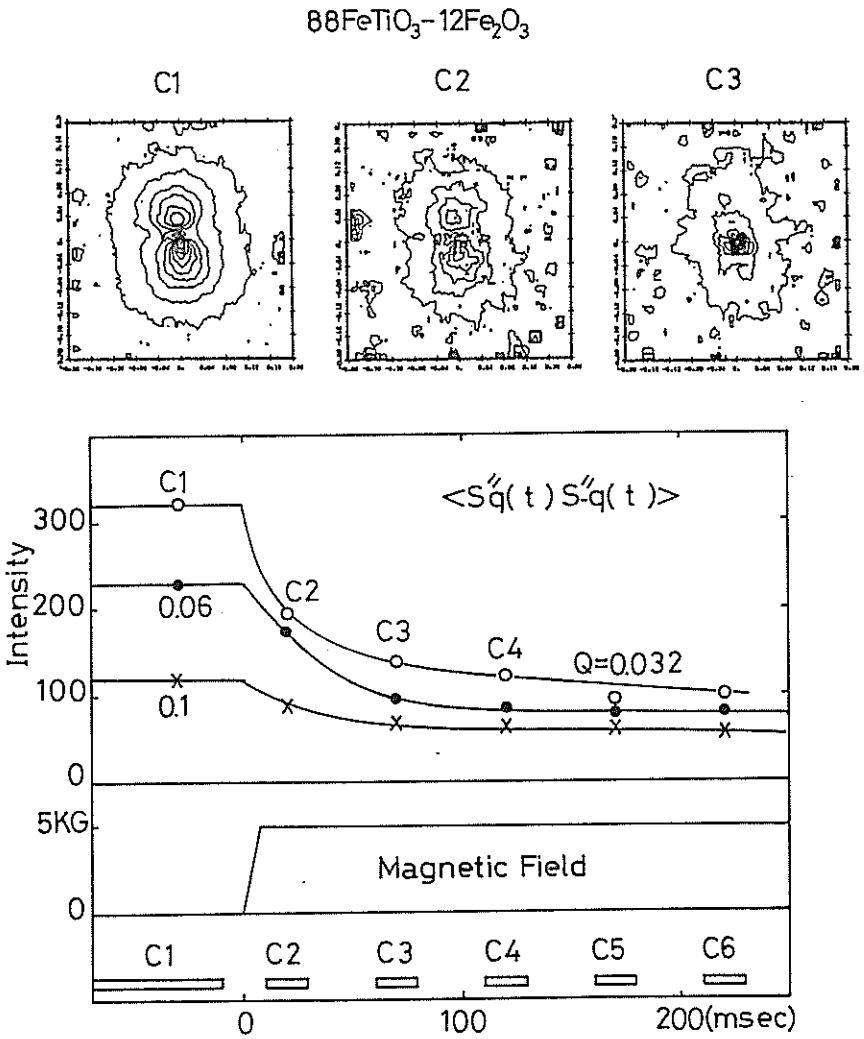

Fig.2 Temporal variation of intensity of small angle neutron scattering when pulsed magnetic field of 5kOe is applied to a cluster type spin glass $88FeTiO_3$-$12Fe_2O_3$.

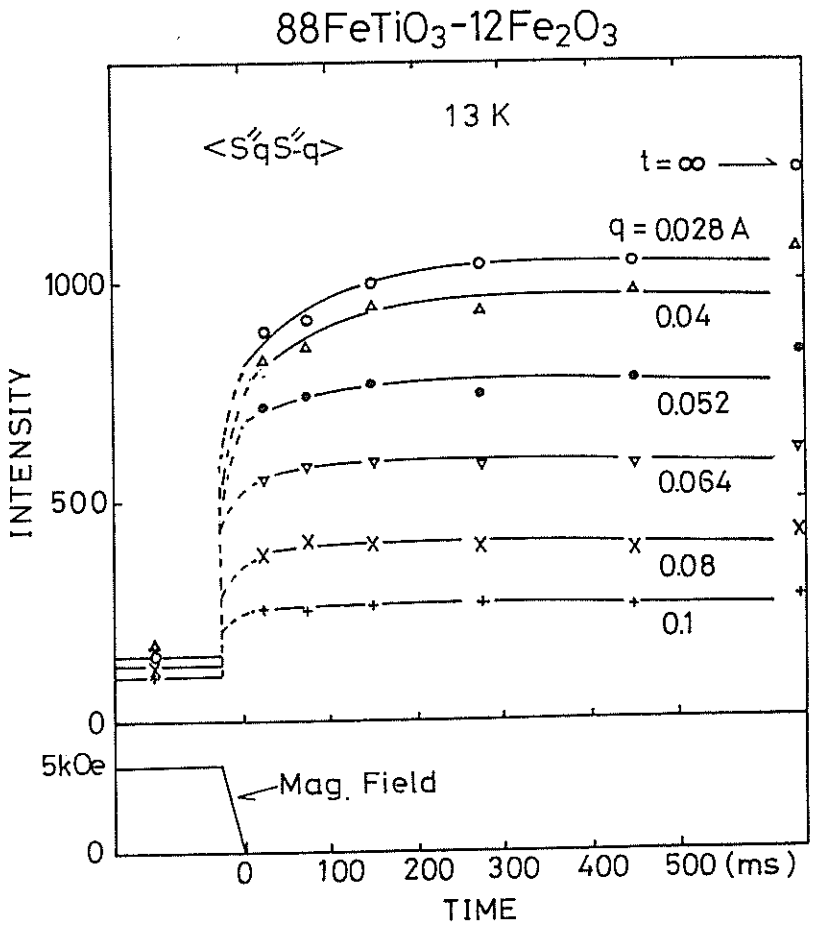

Fig.3 Temporal variation of intensity of small angle neutron scattering when a pulsed magnetic field of 5kOe is switched off.

Spinodal Decomposition in FeCr Alloys Studied by Small Angle Neutron Scattering II

M. Furusaka and Y. Ishikawa

Physics Department of Tohoku University, Sendai, 980, Japan

The kinetics of spinodal decomposition in FeCr alloys has been studied by small angle neutron scattering instruemt(SAN) installed at KENS. Experimental results were reported in earlier papers[1),2)], which showed clearly that the Cahn's linear theory did not work even in the early stage of decomposition. In this paper we attempt to analyze the results based on the current non-linear theory develloped by Langer, Bar-on and Miller[3)] (hereafter referred to as LBM).

According to the theory of LBM, the kinetic equation is written as follows.

$$\frac{dS(k,t)}{dt} = -2MKk^2\{k^2 + \frac{A(k,t)}{K}\} + 2Mk_BTk^2 , \qquad (1)$$

where $S(k,t)$ is k dependent scattering function. M and K are mobility and energy gradient coefficent respectively, T is temperature and k_B the Boltzman constant. $A(k,t)$ in Eq.(1) is given by

$$A(k,t) = \sum_{n=2}^{\infty} \frac{1}{(n-1)!} \frac{\partial^n f}{\partial c_o^n} \frac{S_n(k,t)}{S(k,t)} , \qquad (2)$$

with $S_n(k,t)$ the Fourier transform of the higher order correlation functions and $\partial^n f / \partial c_o^n$ the n th derivative of the free energy with respect to the concentration c_o.

If we assume that $A(k,t)$ is time independent, A, the solution of Eq.(2) is given by

$$S(k,t) = \{S(t=0) - S_\infty\} e^{-2MKk^2(k^2+A/K)\cdot t} + S_\infty , \qquad (3)$$

where S_∞ is the stationary solution of $S(k,t)$ and is given by

$$S_\infty = \frac{k_BT/K}{k^2+A/K} . \qquad (4)$$

If the values of parameters M, A and K are properly chosen, Eq.(3) is found to reproduce the experimental observations satisfactorily as are shown in Fig.1. The solid lines are calculated by Eq.(3) and the squares represent experimental results of Fe - 40at%Cr annealed at 515 C, a temperature close to the classical spinodal line.

It should be noted the value of A obtained by the least square's fit to data is not time independent, and also S_∞ determined from Eq.(3) is not the real stationary sate. In order to resolve this inconsistency, we determined the temporal variation of A(k,t) directly from the experimental results. For this purpose we modified Eq.(1) as follows

$$k^2 + \frac{A(k,t)}{K} = -\frac{1}{2MK}\frac{1}{k^2 S}\frac{dS}{dt} + \frac{k_B T}{KS} \quad , \tag{5}$$

and calculate the right hand side by employing S and dS/dt experimentally measured. For MK and $k_B T/K$ we adopted the values determined in previous analyses. The results of calculations for Fe - 40at%Cr annealed at 515 C are displayed in Fig.2. In the figure a dushed line represents the relation, $f(k) = k^2 + C$, which indicates clearly that $k^2 + C$ really holds for each curve in a wide range of k. This is another experimental support that Eq.(1) reproduces the experimental results. Below $k = 0.08\ A^{-1}$, a clear deviation of the calculated curve from this relation occurs, where other mechanics of scattering may become important. The temperature dependence of A/K obtained by this analysis is plotted in Fig.3, where the results obtained for Fe - 30at%Cr are also presented. In the inset to the figure, the time dependence of μ ($\propto$ - A/K) calculated based on LBM theory[3] at the classical spinodal line is also reproduced for reference.

Note that μ starts from zero because the second derivertive of the free energy must be zero at the spinodal line. Then influenced by higher order terms of A(k,t), μ goes negative but quickly changes sign and stays rougly constant at a small positive value. Our experimental results of the time dependence of A(k,t)/K are in reasonalbe agreement with this behavior, if we assume that our observation is a time range between $2 \leq \tau \leq 10$. Note that the time dependences of A/K, for Fe - 30at%Cr which were annealed above the spinodal line are also quite similar to those for Fe - 40at%Cr. This provides another evidence that the higher order terms play an important role for the decomposition process near the spinodal line.

In conclusion, the early stage of decomposition in FeCr alloy systems near the classical spinodal line could be quantitatively explained by the current theory of LBM. But the small deviation from the theory was detected

except at very early stage of the decomposition.

References

1) M. Furusaka, Y. Ishikawa, S. Yamaguchi and Y. Fujino : KENS REPORT III (1982)69.

2) M. Furusaka, Y. Ishikawa, S. Yamaguchi and Y. Fujino : Physics B120 (1983)383.

3) J. S. Langer, M. Bar-on and H. D. Miller : Phys. Rev. A11(1975)1417.

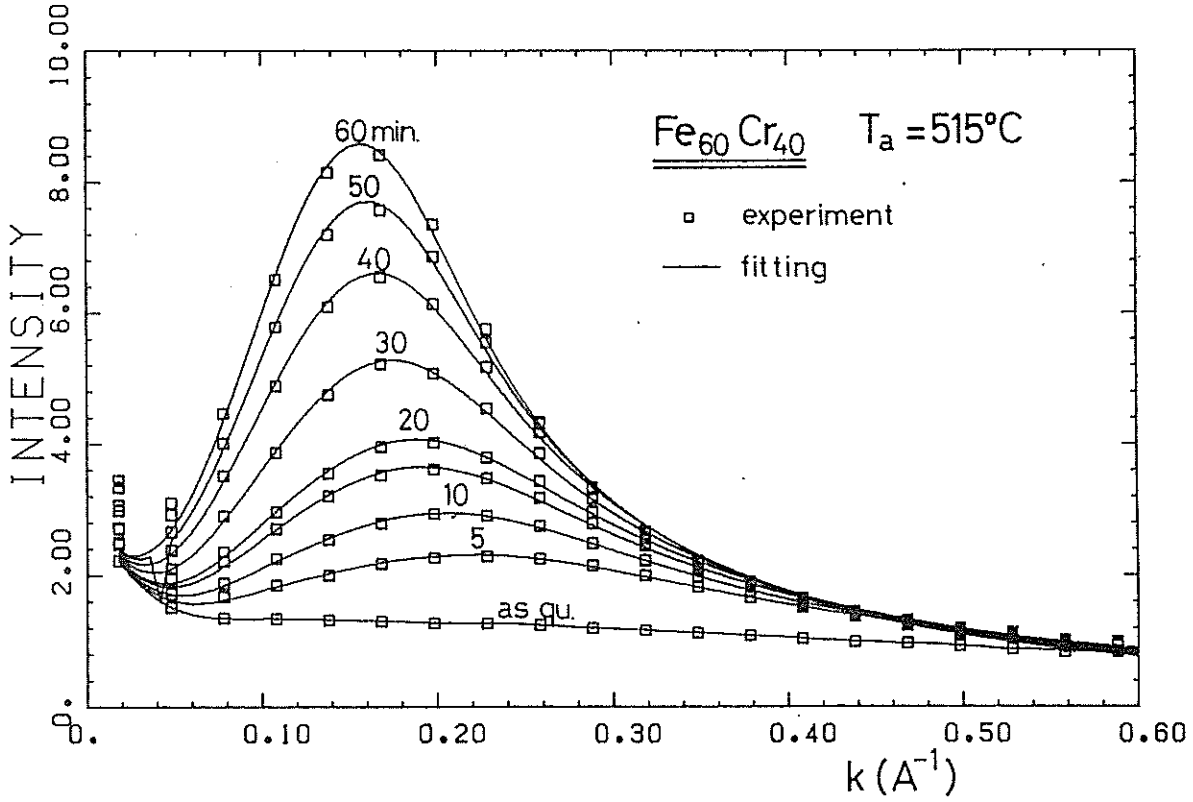

Fig.1. Time evolution of the scattering function S(k,t) of Fe -40at%Cr annealed at 515 C plotted as a function of k. Squares are the experimental results,while solid curves are calculated by Eq.(3) using parameters determined by least square's fit to data.

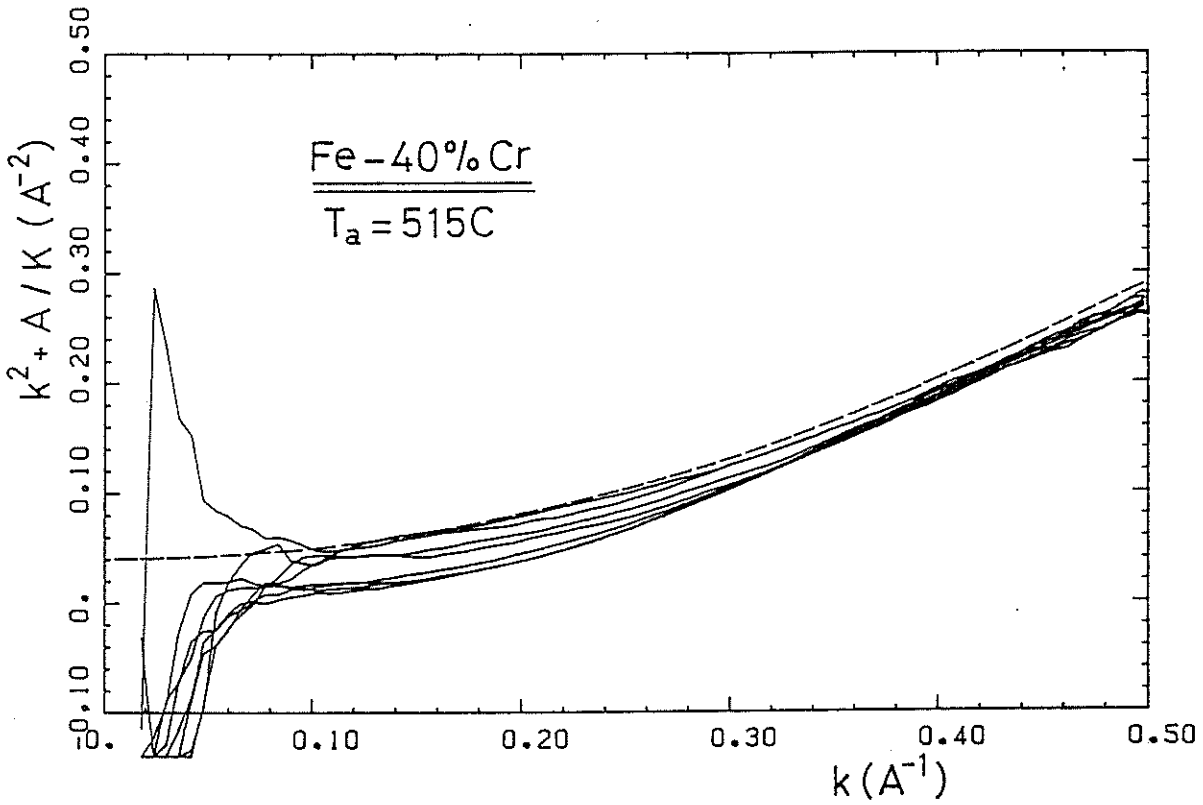

Fig.2. Time evolution of the function $k^2 + A(k,t)/K$ calculated by Eq.(5) using S and dS/dt experimentally obtained. Dashed line shows the relation $f(k) = k^2 + c$.

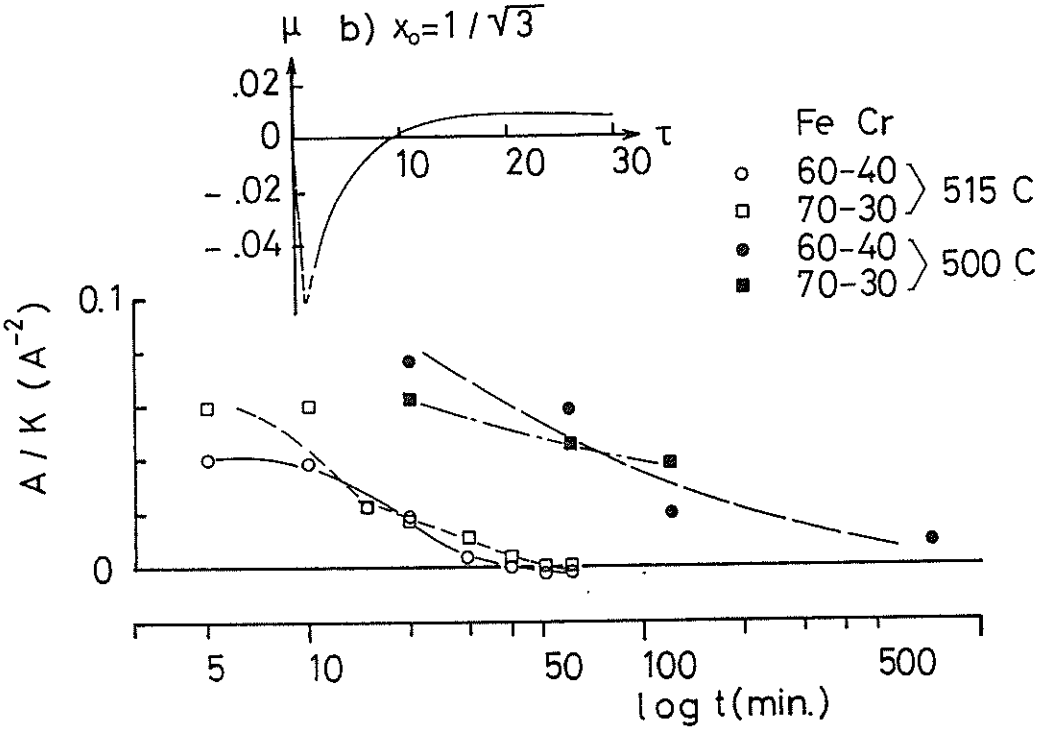

Fig.3. Time evolution of the value A(k,t)/K obtained from Fig.2. Time dependence of $\mu(\propto -A/K)$ at the classical spinodal line calculated by LBM[3] was reproduced in the inset to the figure.

In-situ measurement of phase separation in an Al-Zn alloy with SAN

M. Furusaka, M. Mera and Y. Ishikawa

Physics Department, Tohoku University, Sendai

A special furnace which makes possible the in-situ studies of phase separation by neutron small angle scattering has been installed at SAN in KENS and the very early stage of phase separation process in the Al-6.8at% Zn alloy at room temperature has been studied. The paper reports a preliminary result.

The measurement of the very early stage of phase separation is particularly of importance, because it is only this stage that the experimental results are crucially compared with the current theory made by Langer, Baron and Miller[1] or others[2,3,4,5]. Although the phase separation processes have been studied by a number of investigators for different alloy systems, only few data are available for the very early stage of decomposition. Futhermore, since the precipitated phase has a rather small size in the very early stage of phase separation, the measurements in the wide q range ($0.02 \leq q \leq 0.6 \mathring{A}^{-1}$) are indispensable, which is the privilege of KENS-SAN as shown in a previous study[6].

The outline of the in-situ annealing and quenching system is displayed in Fig.1. The sample was heated by an image furnace consisting of two infrared heaters and a nickel coated curved mirror to focuss the images of the heaters on the sample. The sample was suspended by a stainless tube in a transparent quartz tube 2mm thick and 26mm in diameter which was evacuated by a large rotary pump of 950ℓ/min to remove liquid nitrogen from the sample. The scattering chamber accommodating the image furnace was also evacuated by another vacuum pump to avoid the air scattering. The rapid quenching of the sample from the annealing temperature into a lower temperature (≅-150°C) was achieved by sending a flash of liquid nitrogen from a 100ℓ reservoir onto the sample through the stainless steel tube. The measurement was carried out at this temperature. The sample could be quenched with a cooling rate of 200°C /min but the heating rate was found to be rather slow; 50°C/min. The shortest annealing time achieved by the present experiment was about 1 min. The annealing temperature of 25°C was controlled within ± 1 degree by a convention-

al temperature controller with a cold nitrogen gas flow.

The sample was made by melting 99.999% Al and Zn by a HF furnace and was homogenized at 400°C for 12 hours in the image furnace, followed by quenching to -150°C to start the measurement. The sample was then annealed at 25°C which is below the spinodal line (129±2°C)[7] for a given time, followed by quenching again to -150°C to restart the measurement. The process was repeated until the total annealing time became 10 mins. The typical measuring time of neutron scattering was about 2hrs. The time was rather long because we needed a good statistics for the scattering at high q sides. The preliminary results of measurements are displayed in Fig.2. The results show clearly that (i)the Cahn's theory does not hold even at the very stage of decomposition; the peak of the scattering was continuously shifted to the lower q side with increasing the annealing time, (ii)no cross over phenomenon was observed at the very early stage ($t \leq 4$min) but (iii) the phenomenon seems to appear for longer annealing time ($10 \geq t \geq 5$min).

In conclusion the in-situ measurements of phase separation process at 25°C could be carried out for the wide q range ($0.02 \leq q \leq 0.6 \text{Å}^{-1}$) in an annealing time between 1 min and 10 min. If the heating system is improved to increase the heating rate, the phase separation in shorter annealing time (< 30sec) can be studied with our in-situ system.

References

1) J. S. Langer, M. Bar-on and H. D. Miller : Phys. Rev. A11(1975)1417.

2) K. Binder and D. Stuffer : Phys. Rev. Lett. 33(1974)1006.

3) Y. Saito : J. Phys. Soc. Jpn. 41(1976)1129.

4) J. Marro, A. B. Bortz, M. H. Kalos and J. L. Levowitz : Phys. Rev. B12 (1975)2000.

5) H. Furukawa : Phys. Rev. A23(1981)1535.

6) M. Furusaka, Y. Ishikawa, S. Yamaguchi and Y. Fujino : Physica, to be published.

7) A. Naudon, J. Alain, in collab. with J. Delafound, A. Junqua and J. Mimault: Scripta Met. 8(1975)1105.

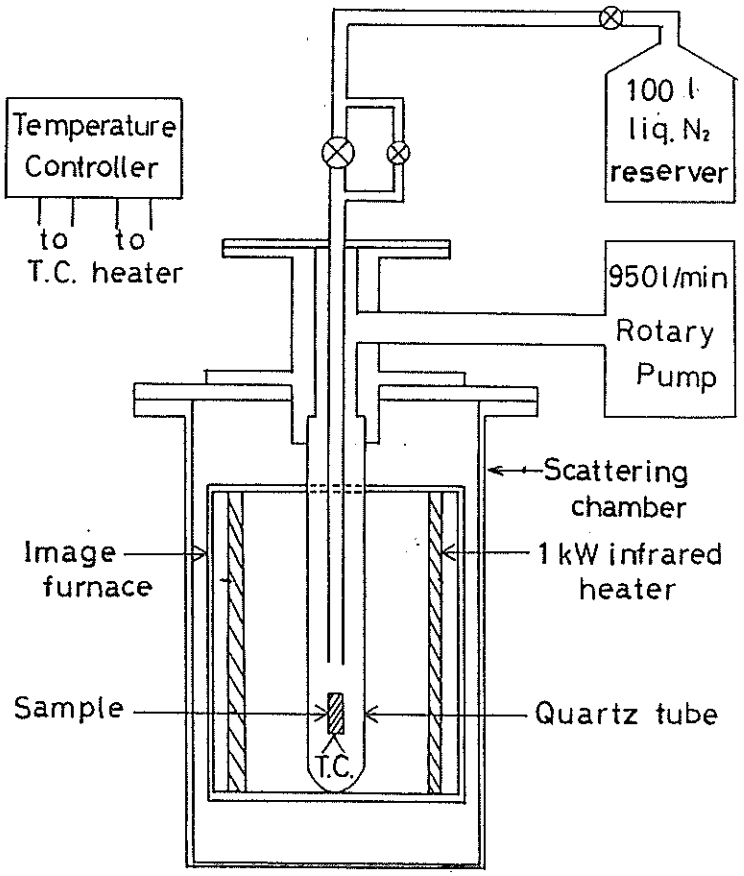

Fig.1 Schematic display of the in-situ annealing and quenching system.

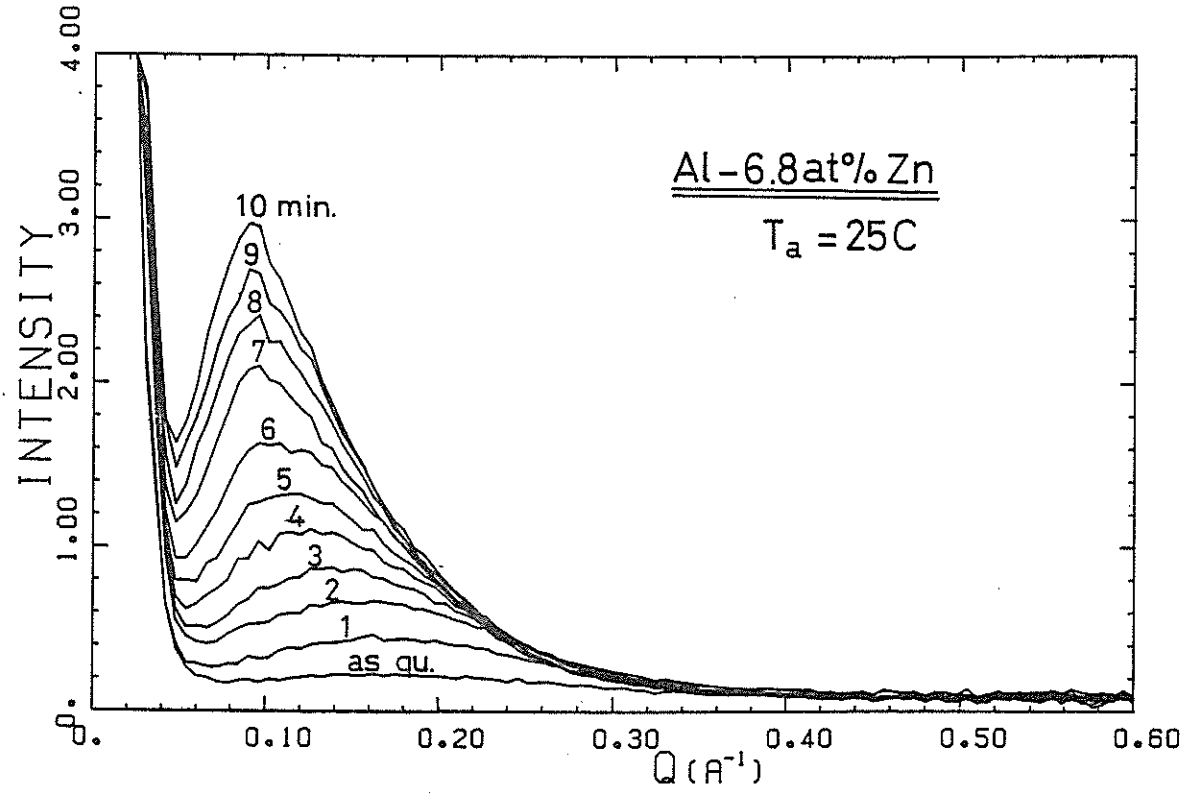

Fig.2 Temporal evolution of scattering intensity for Al-6.8%Zn anneal at 25°C plotted against q.

Small-angle Neutron Scattering from Semi-dilute Polymer Solutions near the Lower Critical Solution Temperature

Kimio Kurita, Shinya Nakajima, Osamu Ozawa, Takashi Nakamura, Tsuyoshi Iizuka, Eiichi Wada, Koji Okano*, Michihiro Furusaka** and Yoshikazu Ishikawa**

College of Science and Technology, Nihon University, Tokyo 101
*Department of Applied Physics, University of Tokyo, Tokyo 113
**Department of Physics, Tohoku university, Sendai 980

In the preceeding paper[1] we reported that for semi-dilute solution of polystyrene in deuterated cyclohexane near the upper critical solution temperature (UCST) the binary cluster integral β_1 changes its sign at about 40°C, the θ temperature, whereas the ternary cluster integral β_2 is almost independent of temperature near θ point. Slightly below the temperature θ we determined compensation temperature $\tilde{\theta}$ at which the excluded volume of the segment actually vanishes due to the opposite contribution of the above two cluster integrals.

In this paper we discuss the compensation temperature in the same sample system near the lower critical solution temperature (LCST).

In the experiment, solution cell was specially designed to withstand a high vapour pressure of cyclohexane ~ 20 atm at 200°C. Two quartz windows of 8 mm in thickness are placed in a steel tube of 40 mm in diameter. Thickness of the sample liquid was 2 mm. Area of the neutron beam at the window was 35 x 14 mm^2. Transmission of these quartz windows was about 70% for our neutron beam of 3 ~ 9 Å in wavelength.

The sample used was living polystyrene (Press. Chem., $M=2.9\times10^5$, $M_w/M_n \leq 1.06$) dissolved in deuterated cyclohexane (C_6D_{12}). Screening lengths ξ of the polymer were measured for three solutions, 0.129 $g\cdot cm^{-3}$, 0.186 $g\cdot cm^{-3}$ and 0.211 $g\cdot cm^{-3}$. These are above the cross-over concentration. All concentrations are quoted for a temperature of 40°C.

The measurements were performed with the KENS-SAN instrument at KEK[2]. The excess scattering intensity of polystyrene solution against the solvent was determined after the transmission correction was made both for the solution and solvent. To compensate the uniform incoherent scattering due to the hydrogen atoms we have added normal cyclohexane into the solvent so that solvent and sample solution have the same number of protons. The measurement for the

solvent was made at 200°C. The incoherent neutron spectrum as well as the detector efficiency of two-dimensional position sensitive detector were corrected for by employing the data of incoherent scattering from water.

The plot of angular dependence of scattered intensity with the resolution of dq/q=0.2 was of Lorentzian type (see Fig. 1) as observed in the vicinity of UCST. From this plot we determined the screening length for each concentration and temperature. The concentration dependence of ξ for several temperatures near the lower θ (θ_L) (Fig. 2) is in good agreement with the prediction of Eq. (1), which was theoretically derived by using a chain approximation. This approximation is legitimate when the intramolecular excluded volume effect is very weak and parameters $z_1 \equiv \beta_1 b^{-3} N^{1/2}$ and $z_2 \equiv \beta_2 b^{-6}$ are small as compared with unity, here b^2 being the mean square length of a segment, N the number of segments in a polymer chain.

$$\frac{1}{\xi^2} - \frac{6}{MA^2} = 12N_A \frac{B_1}{A^2} C + 36N_A^2 \frac{B_2}{A^2} C^2 , \qquad (1)$$

where C is the weight concentration ($g \cdot cm^{-3}$), N_A is Avogadro's number, M is the molecular weight of polymer, A^2, B_1 and B_2 are defined respectively as $MA^2 = Nb^2$, $M^2 B_1 = N^2 \beta_1$ and $M^3 B_2 = N^3 \beta_2$.

By use of Eq. (1) we determined separately the temperature dependences of binary and ternary cluster integrals by B_1 and B_2 (Fig. 3). We recognize from these results that there exists concentration dependent compensation temperature in semi-dilute solution above the temperature θ_L where the binary cluster integral vanishes. We estimated θ_L value, $\theta_L = 191 \pm 2$°C, by the extraporation of the temperature dependent B_1 to $B_1 = 0$.

Fig. 4 shows a plot of B_1 vs. the reduced temperature distances from the θ temperature ($1-\theta/T$) and ($\theta_L/T-1$), with T being the absolute temperature. The temperature dependence of B_1 in the immediate neighborhood of the θ_L is similar to that near the θ.

References

1) K. Kurita, O. Hasegawa, S. Nakajima, E. Wada, K. Okano, M. Furusaka, Y. Ishikawa, KENS REPORT III, 80 (1982); K. Okano, K. Kurita, S. Nakajima, E. Wada, M. Furusaka, Y. Ishikawa, Physica B (1983) in press.

2) Y. Ishikawa, S. Ikeda, M. Furusaka, N. Niimura, KENS REPORT I, 101 (1980).

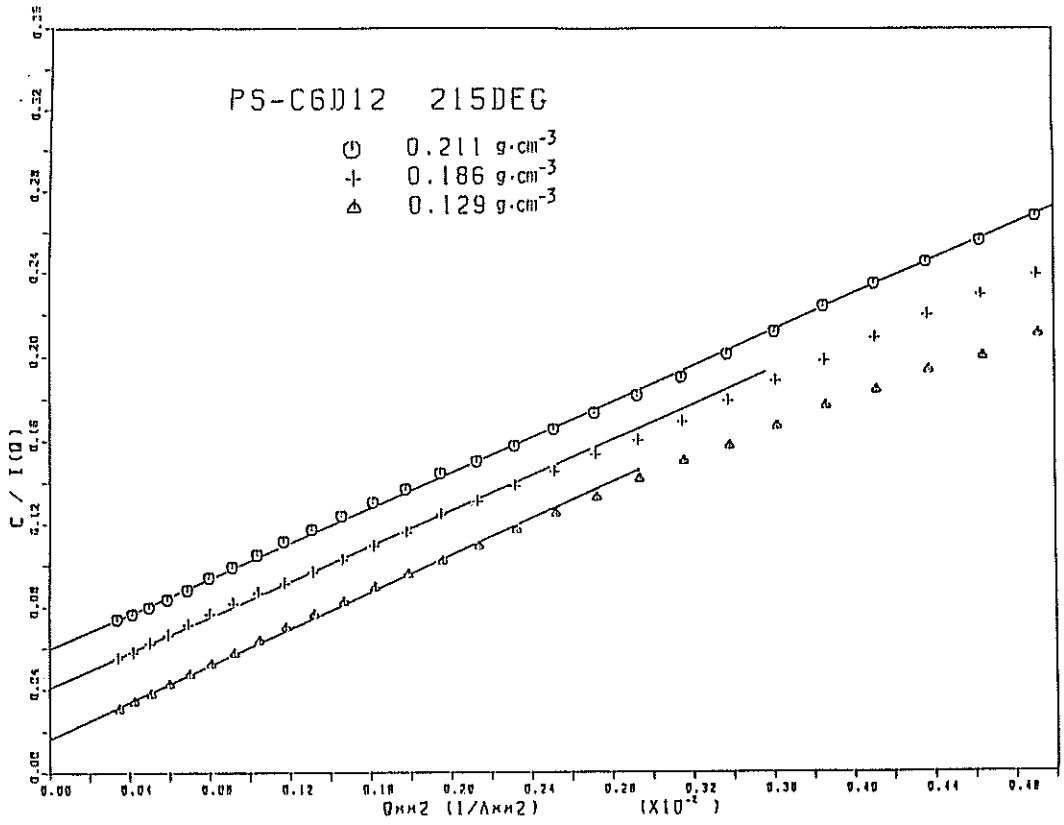

Fig. 1 Zimm plots of the excess scattered neutron intensity for polystyrene in deuterated cyclohexane at 215°C.

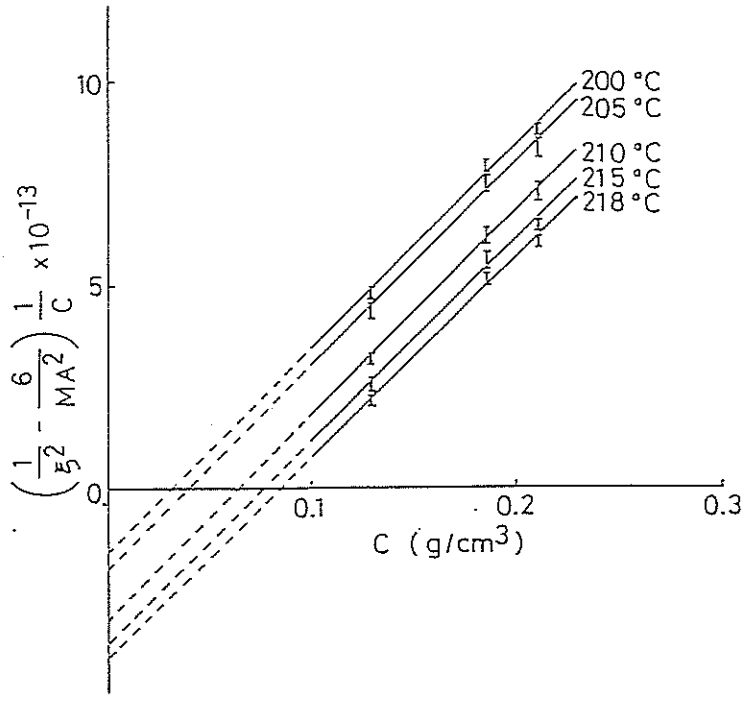

Fig. 2 The concentration dependence of screening length for several temperatures near θ_L.

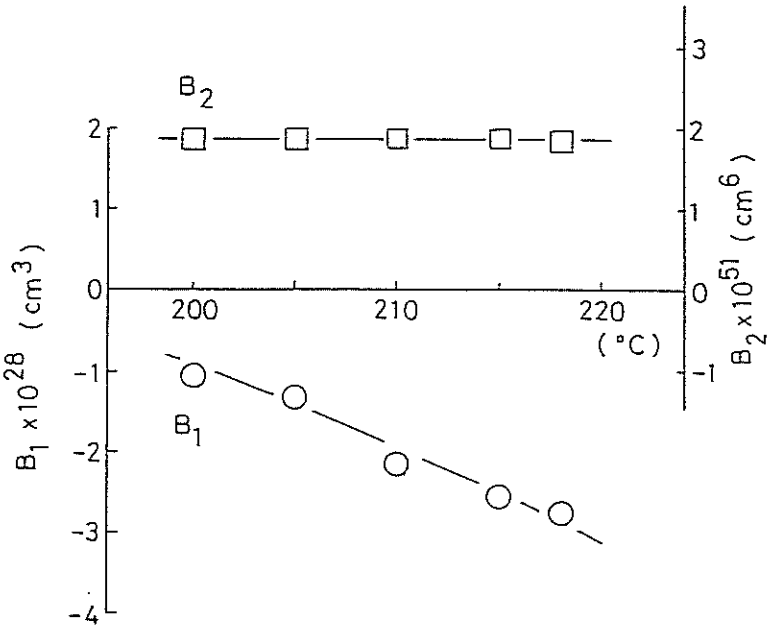

Fig. 3 The temperature dependences of binary (B_1) and ternary (B_2) cluster integrals for polymer segments.

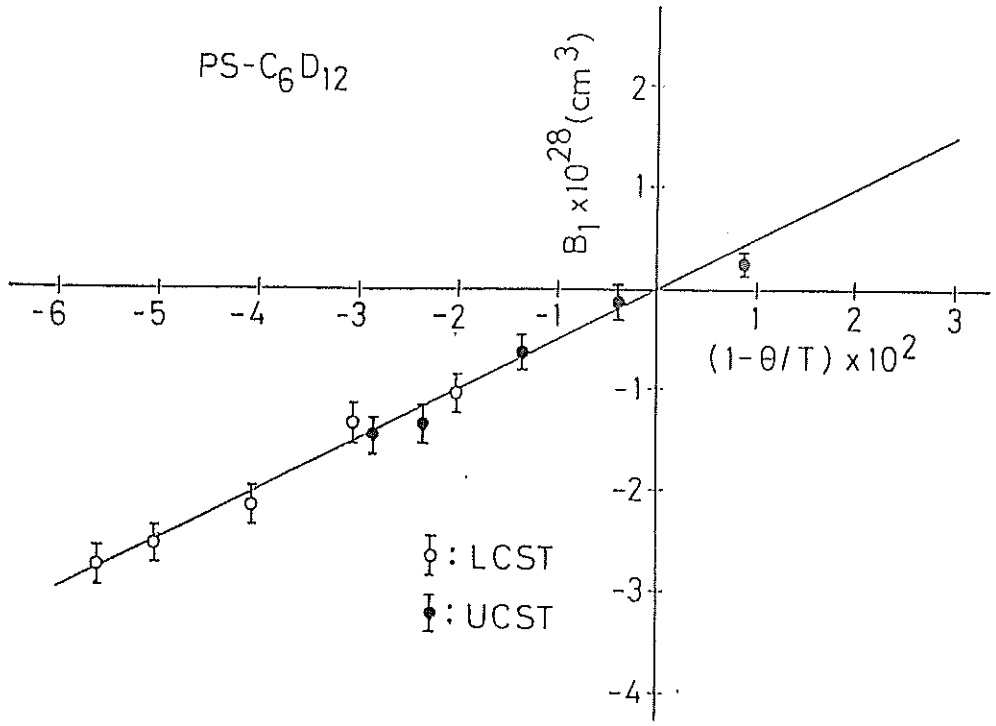

Fig. 4 plot of B_1 as functions of reduced temperature distances from the θ temperature $(1-\theta/T)$ and $(\theta_L/T-1)$, with θ_L being the lower θ temperature where $B_1=0$.

Scaling Analysis of Semidilute Polymer Solutions by Small-Angle Neutron Scattering

Hisao HAYASHI, Fumiyuki HAMADA, Akio NAKAJIMA, Kimio KURITA,* Takashi NAKAMURA,* Shinya NAKAJIMA* and Michihiro FURUSAKA**

Department of Polymer Chemistry, Kyoto University, Kyoto 606, Japan
* College of Science and Technology, Nihon University, Kanda Surugadai, Chiyoda-ku, Tokyo 101, Japan
** Department of Physics, Tohoku University, Sendai 980, Japan

Recent developement of the theories of polymer solutions based on scaling concepts has revealed that there are five regions in the temperature-concentration diagram of polymer solutions.[1] In each of these regions, quantities characterizing the polymer solution, such as osmotic pressure and correlation length, have distinctive asymptotic behavior as functions of molecular weight or concentration. In this report we study the concentration dependence of the correlation length in semidilute polymer solutions in a good solvent.

In the semidilute regime, the pair correlation function g(r) can be scaled in a simple Ornstein-Zernike form:

$$g(r) = n(\xi/r)\exp(-r/\xi) \tag{1}$$

where n is the number density of segments, and ξ is the correlation length. Fourier transformation of eq. (1) and substitution of the relation $g=n\xi^3$ lead to the scattering law S(q) of a Lorentzian form:

$$S(q) = g/(1 + q^2\xi^2) \tag{2}$$

where g is the number of segments per 'blob' of size ξ. The value of ξ can be determined from the slope and intercept of the plot of $S(q)^{-1}$ against q^2. According to the scaling law,[2] concentration dependence of the correlation length is expected to follow the asymptotic form:

$$\xi \sim n^{-\nu/(3\nu - 1)} \tag{3}$$

where ν is the excluded volume exponent ranging from 0.5 to 0.6.

Experimental

Monodisperse polystyrene of molecular weight M_w=110,000 was purchased from Pressure Chemical Co. Deuterated toluene-d_8 (isotopic purity 99.6%) supplied from CEA was used as a solvent without further purification.

Neutron scattering was measured using the SAN facility at KENS with the sample-to-detector distance of 3.0 m. The three-dimensional (x-y-t) scattering data were corrected for transmission and for inhomogeneity of the detector sensitivity, and averaged to obtain one-dimensional scattering curve, *i. e.* scattered intensity versus $q=(4\pi/\lambda)\sin\theta$, θ being half of the scattering angle. The incoherent and background scattering was eliminated by subtracting the scattering of solvent consisting of toluene and deuterated toluene-d_o with the same hydrogen content as in the solution. The sample was contained in a cell 2 mm in thickness with a pair of quartz windows 0.5 mm thick.

Results and Discussion

Figure 1 shows the plots of $S(q)^{-1}$ versus q^2 at various polymer concentrations covering from dilute to semidilute regime. The linearity observed for these plots confirms the Lorentzian form predicted for the scattering law, and validates the evaluation of ξ. The values of ξ determined from Fig. 1 are plotted by the open circles in Fig. 2. The data obtained by small-angle X-ray scattering are also shown by the filled circles. The values obtained by SANS and SAXS are in good agreement. Distinctive asymptotic linearity observed in the region $c \gtrsim 0.05$ g/cm^3 demonstrates the validity of eq. (3) and hence of the underlying scaling concepts. The exponent in eq. (3) determined by the slope of the plot is 0.84±0.09, which is in good accord with the value 0.93 predicted by the equation using the value ν=0.52 obtained from ref. 3.

References

1. M. Daoud and G. Jannink, J. Phys (Paris) 37, 973 (1976).
2. M. Daoud, J. P. Cotton, B. Farnoux, G. Jannink, G. Sarma, H. Benoit, R. Duplessix, C. Picot and P. G. de Gennes, Macromolecules 8, 804 (1975).
3. R. G. Kirste and G. Wild, Makromol. Chem. 121, 174 (1969).

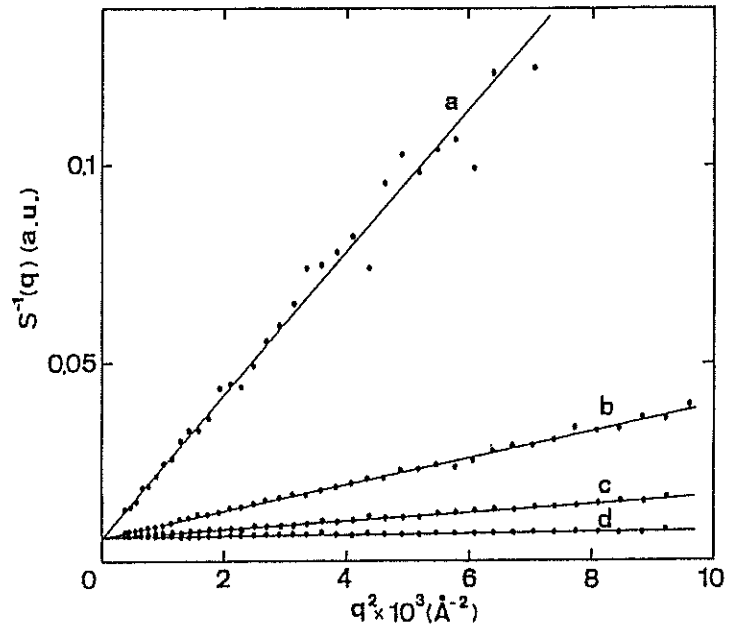

Fig. 1. Plots of $S(q)^{-1}$ vs. q^2 for polystyrene (M_w=110,000) dissolved in toluene-d_8 at concentration of (a) 0.01, (b) 0.05, (c) 0.1 and (d) 0.3 g/cm^3.

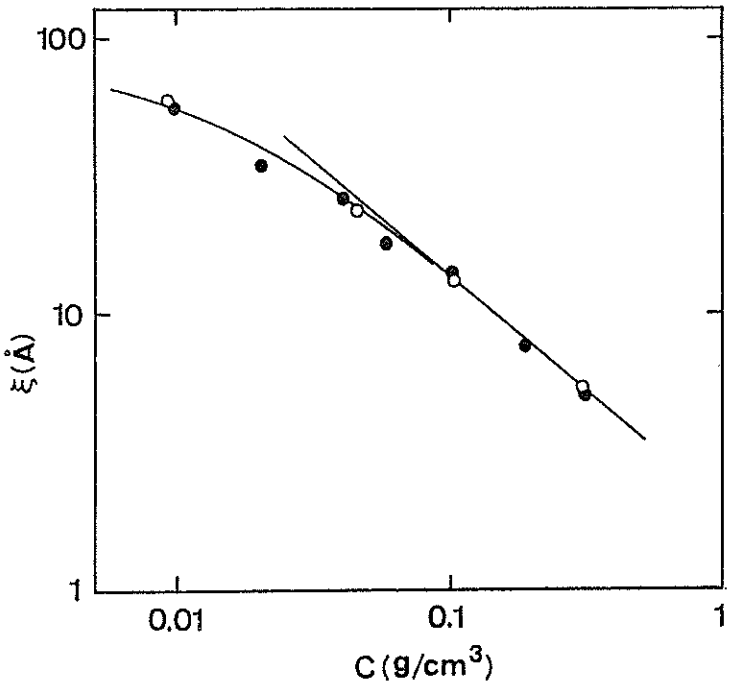

Fig. 2. Double logarithmic plot of the correlation length ξ vs. concentration c measured by SANS (○) and SAXS (●).

TOF Diffraction Study of Fe_3O_4 Single Crystal at Elevated Temperature

I. Kawada, M. Isobe, Y. Masuda, E. Bannai, K. Shibata, F. Izumi, K. Ohsumi* and H. Miyatake**

National Institute for Research in Inorganic Materials, Sakura-mura, Niihari-gun, Ibaraki 305

* Mineralogical Institute, Faculty of Science, University of Tokyo, Hongo, Tokyo 113

** Department of Applied Physics, Faculty of Engineering, Nagoya University, Nagoya 464

In the course of the measurements on the four-circle single crystal diffractometer (FOX) a measurement was undertaken using a newly developed high temperature equipment. The sample investigated was magnetite (Fe_3O_4) rod with about 8 mm in diameter and about 10 mm in length which had been synthesized by floating method.

The heating furnace is an image focusing system of a combination of reflecting mirrors with a heating source of a 1 kW Xenom lamp (Fig. 1.).

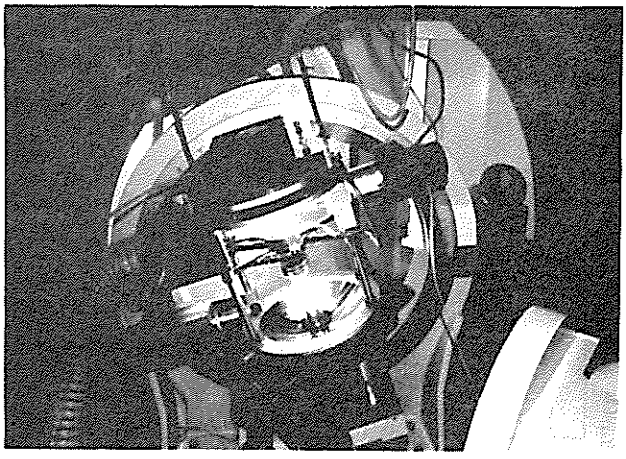

Fig. 1. The heating furnace attached to FOX

The measurements were performed in the selected zones in reciprocal space such as [111]*, [110]* and [100]* at room temperature and at high temperature. In the latter case the temperature was kept at about 1000°C which was measured by an optical pyrometer. The measurement time in each zone was about 6 hours at room temperature and 4 hours at high temperature respectively.

In Fig. 2. diffraction patterns of [111]* at both temperatures at 2θ=90° are shown. Comparing these diffraction patterns, following difference of feature is remarkable: the reflections higher than 999 become hardly observable at high temperature, and reflection intensity changes between both states (e.g. that of 888). These can be attributed to the thermal vibration and to the transition between ferrimagnetic and paramagnetic state of magnetite. Two small peaks at about 1710 and 2560 micro seconds remain not indexed. These may be caused by sample holder.

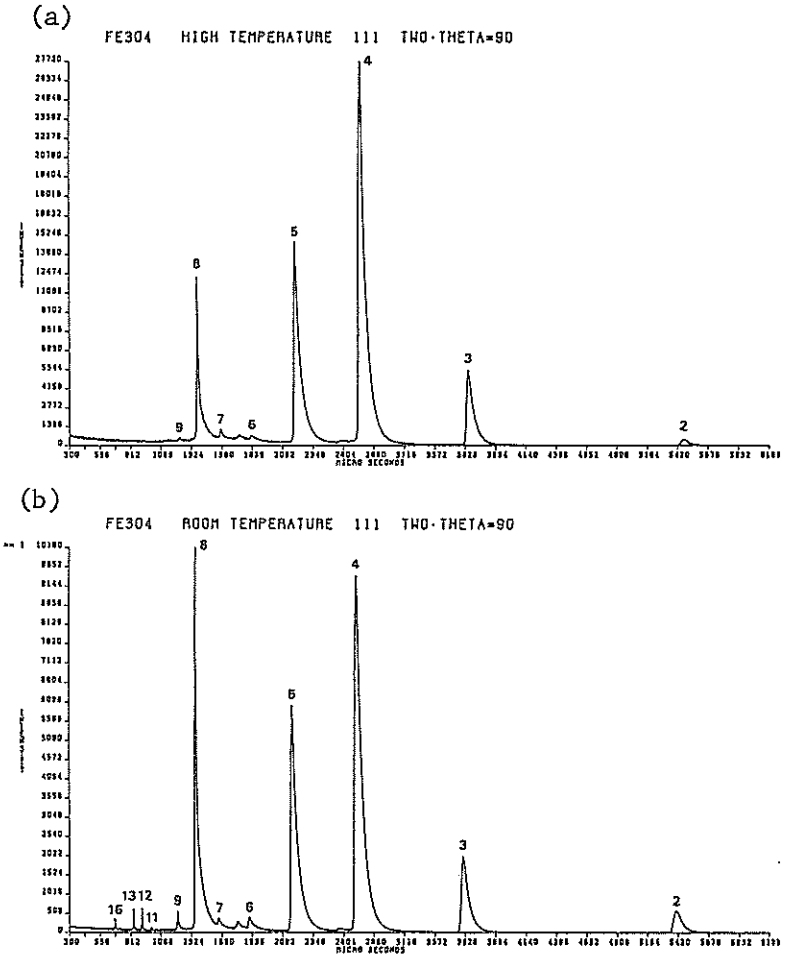

Fig. 2. Diffraction pattern of Fe_3O_4 hhh
(a) at about 1000°C and (b) at about 20°C

We thank Dr. I. Shindo for the guidance and Dr. F. Okamura for the motivation of the construction of this high temperature equipment.

High Resolution Quasielastic Spectrometer Using Pulsed Cold Neutron Source

K. Inoue*, Y. Ishikawa**, N. Watanabe+, Y. Kiyanagi*,
M. Kohgi**, S. Ikeda+ and H. Iwasa*

* Department of Nuclear Engineering, Hokkaido University, Sapporo, 060 Hokkaido, Japan

** Physics Department, Tohoku University, Sendai, 980 Miyagi-ken, Japan

\+ National Laboratory for High Energy Physics, Oho-machi, Tsukuba-gun, 305 Ibaraki-ken, Japan

We have developed a new type of time-of-flight spectrometer(LAM-80) with an energy resolution of the order of 10 μeV by which the observable time scale is in the region up to 10^{-10}sec. The LAM-80 is a quasielastic spectrometer which uses the KENS cold source, the C_2 neutron guide tube and a quasi-backscattering type analyser mirror. Incident neutrons fly through a 25 m flight-path which includes the neutron guide tube. Scattered neutrons from the sample are analysed by a crystal analyser mirror, which contains an array of 72 pyrolitic graphite crystal pieces, the dimensions of which are 12 mm × 12 mm × 2 mm per piece, with a 1.2°

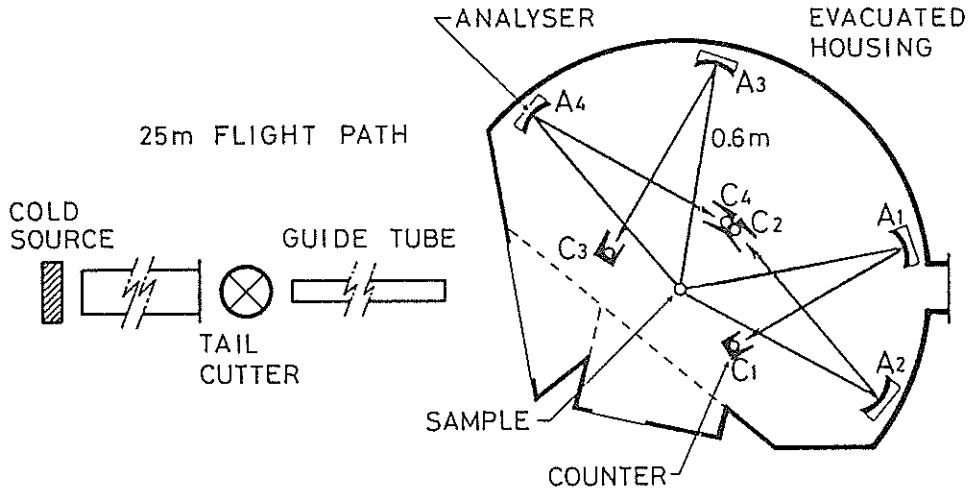

Fig.1 THE TIME-OF-FLIGHT HIGH RESOLUTION SPECTROMETR (LAM-80) AT KENS

mosaicness and a Bragg angle of 80°. Subsequently, the analysed neutrons are detected by an ^{3}He counter. The Q range covered by four counters is 0.15 ∿ 1.7 Å^{-1}. One of the positive feature of this spectrometer is its simplicity due to the usage of the pulsed source and the analyser mirror. Fig. 1 depicts the arrangement of the LAM-80 with four analysers installed in an evacuated housing chamber.

In the case of purely elastic scattering, assuming relevant simplifications [1], the measured neutron intensity is expressed as

$$y(t) = \text{const.}F(t)\int Z(t-t')R^*(t')dt' \qquad (1)$$

where F(t) is the neutron time-of-flight spectrum; Z(τ) is the time-dependent distribution of the neutron pulse emitted from the cold source and R*(t) is the time resolution function of the analyser mirrors. In the case of the LAM-80, the time variance of the analyser mirror was adjusted to match approximately the time variance of the incident neutron pulse, as shown in Fig. 2. The raw data in Fig. 3 shows the spectra from a vanadium sample, measuring 14 mm in diameter, 0.5 mm in thickness and 5 cm in length and from an ethylene glycol sample. These data reveal the wide applicability of the LAM-80 in studies of polymers, associated molecular liquids having hydrogen bonds and so on.

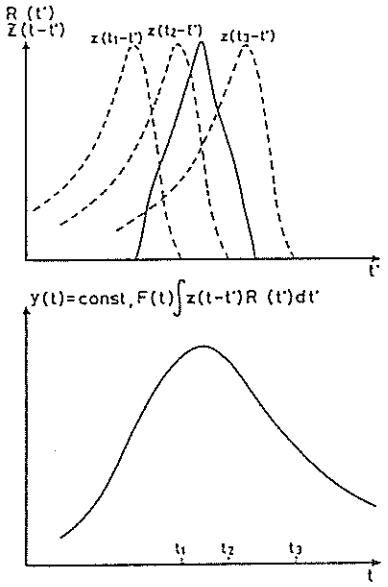

Fig. 2 Typical shape of pure elastic scattering.

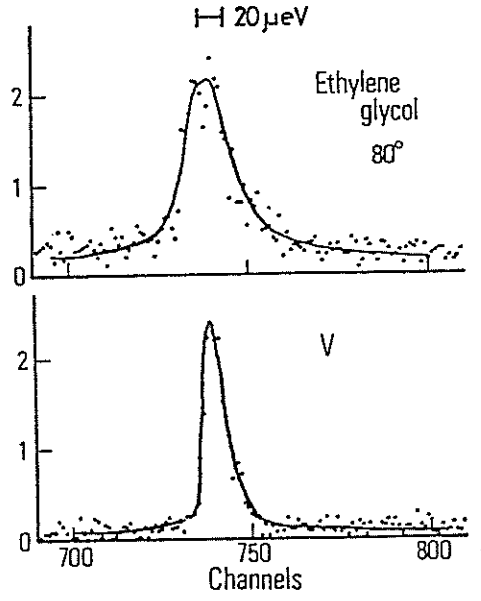

Fig. 3 Scattering spectra from ethylene glycol and vanadium.

Coherent Neutron Scattering from Light Water

Kazuhiko INOUE

Department of Nuclear Engineering, Hokkaido University, Sapporo, 060 Hokkaido, Japan

Utilizing the accelerator-based intense cold neutron source, we have conducted measurements of the differential scattering intensity from light water for the Q range down to 0.2 $Å^{-1}$ with high statistics and high S/N ratio. The predominantly incoherent scattering from light water demanded high statistics. Measurements were carried out using the LAM-40 spectrometer [1] on the KENS. The water sample was held in the LAM-40 standard liquid sample container, which was designed in the form of a 14 mm outer diameter cylindrical sheet having a thickness of 0.1 mm. Angular departure of neighbouring analyseres on the analyser bank was 16°, and then the analyser bank was stepped in seven angular positions from 0° to 16°.

Typical differential spectral data as shown in Fig. 1 were integrated over the time-of-flight abscissa to obtain the differential scattering

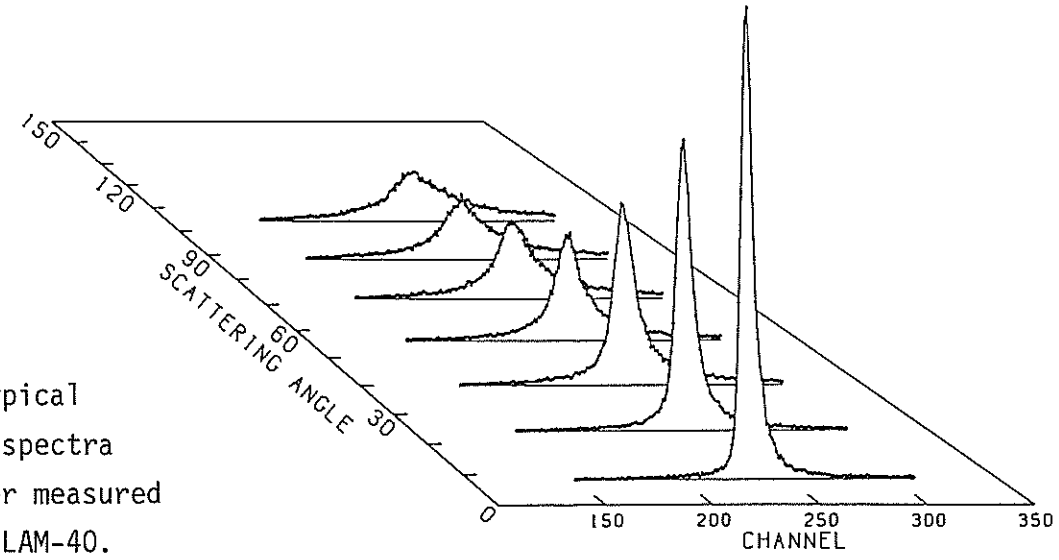

Fig. 1 Typical differential spectra of light water measured by using the LAM-40.

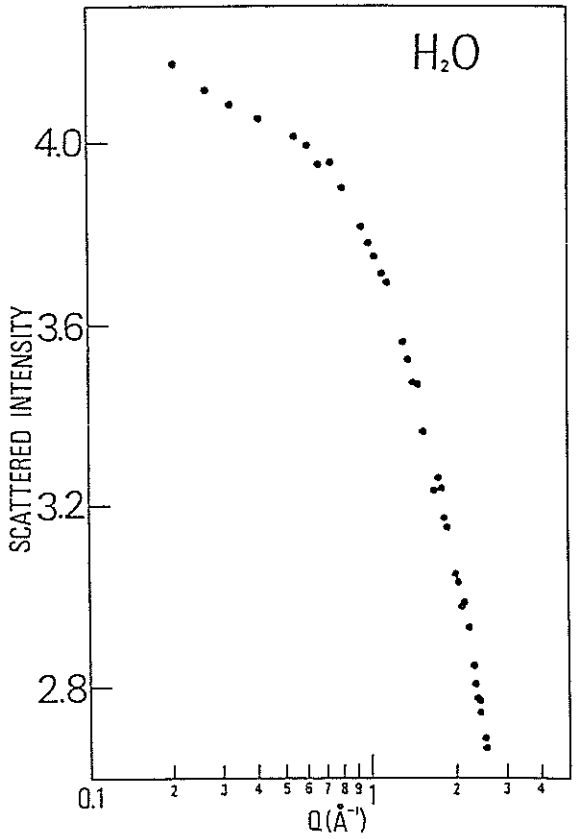

Fig. 2 The differential scattering intensity of light water as a function of Q at ambient temperature.

intensity as a function of the scattering angle. Fig. 2 depicts a preliminary result of differential scattering inteisity from water at ambient temperature. There is a definite indication of a peak at $Q \sim 0.7$ $\mathring{A}^{-1}$, which suggests the existense of a large structure in water. For the Q range larger than about 0.5 $\mathring{A}^{-1}$, Powles et al. made detailed measurements [2], and reported a small peak at about 1.1 $\mathring{A}^{-1}$ and a well established one at 1.9 $\mathring{A}^{-1}$. The present results do not indicate the existense of a small peak at 1.1 $\mathring{A}^{-1}$ but there is definite indication of peaks within the Q range from 1.5 to 2.0 $\mathring{A}^{-1}$. We are presently conducting measurements to guarantee more precise analysis, the results of which will be reported elsewhere.

References

[1] K.Inoue, Y.Kiyanagi, M.Kohgi and K.Kaji, Physica, Y89(1983).

[2] J.C.Powles, J.C.Dore and D.I.Page, Mol. Phys., 24(1972)1025.

Differential Scattering from Deuterated Alcohol Aqueous Solutions

Kazuhiko INOUE

Department of Nuclear Engineering, Hokkaido University, Sapporo, 060 Hokkaido, Japan

We have measured the differential scattering intensities from deuterated tertiary butyl alcohol and deuterated methanol heavy water solutions, $(CH_3)_3COD+D_2O$ and CH_3OD+D_2O, at ambient temperature as a function of Q for the relatively small Q region by using the LAM-40 spectrometer. Fig. 1 and 2 depict that the tertiary butyl alcohol solution has a much steeper slope than that of methanol solution. We can readily understand the steeper slope if we assume that some intermediate angle scattering occurred from the tertiary butyl base of the globular shape for the larger radius of gyration of the tertiary butyl alcohol base as compared to the smaller one of the methanol base. This conclusion was confirmed by the results of measured intensities from ordinary water solutions of $(CD_3)_3COH$ and CD_3OH which reveal similar Q dependencies as the ones from heavy water solutions of $(CH_3)_3COD$ and CH_3OD.

Table 1 shows the preliminary results for the gyration radii obtained under the assumption of dilute solution limit. Cooperation of techniques, selective deuteration and intermediate angle scattering might promise some useful results for some molecular liquid systems such as alcohol, ammomium derivative solutions and so on.

We are conducting investigation on several molecular liquid systemes and will report the results elsewhere.

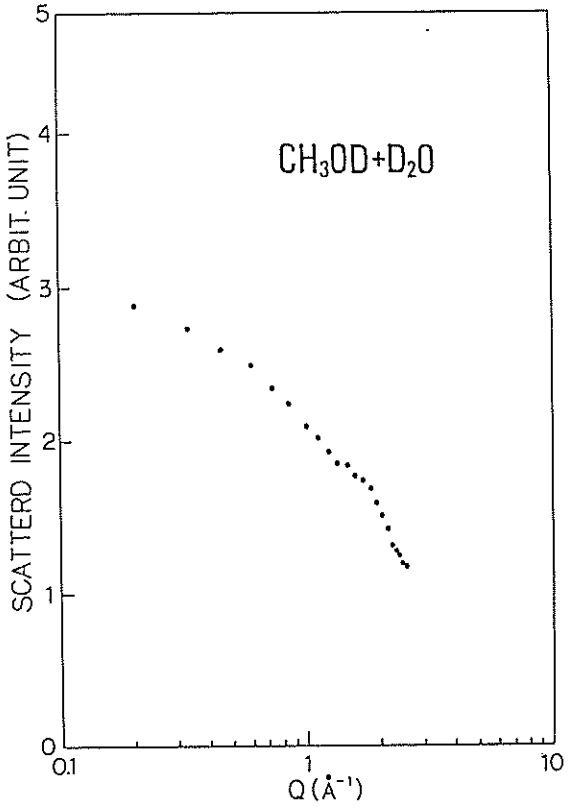

Fig. 1 Differential scattering intensity from deuterated methanol heavy water solution.

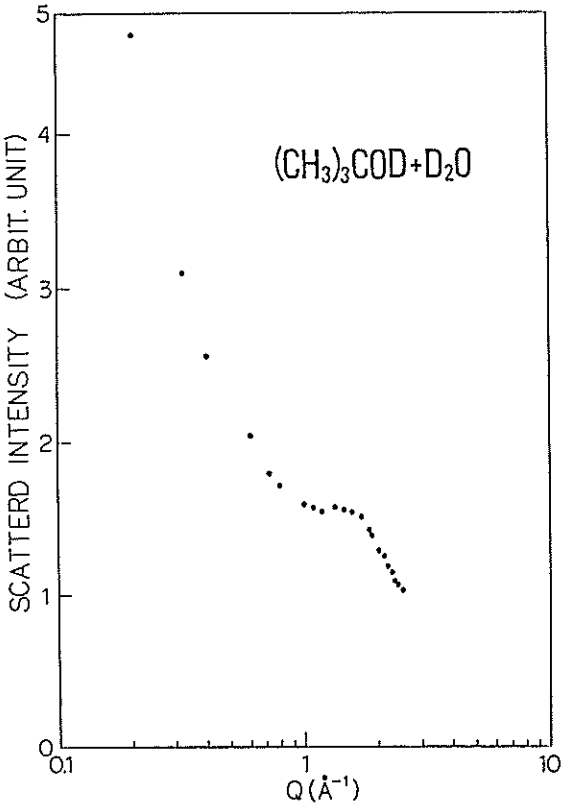

Fig. 2 Differential scattering intensity from deuterated tertiary butyl alcohol heavy water solution.

Table 1. Estimated gyration radii.

case	a (Å)
$CH_3OD + D_2O$	1.39
$(CH_3)_3COD + D_2O$	2.93

Neutron Quasielastic Scattering from Cyclohexane

Yoshiaki KIYANAGI and Kazuhiko INOUE

Department of Nuclear Engineering, Hokkaido University,
Sapporo, 060 Hokkaido, Janan

Cyclohexane is one of the globular molecules and has a plastic crystal phase at the temperature range of 186.1 ∿ 279.7 K. So far cyclohexane has been studied by neutron quasielastic scattering[1∿3]. We have intended to measure the quasielastic spectra with a resolution better than before in order to study the rotational mode in more detail as well as to examine the validity of the rotational diffusion model. Here, we report a preliminary result of quasielastic scattering data.

We measured the neutron quasielastic scattering spectra at 143, 214, 268 and 298 K by using LAM-40 spectrometer at KENS. 143 K data showed no broadening. Figure 1 shows the time-of-flight spectra at 214, 268 and 293 K. The 268 K spectra are similar to the 293 K spectra at large scattering angles, which will be explained by the fact that at large momentum transfer, the rotational diffusion mode was mainly observed. The 214 K data is somewhat different from other ones. We analysed the FWHM of the spectra by a spherical top rotational diffusion model, though, strictly speaking, cyclohexane being a symmetrical top. We used the data at large momentum transfer region to seperate out the quasielastic component from the whole spectra. Figure 2 shows the FWHM of quasielastic parts and the rotational diffusion constants Dr derived from the observed scattering profiles. For liquid phase data analysis we adopted the simple diffusion model of translation. The spherical top model analysis resulted in approximately good fits to the FWHM data of a liquid phase as well as a plastic crystal phase, but the rotational diffusion constants were not so

sensitive to the variation of the FWHM. We are now conducting the detail analysis of spectral shapes with the symmetrical top model.

References

1) L.N.Becka, et. al., J. Chem. Phys., 38(1963)1685.

2) L.A. De Graaf, Physica, 40(1969)497.

3) P.A. Egelstaff, et al., J. Chem. Phys., 53(1970)2590.

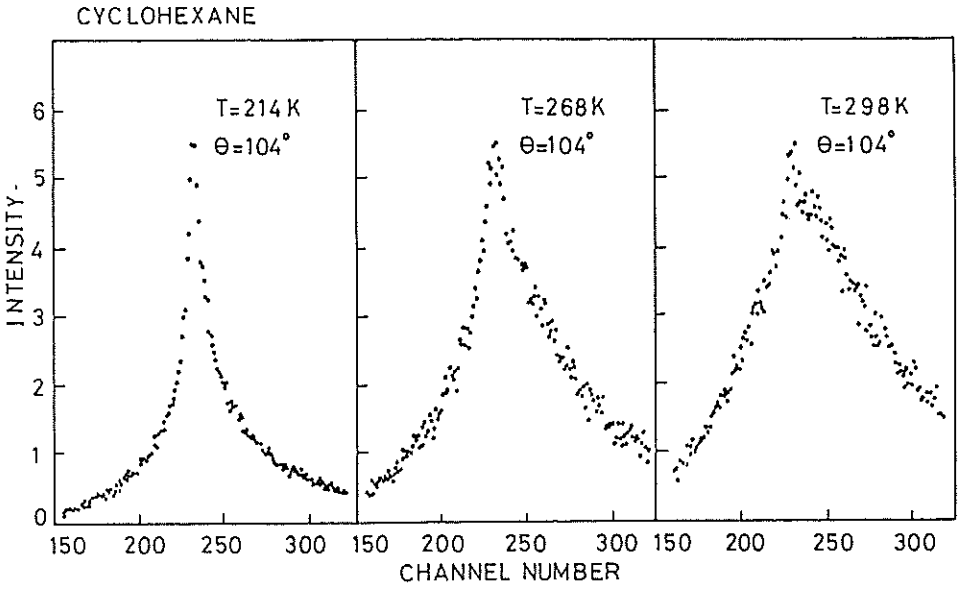

Fig. 1 Time-of-flight spectra from cyclohexane.

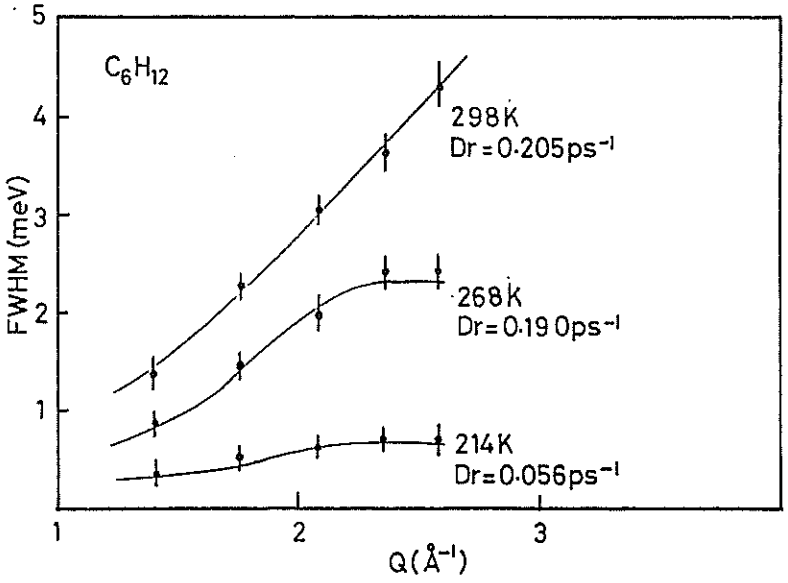

Fig. 2 FWHM of quasielastic spectra.

Hydrogen Diffusion in Ti

Yoshiaki KIYANAGI*, Kazuhiko INOUE* and Kenzo KAI**

* Department of Nuclear Engineering, Hokkaido University, Sapporo, 060 Hokkaido, Japan

** Institute for Iron, Steel and Other Metals, Tohoku University, Sendai, 980 Miyagi-ken, Japan

In (α+β) phase of $TiH_{0.24}$ at about 350°C, we observed the diffusion of hydrogen with a time scale of 10^{-12}sec[1]. Subsequently we have aimed to observe the diffusion of hydrogen in a single phase of β to confirm that the rapid hydrogen diffusion takes place only in β phase. Untill now different values of eutecric points were presented[2], which are about 38 % and 42 % hydrogen atomic percent. Here, we report the results of the quasielastic scattering of $TiH_{0.61}$, at 38 % hydrogen atomic percent, which will be in β phase above about 320°C.

Quasielastic scattering was carried out at 25°C, 334°C and 358°C by using LAM-40 spectrometer at KENS. The temperature was controlled by an electric heater. The spectrum at 25°C in (α+γ) phase indicated no broadening. Figure 1 shows the spectra of 334°C and 358°C. The two spectra are very similar and consist of two components of quasielastic and elastic part. The elastic part can be attributed to the scattering of hydrogens which do not diffuse in time scale of 10^{-12}sec. The ratio of elastic to quasielastic part did not vary so much with temperature. These results indicate that we could not observe the pure quasielastic spectra at this hydrogen concentration, so it is required to measure a 42 % hydrogen atomic percent sample. Figure 2 shows the FWHM of the quasi-elastic parts of the spectra. The diffusion constants derived were 2.1 $\times$ 10^{-5}cm^2/s at 334°C and 2.4 $\times$ 10^{-5}cm^2/s at 358°C, respectively.

The mean residence times were estimated to be about 1 psec. We are now preparing the measurements of $TiH_{0.69}$ and the detail theoretical analysis.

References

1) Y. Kiyanagi, et al., KENS REPORT-III(1982)

2) W.M. Mueller, et al., METAL HYDRIDES(1968)Academic Press.

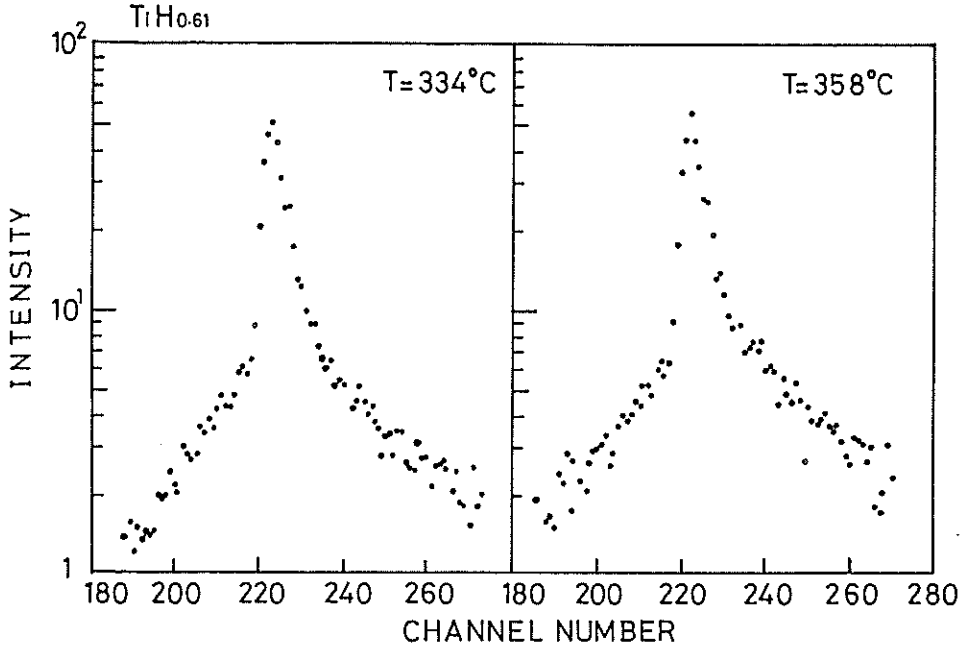

Fig. 1 Time-of-flight spectra from $TiH_{0.61}$.

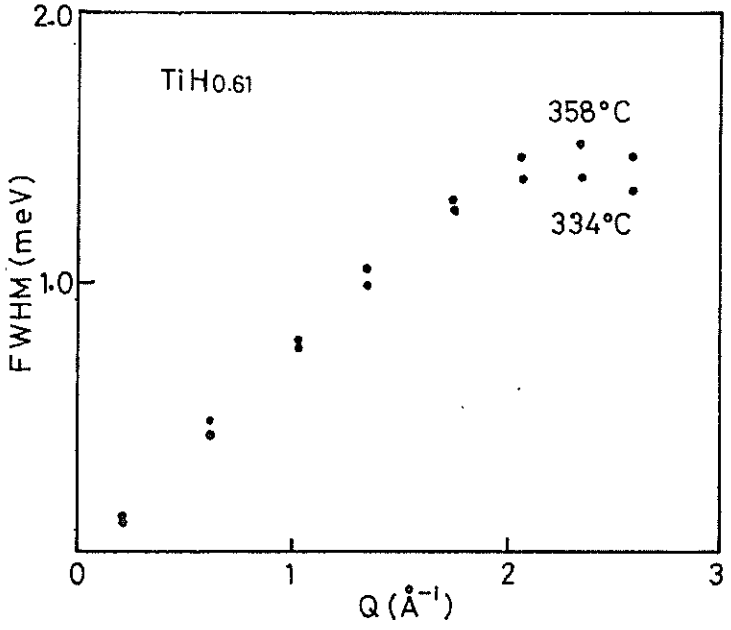

Fig. 2 FWHM of quasielastic component.

Study of Polymer Solution by Neutron Quasielastic Scattering

Yasuhiro MIYAKE, Yoshinobu IZUMI, Katsunari YASUDA,
Kazuhiko INOUE* and Yoshiaki KIYANAGI*

Department of Polymer Science, Faculty of Science,
*Department of Nuclear Engineering, Faculty of Engineering,
Hokkaido University, Sapporo 060

Neutron scattering (NS) measurements are one of the most powerful tools in the study of polymer science, since we can utilize a polymer labeled with its isotope in NS measurement and then obtain the important properties of polymer by this contrast method.[1] That is, we would be able to obtain some information on segmental motions of polymer molecule depending on Q, when we use neutron spin echo and backscattering spectrometers in the measurements of neutron quasielastic scattering (NQES)[2]. Fortunately LAM 80 spectrometer, whose energy resolution is about 10 μeV and Q range is $0.15 \sim 1.7 A^{-1}$, will be completed in KEK and utilized soon. Then we would be possible to study molecular motion of inner region of polymer molecule by LAM 80 to some extent. Such study is very important in the study of polymer conformation, especially relating to phase separation in solution[3)4)]. But it is necessary to select a proper polymer solution to perform the study. Carbon disulfide (CS_2) is a good candidate as a solvent for this aim. It is thought that polystyrene (PS) is a good one for the candidate, CS_2, because θ temperature of PS–CS_2 solution is near $-5^{\circ}C$ according to Higgins et al[2]. However we are afraid whether CS_2 is a true θ solvent for PS, because phase separation of this solution is not appeared even at $-30^{\circ}C$. So we seeked a proper polymer for CS_2 in which phase separation appears. We found that poly(p–chlorostyrene) (PpCS) is suitable for this aim. θ temperature may be near $-5^{\circ}C$ in the solution. In this report, preliminary results obtained on PpCS in CS_2 solution at $22^{\circ}C$ by LAM 40 spectrometer are given. Resolution and Q range of LAM 40 are not so good for this aim in comparison with LAM 80, but the useful and basic results for next study with LAM 80 are obtained. Results are shown in Figs. In Figs., results on three PS in CS_2 solutions obtained with former type LAM 40 spectrometer and on PpCS in CS_2 solution obtained tentatively with new LAM 80 during the manufacture of this spectrometer are shown together. We see from the results that the values of

effective diffusion constant in all systems are appropriate and D_{eff} depends on the samples, molecular weight and concentration of the systems. D_{eff} of PS is larger than that of PpCS in CS_2 solution and D_{eff} of PS 600 is larger than that of PS 17500 and PpCS in CS_2 solutions. These results may be reasonable in the point of view of both molecular structure and segmental motion if D_{eff} reflects a restricted segmental motion of polymer molecule. However the values obtained by LAM 80 are lower than that by LAM 40, as shown in Fig. 1, although molecular weight (4.3×10^4) of PpCS and concentration (20%) of solution are different from other solutions. It is thought that this problem is attributed to the method of data analysis. So we will take into consideration this problem in next paper in details, where results obtained by new LAM 80 will be presented.

References

1)T.Springer, Quasielastic Neutron Scattering for the Investigation of Diffusive Motions in Solids and Liquids, Springer-Verlag(1972); Ed. R.A.Fava, Methods of Experimental Physics, 16(1980)205,480, Academic Press.

2)J.S.Higgins, G.Allen, R.E.Ghosh, W.S.Howells and B.Farnoux, Chem.Phys.Lett. 49(1977)197.

3)D.Richter, B.Ewen, J.B.Hayter, Phys.Rev.Lett. 45(1980)2121.

4)J.P.Cotton, M.Nierlich, F.Boue, M.Daoud, B.Farnoux, G.Jannink, R.Duplessix, and C.Picot, J.Chem.Phys. 65(1976)1101.

Fig. 1. Plot of FWHM vs Q^2 :

LAM 40

●; PS(MW=6×10^2)–CS_2, 40%.

○; PS(MW=1.1×10^5)–CS_2, 10%.

×; PS(MW=1.75×10^4)–CS_2, 40%.

▲; PpCS(MW=2.5×10^5)–CS_2, 10%.

LAM 80

□; PpCS(MW=4×10^4)–CS_2, 20%.

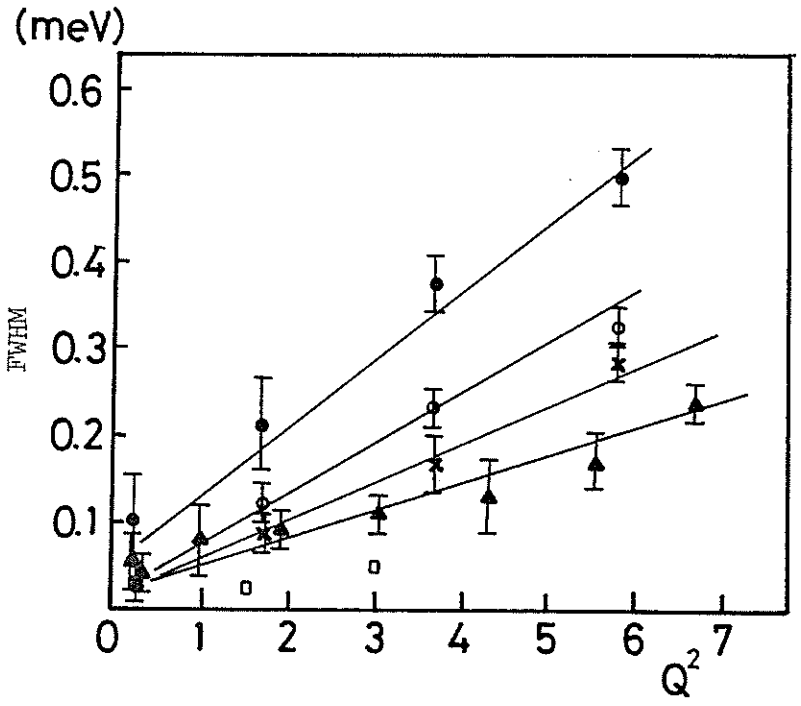

Fig. 2. The energy spectra of quasielastic neutron scattering for Vanadium(A), PpCS(4×10^4)–CS_2, θ=80°(B), and θ=130°(C), by LAM 80

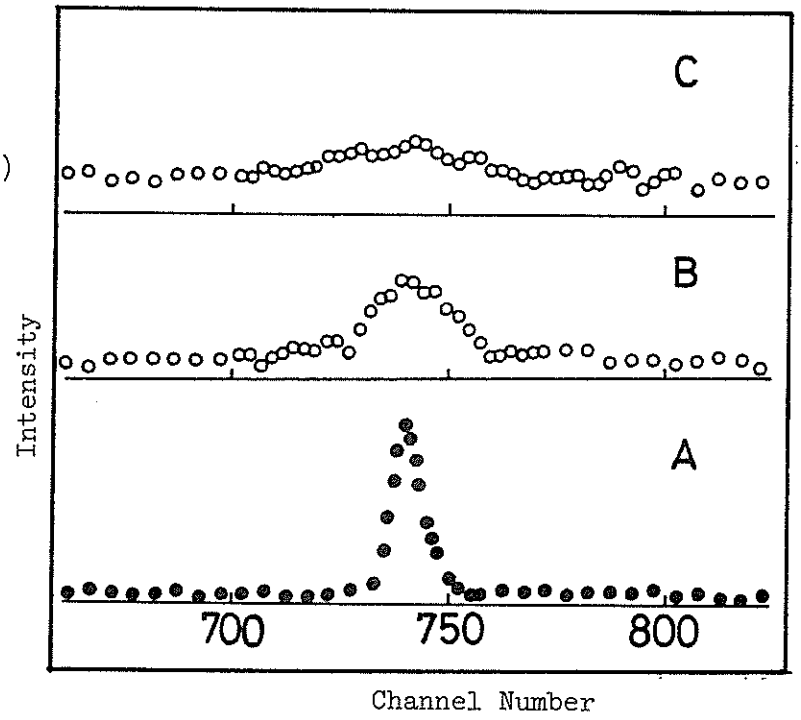

Quasielastic Neutron Scattering of α-Lactalbumin

Yoshinobu IZUMI, Yasuhiro MIYAKE and Kazuhiko INOUE*

Department of Polymer Science, Faculty of Science,
*Department of Nuclear Engineering, Faculty of Engineering,
Hokkaido University, Sapporo 060

In a previous paper, we studied the conformation of α-lactalbumin(αLA) at the native (N), the stable intermediate (A), and the fully unfolded states and transition processes among them using x-ray and neutron small-angle scattering and quasielastic neutron scattering methods[1]. It was found that the conformation of the A state at acid pH was typical of a globular protein and the conformation at the A state had a more or less expanded form than that at the N state. Preliminary analysis and discussion based on the Gaussian approximation were explained by the model of folding[2].

The present work concerns with the determination of the diffusive properties of H_2O and D_2O in αLA solution at the N state. Neutron spectra on αLA solution were measured using quasielastic neutron scattering spectrometer (LAM 40) at KEK. The protein concentration was 9% in a pH 7.0 phosphate buffer.

Quasielastic scattering spectra for the αLA solution and buffer are shown in Fig. 1. The quasielastic scattering is noticeably broader in the buffer solution (1-b and 2-b) than in the αLA solution (1-a and 2-a), especially at higher angles. Multiple scattering effect does not exist. Therefore, it seems unlikely that this is the cause of such a difference between the spectra of αLA and that of the buffer. The spectra are nearly symmetrical in energy transfer because of the inverted geometry spectrometer, even at the highest scattering angle. To obtain more reliable FWHM from these spectra, however, only the spectra at the left-hand side were used[3]. The variation of FWHM with squared momentum transfer Q^2 is plotted for the buffer and the αLA solutions in Fig. 2. The FWHMs for the αLA solutions are smaller than those of the buffers, which suggests the existence of an intermediate phase between the bounded water phase and the free water phase.[4]

The details of this work will be published elsewhere. This work was partly supported by the Grant-in-Aid from the Ministry of Education, Science

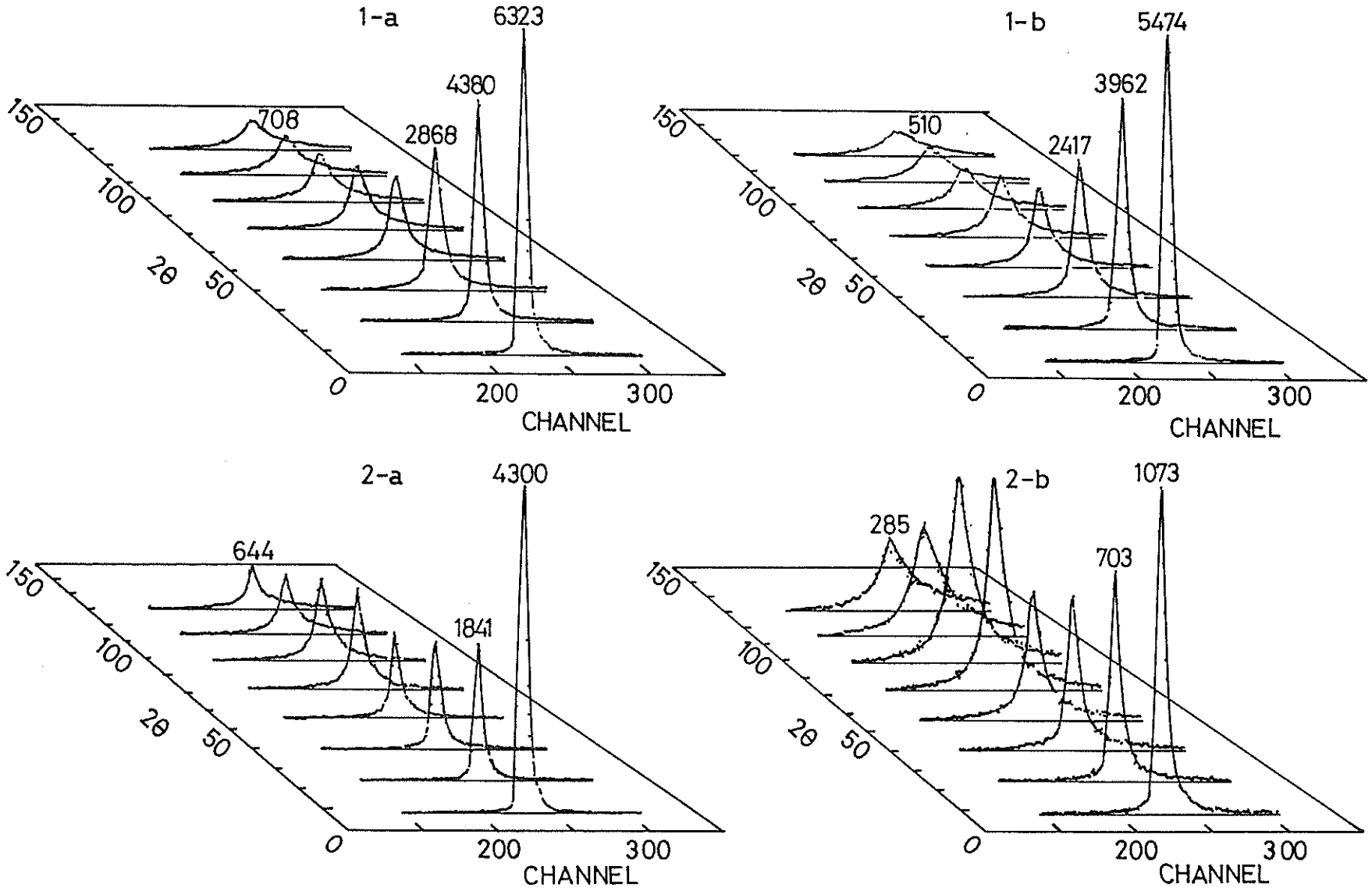

Fig.1. Quasielastic neutron scattering spectra for αLA solution and the buffer:
1—a; αLA—H_2O+buffer solution, 1—b; H_2O+buffer.
2—a; αLA—D_2O+buffer solution, 2—b; D_2O+buffer.

and Culture.

References

1)Y.Izumi, Y.Miyake, K.Kuwajima, S.Sugai, K.Inoue, M.Iizumi and S.Katano, Physica B, 116(1983) in press.

2)K.Kuwajima, J.Mol.Biol. 114(1977)241.

3)K.Inoue, Y.Kiyanagi, H.Iwasa and Y.Sakamoto, Nucl.Instr.Methods, 178(1980) 459. 4)A.M.Hecht and J.W.White, J.C.S. Faraday II, 72(1976)439.

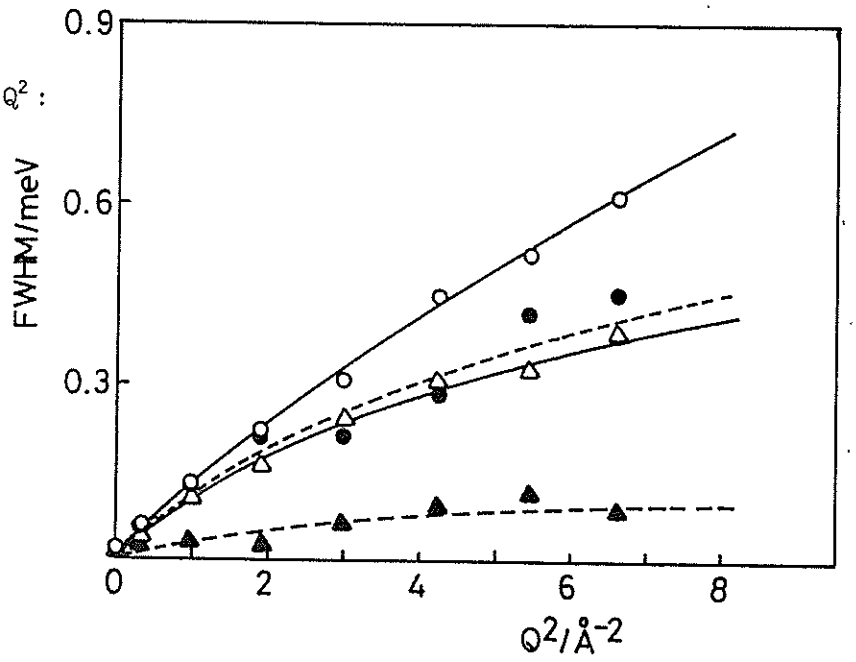

Fig. 2. Plot of FWHM vs Q^2 :
o: H_2O+buffer
Δ: αLA+H_2O+buffer
●: D_2O+buffer
▲: αLA+D_2O+buffer

Temperature Dependence of Structure of $NiCl_2$ Aqueous Solution

Takashi SAKUMA, Kaoru SHIBATA*, Hideshi FUJISHITA* and Sadao HOSHINO*

Department of Physics, Ibaraki University
Mito 310, Japan

*Institute for Solid State Physics, The University of Tokyo
Roppongi, Minato-ku, Tokyo 106, Japan

A quasielastic neutron scattering measurement is one of the powerful methods to study the structure and the dynamical porperties of aqueous solutions in which ions exhibit strong hydrations. We pointed out the importance of analyzing the whole shape of energy spectrum of scattered neutrons.[1] The same method has been applied to the study of aqueous solutions.[2] In the present study we performed quasielastic neutron sacttering measurements to study the temperature dependence of aqueous solution in which an abrupt change of a structure and dynamical properties might occur .

The properties of $NiCl_2$ aqueous solution have been reported by a numbers of authors so far.[3] There is an anomaly in solubility of $NiCl_2$ aqueous solution at about 64°C, which might correspond to a change of a number of water of crystallization from 4 to 2 at this temperature. To confirm the change of a structure and dynamical properties of $NiCl_2$ aqueous solution, we performed quasielastic measurements of 4M solution using the LAM spectrometer. A scattering specimen was prepared in a sample container of 14 mm diameter cylinder, 2 mm in thickness and 80 mm in length. The container with a thin wall was made of quartz. The whole apparatus was housed in an evacuated cage, and the sample container was vacuum-proofed. The quasielastic scattering at 45°C, 55°C, 65°C, 70°C, 75°C and 80°C was measureed at eight different values of scattering angles satisfying $2\theta = 16° + (n-1)\times 16°$ $(n=1,2,\cdots,8)$. The elastic scattering energy corresponded to 4.6 meV. The channel number was 512 and channel width was 32 μsec. The observed energy spectra at 45°C are shown in Fig.1.

Using H_2O as the solvent, most part of the scattering intensity from solution can be regarded as due to the proton incoherent scattering. The incoherent scattering law due to protons in solution is written as

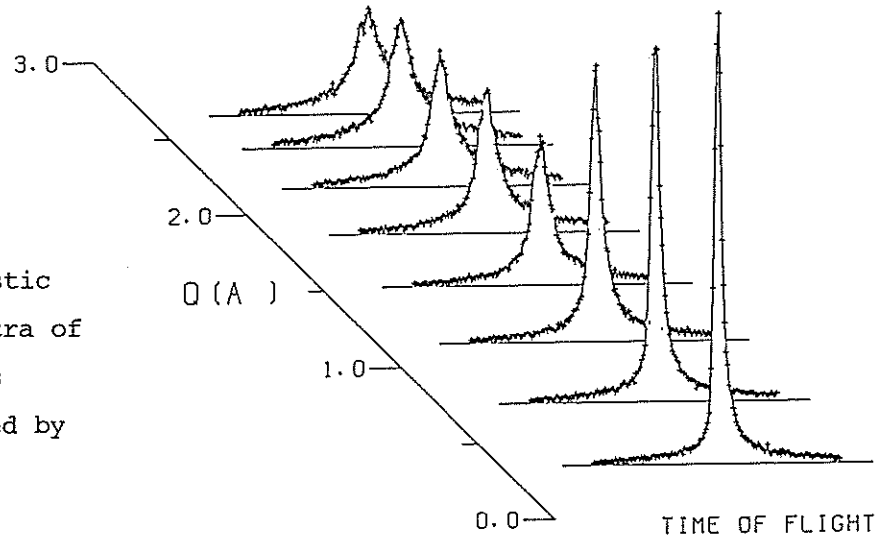

Fig.1 Quasielastic scattering spectra of 4M $NiCl_2$ aqueous solution measured by the LAM at 45°C.

follows;

$$S_{inc}(Q,\omega) \propto \frac{1}{\pi} \{ \delta_b \frac{\Gamma_b(Q)}{\omega^2+\Gamma_b(Q)^2} + \delta_f \frac{\Gamma_f(Q)}{\omega^2+\Gamma_f(Q)^2} \} , \qquad (1)$$

where $\Gamma_b(Q)$ and $\Gamma_f(Q)$ are the half of the full width at half maximum(FWHM) of the Lorentzians for bound water and for free water, respectively. δ_b and δ_f are the numbers of bound water molecules and of free water molecules per cation, respectively. Preliminary estimation was made for qualitative change of the structure and dynamical properties in the solution from the temperature dependence of FWHM of the observed spectrum; it was found that the increase of the FWHM with temperature was not so obvious around 65°C. The detailed analysis of the data of 4M $NiCl_2$ aqueous solution using above scattering law is now in progress.

The authors wish to thank Professor Inoue and his collaborators of Hokkaido University for help in quasielastic neutron scattering measurements.

Reference

1) T.Sakuma, S.Hoshino and Y.Fujii : J. Phys. Soc. Jpn. 46 (1979) 617.
2) P.Martel and B.M.Powell : Solid State Commun. 39 (1981) 107.
3) Y.Waseda and T.Sakuma : Metal Physics Seminar 5 (1982) 201.

Quasielastic Neutron Scattering Study of Polyelectrolyte Solutions

Ichiro Noda, Yuji Higo and Kazuhiko Inoue*

Department of Synthetic Chemistry, Faculty of Engneering, Nagoya University, Furo-cho, Chikusa-ku, Nagoya 464, Japan

*Department of Nuclear Engneering, Faculty of Engneering, Hokkaido University, Sapporo 060, Japan

The effect of electrostatic interaction on the local motion of a polymer chain was studied by measuring quasielastic neutron scattering from polyelectrolyte solutions.

The polyelectrolyte samples used here were poly(sodium acrylates) having two different degrees of ionization α=0.2 and 1.0. The solvent was D_2O. The concentrations of poly(sodium acrylates) with α=0.2 and 1.0 were 0.117 and 0.126 g/cm^3,respectively. The measurments of quasielastic neutron scattering were carried out at room temperature by using the LAM spectrometer at KEK. The sample cell was a standard aluminum cell of coaxial cylinder.

Fig.1 shows the raw data of quasielastic spectra from poly(sodium acrylates) with α=0.2 and 1.0 in D_2O. Fig.2 shows examples of the scattering spectra of poly(sodium acrylates) after subtracting the scattering spectra of D_2O. Fig.3 shows the Q-dependences of the full width at half maximum Γ of the spectra from poly(sodium acrylates) and vanadium. The Γ-values were evaluated by the least-square method assuming that the scattering spectra are single Lorenzian curves as shown in Fig.2. The spectra of vanadium corresponds to the effective resolution of the spectrometer. Fig. 4 shows the corrected Γ-values of poly(sodium acrylate) with α=0.2 after subtracting the Γ-values of vanadium. The corrected Γ-values of poly(sodium acrylate) with α=1.0 are almost equal to zero since its Γ-values are comparable to those of vanadium as shown in Fig.3. This result implies that the local motion of a polymer chain is depressed by electrostatic interaction. However, further experiments are needed to confirm this conclusion by using a cell suitable for aqueous solutions since the sample solutions might be contaminated by ions eluted from the aluminum cell.

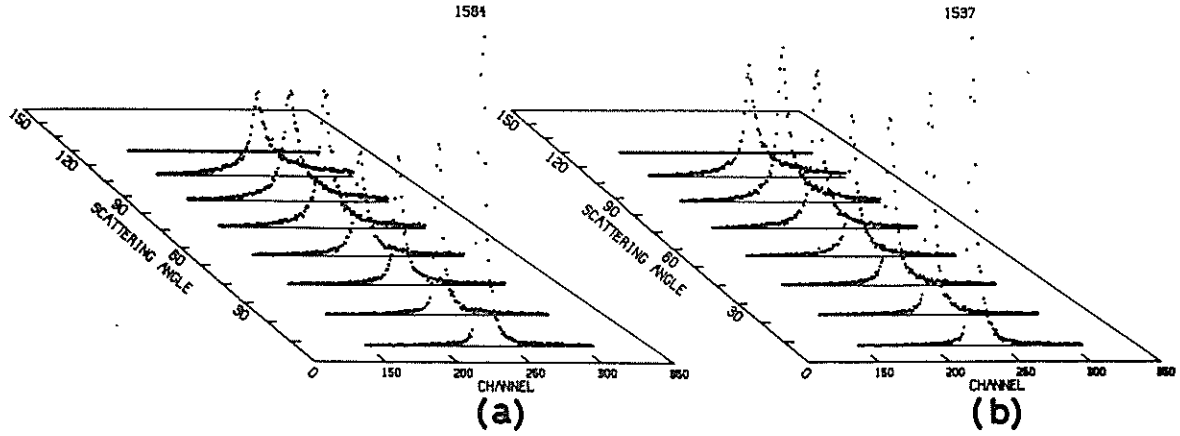

Fig.1. Raw data of quasielastic spectra from poly(sodium acrylates) with α=0.2(a) and 1.0(b) in D_2O.

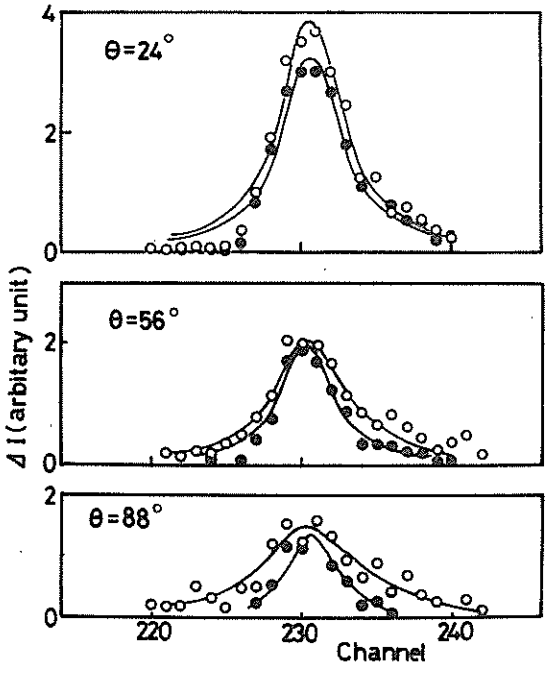

Fig.2. Examples of quasielastic spectra of poly(sodium acrylates) with α=0.2(o) and 1.0(●) at the different angles. The full lines are evaluated by the least-square method.

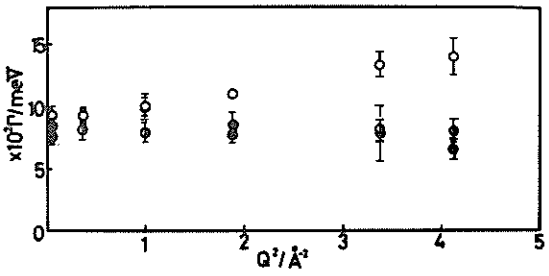

Fig.3. Γ-values vs. Q^2 for poly-(sodium acrylates) with α=0.2(o) and 1.0(●), and vanadium(◑).

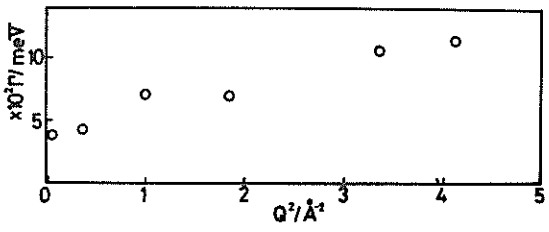

Fig.4. Corrected Γ-values vs. Q^2 for poly(sodium acrylate) with α=0.2.

Diffusive Motions in Rubbers

Kazuhiko INOUE*, Keisuke KAJI+, Toshiji KANAYA+ and Hiroshi AKIE*

* Department of Nuclear Engineering, Hokkaido University, Sapporo, 060 Hokkaido, Japan

\+ Institute for Chemical Research, Kyoto University, Uji, 611 Kyoto-hu, Japan

Neutron quasielastic spectra of a rubber state polymer can provide information on its segmental diffusive motions. As rubber polymers contain bridges, the centre-of-mass diffusion of each chain between bridges is completely suppressed. It has been suggested that the scattered neutron spectra may consist of a central purely elastic component and a broad quasielastic part resulting from localized segmental diffusive motion. In this case, it is possible to distinguish clearly two components whose intensity behaviors, as a function of Q, give information about the nature of segmental motion. We have conducted two series of experiments, one by using the LAM-40 spectrometer with conventional energy resolution and the other by using the LAM-80 with high resolution. Figs. 1 ∿ 4 show the raw data obtained for the rubbers isoprene, chloroprene and butadiene.

These data indicate the possibility of existence of two distinct types of diffusive motions, of which the time-constants τ_1 and τ_2 have several decades times difference. For the shorter time-constant motion, we write the incoherent scattering law as follows,

$$S_{inc}^{(1)}(Q,\omega) = S_{inc}^{(1,e)}(Q,\omega) + S_{inc}^{(1.q)}(Q,\omega), \qquad (1)$$

where e represents elastic and q quasielastic. For the longer time constant motion, the scattering law is

$$S_{inc}^{(2)}(Q,\omega) = S_{inc}^{(2,e)}(Q,\omega) + S_{inc}^{(2,q)}(Q,\omega). \qquad (2)$$

Examining the spectra resulting from the different resolutions used for each spectrometer, we note that the observed spectrum from the LAM-40 is the result of the convolution of the instrumental function and the scattering function

$$S_{inc}(Q,\omega) = a_1\delta(\omega) + b_1 S_{inc}^{(1,q)}(Q,\omega), \tag{3}$$

and that from the LAM-80, is the result of the convolution of the instrumental function and the scattering function

$$S_{inc}(Q,\omega) = a_2\delta(\omega) + b_2 S_{inc}^{(2,q)}(Q,\omega) + c_2 S_{inc}^{(1.q)}(Q,\omega). \tag{4}$$

The third one on the right hand side in Eq.(4) contributes only to produce an almost flat spectrum near the central peak. Accordingly, we can readily assess the tine-constants for the two motions $\tau_1 \sim 10^{-12}$sec and $\tau_2 \sim 5 \times 10^{-11}$sec.

Looking carefully at the spectral features of Figs. 2 and 3 and the τ_1 values, we can see that, following pipe model proposed by de Gennes [1], the fast mode is a transverse and quick rotational diffusive motion inside the pipe due to the thermal fluctuations of many bond angles, and the slow one is a jump motion of the chain along the direction of the pipe.

Reference

[1] P. G. de Gennes, J. chem. Phys., 55(1971)572.

Fig.1 Spectrum from isoprene measured by using LAM-80

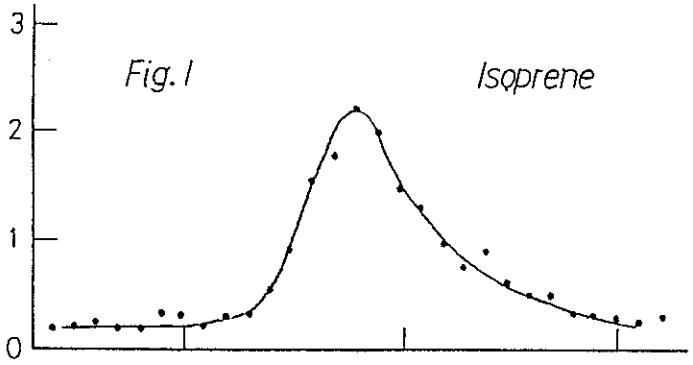

Fig.2 Spectrum from chloroprene measured by using LAM-80

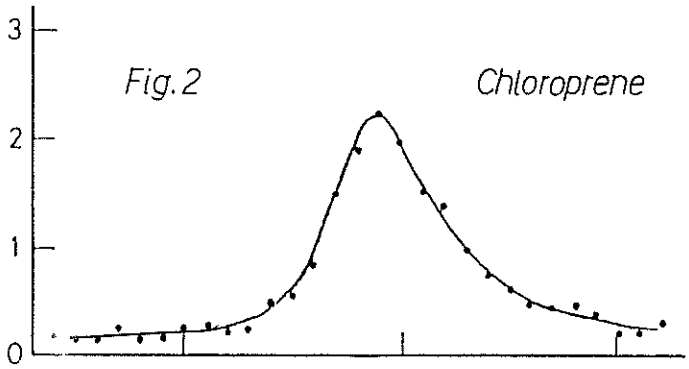

Fig.3 Spectrum from butadiene measured by using LAM-80

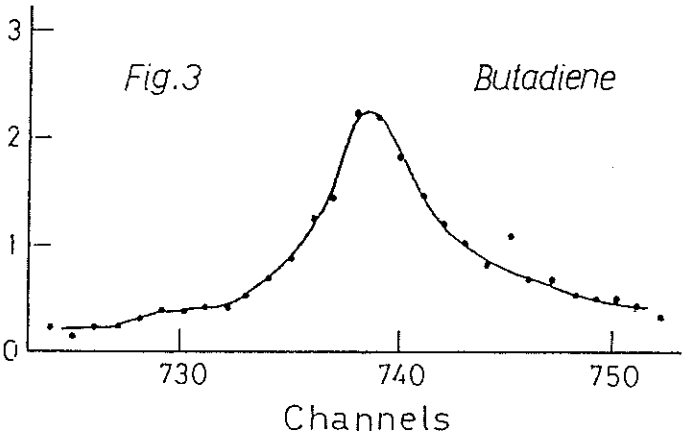

Fig.4 Spectrum from butadiene measured by using LAM-40

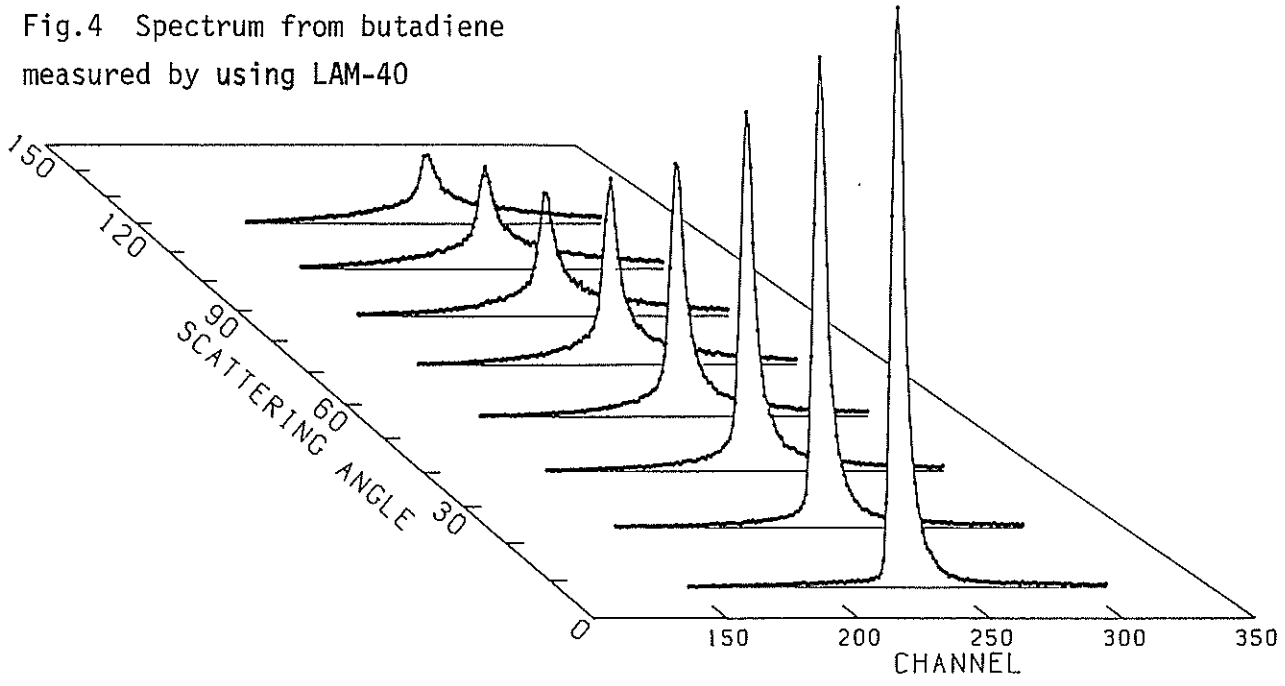

Molecular dynamics of polyisoprene rubber

Toshiji Kanaya, Keisuke Kaji, Hiroshi Urakawa, Ryozo Kitamaru
and Kazuhiko Inoue*

Institute for Chemical Research, Kyoto University, Uji,
Kyoto-Fu 611 and * Department of Nuclear Engineering
Faculty of Engineering, Hokkaido University, Sapporo 060

Micro-Brownian motion of polyisoprene(PIP) rubber was investigated by neutron quasielastic scattering(NQES). NQES measurements were carried out using the conventional energy-resolution quasielastic spectrometer LAM-40 at KENS. The sample was coated on the outer surface of aluminum cylinder 13.8 mm in diameter, 100 mm long and 0.25 mm thick. The thickness of the coated film is less than 0.1 mm. The time-of-flight(TOF) spectrum was obtained simultaneously at eight scattering angles, 8, 24, 40, 56, 72, 88, 104 and 120° at room temperature. The observed TOF spectra are shown in Fig. 1. The spectra evidently consist of at least two components, i. e., the central sharp elastic scattering part and the lower broad quasielastic scattering. The elastic part may arise from the presence of the entanglements of molecular chains in the rubbery polymers. The entanglements are essentially temporary but their relaxation time may be very long so that they can be regarded as permanent bridges because of a limited energy resolution of the spectrometer. On the other hand, the quasi-elastic broad scattering will be related to a local micro-Brownian motion between the entanglements.

The quasielastic scattering was analysed in terms of a rotational jump model proposed by Barnes. The time and distance scales of this model are characterized by the three parameters; the average time between successive jumps τ_1, the radius of jump circle d and the number of jump sites N. In order to determine the three parameters, we compared the theoretical Qd(Q: scattering vector) dependence of full width at half maximum(FWHM) of the quasielastic scattering with the experimental one. The result is shown in Fig. 2. It is found that

the best fit is obtainable in the case of $\tau_1 = 2.7$ ps, d = 1.4 A and $N \geq 5$. This result suggests that the motion observed in this work is related to micro-Brownian motion in very local region.

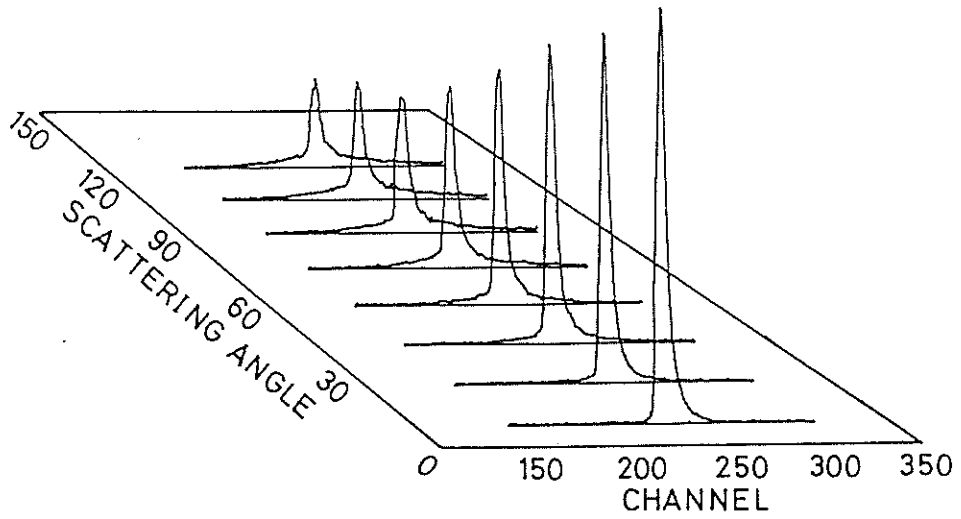

Fig. 1. Time-of-flight spectra of polyiosprene(PIP) at scattering angles from 8° to 120°. A channel width is 32 μs.

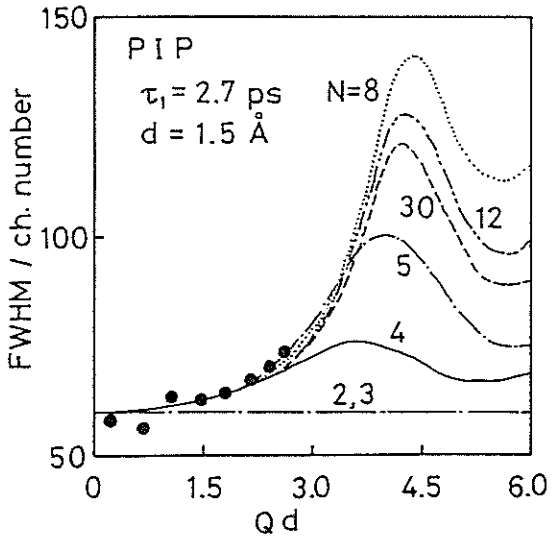

Fig. 2. Qd-dependence of full width at half maximum(FWHM) of quasielastic peak of PIP. FWHM is represented by channel number. Theoretical curves were calculated assuming that: $\tau_1 = 2.7$ ps, d = 1.5 Å, and different numbers of N.

Molecular dynamics of polybutadiene rubber

Toshiji Kanaya, Keisuke Kaji, Hiroshi Urakawa, Ryozo Kitamaru
and Kazuhiko Inoue*

Institute for Chemical Research, Kyoto University, Uji,
Kyoto-Fu 611 and * Department of Nuclear Engineering
Faculty of Engineering, Hokkaido University, Sapporo 060

Investigation on molecular chain dynamics of polybutadiene(PB) rubber was peformed by neutron quasielastic scattering. The quasi-elastic spectra were obtained with the conventional-energy resolution quasielastic spectrometer LAM-40 at KENS. The sample was coated on the aluminum holder and the measurements were made by the same procedure as described in a preceding paper. The observed TOF spectra at various Q-values are shown in Fig. 1. These spectra also comprise both of elastic scattering part and quasielastic one, as observed for other rubber polymers. It was found that full width at half maximum(FWHM) of the quasiealstic scattering dose not depend on Q(Fig. 2). According to a rotational jump model, this result means that the number of jump sites N is 2 or 3. The average time between successive jumps was estimated from FWHM to be 3.8 ps. This value is longer than that of polyisoprene (PIP) as shown in the previous paper. The Q-dependence of EISF(the ratio of the integrated scattering intensity of the elastic part to the total one) suggests that the radius d of jump circle of PB is larger than that of PIP, assuming the number of jump sites N is equal to 3 for PB.

The present results can be understood in terms of molecular structure of polymers. PB has no side group while PIP has a methyl group. For the local jump motion in the rubbery polymer, side methyl group may hinder relatively large motion. Therefore, the jump distance for PIP may be short compared with PB. It is expected that the large motion has the relatively long relaxation time. This picture agrees with the result that the average time between successive jumps of PB is longer than that of PIP.

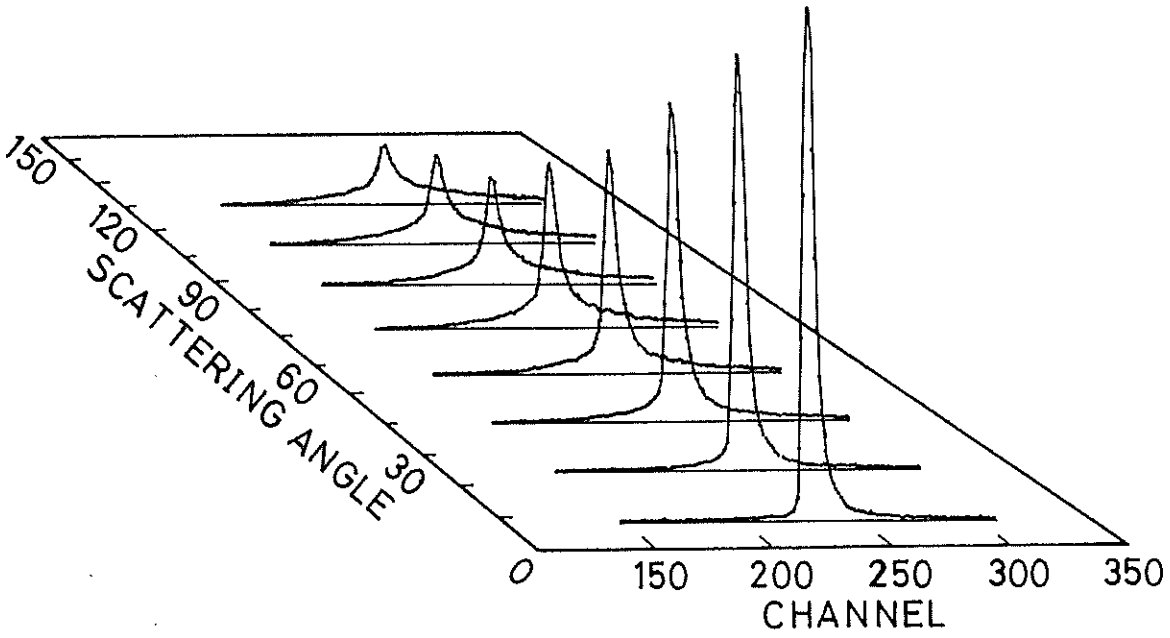

Fig. 1. Time-of-flight spectra of polybutadiene(PB) at scattering angles from 8° to 120°. A channel width is 32 μs.

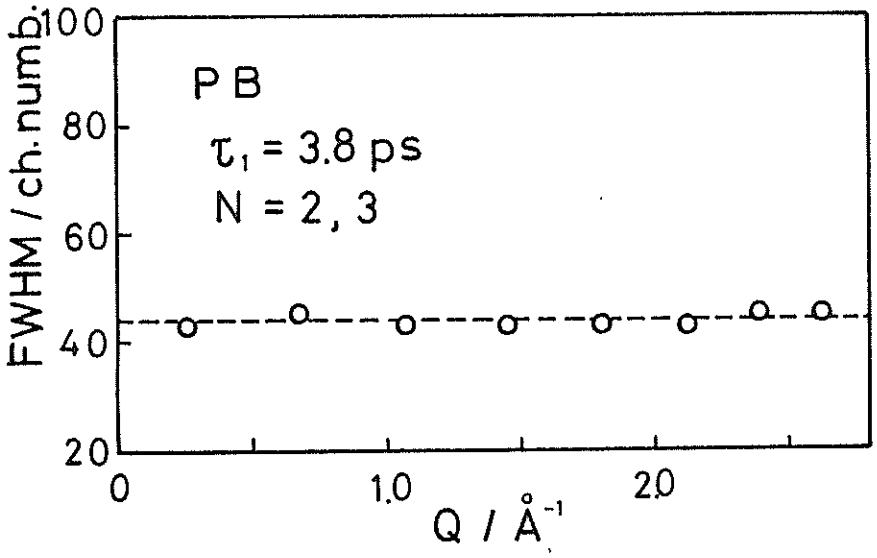

Fig. 2. Q-dependence of full width at half maximum(FWHM) of quasielastic peak of PB. FWHM is represented by channel number.

Spin Dynamics of the Spin Glass $0.88FeTiO_3$-$0.12Fe_2O_3$

Masahumi Kohgi

Physics Department, Tohoku University
Sendai 980, Japan

The randomly mixed system $FeTiO_3$-Fe_2O_3 with small content of Fe_2O_3 exhibits the spin glass anomalies[1]. In this system, the strong negative interactions between Fe^{2+} ions and Fe^{3+} ions in the Ti layer of the $FeTiO_3$ exceed the negative Fe^{2+}-Fe^{2+} interations via Ti layer of the matrix, and force the moments of Fe^{2+} ions to align parallel. This causes the ferrimagnetic ordering for higher concentration of Fe_2O_3 than the percolation limit of the long range ordering (ca 20%)[2], and the super paramagnetic state appears for lower concentration.

The c-axis susceptibility (DC and AC) of $0.88FeTiO_3$-$0.12Fe_2O_3$[1] exhibits the typical spin glass behaviour with the freezing temperature of T_g=38K. The remanence appears below T_g. The small angle neutron scattering experiments[1] revealed that below 100K there exist the ferromagnetic (ferrimagnetic) clusters with the correlation length of about 100Å which are coupled antiferromagnetically each together, and that the spin glass anomalies are strongly correlated with the abrupt increase of the c-axis component of the spin correlations near T_g with decreasing temperature from high temperatures where the components perpendicular to the c-axis are dominant. The muon spin relaxation (μSR) experiments[3] showed that the fluctuation rate of Fe moments changes rather gradually between $T_g<T<3T_g$ compared with the dilute alloy cases (AuFe, CuMn, AgMn), and that below T~30K the onset of the static random local fields starts, indicating the freezing of the c-axis component fo the Fe moments.

The purpose of this work is to get more detailed information on the spin dynamics in this system by means of neutron inelastic scattering. The experiments were carried out on the LAM spectrometer at KENS, which is the inverted geometry TOF spectrometer using a final energy of 4.59meV. The energy resolution is 200 μeV. The sample was a single crystal of $0.88FeTiO_3$-$0.12Fe_2O_3$ which was the same that was used in the small angle scattering experiments.

In Fig.1, typical example of the observed tmeperature dependence of the

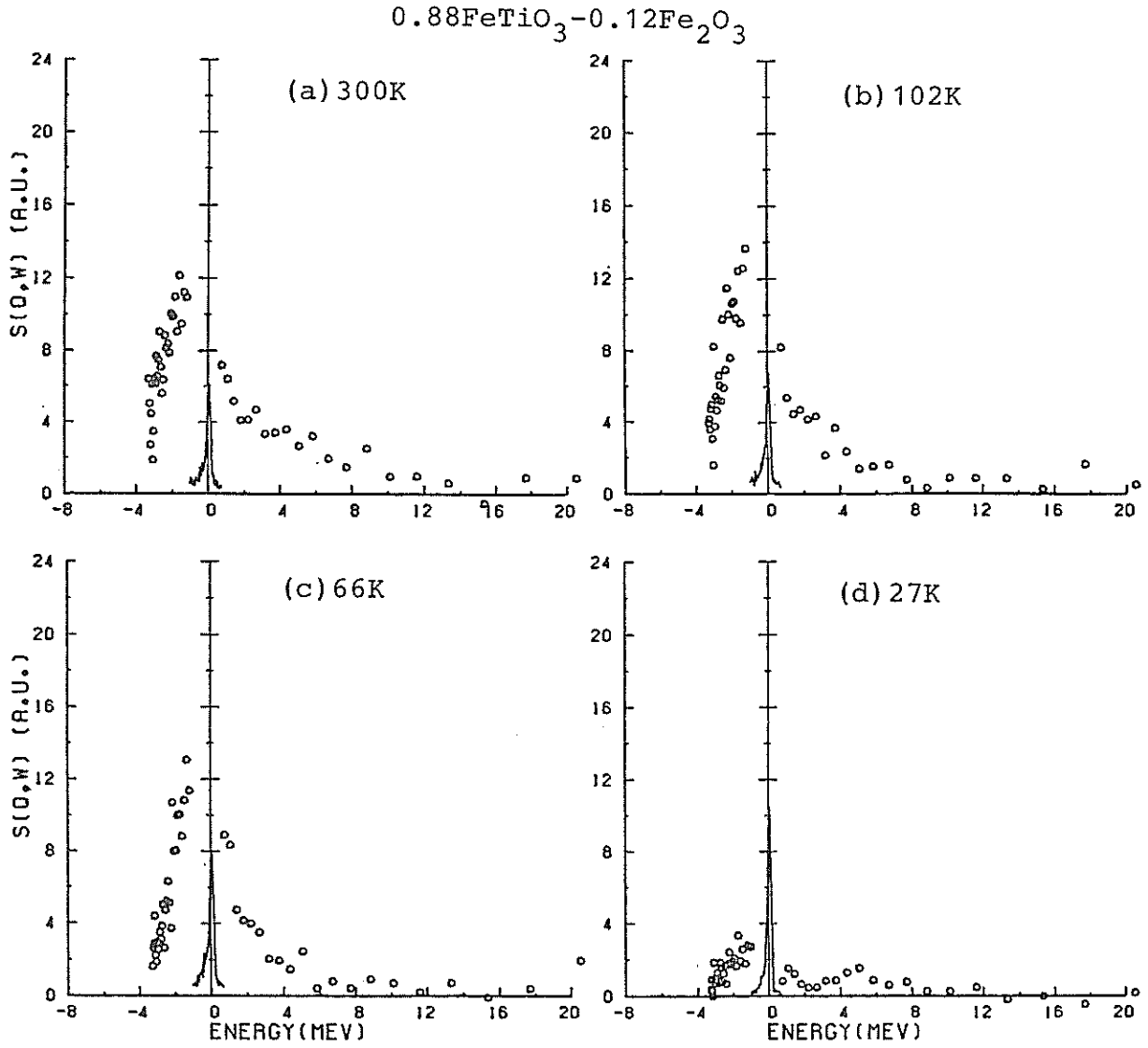

Fig.1. The scattering function $S(Q,\omega)$ VS ω for $Q_o=0.82\mathring{A}^{-1}$ at (a)300K, (b)102K, (c)66K and (d)27K. For the elastic scattering region ($-1<\omega<0.5$meV), they are shown by solid curves on a reduced scale of 1/20.

scattering function $S(Q,\omega)$ is shown. In this case, the scattering vector Q is in the a*-c* plane, the incident neutron wave vector is parallel to the a* axis, and scattering angle is 32° ($Q=Q_0=0.82\mathring{A}$ for $\omega=0$). It is noted that the scattering functions are asymmetric around $\omega=0$. The origin of the asymmetry is not known in this stage, but presumably due to some short range correlations which remain even at room temperature, resulting in strong Q dependence(also ω dependence in TOF experiments) of the scattering intensity. Such asymmetry was seen also in the other scattering angle data to the same order or less. In spite of this complexity, we can clearly see the characteristics of the spin dynamics relevant to the spin glass behaviour of our system as follows:

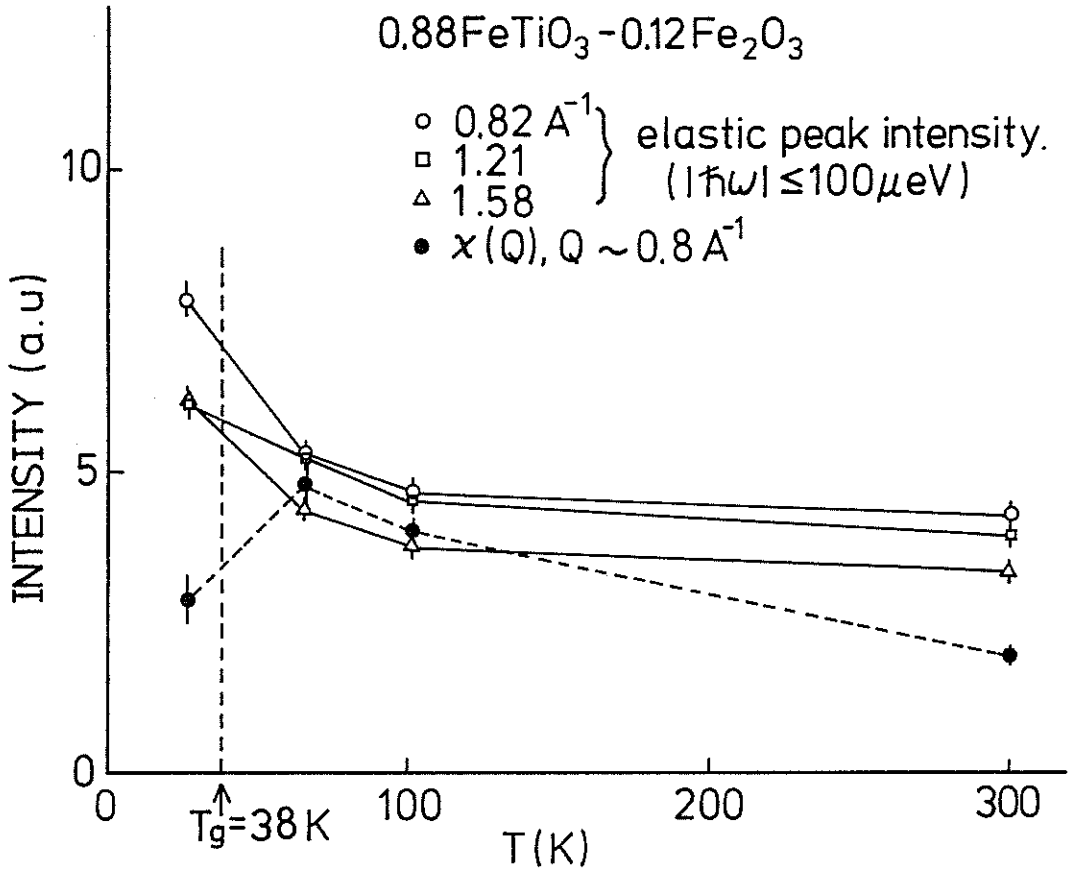

Fig.2. The elastic peak intensity for Q=0.82, 1.21 and 1.58$\mathring{A}^{-1}$, and $\chi(Q)$ for $Q\sim0.8\mathring{A}$ as a function of temperature. The vertical broken line markes the temperature of the maximum in c-axis susceptibility.

i) The low frequency components of the spectral function increase gradually as decreasing temperature from 300K to 66K, and the function changes to a different shape at 27K($<T_g$) which seems to be a summation of a quasi-elastic peak and a broad inelastic peak at 2-5 meV(depend on the scattering angle we observed:32°,48°,54°,70°,86°).

ii) Wave length dependent susceptibility shows a maximum near T=66K and a decrease at T=27K, as shown in Fig.2 by closed circles, which are approximately estimated from the integration of our quasi-elastic (inelastic) scattering data corrected for the detailed balance and energy factors in the scattering function .

iii) Intensities of the "elastic" peaks increase strongly below about 100K. The integrated intensities of them in the energy window of 200 μeV vs. temperature are shown in Fig.2 by open marks for three different Q values.

These features are very similar to the cases of Cu-Mn alloys[4] except that in our case the excitation-like inelastic scattering are seen below T_g(T=27K). As for the inelastic scattering, nearly the same phenomena were observed for the insulator spin glass $Eu_xSr_{1-x}S$ with x=0.5 and 0.52[5].

More detailed study will be done.

references

1) Y. Ishikawa, M. Arai, N. Saito, M. Kohgi and H. Takei:
J. Mag. Mag. Mat. 31-34 (1983) 1381.

2) Y. Ishikawa:
J. Phys. Soc. Jpn. 17 (1962) 1835.

3) Y. J. Uemura, K. Nishiyama, R. Kadono, J. Imazato, Y. Kuno, K. Nagamine, T. Yamazaki and Y. Ishikawa:
J. Mag. Mag. Mat. 31-34 (1983) 1379,

4) A. P. Murani and A. Heidemann:
Phys. Rev. Letters 41 (1978) 1402.
A. P. Murani:
Phys. Rev. Letters 41 (1978) 1406.

5) H. Maletta, W. Zinn, H. Scheuer and S. M. Shapiro:
J. Appl. Phys. 52(1981) 1735.

Neutron Scattering from Zero Alloy

Kazuhiro SAWA*, Kazuhiko INOUE*, Toshiharu FUKUNAGA**,
Masakatsu MISAWA** and Noboru WATANABE+

* Department of Nuclear Engineering, Hokkaido University, Sapporo, 060 Hokkaido, Japan
** Institute for Iron, Steel and other Materials, Tohoku University, Sendai, 980 Miyagi-ken, Japan
\+ National Laboratory for High Energy Physics, Oho-machi, Tsukuba-gun, 305 Ibaraki-ken, Japan

In performing measurements of quasielastic scattering it is customary to use sample containers made of aluminum. Such containers have the disadvantage of producing a strong diffraction peak near $Q \sim 2.6$ Å^{-1} as seen from the spectra measured by the LAM-40 spectrometer depicted in Fig.1. In the case of the liquid scattering sample, a more sophisticated design sample container made of a metal which does not cause coherent scattering is desired. As is well known, vanadium is a typical incoherent scatterer, but it is not very compatible with water and lacks sufficient malleability. In our search for a more appropriate metal, we measured the scattering from a zero alloy cylinder, 68 % Ti and 32 % Zr alloy, by using the LAM-40 spectrometer. Fig. 2 depicts the data obtained, and Fig. 3 shows the total intensity as a function of Q, in which the results were normalized by the measured vanadium intensity.

There is no strong diffraction peak in the Q range from 0 to 2.6 Å^{-1}, but in using zero alloy we noticed some diffuse scattering due to the fact that it is a non-stoichiometric solid solution. Obviously, zero alloy is superior to aluminum for the design of the sample container in that there is no strong variation in the total cross section. However, the total cross section of zero alloy is several times larger than that of aluminum

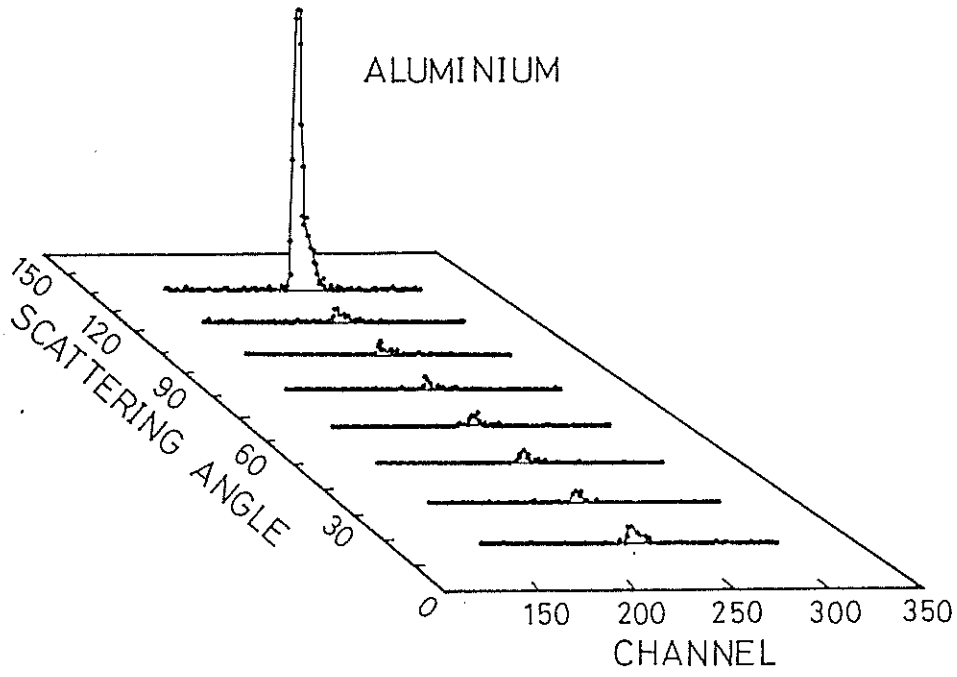

Fig. 1 Time of flight spectra of aluminium cylinder.

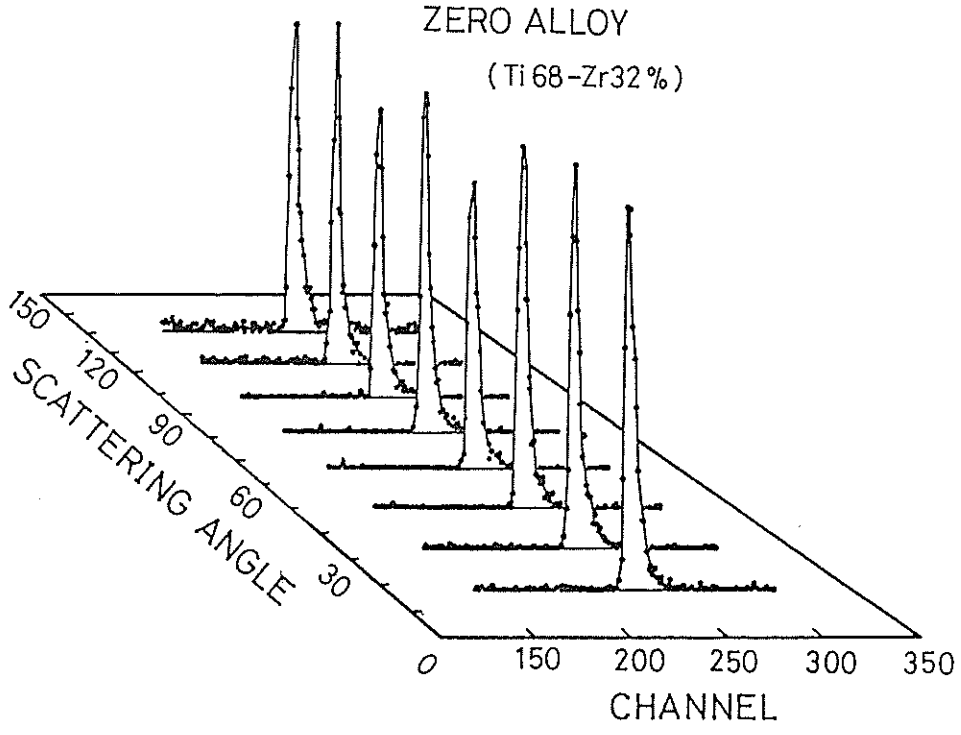

Fig. 2 Time of flight spectra of zero alloy cylinder, 68% Ti and 32% Zr alloy.

du to the incoherent scattering of titanium. Accordingly, if zero alloy is used, the walls of the container should be made thinner.

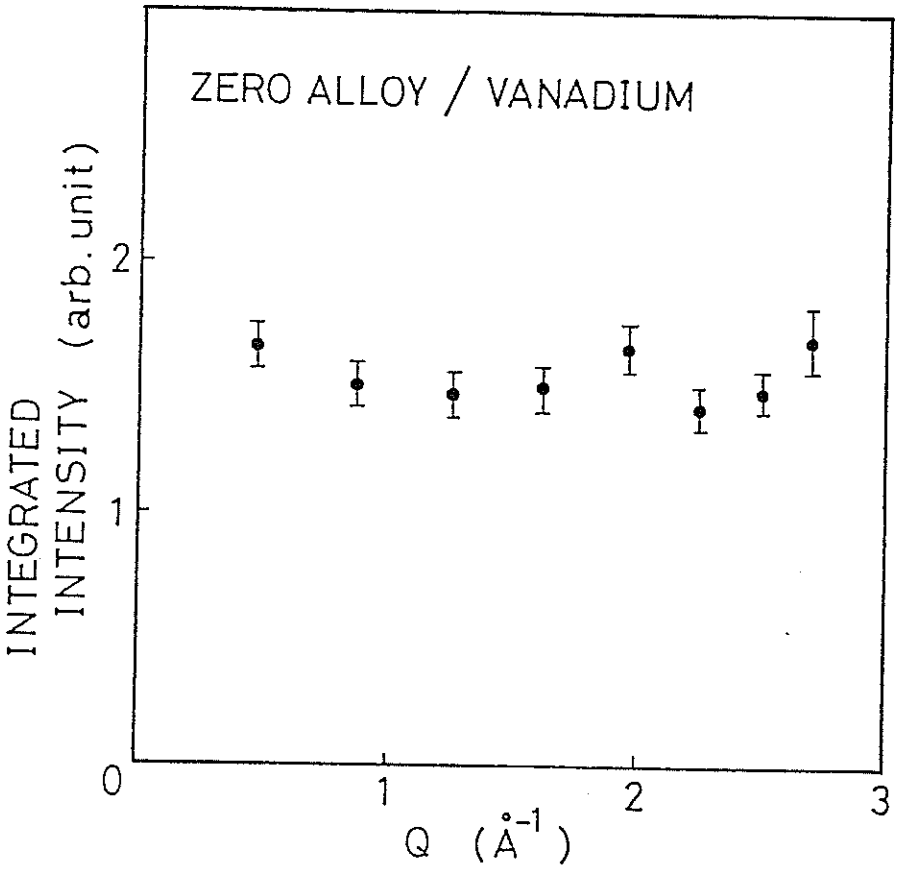

Fig. 3 Total intensity of zero alloy as a function of Q, normalized by measured vanadium intensity.

Scattering Cross Section and Neutron Spectra in the Condensed Methane

Kazuhiko INOUE, Toshiaki HORIMOTO, Hiroshi AKIE,
Yoshiaki KIYANAGI and Hirokatsu IWASA

Department of Nuclear Engineering, Hokkaido
University, Sapporo, 060 Hokkaido, Japan

Condensed methane is known to be the best cold moderator for the pulsed cold neutron source. Several authors have investigated the scattering cross section and neutron spectra of condensed methane. To obtain the optimun design for the pulsed cold source using condensed methane, more comprehensive information on neutron transport in condensed methane is needed. We have begun extensive measurements and analysis to accumulate these data.

First, we conducted preliminary measurements of the activation energy for the diffusive rotation of the methane molecule at the temperature range from 20 K to 100 K by using the LAM-40 spectrometer. Fig. 1 shows the

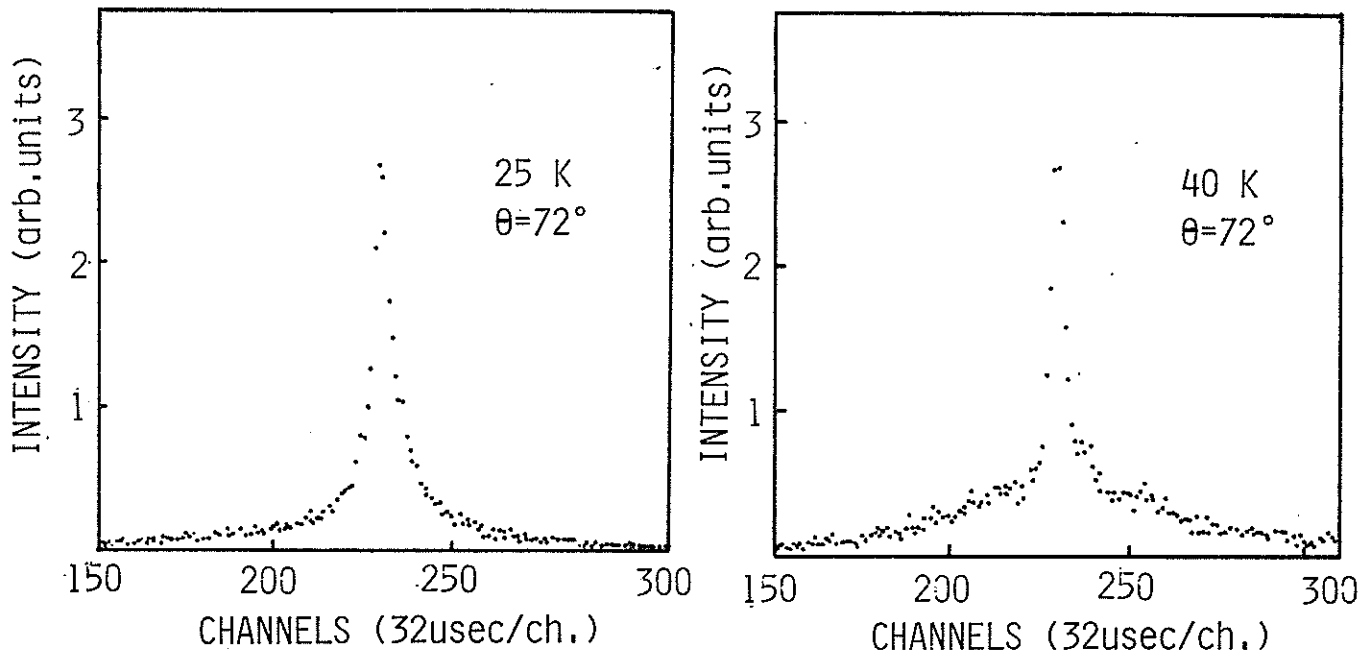

Fig. 1 Time-of-flight spectra from condenced methane at 25K and 100K, a scattering angle of 72°.

typical scattering spectra from condensed methane at temperatures 25 K and 40 K, respectively. Fig. 2 depicts the inverse-temperature dependence of the rotational diffusion constant from which we obtained the value of the activation energy, Ea, as follows:

$$Ea = 1.74 \text{ meV}. \qquad (1)$$

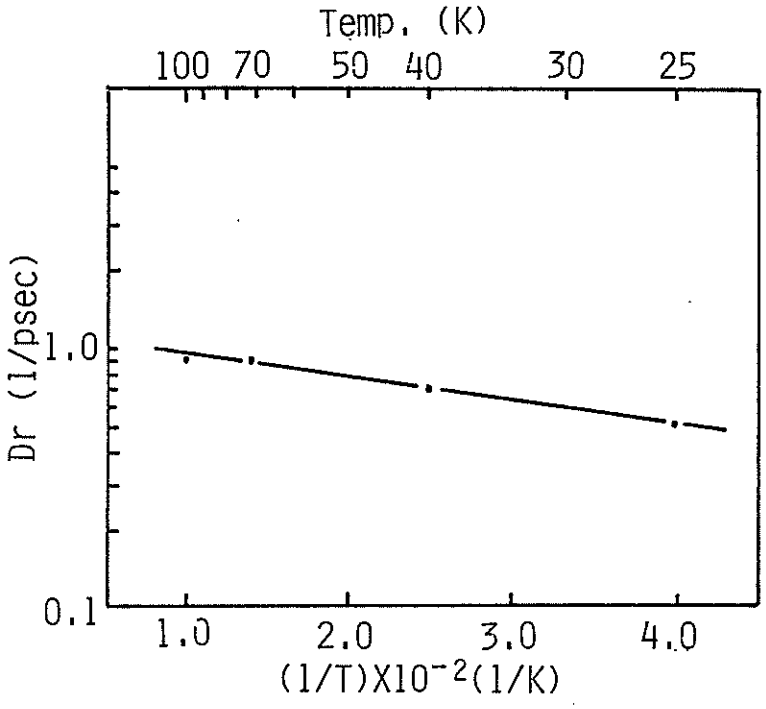

Fig. 2 The rotational diffusion constant as a function of 1/T.

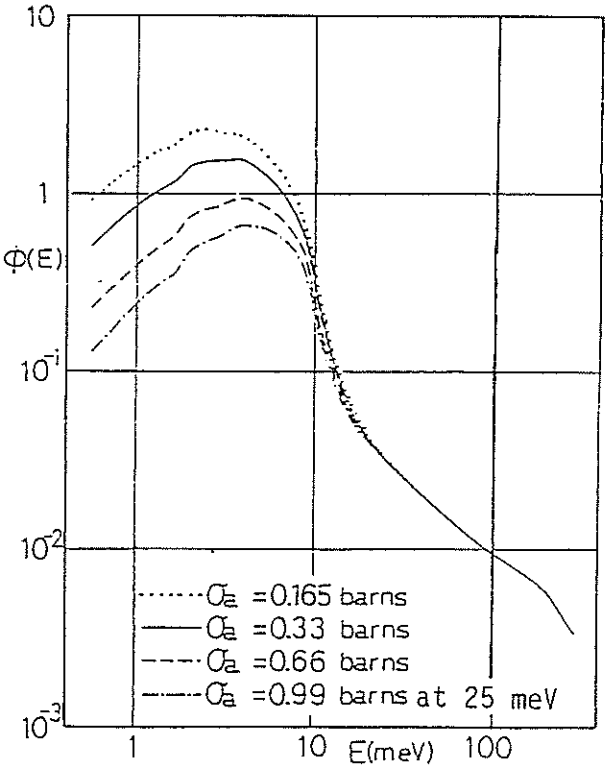

Fig. 3 The calculated neutron energy spectra in 20K methane.

Secondly, we calculated the neutron spectra in the condensed methane solving numerically the transport equation:

$$[\sigma_a(E) + \sigma_s(E)]\phi(E) = \int_0^\infty \sigma(E' \to E)\phi(E')dE'. \qquad (2)$$

Fig. 3 shows a preliminary result for the neutron energy spectra in 20 K methane, and for the cases of larger and smaller absorptions. We used a simplified scattering model in the above calculation. Plans are under way to divise an improved model, including the cross section parameter described above.

Study of Melanin by Neutron Inelastic Scattering

Yasuhiro MIYAKE, Yoshinobu IZUMI, Katsunari YASUDA,
Kazuhiko INOUE* and Yoshiaki KIYANAGI*

Department of Polymer Science, Faculty of Science,
*Department of Nuclear Engineering, Faculty of Engineering,
Hokkaido University, Sapporo 060

In a previous report, neutron inelastic scattering (NIES) profiles of dopa and sepia melanins measured by LAM D (DIX) spectrometer were presented, where we pointed out the differences of profiles over 10–650 cm^{-1} in both NIES spectra. But we found out that previous results were contaminated with NIES from the environmental substances of sample such as air, container and etc. Therefore we measured NIES of both melanins except the effect of environment again. The obtained results are shown in Fig. 1 and infra-red absorption spectra of both melanins are also shown in Fig. 2 for comparison. We can see apparent NIES at 700 cm^{-1} in both profiles, which may be attributed to some of complicated motions of complex ring molecule with nitrogen such as indolequinone[1], even though distinct absorption was not appeared in this region of IR spectra, and we cannot find a characteristic NIES over 10–500 cm^{-1}, where torsional motions of methyl group in polymer exist[2]. Then it seems that melanin will be rodlike and oligomeric complicated molecule constituted from various ring molecules including indole ring and may not have many pendant groups. But it is necessary for us to understand the true structure of melanin and to measure NIES of melanin at very low temperature and its homologues such as indole and dopa in more details, to assign the profile correctly, although our speculation for estimation of profiles may not be so incorrect from considerations of our results of melanin by x-ray scattering and solubility test and so on.

References

1)A.D.Cross, An Introduction to Practical Infra-Red Spectroscopy, 1960, Butterworths.

2)G.Allen and J.S.Higgins, Rep.Prog.Phys. 36(1973)1073.

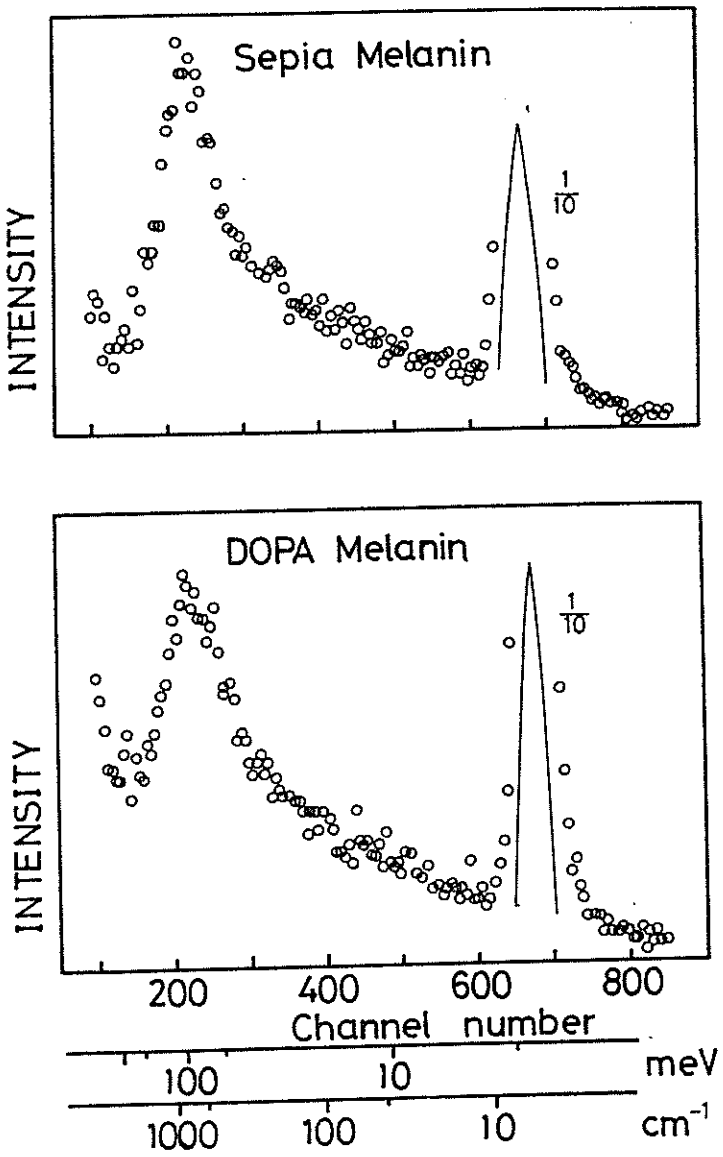

Fig. 1. Time-of-flight downscattering spectra from melanins.

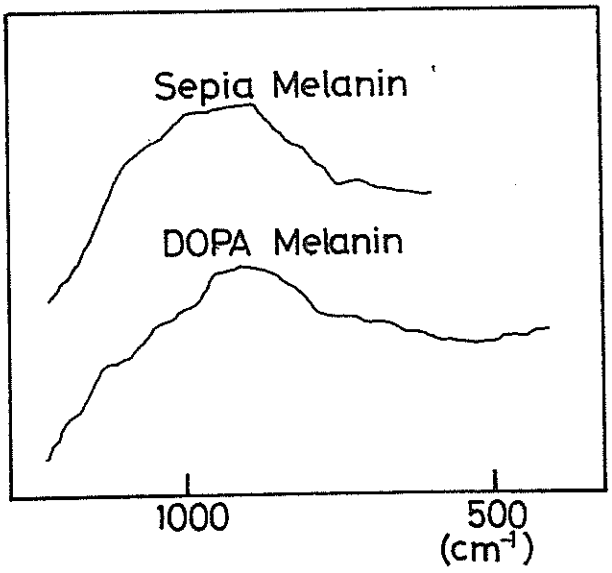

Fig. 2. IR spectra from melanins.

Inelastic Neutron Scattering of Amorphous Selenium

Kaoru SHIBATA, Hideshi FUJISHITA and Sadao HOSHINO

Institute for Solid State Physics, The University of Tokyo
Roppongi, Minato-ku 106, Japan

Dynamical properties of amorphous materials, especially an existence of collective excitations, are interesting subject to study. Neutron scattering studies of amorphous selenium have been reported by several authors in which vibrational density of states(VDOS) was measured[1] and the existence of the collective excitations was reported[2]. In this report, the dynamical scattering function and the vibrational density of states of amorphous selenium measured by LAM-40 and LAM-D spectrometers are presented. They are compared with previous measurements.

Using LAM-40, the low energy part of dynamical scattering function $S(Q,\omega)$ was measured at room temperature with momentum transfers between 0.2 and 2.6 A^{-1} and energies ≤ 9.0 meV. Sample shape was a cylindrical tube with 13.4 mm external diameter, 10 mm internal diameter and about 100 mm length. Fig.1 shows a result of measurements of constant-θ spectra. From the four constant-θ $S(Q,\omega)$ with large θ values, VDOS was obtained in the energy range from 0.3 to 9.0 meV (Fig.2). This averaging procedure was made in order to ensure an application of incoherent approximation preventing the effect of coherent scattering. As seen from Fig.1 no collective excitation peak as was reported by Sacchetti et.al.[2] can be found. Using LAM-D, an inelastic TOF spectrum at $2\theta=110°$ was also measured at room temperature. Sample shape was a rod with 14.0 mm diameter and about 80 mm length. VDOS(Fig.3) was obtained in the energy range from 0.8 to 50.0 meV using this TOF spectrum with the incoherent approximation. In the above analysis an absorption correction and a correction for incident neutron spectrum were made. However corrections for multiple scattering, multi-phonon process and energy resolution effect were not made. In spite of the lack of these corrections, results of VDOS obtained by the above two measurements coincide with each other in the common energy range. Presently obtained VDOS is almost consistent with Gompf's result[1], but the width of optical mode($\omega_{op} \simeq 35$ meV) appeared in Fig.3 is wider than Gompf's result, which

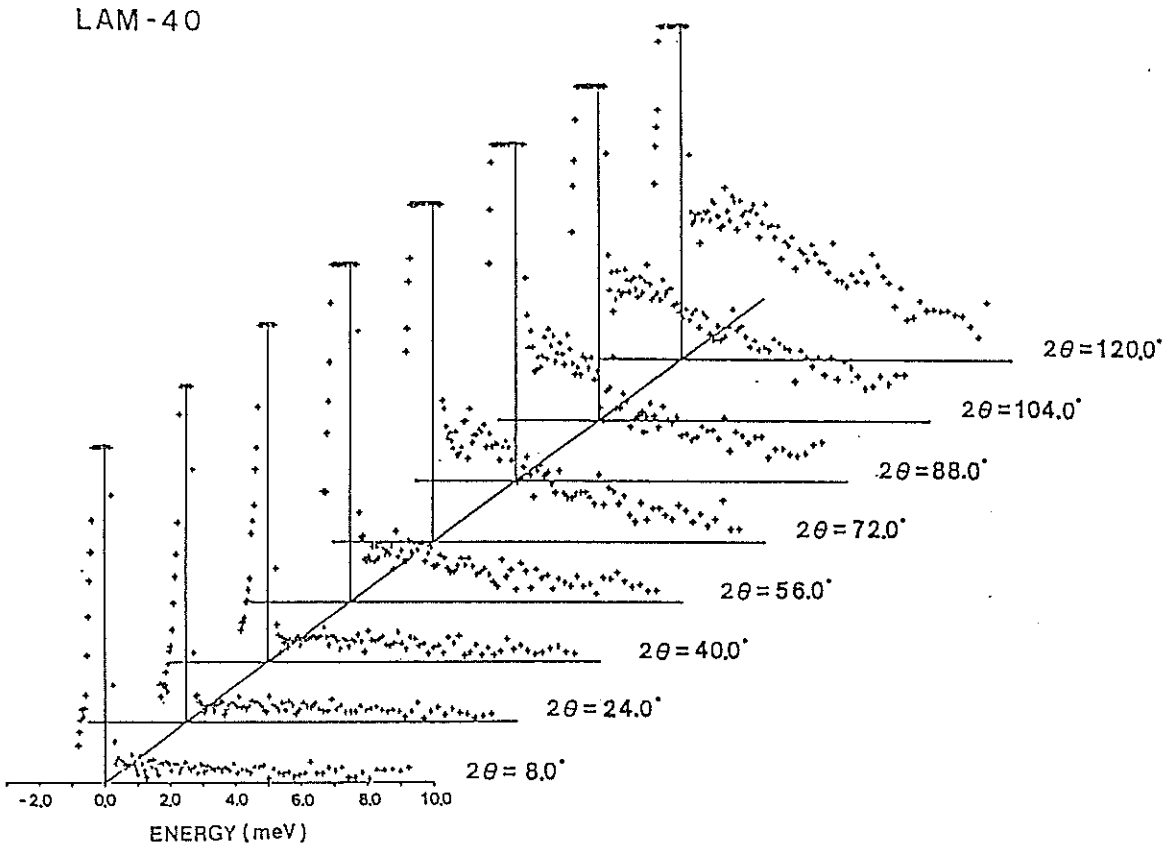

Fig. 1 Dynamical scattering functions of amorphous selenium measured by LAM-40 at room temperature.

may be due to the resolution effect. As shown in Fig.2 low energy part ($\omega \leq 0.5$ meV) of VDOS slightly deviates from a Debye type spectrum($\propto \omega^2$), which might be caused by a Schottky type specpfic heat anomaly[3]. However, in order to obtain a definite conclusion the more precise measurement and its analysis seem to be necessary.

References

1) F.Gompf : The Physics of Selenium and Tellurium, ed. E.Gerlach and P.Grosse(Springer-Verlag, New York,1979)p.64.

2) F.Sacchetti,P.Bosi and F.Menzinger : J.Phys.C15(1982)4483.

3) R.O.Pohl : Amorphous Solids Low-Temperature Properties, ed. W.A.Phillips(Springer-Verlag, New York,1981)p.27.

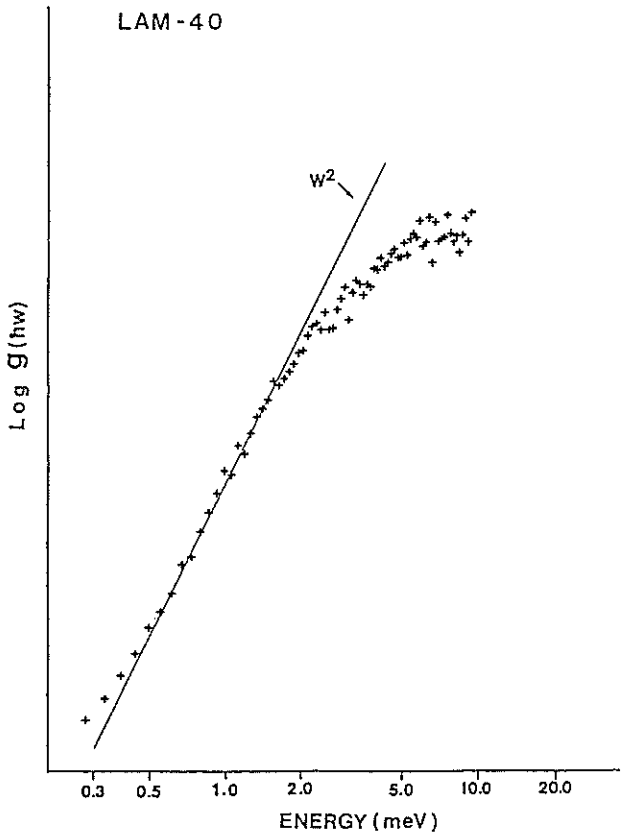

Fig. 2 Vibrational density of states of amorphous selenium reduced from $S(Q,\omega)$ in Fig. 1.

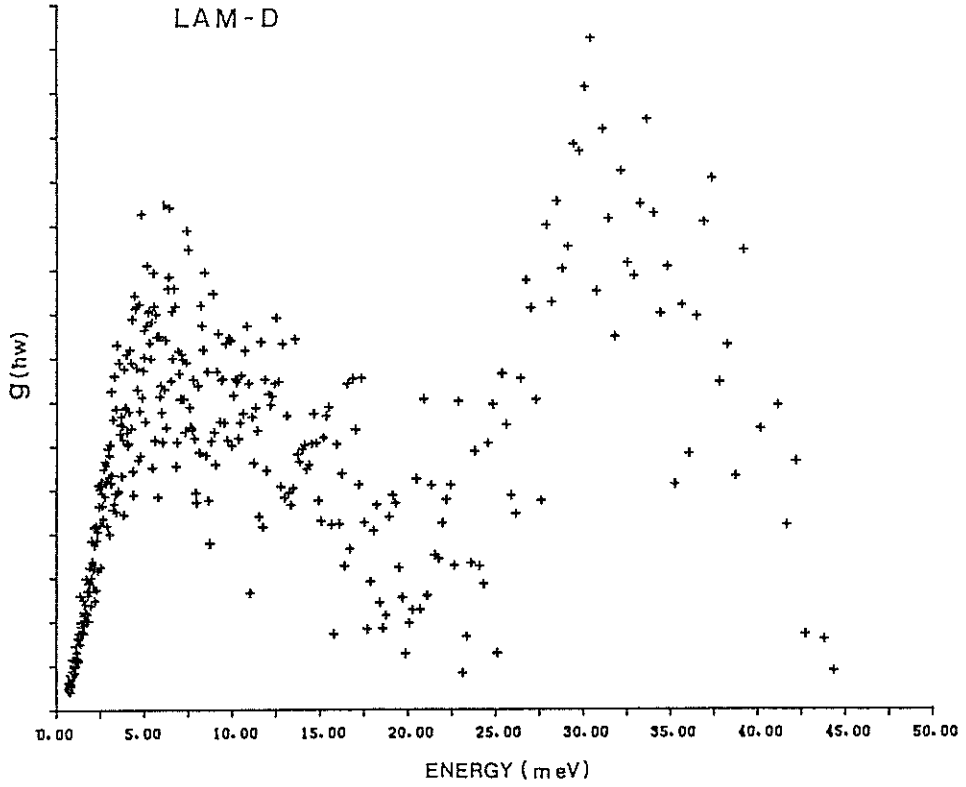

Fig. 3 Vibrational density of states of amorphous selenium measured by LAM-D at room temperature.

Neutron inelastic scattering of partially deutrated poly(vinyl alcohol) film

Toshiji Kanaya, Keisuke Kaji, Hiroshi Urakawa, Ryozo Kitamaru and Kazuhiko Inoue*

Institute for Chemical Research, Kyoto University, Uji, Kyoto-Fu 611 and * Department of Nuclear Engineering Faculty of Engineering, Hokkaido University, Sapporo 060

Extensive studies have been carried out of the vibrational modes of molecules in polymers by infrared(IR) and Raman spectroscopy. However, there are inactive modes in such spectroscopies. On the other hand, neutron inelastic scattering is not limited by the selection rule because neutrons are scattered directly by atomic nuclei. In this work, we investigate the molecular vibrational modes in poly(vinyl alcohol)(PVA) by neutron inelastic incoherent scattering using partially deuterated samples. The incoherent scattering cross-section of deuterium is much smaller than that of hydrogen atom. Therefore, the vibrational modes concerned with deuterated part will disappear in neutron inelastic scattering spectrum. The neutron scattering measurements were carried out using LAM-D spectrometer at KENS. Two kinds of partially deuterated PVA were prepared; one is deuterated in main chain $-(CD_2CD(OH))_n-$:(PVA-DH) and the other in side group $-(CH_2CH(OD))_n-$:(PVA-HD). The unoriented films heat-treated at 160°C for ca. 5 min were used as samples, the thickness of which was ca. 0.25 mm . The observed time-of-flight(TOF) spectra of PVA-DH and PVA-HD are shown in Fig. 1. Referring to the assignments of the vibrational modes from IR spectroscopy,[1),2)] it is found that the vibrational modes concerned with main chain such as C-H streching (2950 cm^{-1}), CH_2 wagging and bending(ca. 1300 cm^{-1}) and CH_2 rocking (ca. 900 cm^{-1}) disappear in the spectrum of PVA-DH and that the modes concerned with the side group such as OH streching(ca. 3500 cm^{-1}) disappear in the spectrum of PVA-HD. Details in the low frequency region is now in consideration.

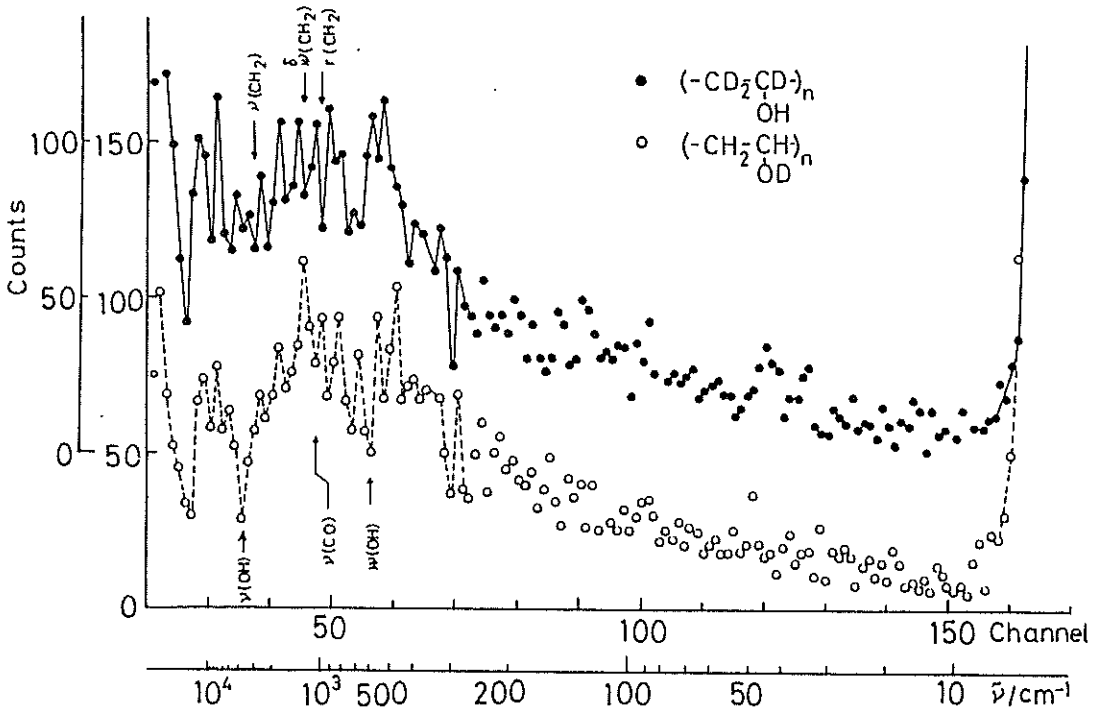

Fig. 1. Time-of-flight spectra of unoriented film of partially deuterated poly(vinyl alcohol) at scattering angle of 60°. The abssicca designates the time of flight of scattered neutrons; the channel width 32 μs. ●: PVA-DH; ○:PVA-HD. ν: streching, δ: bending; w: wagging; r: rocking.

References

1) S. Krimm, C. Y. Liang and G. B. B. M. Sutherland, J. Polym. Sci., 22, 227(1956).

2) H. Tadokoro, H. Nagai, S. Seki and I. Nitta, Bull. Chem. Soc. Jpn., 34, 1504(1961).

Neutron inelastic scattering of partially deuterated poly(vinyl acetate) film

Toshiji Kanaya, Keisuke Kaji, Hiroshi Urakawa, Ryozo Kitamaru and Kazuhiko Inoue*

Institute for Chemical Research, Kyoto University, Uji, Kyoto-Fu 611 and * Department of Nuclear Engineering Faculty of Engineering, Hokkaido University, Sapporo 060

Deuteration of samples is a powerful method for assignment of molecular vibrational modes in neutron inelastic scattering experiment because incoherent scattering cross-section of deuterium atom is much smaller than that of hydrogen atom. In this work, we have studied the vibrational modes in poly(vinyl acetate)(PVAc) by neutron inelastic incoherent scattering, using three kinds of samples; $-(CH_2CH(OCOCH_3))_n-$: PVAc-HH, $-(CH_2CH(OCOCD_3))_n-$:PVAc-HD; $-(CD_2CD(OCOCH_3))_n-$:PVAc-DH. The unoriented films are ca. 0.25 mm thick. The neutron scattering measurements were carried out by LAM-D spectrometer at KENS. The observed TOF spectra are shown in Fig. 1 (a), (b) and (c) for PVAc-HH, PVAc-DH and PVAc-HD, respectively. A broad peak is observed at ca. 250 cm^{-1} in the spectrum of PVAc-HH and at ca. 200 cm^{-1} in the spectrum of PVAc-DH. However, in the spectrum of PVAc-HD, no peak is observed while the scattering intensity in the energy region larger than ca. 400 cm^{-1} is stronger than that in the energy region around ca. 200 cm^{-1}. The peak at 200 cm^{-1} of PVAc-DH is due to the vibrations of methyl group because it disappears in the spectrum of PVAc-HD. It should be assigned to torsional mode of methyl group from the analogy with other polymers.[1] The peak at 250 cm^{-1} of PVAc-HH is also due to torsional vibration of methyl group though the peak position is slightly shifted from that of PVAc-DH. It is considered that this apparent shift is caused by the superposition of the main chain modes, since the vibrational modes of PVAc-HD which are assigned to main chain vibration are observed at the higher energy region larger than ca. 400 cm^{-1}.

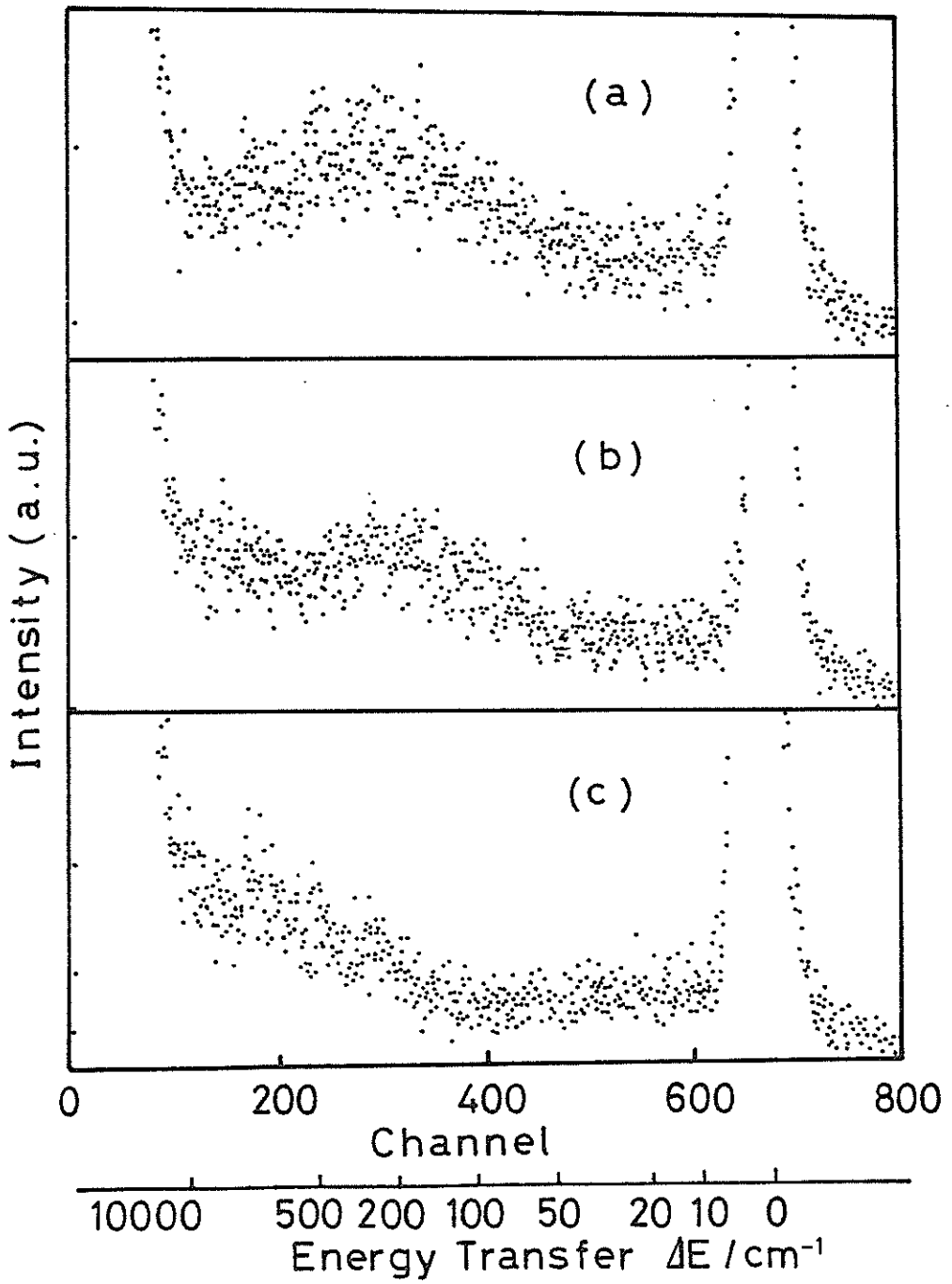

Fig. 1. Time-of-flight spectra of protonated and partially deuterated poly(vinyl acetate)(PVAc) at scattering angle of 60° (a): PVAc-HH; (b): PVAc-DH; (c): PVAc-HD. A channel width is 8 μs.

Reference

1) J. S. Higgins, "Developments in Polymer Characterization-4", Ed. J. V. Dawkins, Appl. Sci. Pub., London, 1983, Chapter 4.

Neutron Spectra Scattered from Amino Acids

Itaru KANEKO and Kazuhiko INOUE

Department of Nuclear Engineering, Hokkaido University,
Sapporo, 060 Hokkaido, Japan

We have conducted some neutron scattering measurements from amino acids, glicine and alanine for the purpose of checking the performance of the LAM-D spectrometer, which is an energy-focusing type time-of-flight spectrometer. As shown in the previous communication [1], the LAM-D is an inverted geometry, downscattering type which enables us to measure a considerably wide range of energy transfer, up to about 2000 $\sim$ 3000 cm^{-1}; this capacity makes it very useful in chemical applications.

The measured spectra are represented in Figs. 1 and 2 for glycine at scattering angles 40° and 90°, and Figs. 3 and 4 for alanine, respectively. Gupta et al. measured the spectra from the glycine and alanine by using a beryllium filter chopper spectrometer installed in a reactor source [2,3]. Comparing our data with theirs, good agreement is found in the frequency region of less than about 500 cm^{-1}. In the case of the direct geometry spectrometer, that is the upscattering type one, it is not feasible to measure the spectra for frequency regions larger than about 500 cm^{-1}. In the case of the LAM-D, however, due to its use of the pulsed neutron source, measurements for frequency regions up to about 3000 cm^{-1} are feasible, as shown in Figs. 1 $\sim$ 4.

References

[1] K.Inoue, Y.Kiyanagi, H.Iwasa and K.Jinguji, KENS REPORT-III(1982)52.

[2] V.D.Gupta and R.D.Singh, Chem.Phys.Lett., 5(1970)218.

[3] V.D.Gupta and M.V.Krishnan, J. Phys., B-3(1970)572.

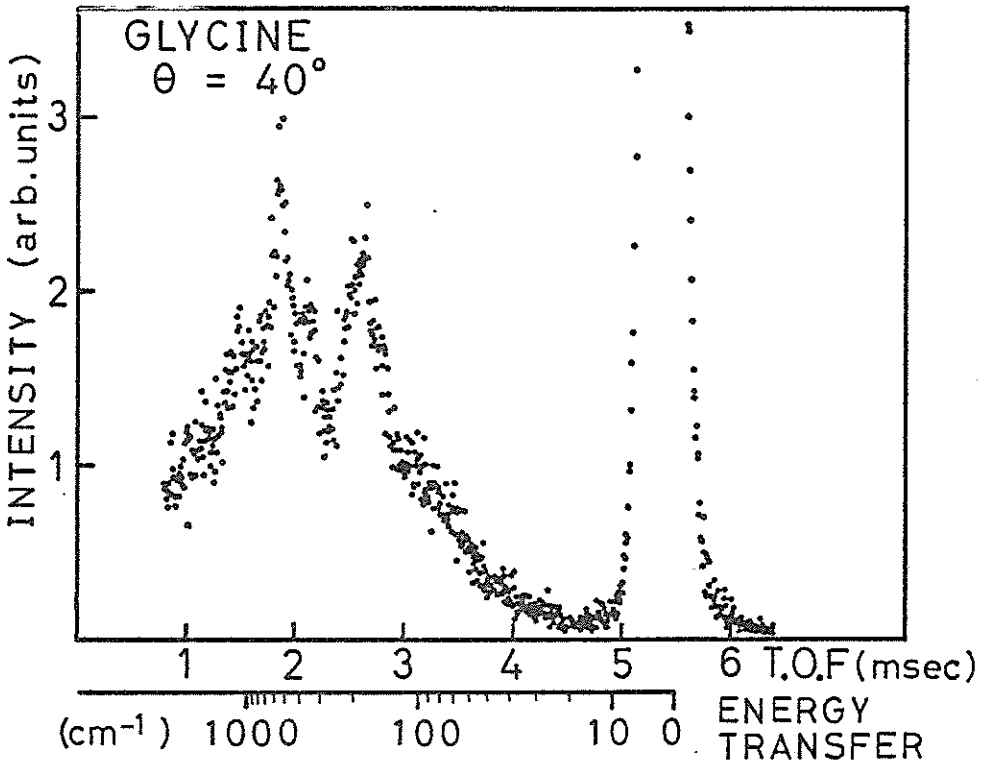

Fig. 1 TOF spectrum of glycine at scattering angle of 40°.

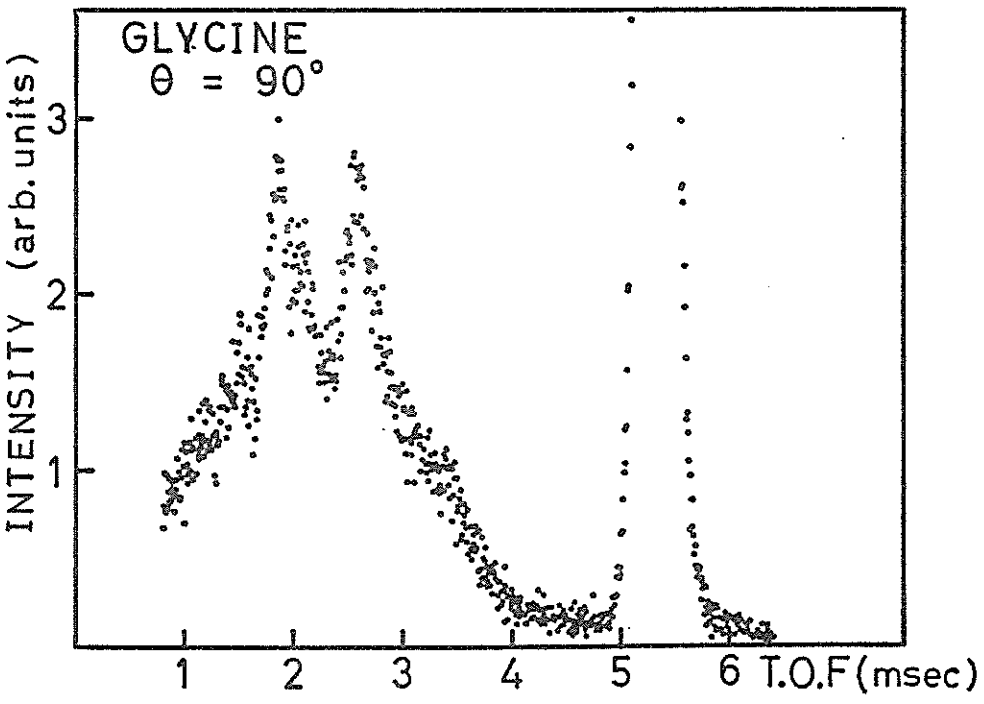

Fig. 2 TOF spectrum of glycine at scattering angle of 90°.

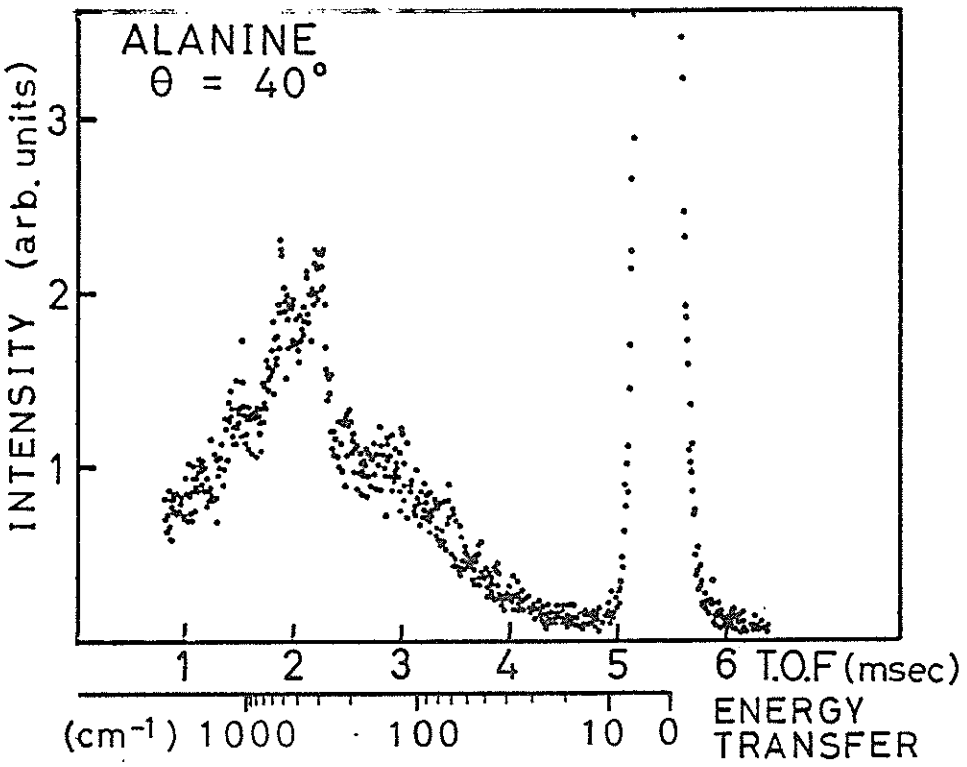

Fig. 3 TOF spectrum of alanine at scattering angle of 40°.

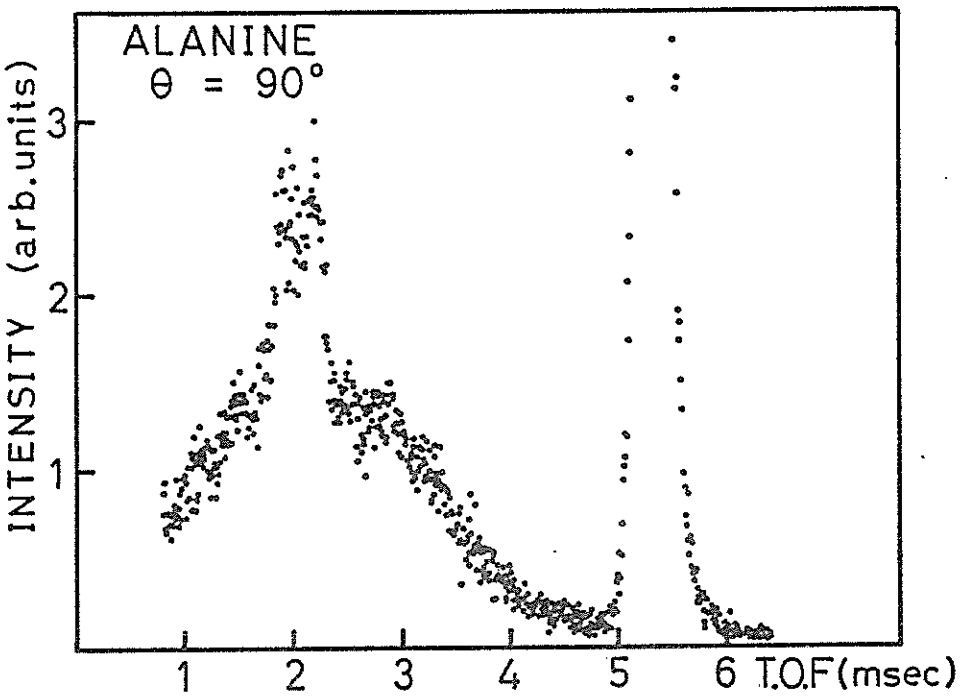

Fig. 4 TOF spectrum of alanine at scattering angle of 90°.

The Observation of the Optical Phonon Mode in TiO_2

K. TAJIMA, N. WAKABAYASHI, Y. TODATE,* S. TOMIYOSHI**
and
Y. ISHIKAWA*

Department of Physics, Keio University,
Yokohama 223, Japan

* Department of Physics, Tohoku University,
Sendai 980, Japan

** Research Institute for Iron, Steel and Other Metals,
Tohoku University, Sendai 980, Japan

Observation of the full phonon dispersion relation is indispensable to the investigation of the coupling mechanism in solids. However, the optic phonon modes are generally in the region of rather high energies and it is sometimes quite difficult to detect them by using a triple axis spectrometer installed at a nuclear reactor.

In order to check the possibility of observing high energy phonon dispersion curves at the KENS pulsed neutron source, a TiO_2 single crystal was examined by means of the MAX spectrometer[1]. Measurements were performed in 2 days along the [100] direction at room temperature.

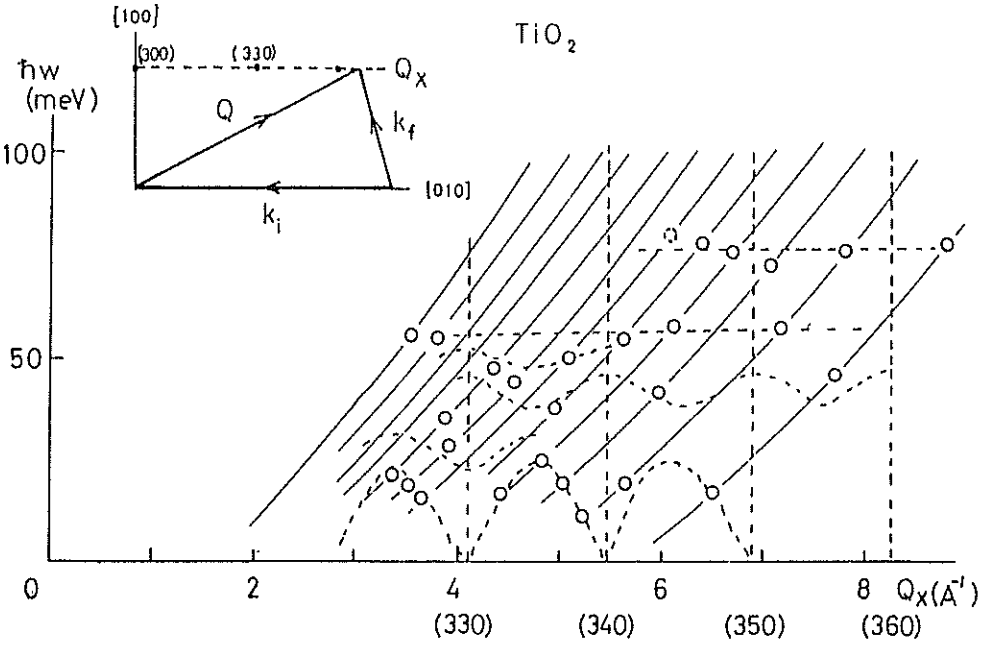

FIGURE 1

The scattering diagram and the range of scans are shown in Figure 1. Observed phonon peak positions are also marked in the figure. As the spectrometer configuration was optimised to observe high energy phonons, the peaks corresponding to the acoustic and lower optic modes were not well resolved. However, the high energy optic phonon peaks were well resolved at the energy around 75 meV. These phonons are longitudinal because the scattered neutron intensities decreased by decreasing the Q_x value. Results are in good agreement with the previous measurement performed at ORNL[2], which are shown by the dotted lines in Figure 1. Since it took only two days to obtain the results presented here, the MAX spectrometer seems to be powerful in measuring high energy phonon dispersion relations.

1) K. Tajima et al. Nuc. Inst. Meth. 201 491 (1982); Physica 120

2) J. Traylor et al. Phys. Rev. B3, 3457 (1971).

Magnetic excitations in a quasi-two dimensional antiferromagnet $MnTiO_3$ measured with MAX

Y. Todate, Y. Ishikawa, K. Tajima*, S. Tomiyoshi**
and H. Takei**

Physics Department, **Institute for Iron, Steel and Other Metals, Tohoku University, Sendai and *Faculty of Science and Technology, Keio University, Yokohama

$MnTiO_3$ has the ilmenite structure in which Mn^{2+} and Ti^{4+} layers alternate along the c-axis of the hexagonal lattice. It becomes antiferromagnetic below T_N=63.5K and has an antiferromagnetic structure with the Mn^{2+} spins aligned antiparallel within each layer,directing along the c axis.The crystal and magnetic structures are shown in Fig.1(a).[1] The static susceptibility exhibits, however, almost no anomaly at T_N, but has a broad maximum around 90°K, as shown in Fig.1(b), suggesting the two dimensional character of this substance. This behavior is quite contrasted with the antiferromagnetism of other ilmenites, $FeTiO_3$, $CoTiO_3$ or $NiTiO_3$[2)3)].

We have studied the magnon dispersions in $MnTiO_3$ by using MAX. One emotion of this study was that $MnTiO_3$ is the most simple antiferromagnet in which the magnetic unit cell contains only one antiferromagnetic spin pair and the spin direction (c axis) allows to have only the 180° domains. Therefore the resolution correction can be made easily to the observed magnon groups to get an accurate information. Another more important emotion was that the MAX has an advantage for studying the collective excitations in the 2D system, because the dispersions are defined only by the function of the distance q_a from the Bragg line(c* axis). Therefore the constant Q scans can automatically be performed with the MAX. Such a characteristic of MAX can be examined for $MnTiO_3$ though the substance is not a perfect 2D antiferromagnet.

The single crystal used in the experiments was made by floating zone method with controlling oxygen pressure,and has the cylindrical shape, 8mm in diameter and 60mm in height. The crystal was mounted in a low temperature cryostat with a cryopump (CRYO-MINI) and the measurements were carried out with MAX either along the c* axis through (101) or along the a* axis through (104) as shown in the inset to Fig.3. If the sample is the perfect 2D anti-

ferromagnet, the scans along different lines parallel to the c* axis are enough to get the whole dispersions which can, in principle, be performed at the same time by a single configuration measurement. The magnon groups observed along a* by one counter at different temperatures are shown in Fig. 2 and the magnon dispersions along c* and a* obtained from the observed groups are displayed in Fig.3. The dispersion relations plotted by the brokedn lines are determined at 5 K for the same sample by employing the triple axis spectrometer TUNS at JAERI, which deviates systematically from those obtained by MAX. The origin of the deviation is not clear, but would be at least partly due to the resolution effect and is a subject of further studies*. For the present resolution of the MAX spectrometer, the deviation is not so significant as indicated by two arrows to the magnon groups at 17 K ing Fig.2.

The magnon dispersions were analyzed by the Heisenberg theory with the magnetic interactions J_i defined in Fig.1(a) and the magnetic anisotropy. The parameters determined from the dispersions by MAX and TUNS are listed respectively in Table 1. Both results are not so much different and they show clearly that only the mangetic interaction between the nearest neighboring Mn^{2+} spins in the same layer predominates over all other interactions. In this table are also listed the molecular field from adjacent spins in the same plane $H^{intra}=\Sigma 2J_i S_i$ as well as that from the spins in the adjacent layers H^{inter}. The ratio of $H^{inter}/H^{intra} = 0.05$ is slightly bigger than that estimated from the critical scattering $H^{inter}/H^{intra} = 0.034\pm0.05$[4]. All results are consistent with the quasi-2D character of the substance. Note that a dotted line in Fig.1(b) was calculated using only an inplane exchange interaction $\bar{J} = \Sigma^{intra} J_i n_i/n_1 = 7.5$ K.

References

1) G. Shirane, S. J. Pickart and Y. Ishikawa ; J. Phys. Soc. Jpn 14(1959)1352
2) R. W. Newnham, J. H. Fand and R. P. Santoro ; Acta, Crystllogr, 17(1964)240
3) J. J. Sticler, S. Kern, A. Wold and G. S. Heller ; Phys. Rev. 164(1964)765
4) J. Akimitsu and Y. Ishikawa ; J. Phys. Soc. Jpn 42(1977)462

* Note added in proof

Recent careful analysis of the spectra of MAX has clarified that the deviation is due to the misindication of analyzer crystal angles. The results by both spectrometers finally agree satisfactorily with each other.

Table 1. Exchange and anisotropy parameters determined from magnon dispersions.

	MAX (°K) (17 K)	TUNS (°K) (5 K)
J_1	-4.52 ± 0.10	-5.65
J_2	0.42 ± 0.04	0.36
J_3	-0.39 ± 0.08	-0.34
J_4	0.054 ± 0.012	0.006
J_5	-0.046 ± 0.025	-0.147
J_6	-0.57 ± 0.08	-1.18
$g\mu_B H_A$	0.48 ± 0.30	1.55
H^{intra} $=(\Sigma 2JiSi)$	88.9	113.3
H^{inter}	4.1	6.2
H^{inter}/H^{intra}	0.047	0.055

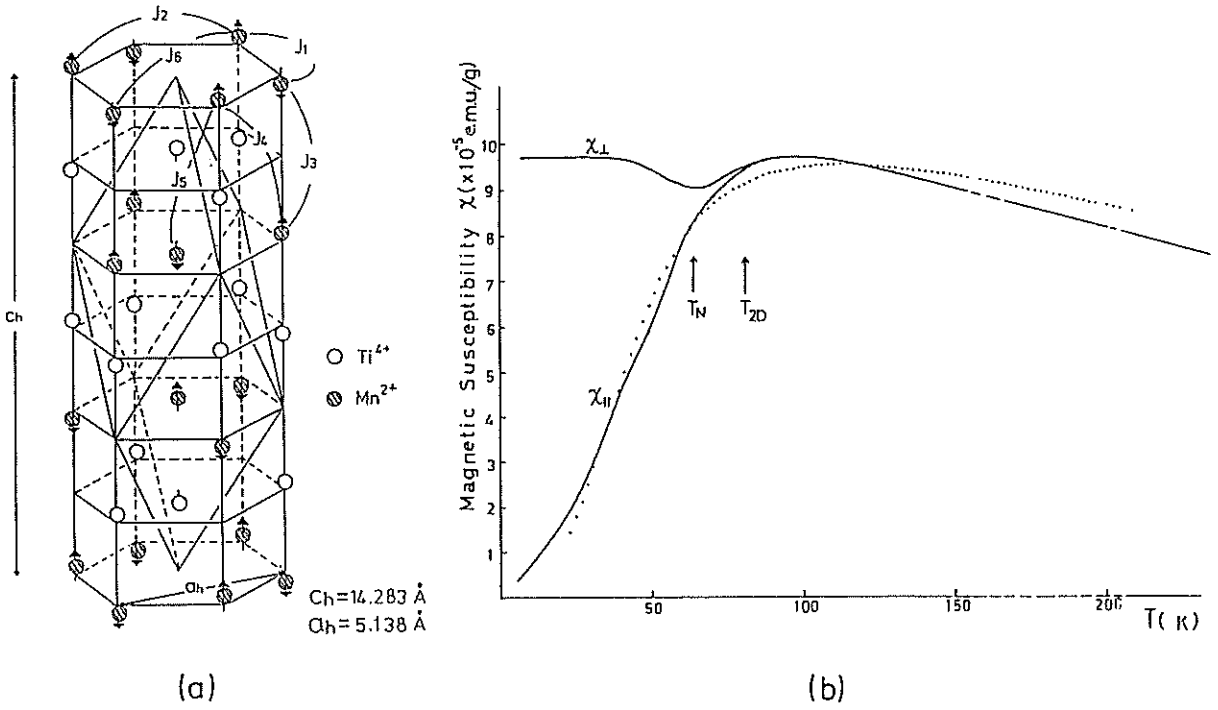

Fig.1 (a)Csystal and magnetic structures of $MnTiO_3$, (b)Static susceptibilities along c, $\chi_{//}$ and perpendicular to it $\chi_{\perp}$. Dotted line was calculated by assuming only an inplane interaction $\bar{J}$ = 7.5K.

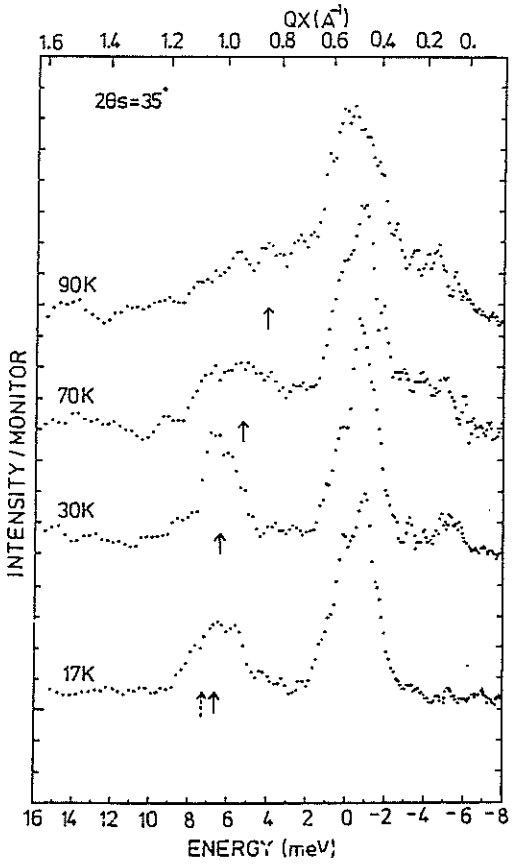

Fig.2 Magnon groups observed by MAX which scans along a*.

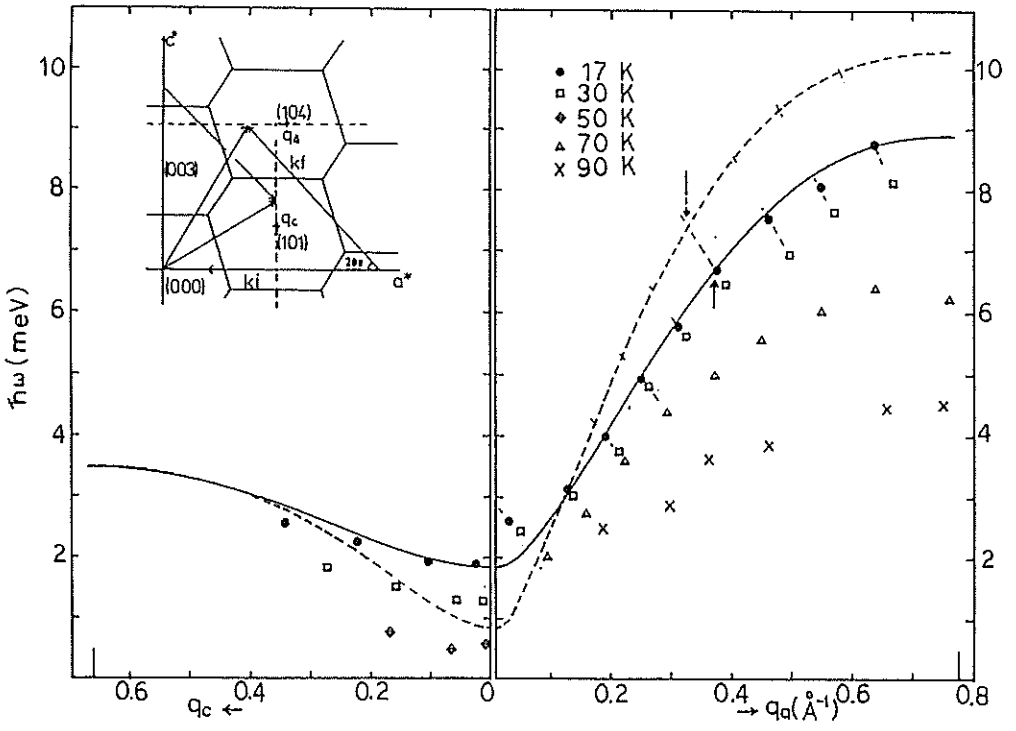

Fig.3 Magnon dispersions of $MnTiO_3$ along a* and c* measured by MAX at different temperatures. Solid lines are calculated by magnon theory. Broken lines are obtained with TUNS.

Use of a Bent Packet of Silicon Wafers as Neutron Monochromator

Shoichi TOMIYOSHI, Yoshikazu ISHIKAWA* and Keisuke TAJIMA+

The Research Institute for Iron, Steel and Other Metals,
Tohoku University, Sendai 980
*Physics Department, Tohoku University, Sendai 980
+Physics Department, Faculty of Science and Technology
Keio University, Hiyoshi, Tokohama 223

As neutron monochromator or analyser an packet of perfect crystal lamellae has been shown to be very promising by several authors.[1-5] Frey[4] reported that a bent packet of silicon crystal lamellae has neutron reflectivity of as high as 87% at the wavelength of 1.83Å and its line width of the rocking curve is only a few minutes of arc. Since such a neutron monochromator is suitable for MAX spectrometer, we also tried to test the feasibility of silicon perfect crystal lamellae as neutron energy analyser. The crystal lamellae we used are commercial silicon wafers produced for semiconductor elements. The wafers we used are not polished and are cut parallel to (111) plane with high precision and also have a cut in [110] direction, so we can assemble the plates in smaller angular divergence.

We measured the neutron diffraction pattern by using the TOF methods. Figure 1 shows the TOF diffraction patterns at the scattering angle of 30° of a flat lamella, a packet of 50 flat lamellae as well as a pyrolytic graphite with the grade ZYB which has been used for MAX spectrometer. The line width $\Delta\lambda$ is connected to the angular width $\Delta\theta$ by the relation $\Delta\lambda/\lambda = \cot\theta \cdot \Delta\theta$, where θ is a half of the scattering angle, so we can determine the angular width from the wavelength spread. The line width of 50 lamellae's packet is almost the same as that of single lamella and is narrower than that of PG. This shows that the as-sliced silicon wafers can be assembled to a packet with the angular divergence of a few minutes of arc. Figure 2 shows the peak intensity as a function of number of flat wehers for several wavelengths. The intensities begin to saturate at about 20

lamellae and are almost saturated at 50 lamellae for all wavelength, so we can not expect an increase of the reflectivity by increasing the number of wafer more than 50.

As is well known the reflectivity can be increased easily by bending the crystals.[1-5] In the present study the wafer disc was bent to have the cylindrical curvature in the scattering plane. Figure 3 shows the peak intensity of single lamella as a function of bending b, where b is related to the radius R of the curvature by the relation; $R = (L^2+b^2)/2b$, where L = 30.3mm. The peak intensities are normalized by each peak value at b = 0. The maximum reflectivity gain is about 3 for wavelength between 1.6 and 4.7 Å. Note, however, that the maximum position shifts depending on the wavelength.

For a packet of 50 lamellae the maximum reflectivity was obtained at about b = 0.3mm. The absolute reflectivity of which was determined by combining the diffraction and the transmission data. In Table 1 the reflectivity of a bent packet of 50 lamellae with b = 0.3mm are given. The reflectivity of PG is also listed for comparison in Table 1. The reflectivity of the bent packet of silicon wafers we attained is lower than that of the previous report,[4] but by selecting better value of curvature and number of wafers we may expect more increase of reflectivity. However, the present value is already about 2/3 to that of PG. Therefore, we think that our silicon weher packet can be employed for the neutron analyzer, especially for the case as MAX where the contamination of the $\lambda/2$ component should be avoided.

References

1) F. Rustichelli: Nucl. Inst. Methods 74 (1969) 219.
2) F. Frey: Nucl. Inst. Methods 96 (1971) 471.
3) F. Frey: Nucl. Inst. Methods 115 (1974) 277,
4) F. Frey: Nucl. Inst. Methods 125 (1975) 9.
5) A. Boeuf and Rustichelli: Acta Cryst. A30 (1974) 798.

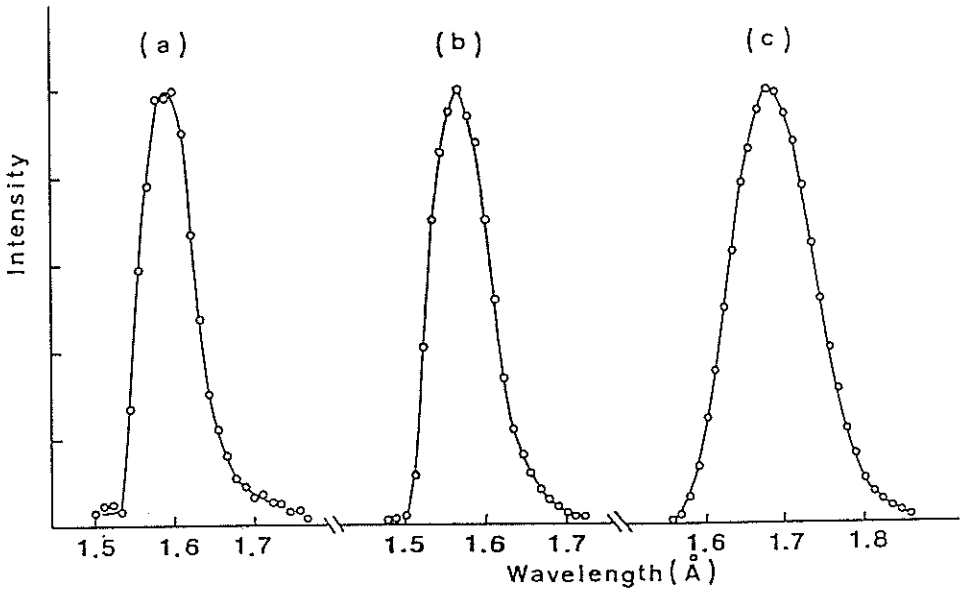

Fig. 1. Line profile of TOF diffraction patterns at the scattering angle of 30°;
(a) Si (111) reflection of a flat lamella,
(b) Si (111) reflection of a flat packet of 50 lamellae,
(c) PG (002) reflection.

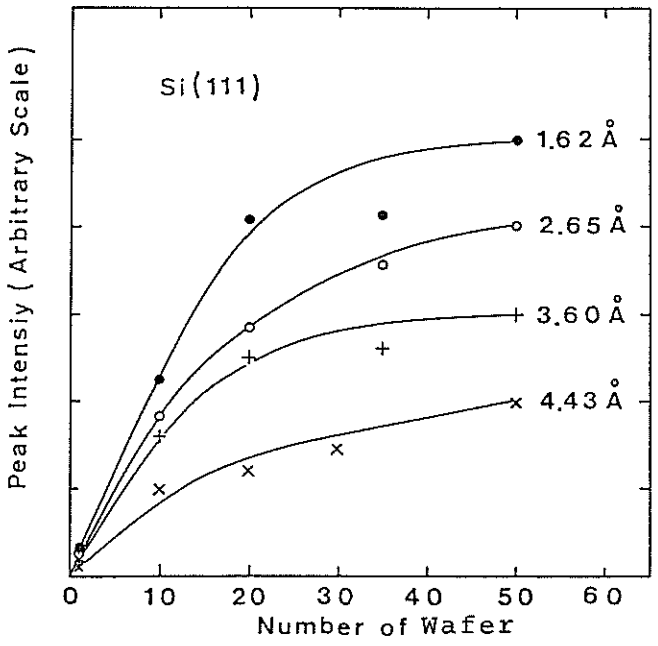

Fig. 2. Peak intensity of Si (111) reflection as a function of number of wafer for four wavelengths.

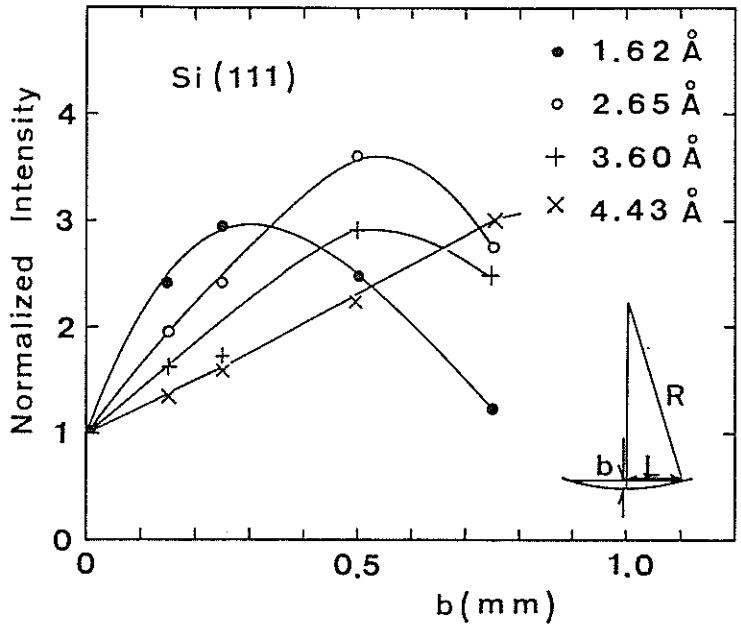

Fig. 3. Normalized peak intensity as a function of bending b for four wavelengths.

Table 1. Reflectivity of a bent packet of 50 wafers with b = 0.3 mm and that of PG.

Scattering angle (°)	30	50	70	90
Wavelength (Å)	1.62	2.65	3.60	4.43
Reflectivity of Si (111) (%)	27.9	45.3	33.5	33.6
Wavelength (Å)	1.74	2.84	3.85	4.74
Reflectivity of PG (002) (%)	42.8	60.7	51.1	46.5

Resonance Detector Spectrometer RAT at KENS

Noboru WATANABE, Susumu IKEDA, Herbert RAUH
Yasuhiro MASUDA and Setsuo SATO

National Laboratory for High Energy Physics
Oho-machi, Tsukuba-gun, Ibaraki 305, Japan

Present paper describes the status of the construction of an eV spectrometer RAT at KENS, and summarizes developing and research activities with this instrument. The spectrometer is an inverted geometry type Resonance Detector Spectrometer. A prototype machine has already been tested[1),2)]. The present instrument utilizes the scattering chamber of the prototype machine with an improved internal shield.

A new data acquisition and processing system has been arranged. Figure 1 shows the block diagram of the system. A camac module type time analyzer has been built which has 4 k channels each (total two inputs) with minimum channel width of 0.125 μs controlled by a 32 MHz quartz. The system has a dedicated mini-computer OKITAC-50/65 for the quick data processing.

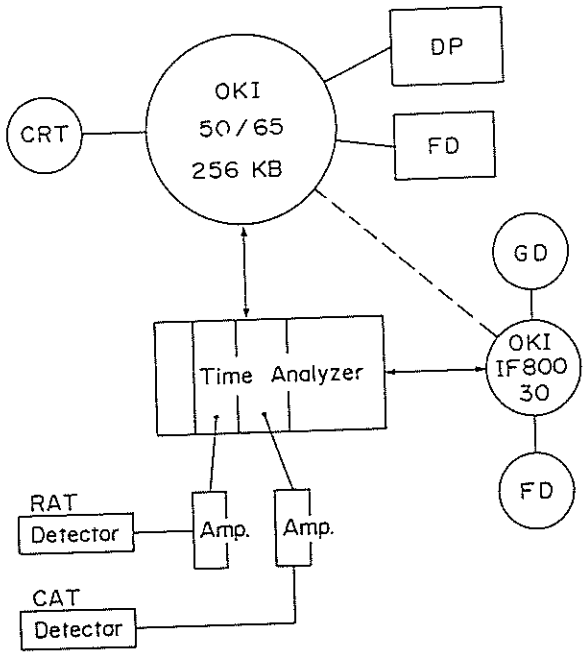

Fig. 1 Block diagram of the data acquisition and processing system for RAT.

A neutron beam monitor has been installed at the entrance of the scattering chamber. The monitor consists of a BGO scintillator which detects gamma rays from the incident beam collimator made of lead. The performance of this monitor is satisfactory for the normalizations of different runs.

The inside of the evacuated scattering chamber is heavily shielded by 10 cm thick borated resin (outer side) and 10 cm thick lead (inner side) to stop the outcoming faster neutrons and energetic gamma rays. In the prototype experiment, signal to background ratio was studied with and without B_4C plate on the inner surface of the shield and no measurable change was found. Prototype experiments were, therefore, performed without the B_4C plate. Figure 2 (a) shows a typical prototype result of high Q scattering from bismuth sample at room temperature, measured with a Sb resonance detector foil (E_r = 6.24 eV) at a scattering angle of 90°. The measured peak could be reproduced reasonably well by a first-principles calculation (solid curve), including Doppler broadened resolution of the resonance detector, time distribution of neutron pulse, and geometrical effects due to the finite extent of the moderator, sample, and detector size. Agreement between measurement and calculation is satisfactory above half height, but not good at both wings. Three origins were considered; (i) neutrons scattered first by the sample and then by the lead shield, (ii) multiple scattering within the sample, (iii) final state correction terms of the scattering function. In order to check the origin (i) we have installed B_4C plates ($\sim$ 90 % B_4C + 10 % resin, $\sim$ 1.5 cm thick) on the inside face of the lead shield, and repeated the measurement with a Ta resonance detector (E_r = 4.28 eV). The result is shown in Fig. 2(b) (solid circles) compared to the result without the B_4C plates (open circles). In the new data the wings disappear especially at lower energy (higher channel) side. Now we conclude that the major contribution of the discrepancy was due to the neutrons scattered first by the sample and then at the lead shield which were not recognized by the previous simple test on signal to background ratio. In the new data there still exists a small discrepancy at the high energy side of the spectrum. We thought this was due to the origin (ii), and have developed a computer code for the first-principles calculation including multiple scattering process in the sample[3]. We found that the new calculation could reproduce the experiment almost perfectly as shown by the solid line in Fig. 2(b).

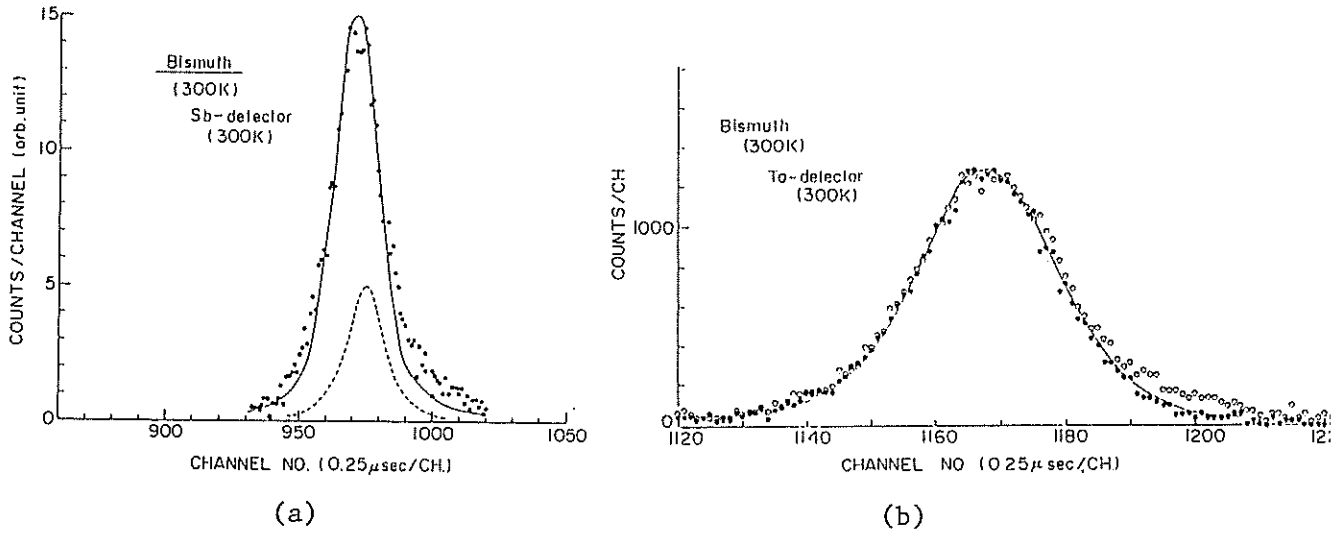

Fig. 2 TOF spectra of high Q scattering from Bi at room temperature measured before (a) and after (b) installation of B_4C plate. Solid curves are first principles calculation.

A time focussing method in the resonance detector spectrometer has been proposed by Carpenter, et al.[4] which allows measurements with improved energy resolution. Extensive measurements gave experimental evidence for the applicability of the theory. A summary of these experiments is given in a separate paper[5], and details will be published elsewhere[6].

In order to have a good understanding of the principle of the high Q scattering, and to examine the performance of the instrument, the same samples as that were used previously, namely Bi, V, Aℓ, and graphite have been remeasured. Furthermore, pyrolitic graphite has also been measured with scattering vector parallel and perpendicular to the c-axis[7]. A striking difference has been detected between both spectra depending upon the different phonon density of state. The results demonstrate the capability of this instrument for the line profile analysis in measurements of high Q scattering, especially in the integral check of the phonon density of state which extends up to higher frequency and no direct measurement of which is possible. Similar high Q scattering from biatomic systems are also in progress.

As a goal of the high Q scattering, arrangements for liquid ^{4}He-II measurement is going on. A preliminary measurement from liquid ^{4}He-I was performed to check the counting rate and signal to background ratio using a existing conventional cryostat. A dedicated cryostat for this experiment has been constructed and is now in test.

Further studies of the resonance detector foil have been performed to improve the energy resolution of the detector. A great deal of measurements has been carried out on various foils such as Ta, and its oxide and carbide, Sb, Sm, Ho, and U-238 at various temperatures, and the detector resolution of 53 meV in FWHM has been achieved by the U-238 foil at 25 K. In a separate paper in this report the results are summarized[8].

The spectrometer utilizes BGO scintillators to detect gamma cascades resulting from the neutron resonance capture in the foil. Cooling of the detector foil is necessary if higher resolution is required as described above. On the other hand a closer coupling of the foil to the scintillator is essentially important in order to realize large solid angle for gamma ray detection as well as high signal to background ratio, and therefore, use of cooled BGO crystals seems to be indispensable. The pulse decay time, however, approaches to 10 μs at temperature below 100 K[9] and an associated time jitter of a few μs might be unavoidable which is much larger than detector resolution at low temperature. In order to overcome this inconvenience a special cryostat has been constructed which can cool the resonance foil separately, and does not affect the BGO crystals located very close to the foil. This system is just under test.

A test of Resonance Filter Detector Spectrometer has started which utilizes a ^{6}Li-scintillator (5 x 5 cm^2, 1 cm thick) as a neutron detector to clarify merit and demerit of this combination compared to the Resonance Detector Spectrometer.

References

1) J. M. Carpenter, N. Watanabe, S. Ikeda, Y. Masuda and S. Sato, KENS Report-III, KEK Internal 82-5 (July 1982) p.119.
2) J. M. Carpenter, N. Watanabe, S. Ikeda, Y. Masuda and S. Sato, Proc. YAMADA Conf.-IV, Neutron Scattering of Condensed Matter (Hakone, Japan, Sep. 1-4, 1982), Physica 120B (1983) 126.
3) H. Rauh, S. Ikeda and N. Watanabe, this report.
4) J. M. Carpenter and N. Watanabe, to be published in Nucl. Instrum. Methods.
5) H. Rauh, S. Ikeda and N. Watanabe, this report.
6) H. Rauh, S. Ikeda and N. Watanabe, to be published.
7) H. Rauh and N. Watanabe, this report, and details to be published.
8) H. Rauh and N. Watanabe, this report, and details to be published.
9) M. J. Weber and R. R. Monchamp, J. Appl. Phys. 44 (1982) 5495.

Experimental Verification of the "Time-Focussing Effect" in the Resonance Detector Spectrometer RAT

Herbert RAUH*, Susumu IKEDA and Noboru WATANABE

National Laboratory for High Energy Physics
Oho-machi, Tsukuba-gun, Ibaraki 305, Japan

A new focussing effect for resonance detector spectrometer was predicted recently[1]. The finite size of moderator, sample and detector foil lead to a spread in the time-of-flight of the neutrons between moderator and detector. This spread may be compensated by the difference in the recoil shift (different scattering angles for the various flight paths), if the moderator, sample and detector foil are mounted at their specific focussing angles. From the fact that the TOF spread is compensated by the recoil energy, we expect that this effect should be large for scatters with small atomic mass number, and that the dominant contribution arises from the sample rather than moderator or detector. The "time-focussing" should be very important for the measurement of the zero-momentum distribution in liquid He-II.

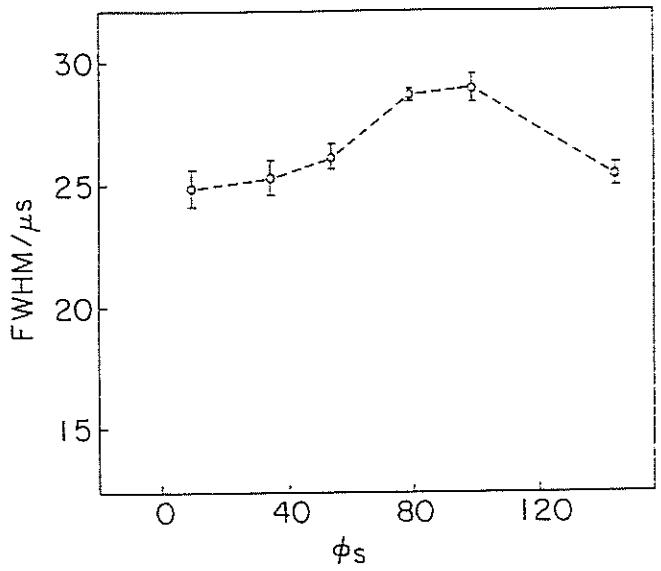

Fig. 1 FWHM values of graphite spectra for different ϕ_s
(o: experimental; ---: guide line to the eye)

---

* Permanent Address: Physikalisches Institut der Universität Würzburg, Röntgenring 8, D-8700 Würzburg, Federal Republic of Germany.

We have measured RAT spectra of polycrystalline graphite with a Ta resonance foil for different "sample angles" ϕ_s (angle between incoming neutron beam and sample plane). The beam size was 3.5 cm in width and 5 cm in height. The sample size was 10 cm x 5 cm x 0.3 cm.

The FWHM values of the RAT spectra are shown in Fig. 1. The line-width varies with ϕ_s, and reaches a maximum value at $\phi_s \simeq 10°$ and a minimum at $\phi_s \simeq 100°$. This is consistent with the theory[1], which predicts $\phi_s = 99.72°$ as focussing angle for the sample. The observed FWHM values are determined by

a) the scattering function, and multiple scattering effects,

b) the neutron capture resonance line-width,

c) the time spread of the moderator neutron distribution,

d) the finite size of moderator and detector, and finally

e) the finite size of the sample.

The contributions a) to d) should be independent of ϕ_s in a very good approximation, and "add" to give Γ_0. Γ_0 is observed at the focussing angle $\phi_s = 100°$, where Γ_{GS}, the contribution arising from the finite size of the sample, vanishes. We have determined $\Gamma_{GS}(\phi_s)$ by de-convolution of the observed spectra using two models.

In the first model we assume that the effect of the finite size of the sample on the RAT spectra can be described by the convolution of two Gaussian functions of widths Γ_{GS} and Γ_0, respectively. Γ_{GS} is then given by

$$\Gamma_{GS}(\phi_s) = \sqrt{\Gamma_{exp}(\phi_s)^2 - \Gamma_0{}^2} \,. \qquad (1)$$

The values of Γ_{GS} calculated with this equation are up to 32 % larger than the corresponding values calculated with the theory[1]. This discrepancy arises

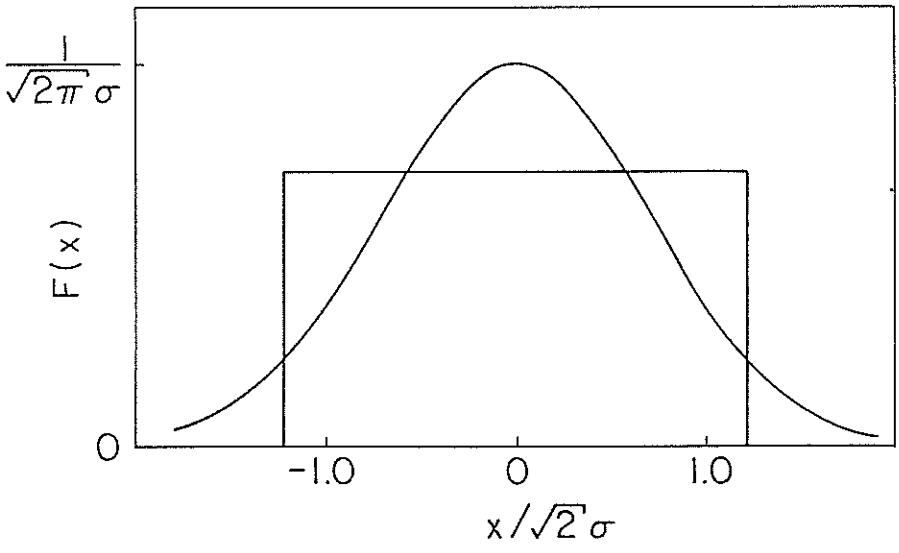

Fig. 2 A square distribution and its "Gaussian equivalent".

from the fact, that the "Gaussian equivalent" of the sample shape overestimates the center of the sample, which contributes very little to the sample-size effect, and underestimates the outer parts of the sample, which are essential (cf. Fig. 2). These faults are overcome in the second model, where we assume that the effect of the finite sample size on the RAT spectra can be described by the convolution of a Gaussian function of width Γ_0 with a square distribution of width Γ_{GS}. The de-convoluted values of Γ_{GS} are shown in Fig. 3 in comparison with the theoretical predictions[1] (full and dashed line). The full line was calculated for a graphite sample of full size 10 cm. The dashed line takes cut-off effects arising from the finite beam-width of 3.5 cm into account. The agreement between theory and experiment is good in this model.

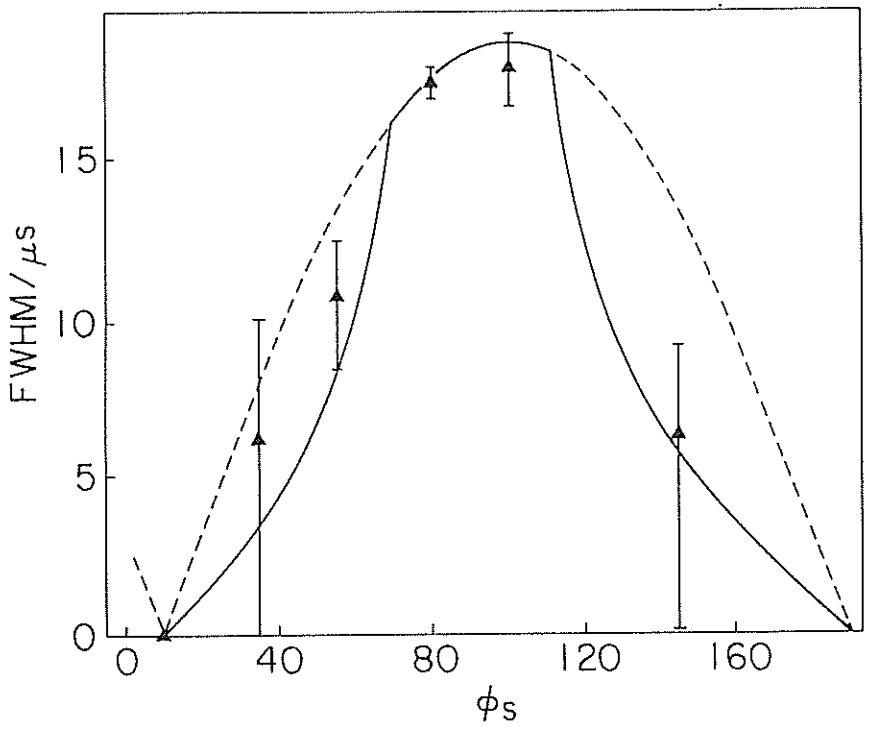

Fig. 3 Γ_{GS} as a function of ϕ_s; Δ: experimental; lines: theory[1] with (——) and without (---) beam size corrections.

For a more detailed study of this effect, measurements using a Be and Li sample are in progress.

References

1) J. M. Carpenter and N. Watanabe, to be published in NIM.

High Q Neutron Scattering by Pyrolitic Graphite
- Determination of the Struck Particle Momentum Distribution

Herbert RAUH* and Noboru WATANABE

National Laboratory for High Energy Physics
Oho-machi, Tsukuba-gun, Ibaraki 305, Japan

The scattering function at high momentum transfer $\underline{Q}$ can be written

$$S(\underline{Q},\omega) = S_{IQ}(\underline{Q},\omega) + S_{FS}(\underline{Q},\omega) \quad . \tag{1}$$

In the limit $Q \to \infty$, the final state correction $S_{FS}(\underline{Q},\omega)$ vanishes, and

$$S(\underline{Q},\omega) \simeq S_{IA}(\underline{Q},\omega) \sim \int d^3\underline{p}\, n(\underline{p}) \cdot \delta(\omega - R - \underline{Q}\cdot\underline{p}/m) \tag{2}$$

where interference terms have been neglected. For an ideal gas, and for a system of harmonic oscillators, $n(\underline{p})$ factorizes

$$n(\underline{p}) = \prod_{i=1}^{3} n_i(p_i) \tag{3}$$

and we find from eq. (2),

$$n(p_i) \sim Q_i S_{IA}(Q_i,\omega)\Big|_{Q_i=\frac{m}{p_i}|\omega-R|} \quad . \tag{4}$$

Therefore, it should be possible to deduce the momentum distribution $n(\underline{p})$ of the scattering system by measuring $S(\underline{Q},\omega)$ at high momentum transfer. This will be of great interest for quantum systems like liquid He-II, where the high-Q spectra should allow to determine the fraction of the scattering atoms which are in the ground state (Bose condensate) and also for the determination of the hydrogen potential in metal hydrides. In this paper we show that such a line-profile analysis is indeed possible with the eV spectrometer RAT at KENS.

For a classical system of scatterers, the scattering function at high momentum transfer is written in the impulse approximation,

$$S_{IA}(Q,\omega) = \frac{1}{\sqrt{2\pi}\sigma} e^{-\frac{1}{2}\left(\frac{\omega-R}{\sigma}\right)^2} \tag{5}$$

$$\omega = E_i - E_f$$

---

* Permanent Address: Physikalisches Institut der Universität Würzburg, Röntgenring 8, D-8700 Würzburg, Federal Republic of Germany.

$$R = \frac{1}{A}(E_i + E_f - 2\sqrt{E_i E_f}\cos\theta)$$

$$\sigma = \sqrt{2k_B T \cdot R}\ .$$

For a solid at $T < \theta_D$, we have to replace the temperature by the effective temperature

$$k_B T_{eff} = \frac{1}{2}\int_0^\infty dE f(E) E \cdot \coth\left(\frac{E}{2T}\right)\ , \qquad (6)$$

which depends upon the effective phonon density of states, defined as the density of states of the lattice vibrations with displacements parallel to the momentum transfer. If we measure the scattering function of a highly anisotropic material like graphite, we expect to observe different line-widths for different directions of $\underline{Q}$ relative to the crystallographic axis.

We have measured the spectra of a pyrolitic graphite sample (PG) at room temperature. The alignment of the sample was such that $\underline{Q} \parallel \underline{c}$ (hexagonal axis) in the first measurement and $\underline{Q} \perp \underline{c}$ in the second. The scattering angle was 90°, and a 12 μm thick Ta foil was used as resonance detector. For each PG alignment three spectra had to be measured:

1) spectrum of sample and holder, with resonance foil,
2) spectrum of sample and holder, without resonance foil (to determine the background),
3) spectrum of the empty sample holder, with resonance foil (to subtract peaks from the aluminium holder).

Fig. 1(a) and 1(b) show the graphite spectra for $\underline{Q} \parallel \underline{c}$ and $\underline{Q} \perp \underline{c}$ respectively after subtraction of the background and sample holder contribution. Comparing both spectra, we clearly observe a difference in the line-widths. The solid line shows the result of first principle calculations of the spectra. In this calculations, the finite time spread of the moderator neutron distribution, the width of the neutron capture resonance line of the detector foil[1], geometrical contributions arising from the finite size of beam, sample and detector[2] and line-broadening due to double scattering[3] were incorporated. The remaining discrepancies for low TOF (high incoming neutron energy) are believed to be due to higher order multiple scattering. The calculated FWHM values agree with the observed line-widths, if $T^{\parallel}_{eff}$ = 550 K for $\underline{Q} \parallel \underline{c}$ and $T^{\perp}_{eff}$ = 1,050 K for $\underline{Q} \perp \underline{c}$. We note that the anisotropic structure of the layered material graphite is very well reflected by the line-broadening of the RAT spectra.

The phonon dispersion of graphite is well known in the low energy range up to about 12 THz. The high frequency modes have been measured by optical methods at the Brillouin zone center only. We may therefore expect that the phonon frequency distribution calculated with lattice dynamical models for

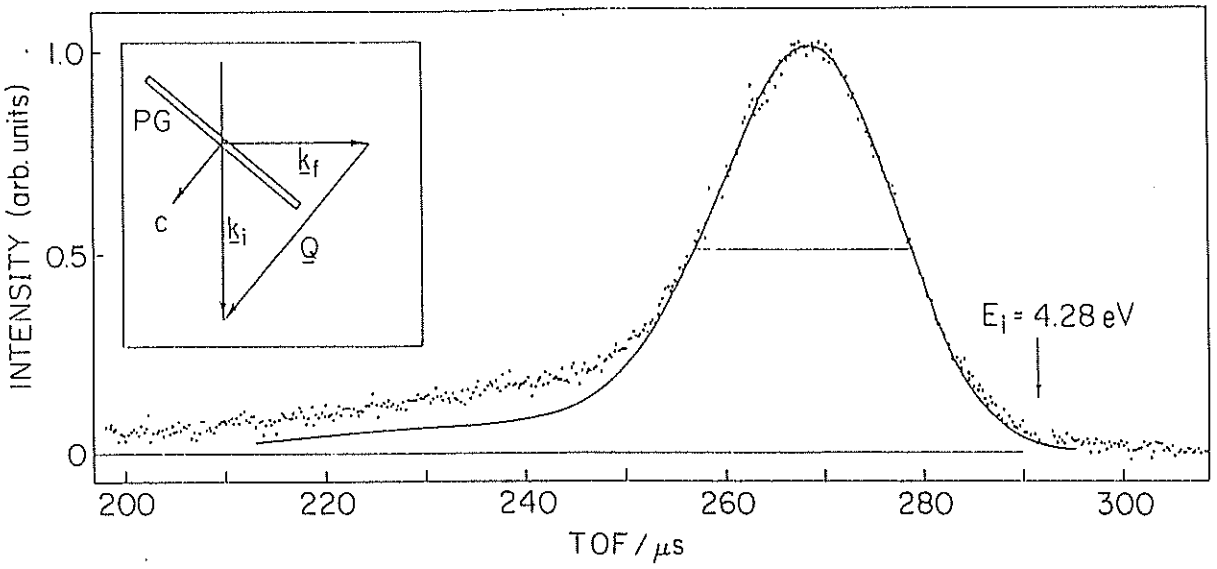

1(a)

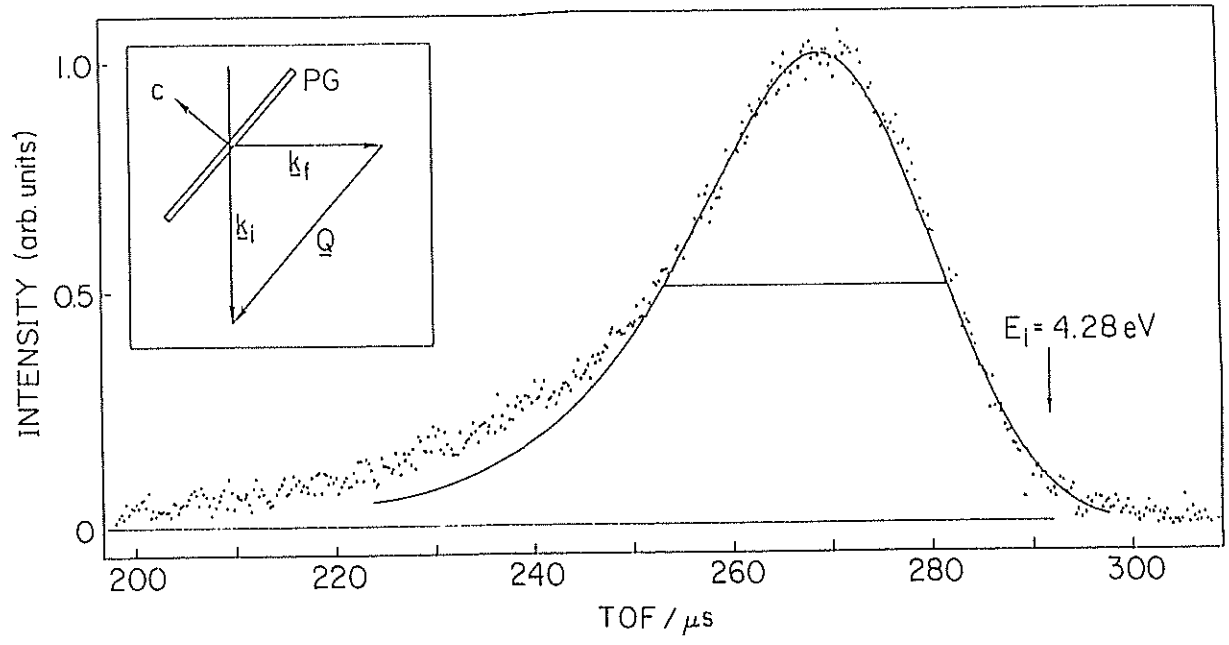

1(b)

Fig. 1 Scattering from graphite for $\underline{Q} \parallel \underline{c}$ (a), and $\underline{Q} \perp \underline{c}$ (b); the points represent experimental data, the solid line has been calculated.

graphite is reliable in the lower energy range, but some deviations may be observed in the high energy region. In order to give an example, we calculate $T_{eff}^{\parallel}$ and $T_{eff}^{\perp}$ using the Young-Koppel model[4] (The authors have provided figures showing the effective density of states for $\underline{Q} \parallel \underline{c}$ and $\underline{Q} \perp \underline{c}$ in their paper.)

	$T_{eff}^{\parallel}$/K	$T_{eff}^{\perp}$/K
Young-Koppel	545	770
RAT spectra	550	1,050

The agreement is good for $\underline{Q} \parallel \underline{c}$, but quite bad for $\underline{Q} \perp \underline{c}$. This is not surprising, because the Young-Koppel model is known to underestimate the high-frequency parts of the phonon density of state.

References

1) H. Rauh and N. Watanabe, Energy Resolution of the eV Spectrometer RAT, KENS Report IV.

2) H. Rauh, S. Ikeda and N. Watanabe, Experimental Verification of the "Time-Focussing Effect" in the Resonance Detector Spectrometer RAT, KENS Report IV.

3) H. Rauh and N. Watanabe, Line Profile Analysis of High-$\underline{Q}$ Scattering Spectra of the Resonance Detector Spectrometer RAT, KENS Report IV.

4) J. A. Young and J. U. Koppel, J. Chem. Phys. 42 (1965) 357.

Line Profile Analysis of High-Q Scattering Spectra of the Resonance Detector Spectrometer RAT

Herbert RAUH* and Noboru WATANABE

National Laboratory for High Energy Physics
Oho-machi, Tsukuba-gun, Ibaraki 305, Japan

An important application of an eV spectrometer will be the determination of the struck particle momentum distribution $n(\underline{p})$. This is of special interest for quantum system like liquid He-II. In order to extract $n(\underline{p})$, the different contributions to the spectrometer response must be known very well. These are:

1. The neutron detector function

In a resonance detector spectrometer the scattered neutrons are detected if their energy is "close to" the resonance energy of the detector foil. The detection probability is given by

$$P_D(E_f,\theta_D) = 1 - e^{-N_d\sigma(E)/\cos\theta_d}$$

where N_d is the area number density of resonance atoms in the foil, θ_D is the angle between scattered neutron beam and normal vector on the foil, and $\sigma(E)$ the resonance absorption cross section. The contribution of the detector function to the energy resolution of RAT has been studied in detail[1] and is well understood.

2. The scattering function

$$S(Q,\omega_{if}) = \frac{1}{\sqrt{2\pi}\sigma_{if}} e^{-\frac{1}{2}\left(\frac{\omega_{if}-R_{if}}{\sigma_{if}}\right)^2} [1 + h(Q,\omega_{if})] \quad . \tag{1}$$

The correction terms $h(Q,\omega_{if})$ can be written as series expansion in powers of $(T_{eff}/R)^{1/2}$ with Hermitian polynominals as coefficients[2]. Figure 1 compares the scattering function with and without correction terms for graphite. We notice that $h(Q,\omega_{if})$ make the scattering function asymmetric in energy, but does not affect the FWHM value drastically.

---

* Permanent Address: Physikalisches Institut der Universität Würzburg, Röntgenring 8, D-8700 Würzburg, Federal Republic of Germany.

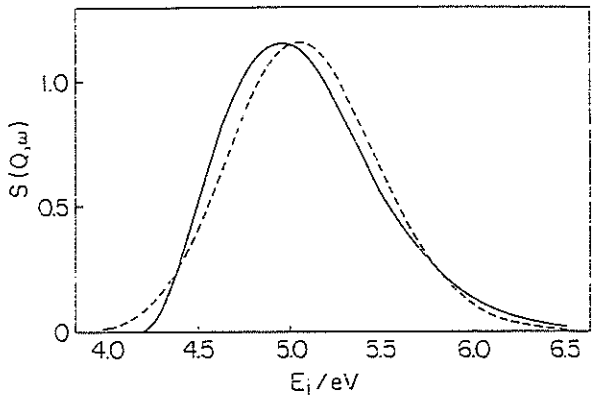

Fig. 1 Scattering function of graphite with (——) and without (---) final state correction terms.

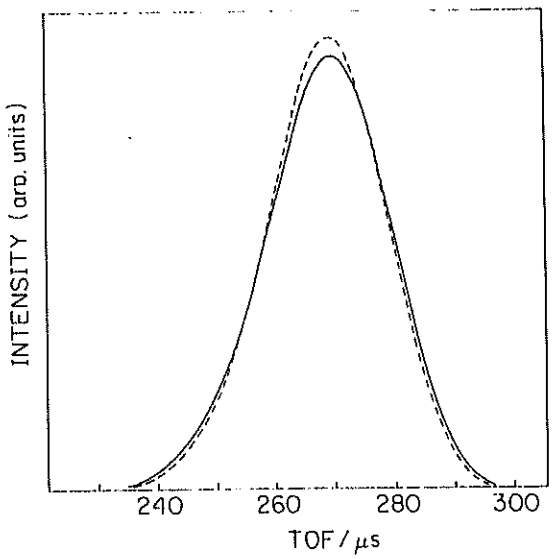

Fig. 2 Effect of the finite detector size on the graphite spectrum: --- zero detector size; —— detector size 5 cm x 5 cm.

3. Geometrical contributions arising from the finite size of sample, detector and moderator[3)]

Among these, the sample contribution is the most important for a scattering system with small atomic mass number. We have studied this contribution in detail for graphite[4)]. In agreement with the theoretical predictions[3)] we found that the sample contribution vanishes for $\phi_s = 100°$, (ϕ_s = angle between incoming neutron beam and plane of the sample). In Fig. 2 we compare the calculated RAT spectra at $\phi_s = 100°$ with and without geometrical contribution. The broadening of the RAT response at this sample angle is mainly caused by the finite size of the detector (5 cm x 5 cm Ta foil).

4. Multiple scattering effects

At the present time the relatively low flux of eV neutrons of a spallation source requires rather big samples. As a typical example, the size of our graphite sample is 10 cm x 5 cm x 0.3 cm. The mean free path of neutrons in graphite is 1.6 cm. Therefore, we expect that multiple scattering effects should clearly be visible in the RAT spctra. Neglecting the geometrical contributions[3)] for a while, we can write down the time spectra of RAT as

$$I(\Omega_3,t) = \frac{\rho_s}{A}\cdot\frac{\sigma}{4\pi}d^3V_1 d^2\Omega_3$$

$$\int_0^\infty dE_1 \int_0^\infty dE_3 \{\phi(E_1, t - \frac{r_1}{u_1} - \frac{r_3}{u_3}) S(\omega_{1,3}, R_{1,3}) P_D(E_3, \theta_D)$$

$$+ \frac{\rho_s}{A}\frac{\sigma}{4\pi}\underbrace{\int dr_2 \int d\Omega_2}_{\text{sample}} \phi(E_1, t - \frac{r_1}{u_1} - \frac{r_2}{u_2} - \frac{r_3}{u_3}) \cdot$$

$$\cdot \int_0^\infty dE_2 S(\omega_{1,2} R_{1,2}) S(\omega_{2,3} R_{2,3}) e^{-\alpha r_2} P_D(E_3, \theta_D)$$

$$+ \cdots\} \qquad (2)$$

where ϕ is the moderator neutron distribution in time and energy. In the above expression the second term describes double scattering, higher order processes, however, are neglected because it is very difficult to calculate them. It is straightforward to incorporate the geometrical effects in eq. (2). In Fig. 3 the contribution of single and double scattering processes to the time spectrum are shown.

We notice that the curves of the single scattering line are shifted by the recoil energy from the position of the elastic line. For double scattering processes, a second shift occurs. Therefore multiple scattering contributions will affect only the high energy part of the spectrum.

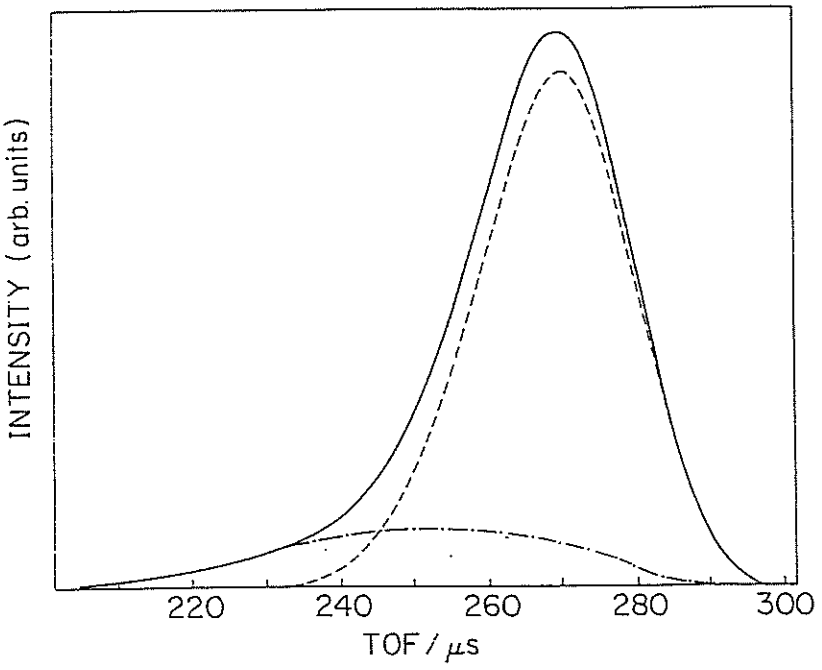

Fig. 3 Graphite spectrum: single scattering contribution (---), double scattering contribution (-•-•-), and the sum of both (——).

5. Comparison with the experiment

We have measured the scattering from a graphite sample (10 cm x 5 cm x 0.3 cm) at focussing angle[3] ϕ_s = 100° using a 12 μm thick Ta foil as resonance detector. The scattering angle was 90°. The points in Fig. 4 represent the experimental data after subtraction of the background. The solid line shows the result of a first principle calculation where all the above mentioned effects have been incorporated. The agreement between measured and calculated spectrum is good at the low energy side of the spectrum and also on the high energy side up to the FWHM value. The discrepancies which are observed for higher energies, are believed to be due to threefold and even higher order scattering processes.

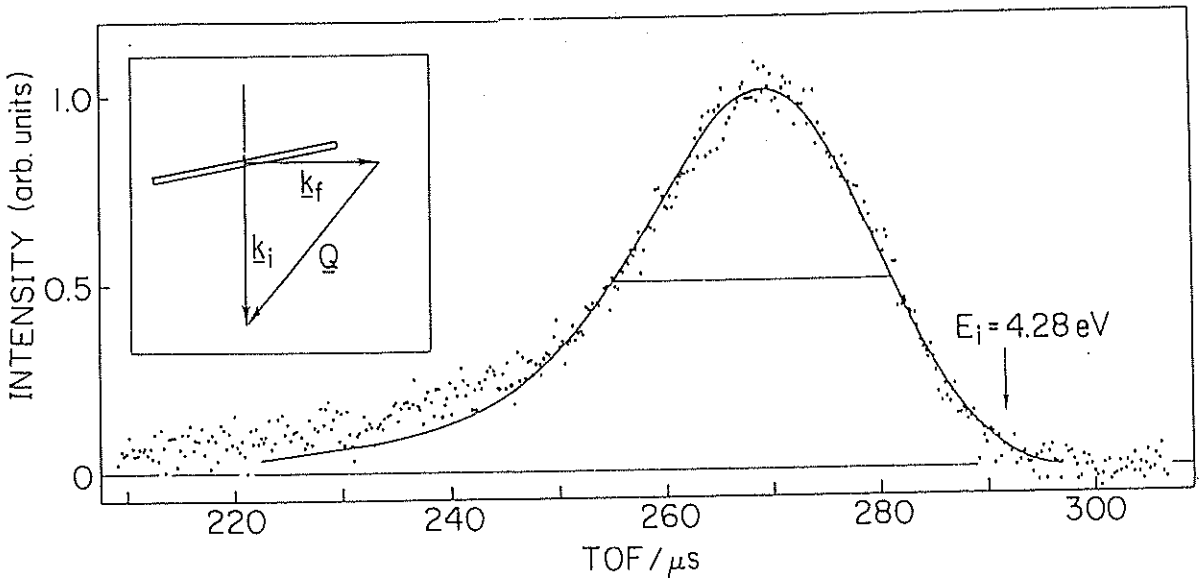

Fig. 4 Comparison between experiment and calculation for graphite scattering.

References

1) H. Rauh and N. Watanabe, Energy Resolution of the eV Spectrometer RAT, KENS Report IV.

2) M. S. Nelkins and D. E. Parks, Phys. Rev. 119 (1960) 1060.

3) J. M. Carpenter and N. Watanabe, to be published in NIM.

4) H. Rauh, S. Ikeda and N. Watanabe, Experimental Verification of the "Time-Focussing Effect" in the Resonance Detector Spectrometer RAT, KENS Report IV.

Energy Resolution of the eV Spectrometer RAT

Herbert RAUH* and Noboru WATANABE

National Laboratory for High Energy Physics
Oho-machi, Tsukuba-gun, Ibaraki 305, Japan

The energy resolution of a resonance detector spectrometer is approximately given by[1)]

$$\frac{\Delta E}{E_r} \simeq \left[\frac{\Delta E_r}{E_r}\left\{1 + \left(\frac{E_i}{E_r}\right)^3\left(\frac{\ell_f}{\ell_i}\right)^2\right\} + \left(\frac{2\delta_m}{\ell_i}\right)^2\right]^{1/2} \tag{1}$$

where E_i, E_r, and ℓ_i, ℓ_f are the neutron energy and flight path length before and after scattering, and δ_m is the FWHM value of the neutron burst from the moderator converted to an effective distance spread. Geometrical contribution to ΔE arising from the finite size of moderator, sample and detector are neglected in eq. (1). For sufficiently small ℓ_f/ℓ_i and δ_m/ℓ_i the energy resolution is mainly determined by the FWHM value ΔE_r of the neutron capture resonance line.

The intrinsic line-width Γ_i of neutron capture resonance levels is typically some ten meV and therefore at least of the order of magnitude of the average phonon energy of the resonance foil material. Thus Lamb's weak binding condition[2)] is met by any foil, and the resonance absorption cross section is given by

$$\sigma = \sigma_0 \Psi(\xi, x) \tag{2}$$

$$\Psi(\xi, x) = \frac{\xi}{2\sqrt{\pi}} \int_{-\infty}^{+\infty} dy \frac{1}{1 + y^2} e^{-\left(\frac{\xi}{2}\right)^2 (x-y)^2} \tag{2a}$$

$$x = \frac{2}{\Gamma_i}(E - E_r - R)$$

$$\xi = \Gamma_i / \Delta$$

$$\Delta = 2\sqrt{k_B T_{eff} R}$$

$$R = \frac{E}{M}$$

---

* Permanent Address: Physikalisches Institut der Universität Würzburg, Röntgenring 8, D-8700 Würzburg, Federal Republic of Germany.

The Doppler width Δ depends upon the temperature and the chemical binding (reflected by the phonon density of states f(E)) through

$$k_B T_{eff} = \frac{1}{2}\int_0^\infty dE f(E) \cdot E \cdot \coth\left(\frac{E}{2T}\right) . \qquad (3)$$

Ground state vibrational motion keeps T_{eff} and therefore Δ finite even in the limit $T \to 0$. For most of the foil materials f(E) is not known. Therefore we have studied the effect of foil temperature and chemical binding experimentally in the so-called direct measurement approach, where the resonance foil is placed at sample position in the eV spectrometer RAT[3),4)].

Temperature effect

We have measured the neutron capture resonance lines of Sb, Sm, Ho, Ta and U-238 (as $UO_2(NO_3)_2 \cdot 6H_2O$) for different temperatures. As an example of the TOF spectra, Fig. 1 shows the resonance lines of the uranium foil at room temperature and 25 K. The different contributions to the observed line-width Γ_{obs} are listed in the table.

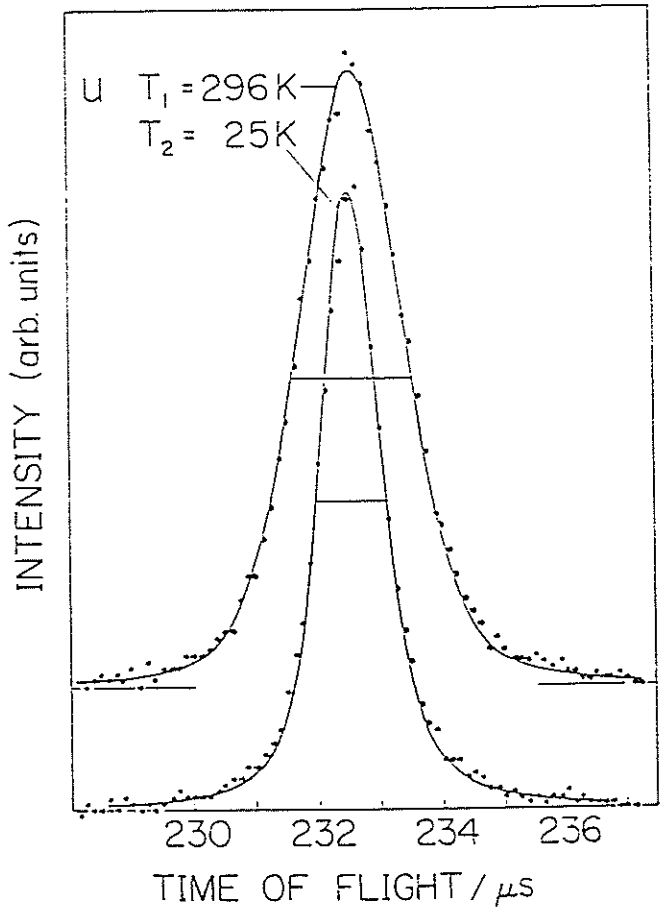

Fig. 1 Resonance line of the uranium foil at 296 K and 25 K.

Table 1

	E_r/meV	Γ_i/meV	Δ/meV	Γ_ψ/meV	Γ_M/meV	Γ_{obs}/meV
296 K	6674	≃ 27	54	106	29	113
25 K			22	53		65

Γ_ψ: FWHM of the Ψ-function, cf. eq. (2).

Γ_M: Energy uncertainty resulting from the time spread of the moderator neutron distribution.

The reduction of temperature from 296 K to 25 K results in an improvement of the energy resolution from 1.7 % (296 K) to 0.97 % (25 K) at resonance energy.

Figure 2 shows the temperature dependence of FWHM of the uranium foil. As a rather unexpected and important result, this figure indicates that the Doppler broadening is still temperature dependent below 25 K. Therefore the energy resolution can be further improved by cooling the uranium foil below 25 K.

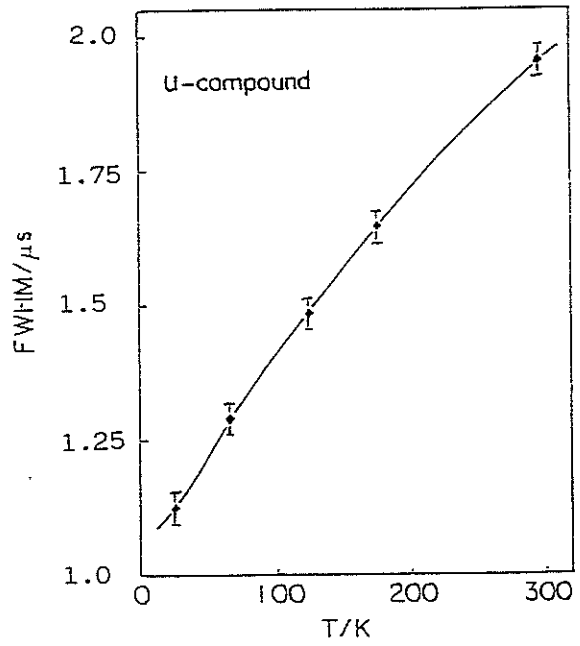

Fig. 2 FWHM of the resonance line of the uranium foil for different temperature (◇ experimental; --- guide line to the eye).

Effect of chemical binding

We have studied the resonance lines of Ta atoms in different crystalline environments (Ta metal, TaC, Ta_2O_5). The effect of the chemical binding on

the FWHM values was found to be rather small compared to the variation with temperature. This is due to the fact that the intrinsic resonance line-width is at least of the order of magnitude of the average phonon energy of the resonance foil material. The situation is therefore quite different from the case of resonant absorption of γ (Mößbauer effect), where the intrinsic line-width is typically some nano-eV.

More details of our study will be published in a separate article[5].

References

1) W. G. Wilson, Pulsed Neutron Scattering, John Wiley & Sons, New York, 1981.

2) W. E. Lamb, Phys. Rev. 55, (1939) 190.

3) J. M. Carpenter, N. Watanabe, S. Ikeda, Y. Masuda and S. Sato, Test of a resonance detector spectrometer, KENS Report III.

4) J. M. Carpenter, N. Watanabe, S. Ikeda, Y. Masuda and S. Sato, to be published.

5) H. Rauh and N. Watanabe, to be published.

Local Modes and Hydrogen Potentials in Some Metal Hydrides

Susumu IKEDA and Noboru WATANABE

National Laboratory for High Energy Physics
Oho-machi, Tsukuba-gun, Ibaraki 305, Japan

The hydrogen potential V(x) is expressed approximately by a linear combination of a harmonic term and a quartic anharmonic term as a function of the deviation x from the hydrogen equilibrium position as

$$V(x) = a_2x^2 + a_4x^4 \qquad (a_2 > 0) \ . \tag{1}$$

If the a_4x^4 is very small, the n-th excitation energy ε_n is given approximately by diagonal terms of Hamiltonian as follows:

$$\varepsilon_n \simeq nh\omega_0 + \beta(n^2 + n) \ , \tag{2}$$

with $\omega_0{}^2 = 2a_2/m$ and $\beta = 3h^2a_4/4m^2\omega_0{}^2$. The hydrogen potential defined by eq. (1) can be classified into three types depending upon the value of β as shown in Fig. 1; that is,

(a) $\beta = 0$: harmonic potential (Fig. 1(a)),

(b) $\beta < 0$: trumpet like potential (Fig. 1(b)),

(c) $\beta > 0$: well like potential (Fig. 1(c)).

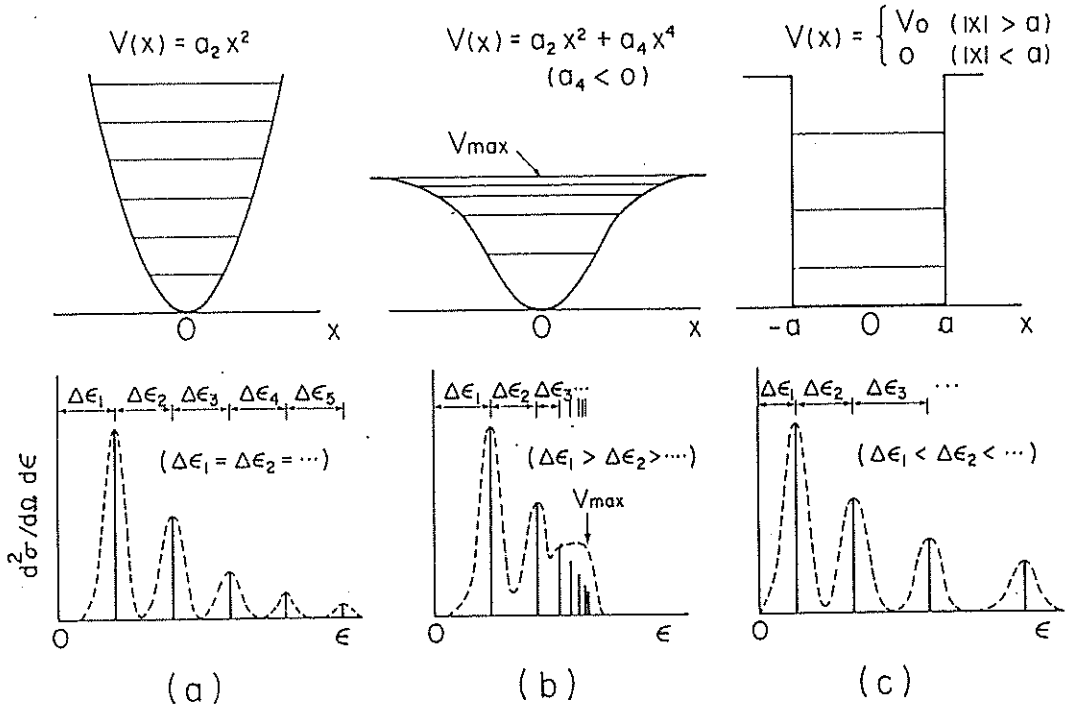

Fig. 1 Three types of hydrogen potential: a) Harmonic potential, b) trumpet like potential, and c) well like potential.

We studied the shape of the hydrogen potentials for tetrahedral site (T-site) in fcc and bcc structures, and for octahedral site (O-site) in bcc structure by measuring the excitation energies of the local modes in β-phase fcc metal hydrides {ZrH_x (x = 1.41, 1.93) and TiH_2} and in bcc metal hydrides {TaH_x (x = 0.1, 0.45, 0.5), $NbH_{0.76}$ and $VH_{0.33}$}, using the CAT spectrometer. We have measured the localized mode spectra up to 5-th excitation ε_5 at about 700 meV for TiH_2, $ZrH_{1.41}$ and $ZrH_{1.93}$ at room temperature (See Figs. 4(b), 5(a) and 5(b) in Ref. (1)), and determined anharmonic parameters β using eq. (2). We obtained β = -2.4 meV with $h\omega_0$ = 147.6 meV for TiH_2 and β = -3.5 meV with $h\omega_0$ = 147.3 meV for $ZrH_{1.41}$[1]. The results indicate that hydrogen potential for T-site in fcc structure is close to the type (a), i.e. almost harmonic potential.

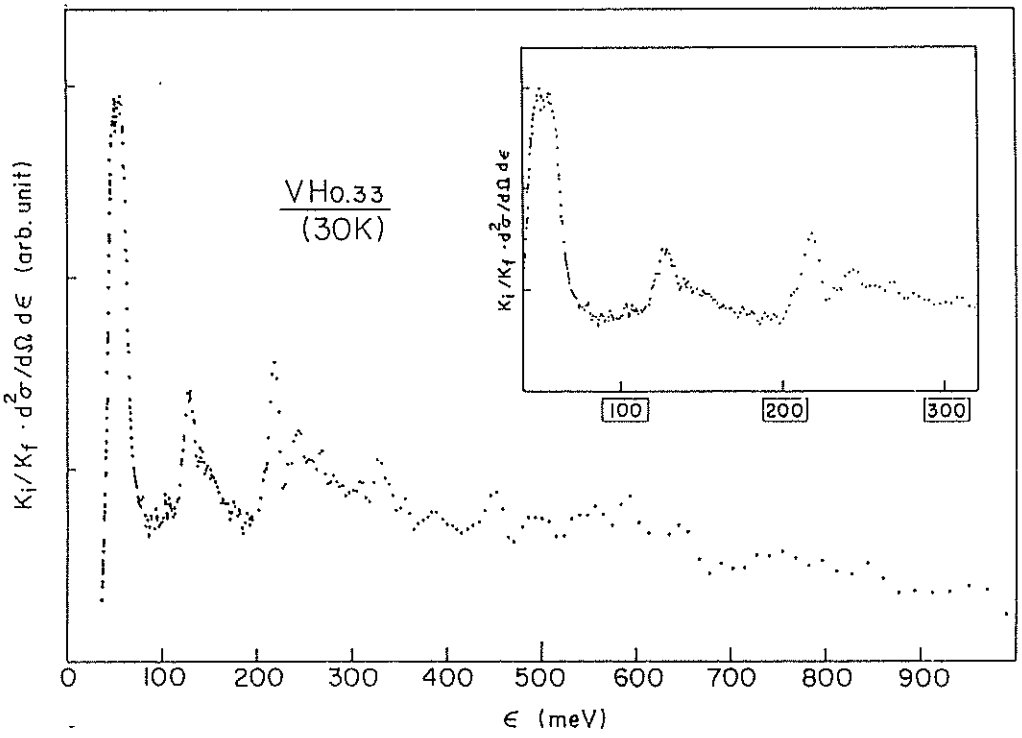

Fig. 2 Local mode spectra of β-$VH_{0.33}$ (30 K).

Figure 2 shows the local mode spectra of β-$VH_{0.33}$ (30 K). The peak at about 55 meV corresponds to the first excitation for x and y directions and the peak at about 220 meV to that for z direction reflecting the symmetry of O-site in bcc (actually bct) structure. The lower first excitation peak at ∿55 meV splits into two peaks at 51 meV and 57 meV. This splitting may be caused by a small monoclinic distortion from tetragonal. A broad peak at about 130 meV is considered to be the second excitation for x and y directions. The value of the anharmonicity determined by using (51+57)/2 meV

and 130 meV is +11 meV. Notice that sign of the β is positive in contrast with that of $TaH_{0.1}$ and the shape of hydrogen potential is like type (c).

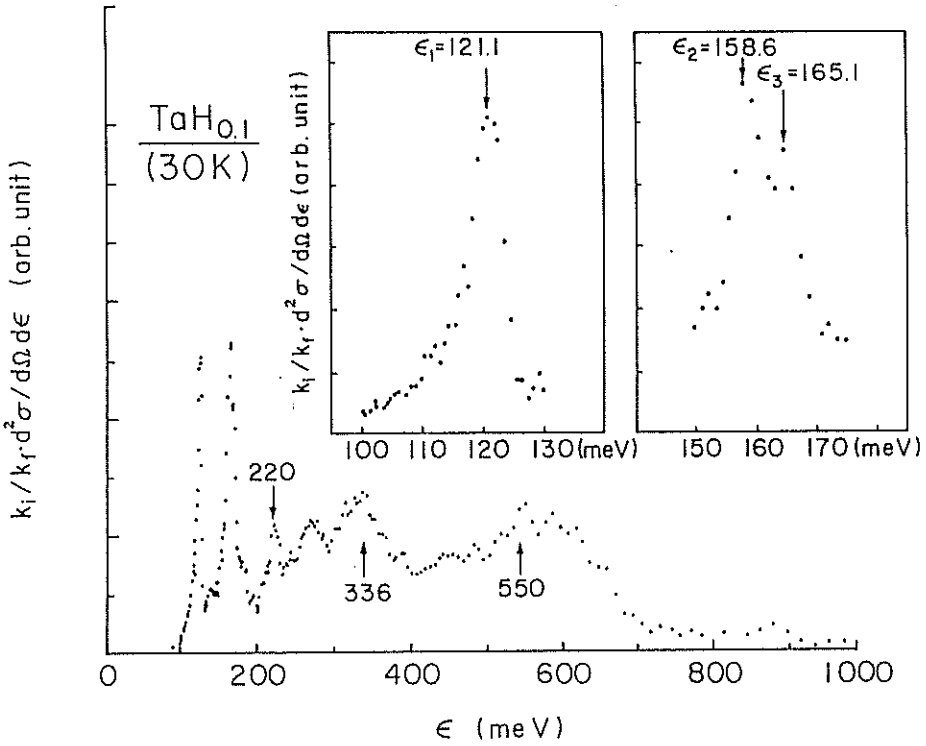

Fig. 3 Local mode spectra of β-$TaH_{0.1}$ at 30 K.

Figure 3 shows the local mode spectra of β-$TaH_{0.1}$ at 30 K. The peak at about 120 meV corresponds to the first excitation for z direction and the peak at about 160 meV to that for x and y directions reflecting the symmetry of T-site in bcc structure. The lower first excitation is found at 121 meV with the line width of 7 meV and the higher first excitation peak splits into two peaks at 159 meV and 165 meV due to the orthorhombic distortion in β-$TaH_{0.1}$ (30 K). This is a first experimental evidence for the splitting of the higher first excitation peak. Hempelmann, et al.[2] calculated an energy ratio of the splitting $\varepsilon_3/\varepsilon_2 = 1.044$ by using the results of X-ray and electron diffraction. The value is consistent with our experimental value of 1.041.

A distinct peak of the second excitation for z direction can be observed at about 220 meV, and a broad peak at about 340 meV seems to be the third excitation of this mode. Careful assignment of higher excitation peaks above 220 meV is under progress. We have obtained anharmonicity parameter β of -11 meV for $TaH_{0.1}$ (30 K) by using eq. (2). The value of $|\beta|$ is fairly larger than those of TiH_2 and ZrH_x. This indicates that the potential is the type (b). Moreover, no discrete level is observed and the

spectrum decrease rapidly beyond $\varepsilon \sim 700$ meV. The result may suggest that V_{max} is about 700 meV.

However, the measured V_{max} cannot be reproduced by eqs. (1) and (2) with the measured β because eq. (2) holds only for small perturbation a_4x^4.

We made a preliminary calculations to determine the total shape of hydrogen potential in $TaH_{0.1}$ by taking account of off-diagonal terms in Hamiltonian. We assumed that the z-component of the hydrogen potential in $TaH_{0.1}$ is given by

$$V(z) = a_1z + a_2z^2 + a_4z^4 \qquad (a_4 < 0) \tag{3}$$

and has maxima at positions A and C shown in Fig. 4. The values of a_1, a_2 and a_4 were determined by using experimental values of 121 meV, 220 meV and 340 meV for z direction. The calculated hydrogen potential and the energy levels are shown in Fig. 5. The results suggest that the peak due to ε_4 of z motion can be found at $\varepsilon = \sim 530$ meV and V_{max} is about 650 meV. The result is consistent with our data.

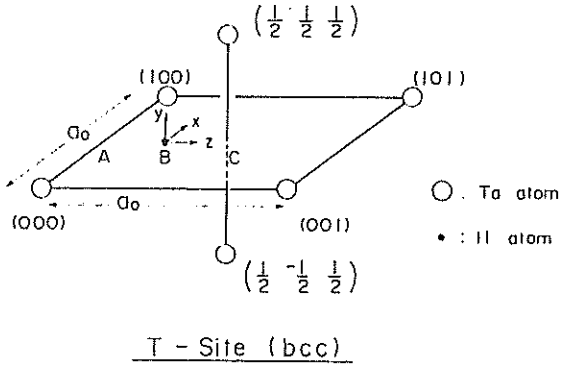

Fig. 4 T-site in bcc structure.

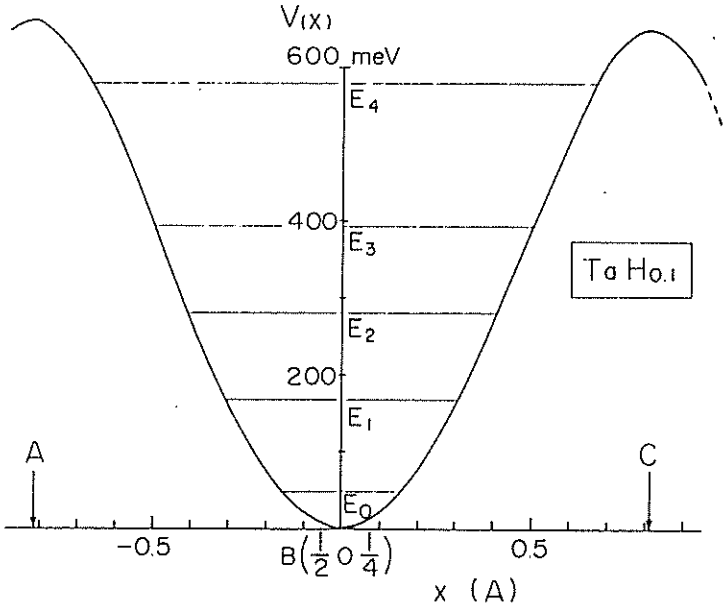

Fig. 5 Calculated potential of β-$TaH_{0.1}$.

References:

1) S. Ikeda, N. watanabe and K. Kai, Proc. Yamada Conf.-VI (Neutron Scattering of Condensed Matter)(Hakone, Oct. 1-4, 1982), to be published in Physica B.

2) R. Hempelmann and D. Richter, Z. Phys. B - Condensed Matter 44 (1981) 159.

Local Vibration Energy Spectra of H Atoms in Amorphous and Crystalline $ZrNiH_x$

Kenzo KAI, Noriyuki HAYASHI, Yuuji TOMITSUKA, Susumu IKEDA*, Noboru WATANABE* and Kenji SUZUKI

The Research Institute for Iron, Steel and Other Metals, Tohoku University, Sendai 980, Japan

*National Laboratory for High Energy Physics, Oho-machi, Tsukuba-gun, Ibaraki-ken 305, Japan

Hydrogen and deuterium atoms are easily absorbed into the interstitial hole in metallic atom polyhedra existing in metallic glasses consisting of a combination of early and late transition metals in the periodic table. Therefore, the metallic glasses are expected as a promising candidate for hydrogen energy conversion and storage materials, while hydrogen and deuterium atoms can be used as a sensitive probe for investigating the atomic scale structure and dynamics of the metallic glasses[1]. In this study the local environment of hydrogen atoms absorbed into ZrNi glass is examined by inelastic scattering using short wavelength pulsed neutrons.

ZrNi glass was solidified into a form of thin ribbons with about 2 mm in width and 30 μm in thickness by ejecting rapidly the melt onto a rotating roll under argon gas atomosphere. H atoms were introduced into the ZrNi glass ribbons from the gas phase under the total pressure of about 20 kg/cm^2 around the temperature of 100 °C. Measurements of the local vibration energy spectrum of H atoms in amorphous and crystalline $ZrNiH_x$ ($x=0.36 \sim 1.84$ for amorphous and $x=0.64 \sim 2.80$ for crystalline phase) were carried out at room temperature by using the Crystal Analyser Time-of-flight spectrometer (CAT) installed at the spallation neutron source in National Laboratory for High Energy Physics in Japan. Details of the performance for the both neutron spectrometers and the data processing procedure have been described in a previous paper[2].

The double differential cross-sections $d^2\sigma/d\Omega d\omega$ for incoherent neutron scattering from amorphous and crystalline $ZrNiH_x$ are shown as a function of the energy transfer $\hbar\omega$ in Fig. 1. In the local vibration energy spectrum of H atoms in crystalline $ZrNiH_{0.64}$, a main peak is divided into three peaks

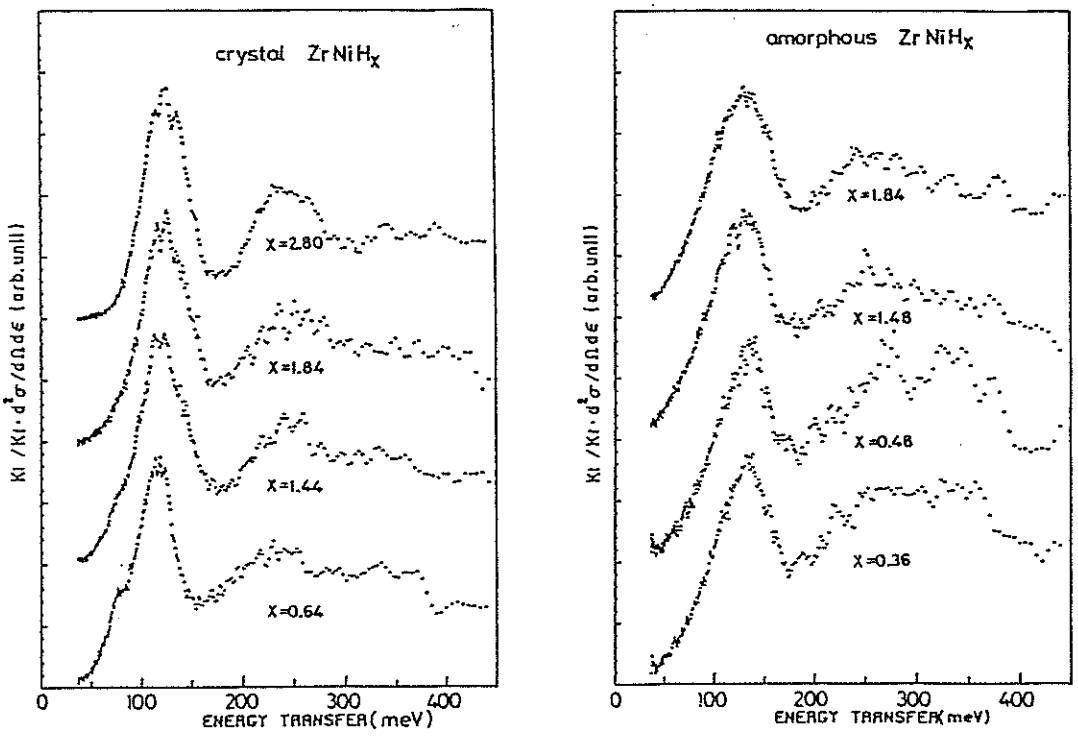

Fig. 1. Local vibration energy spectra of H atoms in crystalline and amorphous $ZrNiH_x$ ($x=0.64 \sim 2.80$ for crystalline and $x=0.36 \sim 1.84$ for amorphous phase)

located over the energy region of $\hbar\omega=110 \sim 120$ meV and a shoulder appears around $\hbar\omega \sim 80$ meV. With increasing H content, the shoulder gradually disappears, while the main peak shifts toward higher energy region. The main peak in the spectrum for crystalline $ZrNiH_{2.8}$ is still separated into three peaks located at $\hbar\omega=112$, 123 and 134 meV respectively and another shoulder takes place on the high energy side of the main peak around $\hbar\omega \sim 150$ meV.

The local vibration energy spectra of H atoms in amorphous $ZrNiH_x$ do not indicate the disappearance and energy shift of peaks and shoulders as shown in Fig. 1. The peaks are generally broader even in amorphous $ZrNiH_x$ with low H content. Higher order vibrations of H atoms are still observed in amorphous $ZrNiH_x$ as well as in crystalline one. It is noteworthy that the main peak position is almostly fixed around $\hbar\omega=130 \sim 135$ meV over the whole H content studied in this work.

H atoms in crystalline ZrNiH occupy selectively the interstitial hole tetrahedrally surrounded by 4Zr atoms(a-site) to induce the lattice distortion from an orthorhombic to a triclinic structure, while H atoms in crystalline $ZrNiH_3$ sit in two different kinds of sites, namely the

tetrahedral hole surrounded by 3Zr and 1Ni atoms(c-site) and the hexahedral hole by 3Zr and 2Ni atoms(b-site) with emptying the a-site and reverting the lattice to an orthorhombic structure[3]. Figure 2 shows the geometrical dimensions of a, b and c-site existing in crystalline ZrNiH and $ZrNiH_3$. Based on the neutron total scattering measurement of amorphous $ZrNiD_x$[4], it has been confimed that D atoms in amorphous $ZrNiD_x$ with low D content prefer to occupy the interstitial hole surrounded by 4Zr atoms. With increasing D content, D atoms occupy asymptotically the 4-coordinations site consisting of 3Zr and 1Ni atoms on the average. The D-Zr atomic distance in the 4Zr atoms tetrahedron occupied by a D atom in amorphous $ZrNiD_{0.3}$ is about 2.10 A, which is obviously shorter than the D-Zr atomic distance (2.20 A) in the a-site in crystalline ZrNiD and rather close to the D-Zr atomic distance(2.08 A) in the 4Zr atoms tetrahedron in crystalline ZrD_2. Therefore, we can understand that the energy position of the main peak in the local vibration energy spectra of H atoms in amorphous $ZrNiH_x$(x=0.3 and 0.48) with low H content is about 10 to 15 meV higher than that of crystalline $ZrNiH_{0.64}$. This study indicates that there is no hexahedral b-site with 5-coordinations in amorphous $ZrNiH(D)_x$ even with approaching a maximum H(D) content.

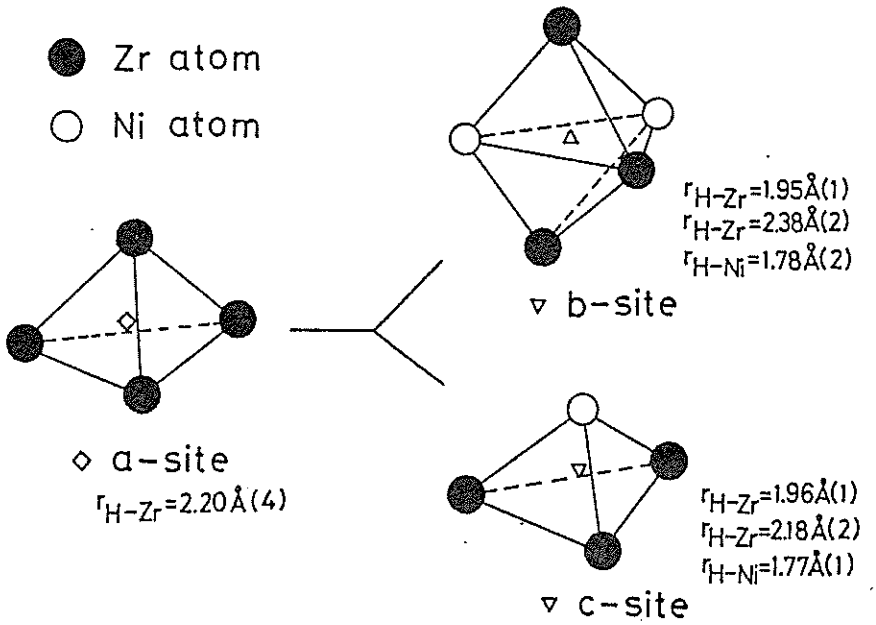

Fig. 2. Polyhedral sites occupied by H(D) atoms in crystalline ZrNiH(D) and $ZrNiH(D)_3$ proposed by Westlake et al[3].

References

1) K. Suzuki, J. Less-Common Metals 89 (1983) 183.

2) S. Ikeda, K. Kai and N. Watanabe, Physica B+C (1983) (Proc. Yamada Conf. VI).

3) D. G. Westlake, H. Shaked, P. R. Mason, B. R. McCart, M. H. Mueller, T. Masumoto and M. Amano, J. Less-Common Metals 88 (1982) 18.

4) N. Hayashi, Y. Tomitsuka, T. Fukunaga, K. Kai, N. Watanabe and K. Suzuki, Neutron Diffraction of Hydrogenated Alloy Glasses Zr-Ni-D, in this volume.

Instrumental Improvements and Further Tests of the CAT

Susumu IKEDA and Noboru WATANABE

National Laboratory for High Energy Physics
Oho-machi, Tsukuba-gun, Ibaraki 305, Japan

Itaru KANEKO

Department of Nuclear Engineering, Hokkaido University
Sapporo, Hokkaido 060, Japan

The CAT is a high resolution ($\Delta\varepsilon/\varepsilon \sim 0.02$) crystal analyzer TOF spectrometer designed for the measurements of incoherent neutron scattering in the energy transfer range ε = 50 - 1,000 meV. The spectrometer was built in FY 1981 and preliminary tests of this instrument were already accomplished[1-3]. Some of the experimental results achieved by this spectrometer have also been reported[3-8]. Higher performances of this instrument, particularly capabilities for high resolution, wide dynamic range (up to higher energy transfer) and high signal to background ratio have been demonstrated. The qualities are the highest among the existing spectrometers of this kind in the world. Present paper reports some instrumental improvements achieved in FY 1982 and the results of further tests of the fundamental performances of this spectrometer.

In the previous experiment, the CAT did not have its own time analyzer but tentatively utilized a part (one input) of the HIT time analyzer (24 bit 1 k channels x 16 inputs, 2 μs/ch. below 0.5 k ch. and 4 μs/ch. above 0.5 k ch.) Therefore, the total number of channels was not adequate for covering the full spectrum including the elastic peak with a required channel width. A dedicated data acquisition and processing system has been constructed which consists of a Camac type time analyzer (16 bit 8 k channels x 2 inputs, minimum channel width: 0.5 μs) and a computer system common to that of the RAT[9] for quick data processing. As an example a set of full TOF spectra for a sample (TiH_2 at room temp.) and for the aluminium holder is shown in Fig. 1. Channel width is 2 μs/ch. The background counts have been decreased by an improvement of the inside shielding of the spectrometer (See Aℓ holder run in Fig. 1).

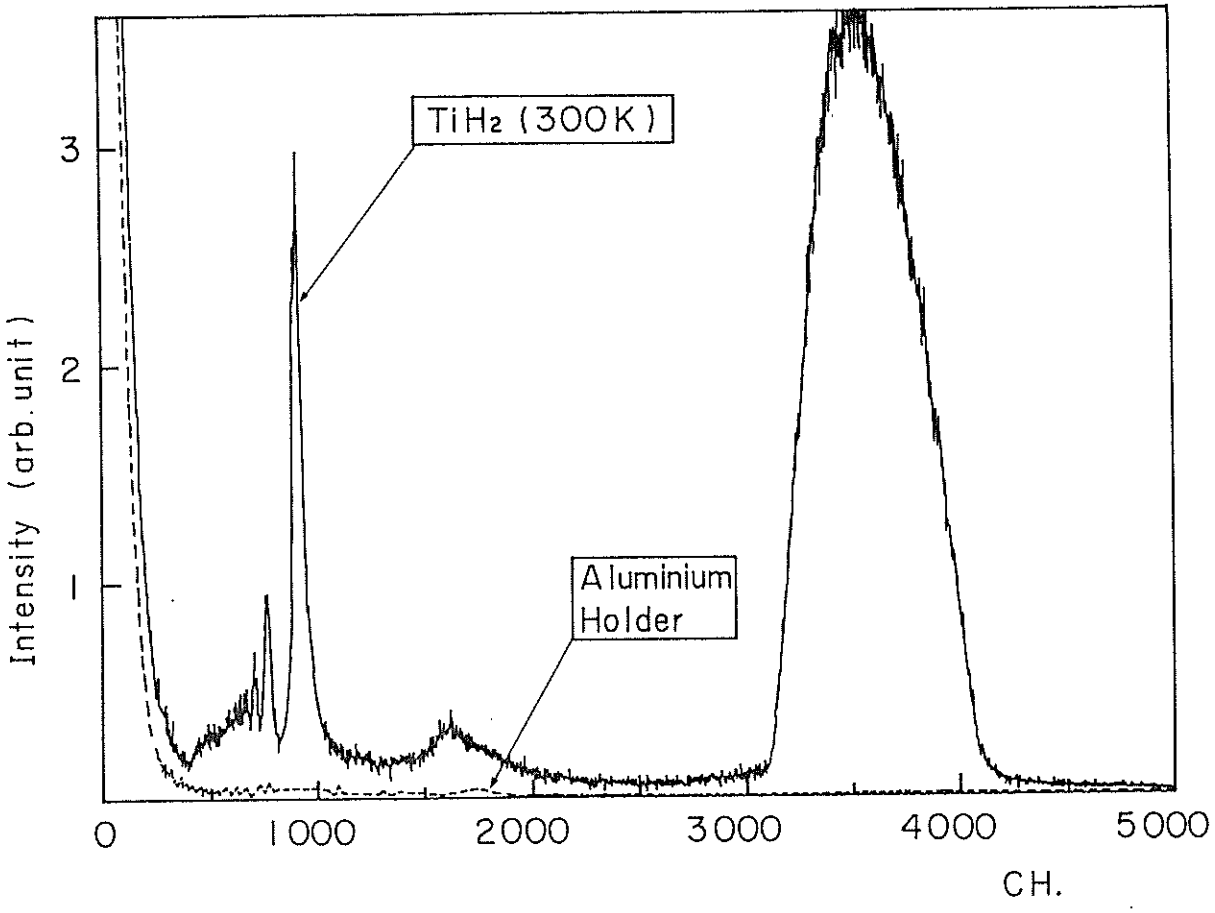

Fig. 1 Full TOF spectra for the sample (TiH_2 at room temp.) and for the aluminium holder with the new time analyzer.

A liquid nitrogen cryostat for beryllium filter cooling was removed and a small closed cycle refrigerator (Cryo-mini S) has been installed for this purpose. This alternation has largely saved our labors in the machine operation. Filter temperature of about 20 K has been attained.

Exact energy distribution of the detected neutrons P(E) is very important. We have calculated P(E) by a Monte Carlo computer simulation. In order to check the calculated P(E), we compared it with a measured elastic peak from $NbH_{0.76}$ at room temperature (β-phase). In Fig. 2 are shown the measured and the calculated elastic peaks (almost identical two curves assigned λ_{PG} with filter) in time scale. The calculated elastic peak is the P(E) modulated by the measured incident spectrum $\phi(E)$. The agreement between measurement and calculation is almost perfect and the calculated value of E_f = 3.6 meV is now justified.

Another important problem which must be checked in this instrument is the spectral contamination by the higher order reflections of the analyzer crystal, because neutrons having the energies larger than beryllium cut-off may leak, more or less, by multiple scattering in the filter. In order to examine this effect, measurements with and without the beryllium filter have been performed. The results are also shown in Fig. 2 in the case of $NbH_{0.76}$ sample at room temperature. Note that "without filter spectrum" is scaled down by 1/15. For the simplicity if we notice the leakage spectrum corresponding to the third order elastic, we cannot recognize any trace of the third order elastic peak in the "with filter spectrum" as demonstrated in the figure.

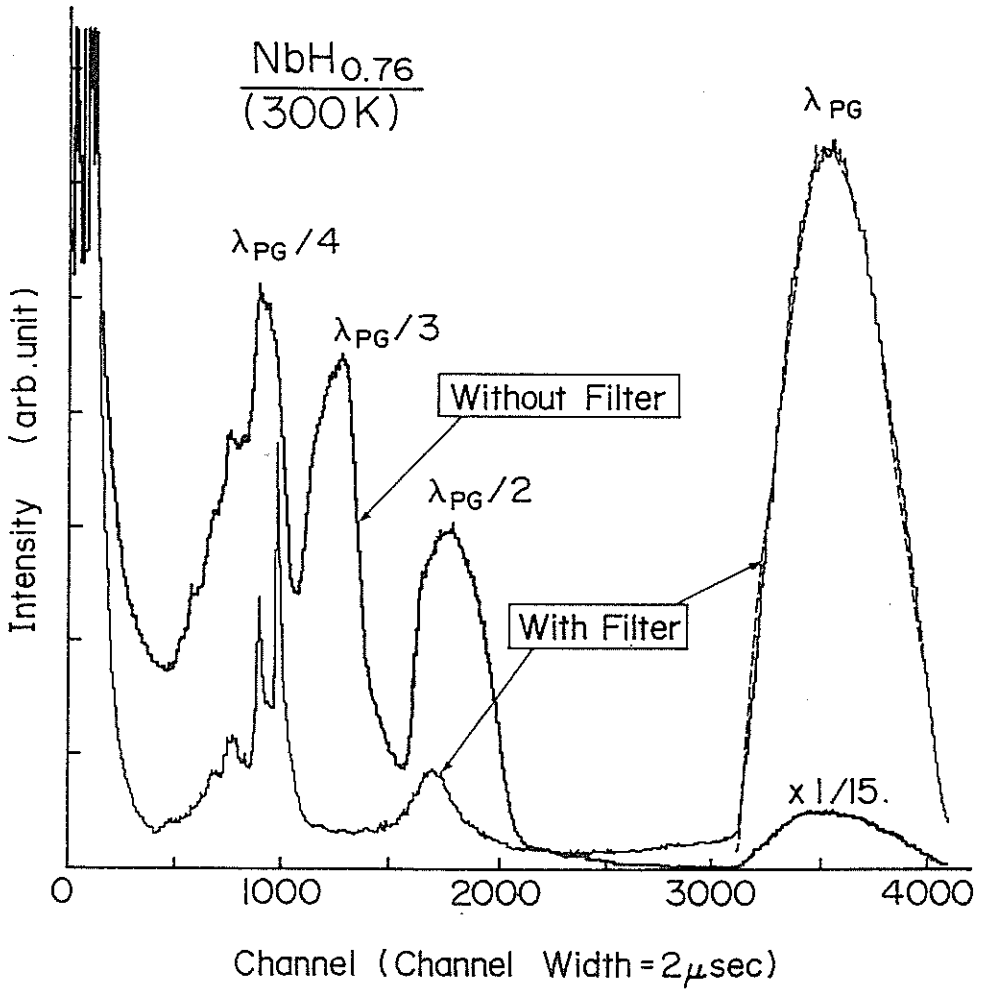

Fig. 2 With and without filter spectra for $NbH_{0.76}$ at room temperature and comparison of measured TOF spectrum for elastic peak (solid line) with calculation (broken line).

Thermal neutron transmission in this beryllium filter with the post cross collimator has been confirmed to be less than 10^{-3} from this result. At Tohoku linac a direct measurement of the transmission in a similar filter-post collimator system was performed and the measured transmission was also less than 10^{-3}. We can, therefore, conclude that the spectral contamination in this instrument is negligibly small, at least, for hydrogeneous samples.

Further improvement in energy resolution is possible with present incident path length by changing the present He-3 counters to a ^{6}Li glass scintillation detector; for instance, effective thickness of the NE-905 scintillator is less than 0.5 mm for $E_f \sim 4$ meV. Using this detector with shorter channel width of 1 μsec, we can realize overall resolution about 1 %. Background counting rate due to the spontaneous α-decay in the scintillator is estimated to be about 0.3 counts/day-μsec-channel which is negligible.

References

1) S. Ikeda, N. Watanabe, K. Kai and S. Yamaguchi, KENS Report, KEK Int. 82-5 (1982) 104.
2) N. Watanabe, S. Ikeda and K. Kai, Proc. ICANS-VI (Argonne, June 28 - July 2, 1982) 279.
3) S. Ikeda and N. Watanabe, to be published.
4) S. Ikeda, N. Watanabe and K. Kai, Proc. YAMADA Conf.-VI (Neutron Scattering) (Hakone, Sept 1 - 4, 1982) to be published in Physica B.
5) K. Kai, S. Ikeda, T. Fukunaga, N. Watanabe and K. Suzuki, ibid.
6) S. Ikeda, N. Watanabe and K. Kai, KENS Report III, KEK Int. 82-5 (1982) 109.
7) K. Kai, S. Ikeda, N. Watanabe and K. Suzuki, ibid 112.
8) S. Ikeda and N. Watanabe, KENS Report IV.
9) N. Watanabe, S. Ikeda, H. Rauh, Y. Masuda and S. Sato, KENS Report IV.

Depolarization Study of the spin fluctuation in FeCr spin glass

Setsuo Mitsuda, Yasuo Endoh and Susumu Ikeda*

Department of Physics, Tohoku University, Sendai 980

* National Laboratory for High Energy Physics
Oho-cho, Tsukuba, Ibaraki 305

We have shown that the measurements of neutron depolarization using the wide range of the continuous spectra of pulsed polarized neutrons give us more direct concept of the theory by Halpern and Holstein than those of the steady beams of single wave length. Then we have applied this technique to the studies of inhomogeneous ferromagnets, such as alloys of 3d transition metal elements, spin glasses, the random mixtures of the magnetic compounds and even amorphous materials. We could also show that the technique is complimentarily useful to study the slow spin fluctuations which are often difficult to be detected with the conventional scattering experiments. Recently we have elucidated the depolarization of the transimitted neutrons through the spin glass materials. We domcument here a brief thoretical back ground concerning to this experiments as well as some brief results from $Fe_{22}Cr_{78}$ which is known as the reentrant spin glass.

Within the Born approximation, the depolarization is due to the scattering of polarized neutrons by the magnetic inhomogeneity. In the language of the classical treatment by Harpern and Holstein, the neutron polarization obeys the classical equation of motion.

$$\hbar\dot{p} = g_n [\vec{P} \times \vec{B}] \qquad (1)$$

, where B represents the magnetic induction in the magnetic specimens. We assume that B is the sum of the constant field, B_o and fluctating one, b. B_o is the average value of <B> and then <b> = 0. Therefore b causes the wave length dependence of depolarization and in particular it results the decay of polarization with respect to the wave length. Eq.(1) is changed to the integral form as,

$$\vec{p}(t) = p_o + g_n \int_0^t dt' \, [\vec{P} \times \vec{B}]$$

$$= p_o + g_n \int_0^t dt' \langle [\vec{P}_o \times B(t')] \rangle + (g_n)^2 \int_0^t dt' \int_0^{t'}$$

$$\langle [\vec{P}_o \times B(t'') \quad B(t') \rangle . \qquad (2)$$

Under the above mentioned approximation, eq(2) is written in terms of the correlation function of b(t), when $P_o // B_o$,

$$\frac{\Delta p}{p} = -\frac{g_n}{2} \int_0^t dt' \int_0^t dt'' \langle b(t')b(t'') + b(t'')b(t') \rangle . \qquad (3)$$

We assume that the random field in the ferromagnet, H(t), is approximated by the Gaussian form, then the random field correlation function is written as follows,

$$\langle H_\perp(t_o) \; H_\perp(t_o+t) \rangle = \frac{\Delta^2}{\gamma^2} \; e^{-\nu t} \qquad (4)$$

The wave length dependence of depolarization is derived from (3) and (4) with further assumption that H(t) = b(t). Therefore the result of Fig.1 is interpreted qualitatively that the oscillation with respect to the wave length arises by the appearance of B_o, and the exponential decay of the polarization is due to the random field.

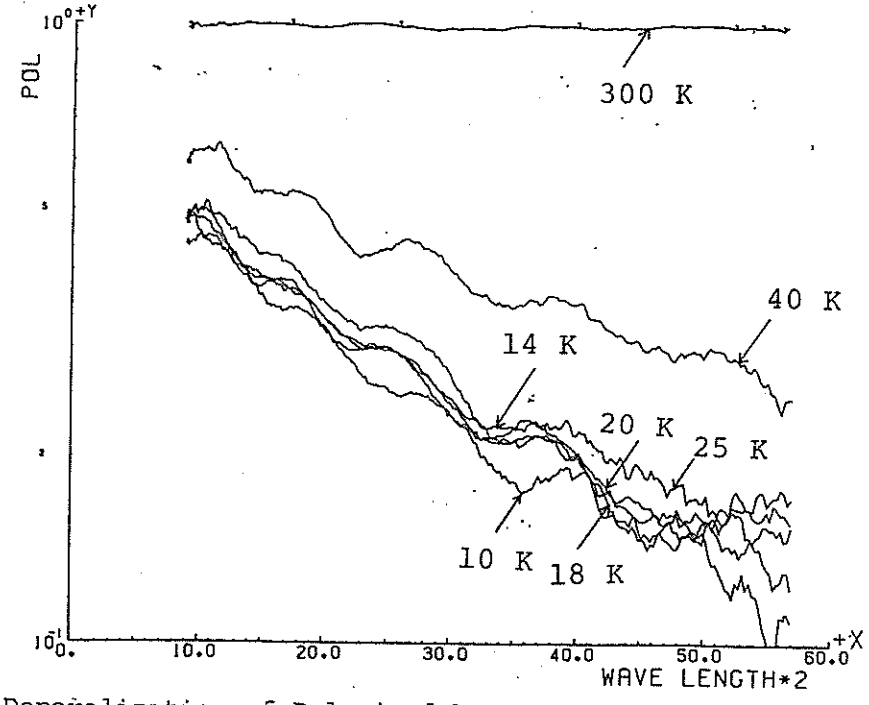

Fig.1. Depolarization of Polarized beams through $Fe_{22}Cr_{78}$ polycrystalline plate.

Neutron Depolarization and Mössbauer Studies of Domain Structure of Amorphous $(Co_{0.94}Fe_{0.06})_{74.5}Si_{13.5}B_{12}$ Alloy

E. Torikai, A. Ito*, S. Mitsuda** and Y. Endoh**

Doctoral Research Course in Human Culture, Ochanomizu University, Tokyo 112, Japan

* Department of Physics, Ochanomizu University, Tokyo 112, Japan

** Physics Department, Tohoku University, Sendai 980, Japan

The depolarization analysis of polarized neutrons passing through magnetic materials has been suggested as a useful technique for the study of domain structures[1,2]. We applied this technique to an amorphous $(Co_{0.94}Fe_{0.06})_{74.5}Si_{13.5}B_{12}$ alloy whose domain structure is difficult to observe by conventional methods. Here, we report some preliminary results of the study.

The amorphous $(Co_{0.94}Fe_{0.06})_{74.5}Si_{13.5}B_{12}$ alloy (in the form of a long ribbon width of 5 mm, thickness of about 23 μm) is one of the promising soft magnetic materials with practical applications. It is characterized by high magnetic permeability, low coercive force and nearly zero magnetostriction constant. Magnetic properties of this kind of alloy have been studied extensively[3-7], but microscopic ones are far from understanding. The as-prepared sample shows a uniaxial magnetic anisotropy as a macroscopic property against early expectation that the amorphous alloy with vanished magnetostriction should have isotropic properties.

To study the microscopic properties of the amorphous alloy in relation to its atomic constituent arrangement, we used the Mössbauer spectroscopy[8]. In this method, the areal ratio of absorption lines depends on the angle between directions of incident γ-rays and those of the internal magnetic fields at the individual nucleus site, which generally corresponds to the directions of the magnetic moments. Using these characteristics, we can obtain the directional distribution of magnetic moments microscopically. The Mössbauer study of an as-prepared sample has revealed that the directions of local magnetization axes are laid in the ribbon plane but are widely distributed around the ribbon's

long direction. Such a large distribution of the magnetization axes, which cannot be expected in crystalline solids with uniaxial magnetic anisotropies, is a distinctive property of an amorphous alloy with structural randomness. We have not succeeded in observing the domain structure of our sample by conventional methods. The domain structure of the amorphous $Co_{70}Fe_5Si_9B_{16}$ alloy, whose concentration is close to ours, has been observed using the Kerr effect by H. Kronmüller et al., which is not consistent with our results[9].

The observation of the depolarization of polarized neutrons is expected to give information about the bulk domain structure of the ferromagnet. During the passage of neutrons through a ferromagnet, spins of neutrons are rotated around magnetic moments of domains on those paths. Applying the classical equation of motion, the depolarization of neutrons is expressed by the mean magnetization and the mean domain size. On the other hand, Mössbauer measurements give information concerning the directions of local magnetization axes as mentioned above but not the dimensions of domains. Therefore the combination of these methods, which are complement with each other, will be useful for the study of the magnetism of the amorphous alloy.

The experiment of the neutron depolarization has been carried out using TOP spectrometer installed at KENS in KEK. The as-prepared sample was annealed at 753 K for 5 min for a stress-release, then was annealed in the magnetic field parallel to the ribbon's long direction at 423 K for 100 hr. The Mössbauer measurements showed that almost all of the local magnetic moments of the sample were aligned along the ribbon's long direction[10]. Since the sample does not show the net magnetization under zero magnetic field, the result is interpreted as that its domain structure is close to 180° domain along the ribbon's long direction. We examined this sample with induced uniaxial magnetic anisotropy as a standard material for the neutron study. The ribbon's long direction was set parallel (// geometry) or perpendicular ($\perp$ geometry) to the initial spin axis of polarized neutrons (z-axis). The magnetic field was applied in the z-direction.

Figure 1(a) shows the polarization of neutrons after transmission through the sample in the // geometry. By remembering the fact that when the polarization is kept (lost) completely, the value of the polarization is 1.0 (0.0), we see in Fig. 1(a) that the initial polarization is kept rathr well and is independent of the wavelength of the neutrons. Under the low applied field (~6 Oe), the depolarization of neutrons is less

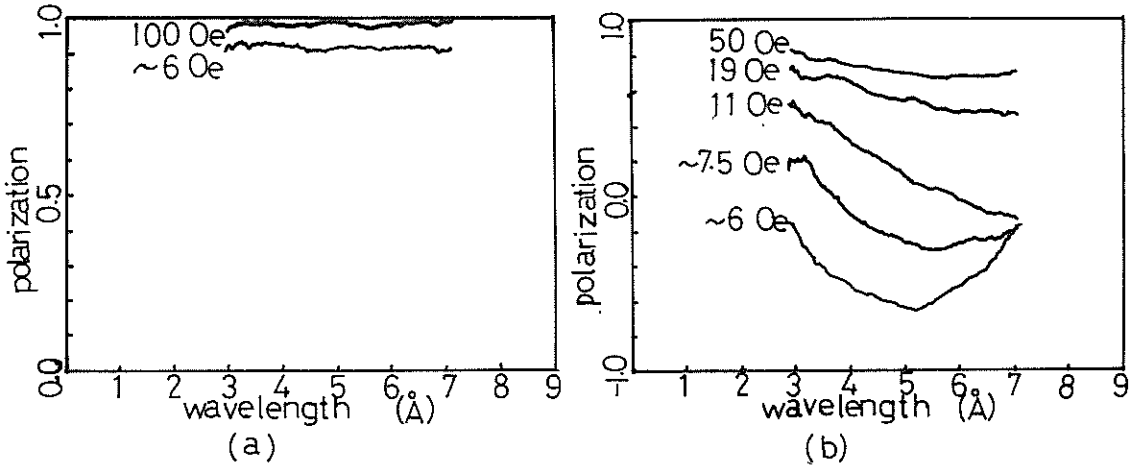

Fig. 1 The polarization of neutrons after transmission through the sample with induced magnetic anisotropy along the ribbon's long direction. The direction of the initial polarization of neutrons is parallel to (a) the ribbon's long direction and (b) the ribbon width.

than 20 %. When the magnetic field is increased up to 100 Oe, the depolarization decreased noticiably but not completely.

The neutron depolarization in the $\perp$ geometry is shown in Fig. 1(b). The negative value of the polarization means that the neutron spins direct to - z axis at the exit. The polarization varies sinusoidally as a function of wavelength under the low applied field (~6 Oe). The net magnetic flux density along the neutron's paths is roughly estimated to be about 0.58 T from the observed period of the polarization spectrum, where the saturation magnetic flux density is 0.8 T. This fact indicates that the most of magnetic moments which lie on an individual neutron's path are aligned in the same direction; the direction of the magnetic moments rotates from the easy axis but does not attain to the z-axis. If we assume the single domain structure in the ribbon plane, the angle between the z-axis and the magnetic moment is estimated as about 66°. When the magnetic field is increased, the sinusoidal aspect of the polarization spectrum disappears. The polarization shows monotonic decrease with increasing the wavelength of neutrons above about 11 Oe, indicating that the domain structure consists of small random domains.

The results of the neutron depolarization and the Mössbouer studies suggest that the sample with induced magnetic anisotropy along the ribbon's long direction has 180° domain structure in the ribbon plane, and the domains are not divided along the ribbon's thickness under low magnetic field; by increasing the magnetic field along the ribbon's width (i.e. perpendicular to the magnetic easy axis) the domains collapse into

small domains. This feature is considered to be reasonable as a magnetization process of this amorphous alloy. The magnetization process of the as-prepared sample and samples annealed under the other conditions will be investigated later using the similar methods.

References

1) O.Halpern and T.Holstein, Phys.Rev., 59 (1941) 960

2) M.Th.Rekvelt, Z.Physik, 259 (1973) 391

3) H.Fujimori, H.Morita, Y.Obi and S.Ohta, Amorphous Magnetism II, eds. R.A.Levy and R.Hasegawa(Prenum Press, New York, 1977) 393

4) K.Arai and N.Tsuya, IEEE Trans.Magn.MAG-13 (1977) 1550

5) T.Miyazaki and M.Takahashi, Jpn.J.Appl.Phys., 17 (1978) 1755

6) H.Sakakima, H.Senno, Y.Yanagiuchi and E.Hirata, J.Appl.Phys., 52 (1981) 2480

7) T.Matsuyama, K.Ohta, M.Kajiura and T.Teranishi, J.J.A.P, 19 (1980) 55

8) A.Ito, E.Torikai, S.Morimoto K.Shiiki and M.Kudo, Jpn.J.Appl.Phys, 20 (1981) 797

9) H.Kronmüller, M.Fähnle, M.Domann, H.Grimm, R.Grimm and B.Gröger, J.M.M.M., 13 (1979) 53

10) E.Torikai, A.Ito, S.Morimoto, K.Shiiki and M.Kudo, Proc. 4-th Int. Conf. on Rapidly Quenched Metals, Sendai, eds. T.Masumoto and K.Suzuki (1981) 1129

Polarized neutron diffraction from Fe/Sb and Fe/V ASF(Interface magnetism of Fe metals)

Nobuyoshi Hosoito, Kenji Kawaguchi and Teruya Shinjo

Institute for Chemical Research, Kyoto Univerisity
Uji Kyoto, 611

and

Y. Endoh
Department of Physics, Tohoku University
Sendai, 980

We have continuously elucidated the effects of interface on ferromagnetism using the tailor made artificial superstructure magnetic films(ASF)[1]. We now focus the studies on the effects of various interfaces on the Fe ferromagnetism. A dominant effect arises from the change of the electronic structure of d bands carrying the magnetic moment near the surface. Since the energy shift or work function varies with the contacting materials at the Fe surface, we expect the various effect with different combinations of bilayers.

We have been looking at a series of Fe ASF where the materials contacting with the Fe metal are varied such as insulators, semimetals, simple metals and transition metals.

In order to extract the interface effect of ferromagnetism, explicitly, we must determine the spatial distribution of magnetization densities along the normal direction to the surface of ASF. Since we could observe the limited numbers of higher ordered reflections, we need an approximation in our situation. Thus we have made polarized neutron diffraction to look at the first order reflection from the series of Fe/Sb as well as Fe/V ASF with different ratio of the thickness of Fe layers with respect to the bilayer thickness. Using the kinematical theory the flipping ratio of the first ordered reflection should be independent upon these specimens, if there exists no surface anomaly in the magnetization density. It should be noted that the extinction effect should be estimated properly.

We have examined the effect of the primary extinction which is dominant due to the fact that the width of the Bragg angle distribution of the superlattice reflection is narrow compared with the wavelength distribution of λ.

Then we have applied the conventional approximation form of

$$R = qQ\tanh(nq) \qquad (1)$$

, where q,n are repectively the scattering power, and the number of layers[2]. R is the intergrated intensity but is approximated by the flipping ratio, because R is several 10th of order[1]. The modified flipping ratios of p = R-1/R+1 are plotted in Fig.1 and they are compared with the functional form of eq.(1). Although more detailed corrections such as the width of the Bragg reflection,and scattering power should be taken,the wave length dependence of the flipping ratio is shown to be a good measure of the primary extinction effect.[2,4]

After the correction we could estimate the magnetization density distribution using an ab initio magnetic scattering potential distribution. The results are summarized in Fig.2. The interesting points are emphasized that only a nearest neighbour Fe layer contacted on the other constituent metallic layers has a significant modulated magnetization from that of the bulk materials.

These results are in good agreement with that of the recent band calculation by Freeman et.al.[3]

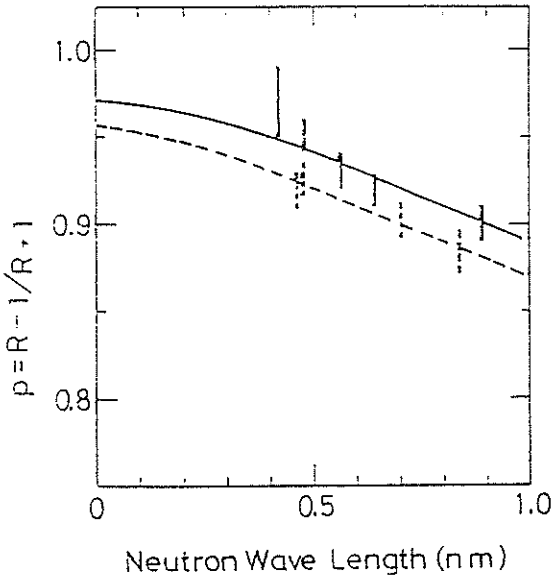

Fig. 1. Wave length dependence of the modified flipping ratio of p = R-1/R+1 for the first order superlattice reflection in Fe/Sb ASF. Two different Fe/Sb are measured.

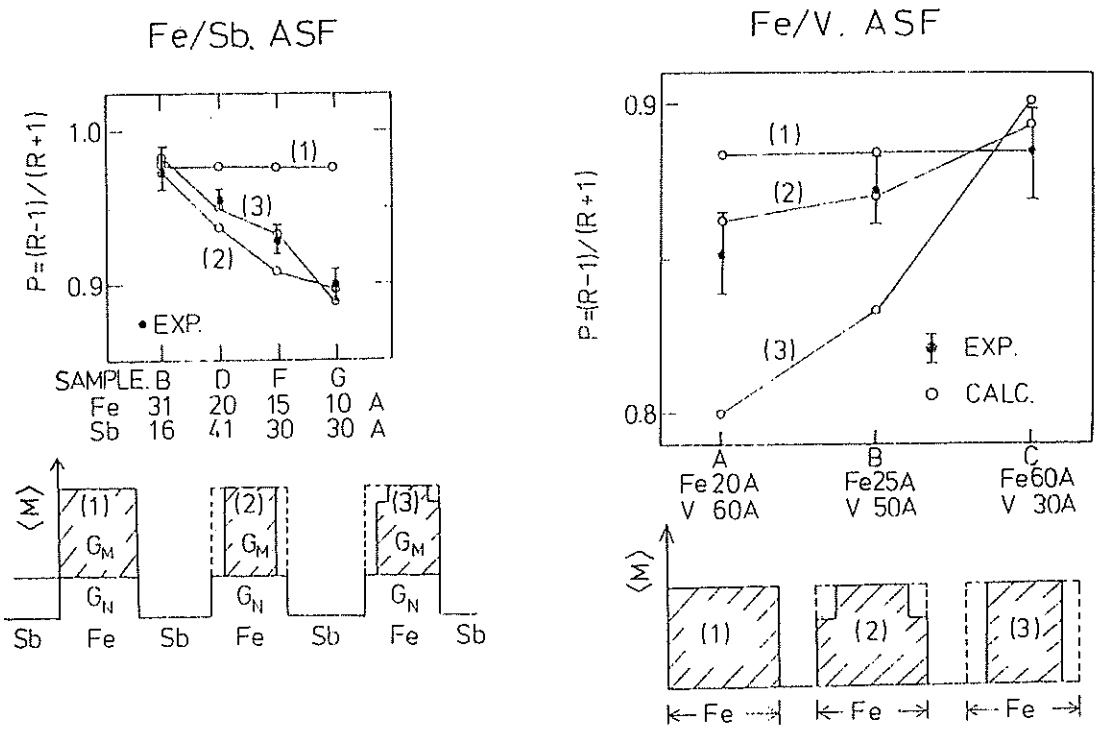

Fig. 2. Schematic model of the magnetization density distribution in Fe/Sb and Fe/V ASF.

References

1) Y. Endoh, N. Hosoito and T. Shinjo, JMMM 35 (1983) 93

2) M. Sato, K. Abe, Y. Endoh and J. Hayter, J. Phys. C 13 (1980) 3567

3) T. Jarlborg and A.J.Freeman, Physica 107 B+C (1981) 69

4) Y. Endoh, J. de Physics C7(1982)159

Determination of helix winding in MnSi

Masayoshi Ishida, Yasuo Endoh, Setsuo Mitsuda and
Yoshikazu Ishikawa

Department of Physics, Tohoku University, Sendai 980

Very recently Nakanishi et al.[1] and Bak and Jensen[2] have presented an interesting theory concerning the helical structure of MnSi. They have shown that the screw structure in MnSi is caused by the antisymmetric exchange interaction, often called as Dzaloshinski-Moriya(D-M) interaction due to the fact that the cubic MnSi has no inversion symmetry of P213. They also predicted that only a single helix of either clockwise (right handed) or anticlockwise (left handed) winding exists in MnSi. On the contrary there is no difference in energy between clock wise and anticlock wise helix in the screw strucure caused by the competition of the magnetic exchange interaction.

Our interest is therefore to test their theory as well as to determine the direction of helix winding by polarized neutrons. Determination of the helix in MnSi provides the sign of the coefficient of the D-M interaction, which may contribute to further theoretical development exploring the domi nant contribution of the spin-orbit coupling to the D-M interaction.

We were aware of possible existence of the crystal structure with a right handed or a left handed coordinate during the course of experiments. After determining the crystal symmetry by means of the converging electron diffraction, we have performed careful polarized neutron diffraction studies on the TOP spectrometer. Since the detailed procedure is described in a recent publication, essential results are documented here[3].

Our experimental set up is such that the magnetic field is applied along the scattering vector which is also parallel to one of the propagation vector of helix. The schematic drawing of the experimental set up is illustrated in the figure. We should observe from this configuration that the only one particular polarized neutrons are scattered by single helix at a magnetic superlattice Bragg point correponding to the inverse of a period of the helix.

We measured the dependences of the magnetic field, the process of cooling through the magneic transition and the samples. Then we found the

clockwise or right handed helix with respect to the propagation vector, which is independent of the cooling process, specimens and domain distributions. The magnetic field dependence of the intensities of the Bragg reflections indicates the irreversible change of the domain distribution without the change of the helix winding. It should be noted that the ratio of neutron counting of both counters with respect to the neutron spin flipping shown in Fig.1 is not exactly same as the flipping ratio of the incident polarized neutrons. However we think that we have observed a single helical state and that the small reduction of the flipping ratio is caused by the extinction effects.

To conclude we could determine the positive sign of the coefficient of the D-M interaction in the cubic crystal of MnSi with the right handed coordinate.

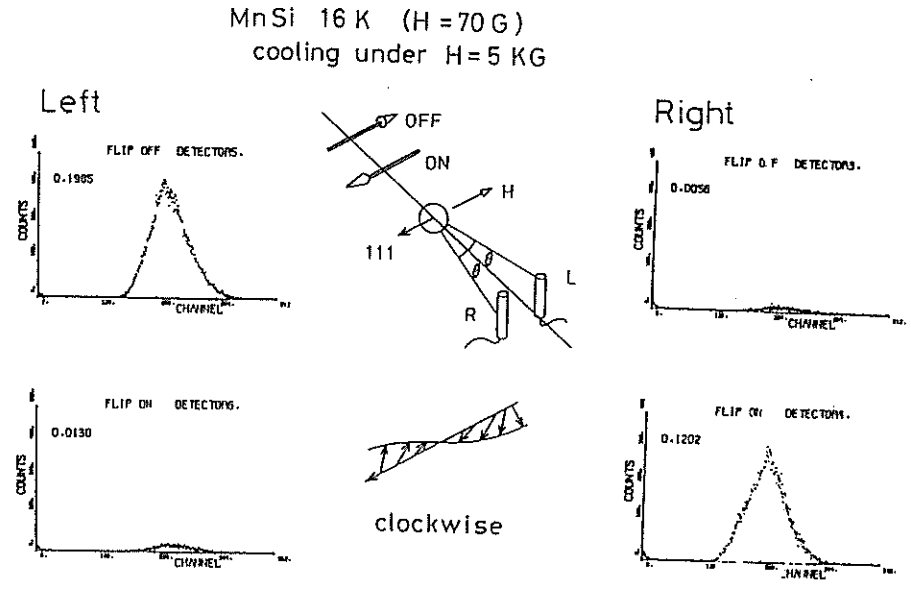

Fig.1 Polarized neutron diffraction results of MnSi at 16K.

References

1) O. Nakanishi, A. Tanase, A. Hasegawa and M. Kataoka; Solid State Commun. 35, 995(1980)

2) P. Bak and M. H. Jensen, J. Phys. C13 L881(1986)

3) M. Ishida, Y. Endoh, Y. Ishikawa, S. Mitsuda, M. Tanaka and H. Mitsuyoshi; submitted to J. Phys. Soc. Jpn.

Tests of Polarizability of Supermirror and Soller Mirror

Yasuo Endoh, Setsuo Mitsuda, Susumu Ikeda* and Mitsugu Onodera

Department of Physics, Tohoku University, Sendai 980

*National Laboratory for High Energy Physics, Oho-cho
Tsukuba, Ibaraki 305

The Soller Mirror polarizers and analyser presently situated on the TOP spectrometer are insufficient in the sense that the polarization drops appreciably in the longer wave length region than 8 A. In our experimental condition the lower critical wave length is chosen to be 3.5 A, and the critical average angle viewing the polarizer mirrors is 0.5 degree.

A reason of the decrease of polarization is the mismatching of both the magnetic and nuclear scattering amplitude of polarizing mirror materials. It may be caused by either the stretching of the films or shift of the FeCo concentration occurred at the evaporation stage.

We have examined the polarizability of testing Soller type polarizers fabricating approximately 3 sheets of FeCo films, which were made by evaporating with a newly constructed electron gun machine. We have chosen $Co_{70}Fe_{30}$ and $Co_{65}Fe_{35}$ of alloy concentration so as to reduce the average nuclear scattering amplitude.

Using the conventional shim method we have determined the polarizability which are shown in Fig.1. First of all we are immediately aware of the improvement of the polarizability in the longer wave length range. Second, the difference of polarizability between these two alloy concentrations is not appreciable, from which we notice the optimal concentration in order to obtain the matching.

At the same time we have examined the supermirror polarizer which were kindly offered by F. Mezei. Although the polarization is better and is constant up to 7.5 A as is shown in Fig.2, the neutron beam spectra out of the supermirror are not suitable for our purpose because of non monotonic dependence with respect to the wave length. (The spectrum is not shown here.)

To conclude we must ontinue to make efforts for making an ideal Soller mirror polarizer for our purpose.

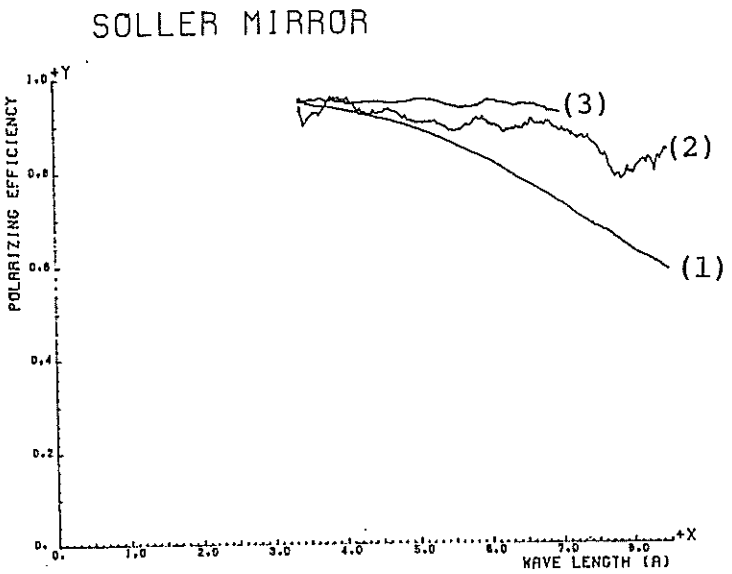

Fig. 1. Polarizability of FeCo Soller type magnetic mirrors.
(1) Currently used at TOP, (2) $Co_{70}Fe_{30}$ (Testing),
(3) $Fe_{65}Co_{35}$ (Testing)

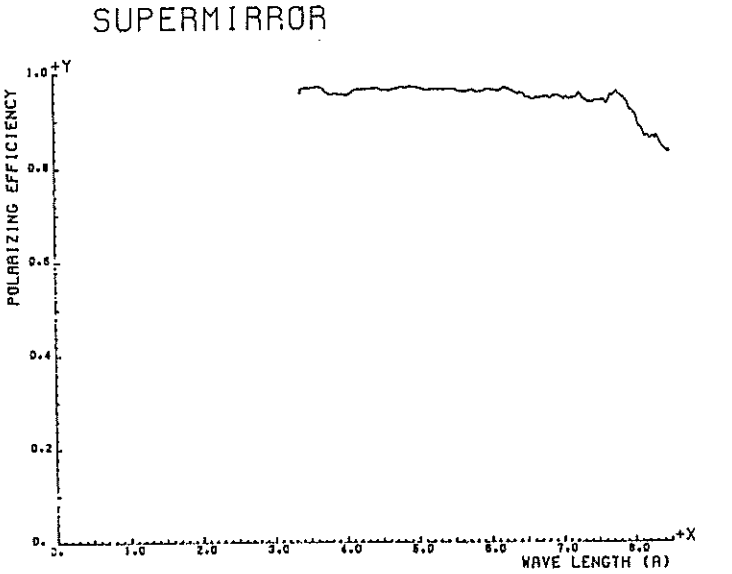

Fig. 2. Polarizability of AgFe Super mirrors

Polarized Epithermal Neutron Spectrometer PEN and Its Preliminary Performance

Masayoshi ISHIDA, Masahumi KOHGI, Yasuhiro MASUDA*, Shigenori HIRAMATSU*, Shigeru ISAGAWA*, Yoshikazu ISHIKAWA, Sigeru ISHIMOTO*, Akira MASAIKE*, Kimio MORIMOTO* and Tetsuo NAKAJIMA*

Physics Department, Tohoku University
Sendai 980, Japan

*National Laboratory for High Energy Physics
Oho-machi, Tsukuba-gun, Ibaraki 305, Japan

Introduction

The Polarized Epithermal Neutron spectrometer (PEN) is a multi-purpose spectrometer utilizing white epithermal polarized neutron beams, which is installed on the H8 thermal neutron beam port at KENS[1]. The neutron polarization is achieved by passage through a dynamically polarized proton filter (DPPF)[2),3)]. Since the DPPF polarizes all thermal and epithermal neutrons efficiently, the PEN spectrometer is designed to be used for various purposes, examples of which are as follows:

1) study of the process of the dynamical polarization of protons (Station 1),
2) magnetic structure determination of amorphous magnets (Station 2),
3) observation of high energy magnetic excitations in metallic ferromagnets (Station 3), and
4) study of spin parity of nuclear state.

Scattering system in the spectrometer

The layout of the spectrometer is displayed in Fig. 1, where the cooling system for the DPPF is omitted. The polarizing filter assembly is installed inside a shield house with a distance of 5.2 m from the neutron source. The shield house has several beam holes glancing at the filter in order to make possible the measurement of neutron scattering from the filter material (Station 1). The Q range of the scattering is about $0.4 \sim 60\ A^{-1}$, where the resolution varies as $\Delta Q/Q = 0.15 \sim 0.01$. A detector bank is also installed 4.5 m downstream from the filter for the small angle scattering.

A two-dimensional converging Soller slit system, which is almost the same as that installed at SAN[4], is inserted before the filter for small angle scattering, giving a resolution of $\Delta Q/Q = 0.1$ for $Q = 0.03 \sim 1.1$ A^{-1}.

An assembly of a sample table, detectors and their shield is placed in front of the polarized neutron exit from the shield (Station 2). The position of the assembly can be changed along the incident neutron beam path. The station with an electromagnet serves for the measurement of elastic or quasi-elastic magnetic scattering. The covered Q range is about $0.3 \sim 60$ A^{-1}.

There is another detector bank for inelastic scattering (Station 3) connected with the sample table in Station 2. Since the detector bank as well as the sample table is equipped with the air pad mechanism, neutron flight paths L_1 (from source to sample) and L_2 (from sample to detector), and scattering angle θ can be changed accurately and easily. We adopted this system because we found that the critical selection of the flight paths and the scattering angle is indispensable for the accurate measurement of high energy magnetic scattering. Here variable ranges of L_1, L_2 and θ are $L_1 = 6.5 \sim 9$ m, $L_2 = 1 \sim 3$ m, and $\theta = 5 \sim 60°$, respectively. In order to perform the inelastic scattering experiments, a chopper system will be introduced to the spectrometer. The covered energy transfer range is about $20 \sim 200$ meV with a resolution of $\Delta E/E = 0.1$.

Polarizing filter assembly

In order to cool the filter, a ^{3}He cryostat is used, the outline of which is shown in Fig. 2. ^{3}He gas is liquefied by passing through a heat exchanger in a ^{4}He pot at 1 K. The filter is cooled down to below 0.5 K by pumping on liquid ^{3}He using a Roots pump system (Alkatel-2000). Contrary to Pre-PEN[1] the transverse polarization scheme (neutrons are polarized transversely to the beam direction) is adopted; a Helmholtz type superconducting magnet with the magnetic field in the vertical direction is used, in which the ^{3}He cryostat is inserted vertically. The superconducting magnet is specially designed so as to produce 25 kG with a homogeneity of 5×10^{-5} in the volume of $30 \times 40 \times 20$ mm^3 and with no zero field in the neutron beam path in order to avoid the depolarization of neutrons.

Spin-flipper system

In order to reverse the direction of the polarization of white neutrons, a non-adiabatic spin flipping device with a superconducting Nb thin plate ($60 \times 70 \times 1$ mm^3) was adopted. The Nb plate in a ^{4}He cryostat is

inserted into the beam path with the surface normal to the beam direction, which serves to decouple the magnetic fields in the beam paths of both sides of the plate. The neutron-spin flip is achieved by reversing non-adiabatically the field direction of one side. In order to flip the spins of neutrons with a defined energy which will be used for inelastic scattering, a Mezei type flipper will be used.

Performance of the polarizing filter assembly

Preliminary performance tests for the polarizing filter assembly were carried out. The filter material was ethylene glycol containing a few percents of Cr^{V} complex. The filter material was set in a sample container in the ^{3}He cryostat, as shown in Fig. 2. It was cooled down by pumping on liquid ^{3}He to 0.3 K. The container was also used as a microwave cavity, into which microwave of about 70 GHz was supplied with enough intensity to saturate ESR of Cr^{V} complex. An RF coil was inserted into the cavity to detect NMR absorption signals at 106.4 MHz. The polarization of the dynamically polarized protons was determined by comparison between the enhanced signal and thermal equilibrium one obtained without supplying microwave at 0.6 K.

For the test experiments, two types of sample (filter) containers were used. One was for checking the maximum proton polarization and the other was for production of polarized neutrons. The former container was a box with the volume of 29 x 30 x 15 mm^{3}, in which beads of the filter material with about 1.5 mm in diameter were packed. Liquid ^{3}He was poured directly into the box. The microwave was supplied to the filter material, and the build-up of the proton polarization was observed. The microwave power was about 100 mW at the output of a klystron. The build-up was saturated in one hour. Then the microwave was switched off and the relaxation of the proton polarization was observed. The relaxation time was about 300 min at 0.3 K. The results are shown in Fig. 3. Two extreme proton polarizations were achieved at the microwave frequencies of 69.24 GHz and 69.50 GHz, which corresponded to the parallel and anti-parallel polarization to the thermal equilibrium polarization, respectively. The absolute values of the polarizations were about 80 % with about 5 % difference between each other. The difference was due to too high Q value of the RF coil. The asymmetry will be improved by using the RF coil with small Q value. The value of polarization of 80 % is almost the maximum one hitherto attained at KEK by this technique and material, indicating that our DPPF system has a satisfactory performance.

For the production of polarized neutrons, we used a sample (filter) container, which was made and tested in the Pre-PEN experiments[1]. It was composed of three layers. The center layer was made of the filter material, the volume of which was 20 height x 6 width x 10 thickness mm^3. The side layers were filled with liquid ^3He. This container was specially designed so as to exclude ^3He nuclei from the neutron beam path. The maximum proton polarization attained was about 50 %. The neutron polarization obtained by using this polarized proton filter was detected to be about 70 % at 100 meV and 40 % at 1 eV. These values are almost the same as those obtained by Pre-PEN experiments[1], suggesting that this may be the limitation of this type of the filter container. Therefore, in order to achieve the better proton polarization comparable to the one obtained with the beads sample, but with a good neutron transmission, another filter system should be adopted, which is now under development.

References

1) Prior to the installation of the PEN spectrometer some test experiments were carried out (Pre-PEN experiments); J. M. Newsam, M. Ishida, S. Isagawa, Y. Ishikawa, S. Ishimoto, M. Kohgi, A. Masaike, Y. Masuda, K. Morimoto and T. Nakajima, KENS Report-III, KEK Internal 82-5 (1982) 123.

2) V. I. Lushchikov, Yu. V. Taran and F. L. Shapiro, Sov. J. Nucl. Phys. 10 (1970) 669.

3) S. Hiramatsu, S. Isagawa, S. Ishimoto, A. Masaike, K. Morimoto, S. Funahashi, Y. Hamaguchi, N. Minakawa and Y. Yamaguchi, J. Phys. Soc. Jpn. 45 (1978) 949.

4) Y. Ishikawa, S. Ikeda, M. Furusaka and N. Niimura, KENS Report-I, KEK Internal 80-1 (1980) 101.

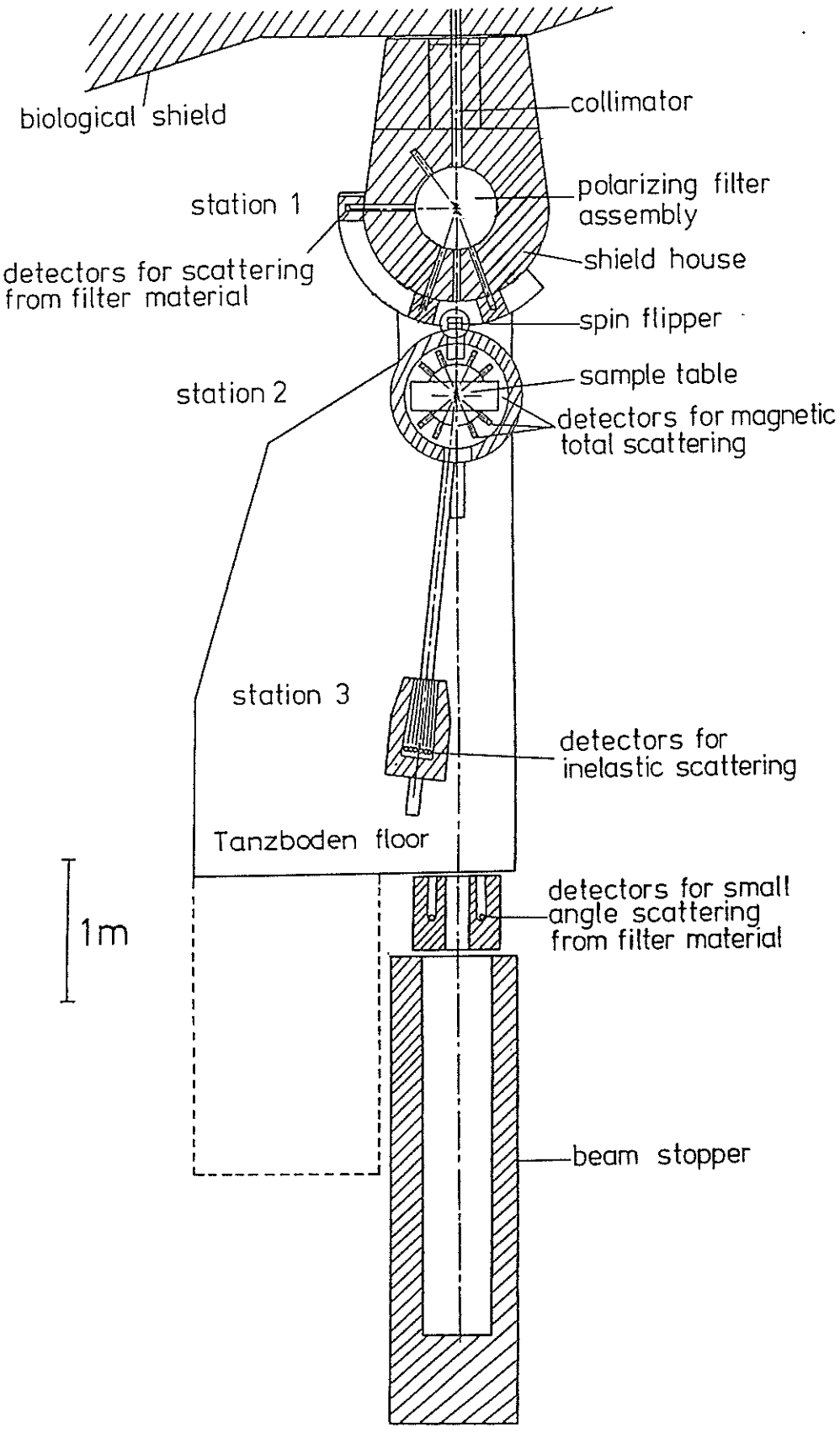

Fig. 1 Layout of the PEN

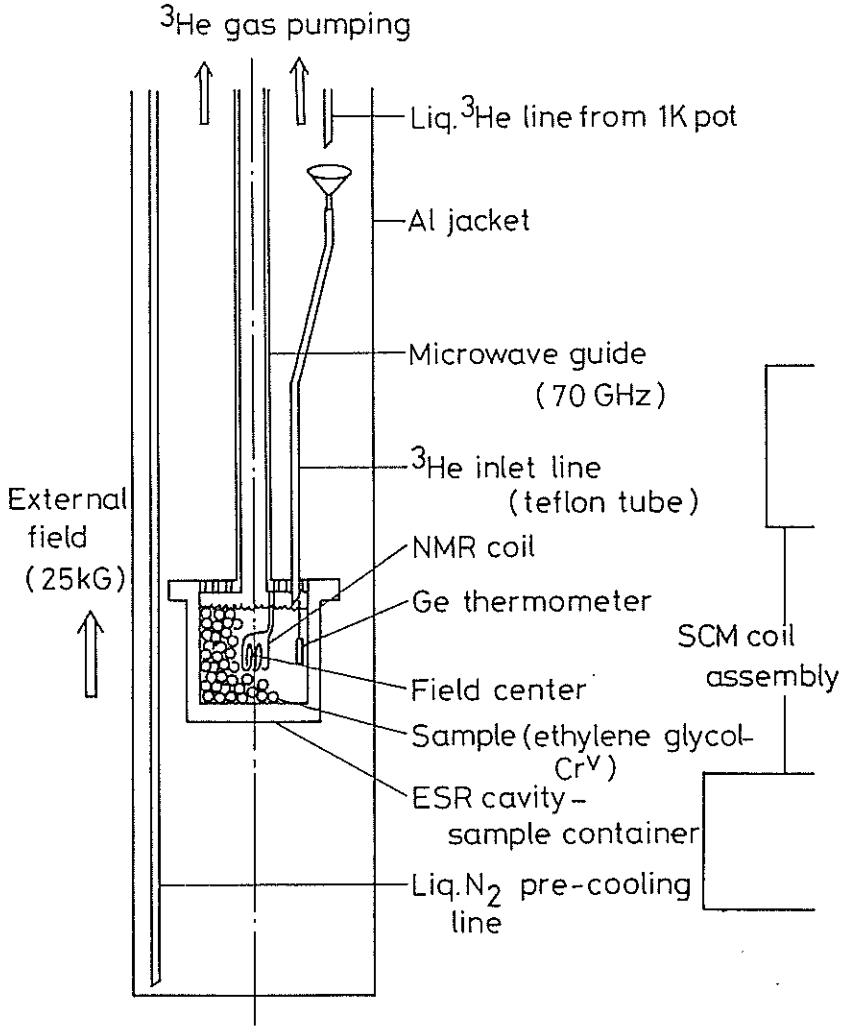

Fig. 2 Sample container and its periphery designed for realization of optimum proton polarization condition. Sample container also worked as a liquid ^{3}He container and an ESR cavity. Ethylene glycol-Cr^V was shaped into small beads for high cooling efficiency. Superconducting coils are wound coaxially around the center axis.

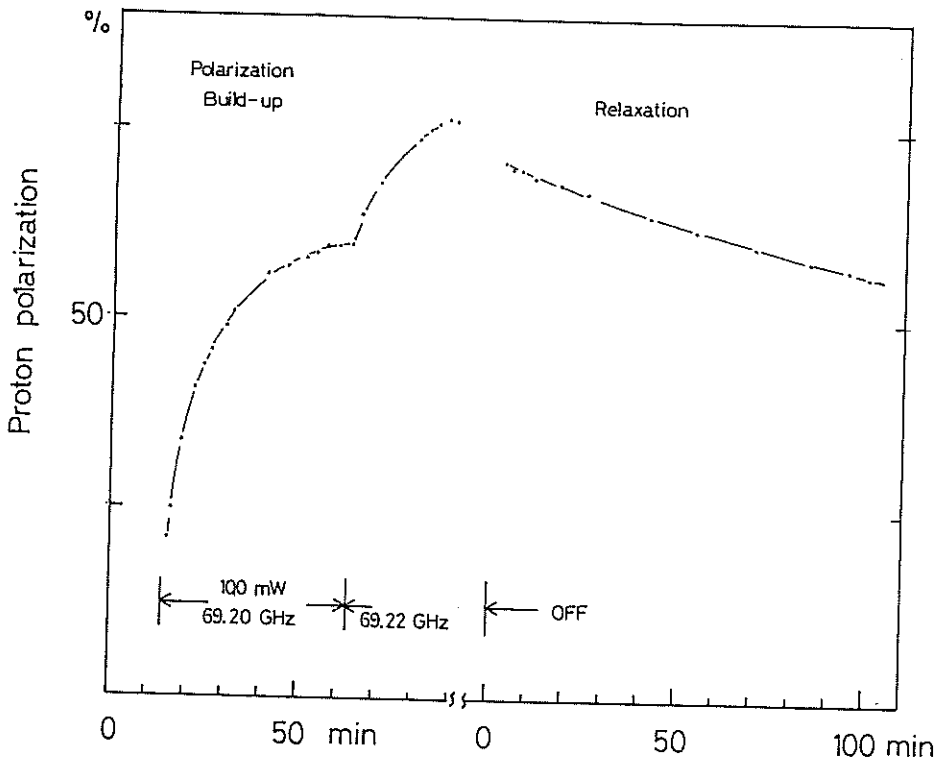

Fig. 3 Polarization build-up and relaxation. Dynamic polarization of protons was started with microwave of 100 mW at 69.20 GHz. After about 60 min the polarization was saturated. In order to get high polarization the frequency of microwave was changed to 69.22 GHz. Then the microwave was switched off. The polarization gradually decreased with relaxation time of about 300 min. The Ge thermometer indicated the temperature of 0.3 K in that time.

Preliminary Report on the Effect of D_2 and D_2O Infused Upon a Vacuum Vessel

Hajimé YOSHIKI and Hiroyuki UEDA[§]

National Laboratory for High Energy Physics
Oho-machi, Tsukuba-gun, Ibaragi 305, Japan

[§]Nuclear Technology Department, Hokkaido University
Sapporo 060, Japan

It has been shown by Mampe et al[1] that the storage time of the ultra cold neutrons (UCN) in storage vessels rather strongly depends upon how the surface of the vessels is cleaned. They established the direct correlation between reflection losses of UCN and the surface hydrogen concentration and concluded that main cause of UCN losses is due to upscattering by warm hydrogen on the surface of the vessel. Before going into UCN production and storage experiments, we conducted a series of operations introducing D_2 or D_2O into a proposed UCN storage cavity and temporary vessels which contain its components, either by glow discharge or simply filling them with these gases. After each operation, we evacuated them and observed the behaviour of the deuterium compounds by a mass spectrometre for a certain period. This is a preliminary report on a particular component among such operations.

Figure 1 shows the system employed. In storing UCN, which is produced by means of superthermal liquid helium[2], it is necessary to operate a UCN valve deep inside the cryostat. A SUS rod, 6 mm in diametre and 1500 mm in length, shown in the centre of the figure was fabricated. The thermal shielding fins , etc., are omitted from the figure. This was placed in a SUS pipe via an electric insulator and the pipe was pumped down by a 200 l/sec turbo molecular pump. The system was made to clean the rod by deuterium ion bombardment.

In Fig.2, the measured partial pressures of masses between 16 and 20 over a period of 2300 hours are shown. What have been done during times where no pump was on, indicated by A,B,C,D and E in the figure are as follows. A) The

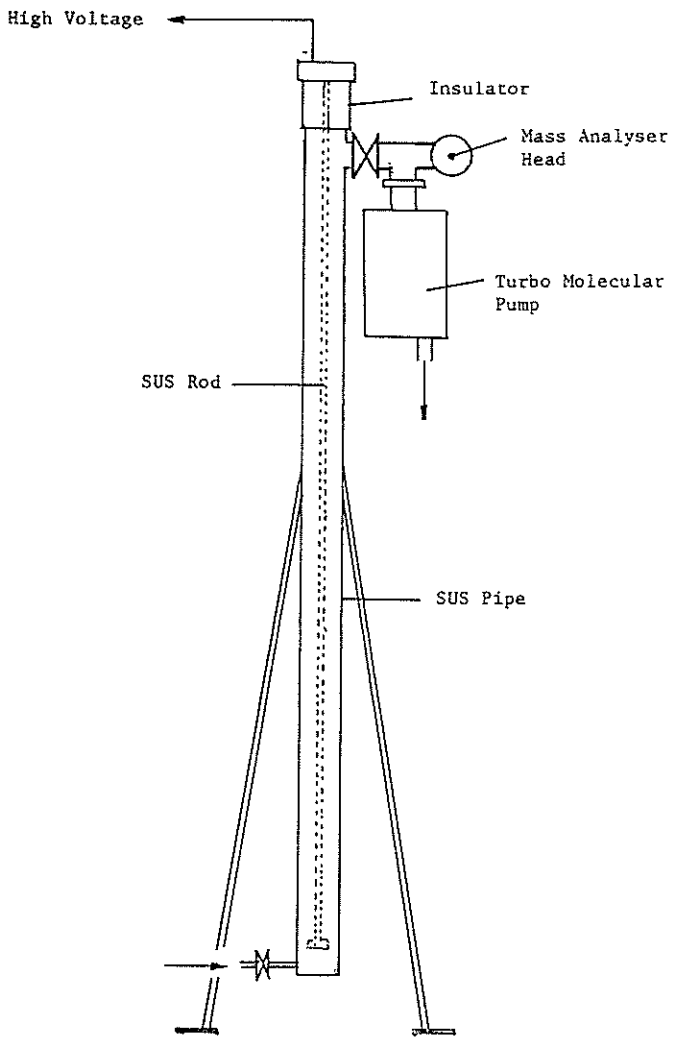

Fig. 1 The Vacuum System used for this Report

SUS pipe was heated up to 190°C evenly and D_2 gas was introduced from the bottom. The glow discharge was continued for 20 min. at 420 volts with 30 mA while the gas flow was kept constant. After pumping down for an hour, D_2O vapour was injected up to several Torr. The heaters were then cut off and the system was pumped down for another hour. When it became close to the room temperature (about 70°C), D_2O vapour was injected again till it saturated. B) The system saturated with D_2O vapour was left at room temperature, sealed, for 310 hours. C) The system kept under vacuum, sealed, for 1580 hours. The

pressure at the time of sealing was 1.5 x 10^{-7} Torr. D) With heaters on, we performed glow discharge at 500 volts, 30 mA for 20 minutes for two times, separated by 10 minutes pumping. Then the heaters were cut and D_2O was filled up to 8 Torr for 40 minutes followed by pumping down for an hour. Then the system was filled with D_2O vapour again up to 6 Torr for a while and pumped down. In three hours the vacuum got to 3 x 10^{-7} Torr. E) The rod was removed from the system to incorporate it in the UCN system. The mass analysis was done to the rest of the system after this.

Most likely candidates for mass 16 are O and CH_4; for 17, OH, CDH_3; for 18, H_2O, OD; for 19, DHO; and for 20, D_2O. We assume that no other candidates like NH_3 or Ar would influence much of the spectrum. Except immediately after the D_2O vapour was injected, the spectrum is dominated by mass 18, followed by 19, 17, 20 and 16. The background spectrum in common vacuum works normally shows no peaks at masses 19 and 20, which implys that these are due to the deuterium injection. If the ordinary cracking pattern of H_2O applies to D_2O, mass 18 should have not more than 10% of OD, and very likely only a few percent. The ratio of mass 18 to mass 17 which is close to the usual cracking ratio of light water also supports this view. It is worth to note however that once D_2 and D_2O are introduced to the vessel, the deuterium compounds remain there as remnant molecules for a long period of time together with hydrogen and its compounds. This is different from the behaviour of other gases like N_2 or Ar. To what extent these deuterated molecules are really coming from the surface of the vessel is still an open question and subject to further investigations.

1) W.Mampe et al, Z.Phys.B, Condensed Matter 45, 1(1981)
2) R.Golub et al, Phys. Lett.,62A 337 (1977)

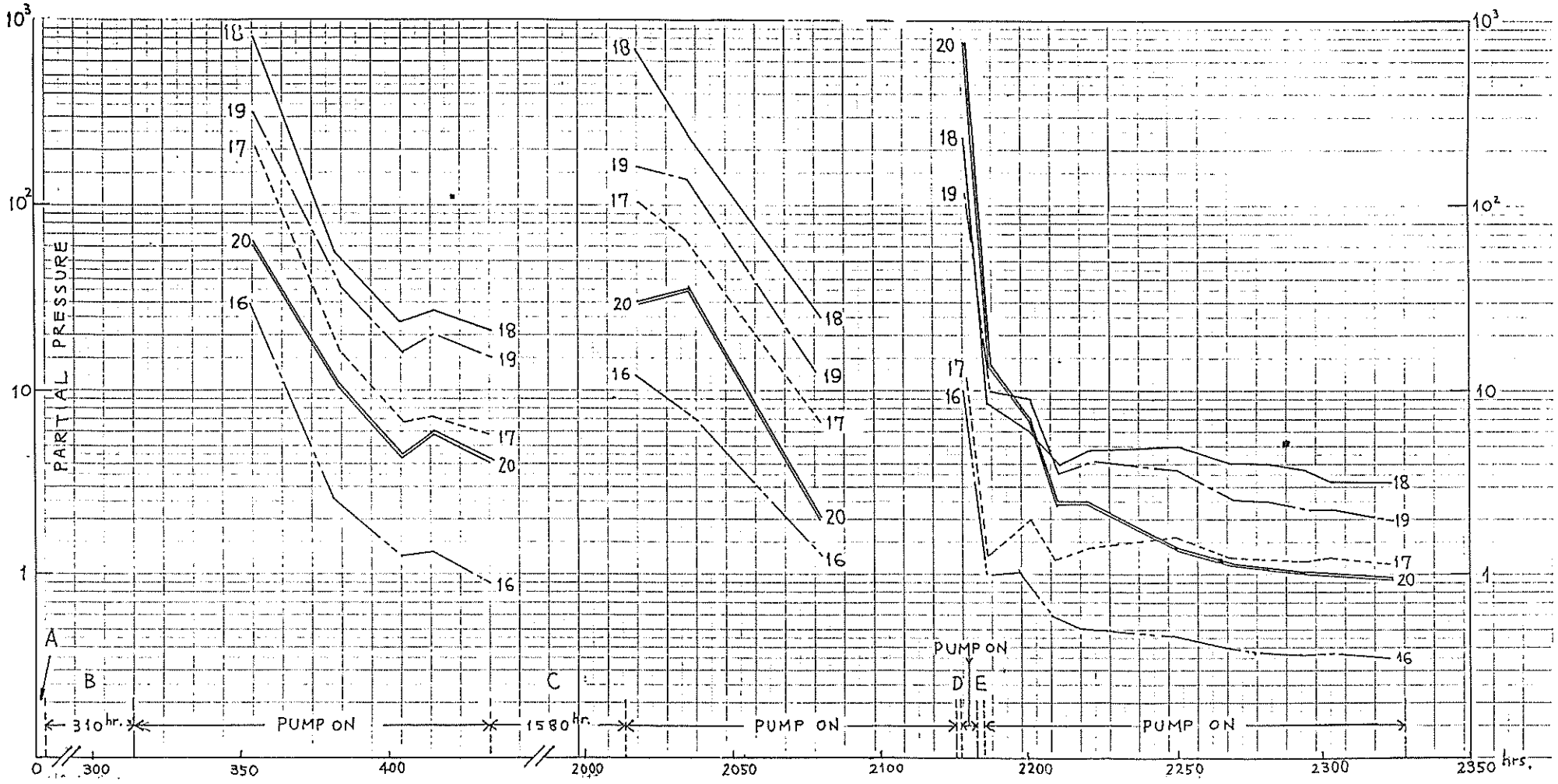

Fig. 2 The Result of Mass Analysis for this Report (Partial Pressures are in Arbitrary Unit)

Linear Position Sensitive Neutron Detectors Using ^{6}Li Glass Scintillators

N. Niimura, K. Yamada, T. Kubota and M. Satoh

Laboratory of Nuclear Science, Faculty of Science
Tohoku University, Mikamine, Sendai 982, Japan

In time-of-flight (TOF) measurements the dead time of detectors is required to be less than 100 nsec and a ^{6}Li-glass scintillator meets the requirement. If a proper method for defining the position of the scintillation event can be developed, it may be used in a position sensitive detector (PSD). We have designed and constructed a new type of a linear PSD using ^{6}Li glass scintillators (L-GS). The feasibility test experiment of this PSD has been performed by using KENS cold neutron. The preliminary result is presented.

The principle of the linear PSD is illustrated in Fig. 1. A stripe of the scintillator is sticked on the light transmitter. Scintillation photons created by a neutron are separated and propagate towads the ends where photomultipliers (PM) are placed. The position where the neutron is captured in the scintillator is determined by the following expression;

$$\ell_A = \frac{1}{2}\{\ell_0 - \frac{1}{\mu}\ln(\frac{I_A}{I_B})\} \quad , \qquad (1)$$

where μ is a linear absorption coefficient of the total optical system, I_A and I_B are the intensity of the photomultiplier A and B respectively, and ℓ_A and ℓ_0 are the length of the scintillator as shown in Fig. 1.

We have constructed the linear PSD. The scintillator is 16 cm in length, 1 cm in width and 0.2 cm in thickness. Experimentally the position where a neutron hits the scintillator is defined with the Bragg reflection from a pyrolytic graphite (PG) single crystal, since in the TOF technique the direction of the Bragg reflection is changed by rotating the PG.

The pulse height distributions from PM-A and PM-B are shown in Fig. 2 when the Bragg reflection from the PG hit the scintillator. The direction of the Bragg reflection is illustrated in Fig. 2. The peak position of the pulse height distribution of the PM-A or PM-B corresponds to the quantity of the scintillation photons, that is, I_A or I_B in eq. (1). When the neutron hits the scintillator at B, the intensity from the PM-B

is stronger than that from the PM-A. When the direction of the Bragg reflection is changed from B to A, the peak position of the pulse height distribution shifts. The results of the experiments do not conflict with the above consideration as shown in Fig. 2. However, we have found that the realization of the linear PSD of this type has several problems to be solved. One of the biggest problems is to measure the quantity of scintillation photons which reach to the both ends accurately.

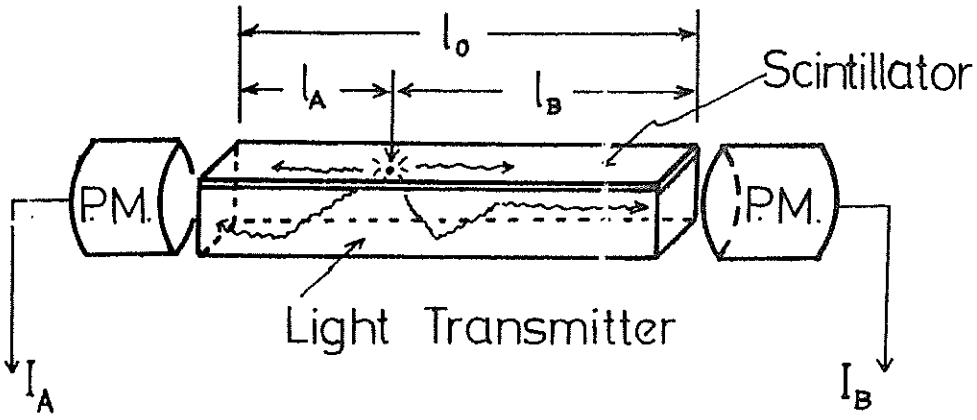

Fig. 1. Principle of a linear position sensitive detector.

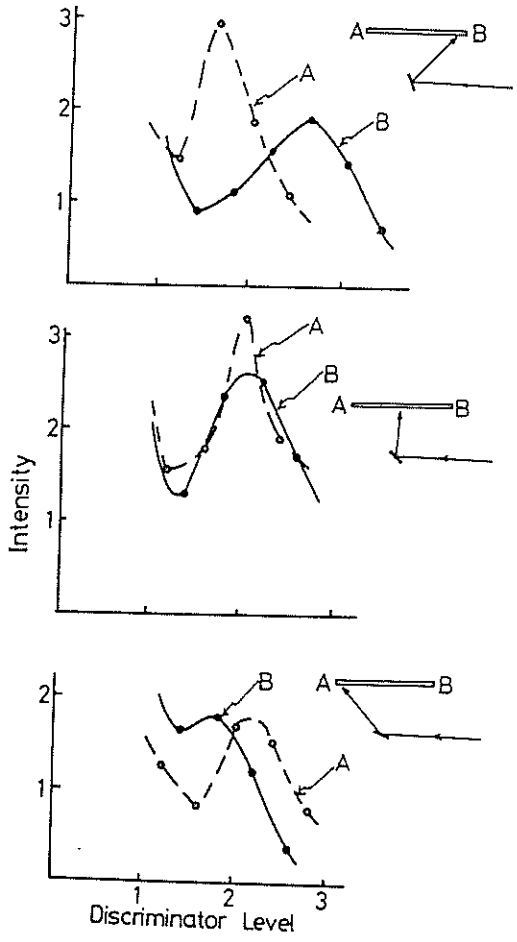

Fig. 2. Pulse height distributions from PM-A and PM-B when the neutron hits the end B, the center and the end A respectively.